UNIVERSITY OF SOUTHAMPTON
FACULTY OF ENGINEERING, SCIENCE & MATHEMATICS
School of Ocean and Earth Science

PHYTOPLANKTON INDUCED CHANGES OF AIR BUBBLE RESIDENCE TIME IN SEAWATER

by

Verena Dauben BSc. (Hons)

Thesis for the degree of Doctor of Philosophy

November 2005

Graduate School of the National Oceanography Centre, Southampton

This PhD dissertation by

Verena Dauben

has been produced under the supervision of the following persons

Supervisors

Dr. Duncan A. Purdie – National Oceanography Centre, Southampton

Dr. Ulrich Horstmann – Leibniz Institute of Marine Sciences Kiel

Chair of Advisory Panel

Prof. Patrick M. Holligan

UNIVERSITY OF SOUTHAMPTON

ABSTRACT

FACULTY OF ENGINEERING, SCIENCE & MATHEMATICS

SCHOOL OF OCEAN & EARTH SCIENCE

Doctor of Philosophy

PHYTOPLANKTON INDUCED CHANGES OF AIR BUBBLE RESIDENCE TIME IN SEAWATER

By Verena Dauben BSc. (Hons)

Air bubbles in the ocean, naturally induced by breaking waves or artificially entrained by ships, remain in the water for different periods of time. Knowledge of the factors accounting for the differences in air bubble residence time (BRT) is essential for understanding processes of air sea-gas exchange as well as for the detection of underwater ship wakes in defence applications. Reasons for the differences in BRT have been found mainly with respect to physical and chemical properties of seawater, such as temperature, salinity and gas saturation level. The impact of biological factors on the behaviour of air bubbles in seawater has not previously been investigated. It is hypothesised that phytoplankton influence BRT through the production of dissolved organic material (DOM) and oxygen.

Laboratory experiments were carried out in a seawater mesocosm tank system to investigate the influence of phytoplankton growth on the BRT of artificially injected air bubbles of a wide size range (10-1000 µm diameter) using both natural phytoplankton populations from Kiel Firth and phytoplankton monocultures. BRT was determined acoustically and several phytoplankton growth-related parameters (chlorophyll concentration, dissolved inorganic nutrients, dissolved organic carbon (DOC), oxygen saturation, bacteria numbers) as well as physico-chemical parameters (surface tension and viscosity) were monitored.

BRT showed statistically significant covariation with oxygen saturation and chlorophyll *a* concentration during phytoplankton growth periods in the tank. Increases in BRT of a factor of > 2 were found during the chlorophyll maxima, provided that the water was sufficiently supersaturated with oxygen (~>110%). When the seawater was undersaturated with oxygen, BRT changed only marginally regardless of the chlorophyll *a* concentration. No clear relationship was evident between BRT and measurements of DOC, surface tension and viscosity.

Investigations of the influence of dissolved oxygen on BRT through variation of oxygen saturation of deionised water showed that oxygen saturation alone has no apparent effect on BRT. The influence of phytoplankton on the rheological properties of an air/water interface was investigated in small scale experiments using different phytoplankton monocultures. An increase in surface shear viscosity was detected for only one of the four species of microalgae tested, *Nitzschia closterium*. Dependency of BRT on the combination of oxygen supersaturation and other phytoplankton growth-related parameters are discussed.

LIST OF CONTENTS

LIST OF TABLES

LIST OF FIGURES

DECLARATION OF AUTHORSHIP

I, Verena Dauben, declare that the thesis entitled Phytoplankton induced changes of air bubble residence time in seawater and the work presented in it are my own.
I confirm that:

- this work was done wholly or mainly while in candidature for a research degree at this University;
- where any part of this thesis has previously been submitted for a degree or any other qualification at this University or any other institution, this has been clearly stated;
- where I have consulted the published work of others, this is always clearly attributed;
- where I have quoted from the work of others, the source is always given. With the exception of such quotations, this thesis is entirely my own work;
- I have acknowledged all main sources of help;
- where the thesis is based on work done by myself jointly with others, I have made clear what was done by others and what I have contributed myself;
- none of this work has been published before submission.

Signed:…….

Date:…….

ACKNOWLEDGEMENTS

I would like to thank my supervisors Dr Duncan Purdie and Dr Ulrich Horstmann for their guidance and support throughout this project.

Thank you to my PhD colleague Alex for a wonderful time together in the office, inspiring discussions and much help with the computer!

Thank you to my colleagues and "helping hands" at FWG Uwe Knispel and Hauke Voß for setting up that tank system and for all their help and support! Thank you also to Heiko Lass, Michael Krüger, Jens Benecke, Marc Florescu, Kai Haacks and Dr Doris Milkert at FWG for their help with various bits and for making my time there enjoyable!

A big thank you must go to Peter Fritsche, Kerstin Nachtigall and Regine Koppe for their assistance in the lab and their generous loan collections of all sorts of lab equipment. Thank you to Tobias Steinhoff for his help with the HTCO.

Many thanks are also due to Dr Jürgen Krägel and Dr Reinhard Miller for the very enjoyable co-operation, and their patient attempts to familiarise me with physical chemistry. You have been really supportive, friendly and approachable! Also thanks to Dr Kamil Wojciechowski for his kind offer to do some surface tension measurements on the phytoplankton cultures.

Thank you to Jeanette Göbel for her help with the phytoplankton cultures!
Thank you also to Siggi Podewski for her encouragement and for valuable scientific discussions. Thanks are due to Dr David Woolf for his advice and expertise on air bubbles.

I would like to thank FWG for funding this research.

Most of all I am grateful to my family – my parents, Christiane and Daniel for all their support, love and encouragement to hang in there!

"Let me tell you the secret that has led me to my goal: my strength lies solely in my tenacity"

Louis Pasteur

LIST OF ABBREVIATIONS

A/D	=	analogue/digital
BRITTA	=	Bubble Reverberation In The Tank
BRT	=	bubble residence time
mf BRT	=	median-filtered bubble residence time
BST	=	bubble surface tension
CCMP	=	Centre for Culture of Marine Phytoplankton
CDOM	=	chromophoric dissolved organic material
Chl *a*	=	chlorophyll *a*
CMC	=	critical micelle concentration
CV	=	coefficient of variation
dB	=	decibel
DF	=	degrees of freedom
DOC	=	dissolved organic carbon
DOM	=	dissolved organic matter
FA	=	fulvic acid
FW	=	Firth water
FWG	=	Forschungsanstalt der Bundeswehr für Wasserschall und Geophysik
GF/F	=	glass fibre filter
HF	=	high frequency
HTCO	=	high temperature catalytic oxidation
ISR	=	interfacial shear rheometer
JGOFS	=	Joint Global Ocean Flux Study
kHz	=	kilo hertz
LF	=	low frequency
MCC	=	mean carbon content
PAT	=	profile analysis tensiometer
POC	=	particulate organic carbon
SP	=	surface pressure
TBB	=	total bacterial biomass
TBN	=	total bacteria number
TEP	=	transparent exopolymer particles
TOC	=	total organic carbon

1 Chapter One. Introduction

1.1 Significance of air bubbles in the ocean

Air bubbles in the upper layer of the ocean play an important role in several physical processes of geochemical significance (Thorpe, 1982; Woolf, 1997). Air bubbles act as a vehicle for the transport of material to the surface microlayer (Scott, 1975; Gershey, 1983; Wallace and Duce, 1995). The primary mechanism by which organic particles are transported upward across the boundary between the ocean and the atmosphere is associated with the production of aerosol particles which is, in turn, the result of bubbles bursting at the sea surface (Blanchard and Woodcock, 1957; Blanchard, 1963; Deane and Stokes, 1999; Monahan and Dam, 2001). Tsen *et al*. (1992) explain the significance of surface active material (surfactants) transported to the atmosphere from the sea by bursting bubbles. These surfactants, which are attached to sea-salt particles, may influence the formation of rain, the evaporation of water from the sea and the ocean-to-air flux of charged particles. Air bubbles are also involved in the exchange of gases between the atmosphere and the ocean (Merlivat and Memery, 1983; Asher *et al*., 1995; Woolf, 1995; Nightingale and Liss, 2004). Wallace and Wirick (1992) found that increased wave action results in increased oxygen concentrations in the sea via bubble entrainment. Air-sea gas exchange is an important process in the geochemical cycling of carbon dioxide (Liss and Merlivat, 1986; Farmer *et al*., 1993). Wallace and Wirick (1992) also discussed the importance of air bubbles in the cycling and global budget of trace gases.

Two major mechanisms are responsible for the entrainment of air bubbles in the ocean. The first mechanism is the breaking of waves. The second mechanism is the formation of bubbles in the wakes of ships by propeller rotation, a process known as cavitation. Cavitation is the creation of vapour bubbles in low pressure fluids.

Due to the large acoustical cross section of air bubbles, they are responsible for the continuing acoustical signatures of ship wakes (Trevorrow *et al*., 1994), especially as these signatures may persist for periods of half an hour or more, often long after visible traces of the ship's passage have disappeared. Ship wakes are important for naval warfare because they may interfere with the successful operation of acoustic devices by scattering and absorbing sound or they may provide a method for detecting, tracking or identifying the ship which has produced the wake (Wildt, 1968).

1.2 Formation and distribution of air bubbles in the ocean

In the ocean, the major mechanism of natural bubble entrainment is the break- up of large volumes of air by breaking waves. Breaking waves dissipate up to 40% of their energy and up to 50% of this energy lost is expended in entraining air bubbles (Rapp and Melville, 1990). Cipriano and Blanchard (1981) report from their experiments that the total rate of air entrainment by a breaking wave gave a value of 125± 17 cm^3 s^{-1}, nearly a third of their volume flow of water (~410 cm^3 s^{-1}), illustrating the efficiency with which air is entrained by falling water. However, the total value of air entrainment varies with wind speed and thus the force of the wave breaking. The wave breaking and the first seconds of bubble plume formation have been assessed by Deane and Stokes (1999), who found that a sequence of events is leading to bubble formation. Immediately before a wave breaks, an overturning jet is formed at the top of the wave crest. This jet is a common feature to both, spilling and plunging breakers (Longuet-Higgins and Cokelet, 1978). As the jet forms, it may become turbulent, entraining air before impacting on the ocean surface. Once the air-containing jet impacts the forward surface of the wave crest, additional entrainment occurs at the entry point, forming jet intrusions, composed of thin filaments of air. These filaments then break up into sub-millimetre sized bubbles. Another process of air entrainment also investigated by Deane and Stokes (1999) occurs directly by the overturning wave crest containing an air cavity which then breaks up into small bubbles. In the first second of breaking, these processes result in one or several high void fraction (void fraction = the volume fraction of air in the total volume) bubble plumes beneath the wave. Bubbles may also be entrained artificially by cavitation through a ship's passage. A detailed account of the formation of air bubbles by cavitation has been given by Wildt (1968). When a cavity is created in water by a ship's propeller, gas diffuses into the cavity from the surrounding water. When the cavity collapses, the gas which has diffused into it is compressed and a bubble forms. The radius of this bubble is determined by the equilibrium of the gas pressure inside the bubble and the hydrostatic pressure outside.

Bubble concentration as well as the penetration depth of bubbles increase with increasing wind speed (Figure 1.1 Kolovayev, 1976; Johnson and Cooke, 1979; Wu, 1981; Thorpe and Hall, 1983; Crawford and Farmer, 1987; Wu, 1988). This rapid increase of bubble population with wind velocity is believed to be due to a more widely spread as well as more violent wave breaking (Wu, 1988). In plunging breakers, the average void fraction decreases from 30-40% to 1% in the first wave period after breaking (Loewen *et al*., 1996). This rapid degassing of the bubble plume is caused by the quick rise of larger bubbles back

to the surface (Crawford and Farmer, 1987; Loewen *et al*., 1996). After the high void fraction plume has degassed, a diffuse cloud of microbubbles is left behind. These microbubbles can persist in the water for long periods of time because they have small rise velocities and are carried and dispersed by the near surface turbulence (Kolovayev, 1976; Thorpe, 1988; Wu, 1994). The dimensions of bubble plumes as well as the bubble distribution in the plumes are strongly dependent on the strength of turbulent shear flows. However, bubble plumes are mostly V-shaped (Thorpe and Hall, 1983). This is due to a decrease in turbulent flow with depth, thus mean vertical profiles of bubble concentration decrease roughly exponentially with depth (Kolovayev, 1976; Johnson and Cooke, 1979; Thorpe and Hall, 1983; Wu, 1981, 1988) and the size spectrum narrows. Kolovayev (1976) found that the most numerous bubbles in the depth range 1.5-8 m are those with radii of about 70 µm and very few bubbles have radii greater than 300 µm (Figure 1.2). According to Kolovayev (1976), this is due to two reasons. First, larger bubbles do not penetrate to great depths. Larger bubbles have a greater buoyant force, thus, turbulent flows, whose velocities decrease with depth, are incapable of entraining larger bubbles to a greater depth compared to smaller bubbles. Secondly, larger bubbles disappear more quickly due to their fast rise.

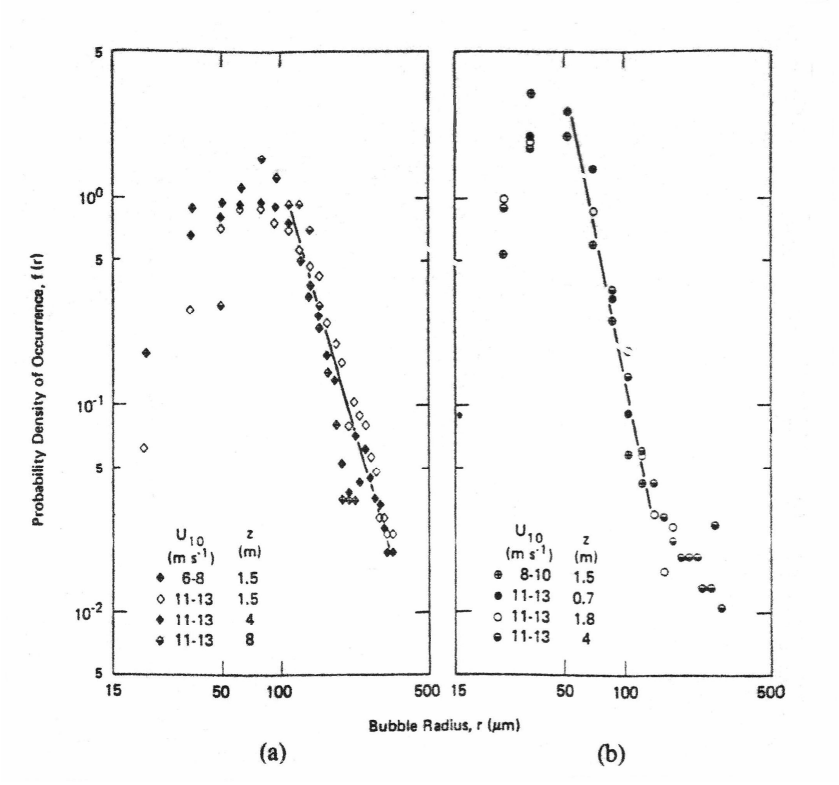

Figure 1.1 Bubble spectra at various depths and wind velocities.
Results were obtained by (a) Kolovayev (1976) and (b) Johnson and Cooke (1979) from Wu (1981).

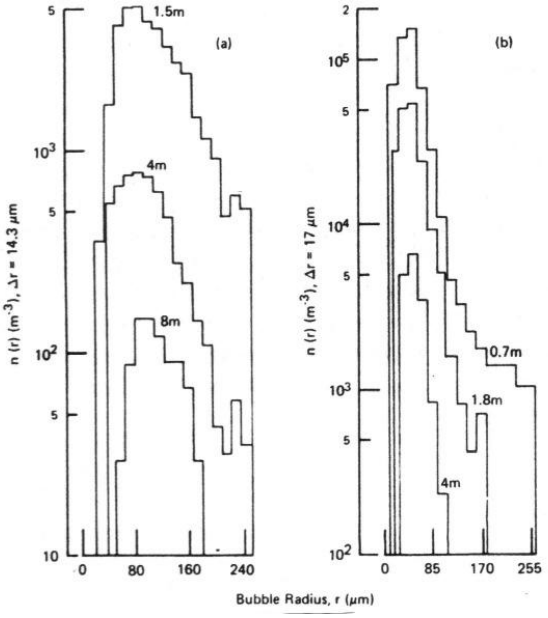

Figure 1.2 Distributions of bubbles at different depths.
(a) by Kolovayev (1976) at depths 1.5,4 and 8m obtained at U10 = 11-13 m s-1 and (b) by Johnson and Cooke (1979) summarised in Wu (1981) at depths 0.7, 1.8 and 4m obtained at U10 = 1-4 m s^{-1}.

1.3 Factors influencing air bubbles in the ocean

1.3.1 Salinity

Reference	Technique	Water type	Salinity	Results
Monahan and Zietlow (1969)	Photographic; whitecap simulation tank	Freshwater 35 psu NaCl	0 35	Salt water bubble coverage decreases less rapidly than for freshwater
Scott (1975)	Photographic; bubble creation by N_2 gas flow	Freshwater Artificial seawater	0 8, 35	Between salinity 0 and 8, bubble size in seawater decreased but quantity increased; For salinity 35 a further size decrease was found
Peltzer and Griffin (1988)	Photographic; bubble production by compressed air through porous glass disc	Type I reagent grade water Artificial seawater Atlantic Coastal SW	0 8, 12, 16, 26, 35 26	Decrease in bubble size only between salinities 0-16. Salinities 26 and 35 had no further influence on bubble size.
Wang and Monahan (1995)	Video camera; bubble production by a tipping bucket	Tap water Seawater	0 2, 4, 6, 20	Bubble concentration increased with salinity. The maximum bubble concentrations for r = 300 µm were: 1800 m^{-3} μm^{-1} for salinity = 0 8600 m^{-3} μm^{-1} for salinity = 6 >48000 m^{-3} μm^{-1} for salinity = 20. Mean bubble radius decreased with salinity: r_{mean} = 2480 µm for salinity = 0 r_{mean} = 1132 µm for salinity = 6 r_{mean} = 320 µm for salinity = 20

Table 1.1 Differences of freshwater and saltwater bubbles found by various investigators.

Several studies have shown that the behaviour of bubbles in freshwater may be different from that of bubbles in seawater (Table 1.1). These findings show that more bubbles are produced in seawater and the seawater bubbles are smaller than bubbles in freshwater, as illustrated in Figure 1.3. The decrease in bubble size in seawater compared to freshwater may be accounted for by a reduced degree of bubble coalescence (Cartmill and Su, 1993; Craig *et al*., 1993). In freshwater, small bubbles coalesce, forming less numerous but larger bubbles. In seawater, coalescence is reduced due to ionic repulsion (Cartmill and Su, 1993). However, opinions on bubble coalescence as the main factor accounting for the observed size and density changes between fresh-and seawater bubbles are split. Craig *et al*. (1993) state that bubble coalescence is inhibited by some salts whereas others have no effect and that this inhibition occurs only upon the 'matching' of a two-valued empirical property assigned to each anion and cation. Some salts were found to have no effect on coalescence (Craig *et al.*, 1993). The strongest degree of coalescence was found in HCl (almost 100% independent of concentrations), where for $MgSO_4$, a concentration of 0.001 mol l^{-1} starts to reduce coalescence and at a concentration of 0.1 mol l^{-1}, coalescence is inhibited. These results are in good agreement with findings of Slauenwhite and Johnson (1999), who detected an increased number of bubbles in NaCl solution that was supplemented with $MgSO_4$ or $MgCl_2$ as well as with results of Shatkay and Ronen (1992), who also found that $MgSO_4$ and $MgCl_2$ reduced the degree of bubble coalescence with increasing concentrations. Another important factor differing between fresh and seawater bubbles is their rate of dissolution, which is, in turn, strongly dependent on the saturation of water with dissolved gases. Studies by Detsch (1990) and Harris and Detsch (1991) indicate that bubbles in freshwater dissolve faster than bubbles in seawater. For larger bubbles in seawater (diameter > 200 µm), the rate of dissolution is independent of bubble diameter but it is linearly dependent on the percentage air saturation (Detsch, 1990). For larger bubbles in freshwater with a diameter > 100 µm, Harris and Detsch (1991) found that in saturated water, these bubbles dissolve slowly, even though their dissolution was nonlinear. For smaller freshwater bubbles < 80 µm in diameter, dissolution proceeded at a much faster rate. In comparison, bubbles in saturated seawater with a diameter < 80 µm dissolved more slowly than bubbles of the same size in freshwater. A reason for the decelerated dissolution of seawater bubbles may be the accumulation of surfactants and particles on the surface of seawater bubbles (Harris and Detsch, 1991, Slauenwhite and Johnson, 1999). The surfactants present in seawater as well as the ions themselves also have an effect on the rise velocity of bubbles. A study carried out by Detsch (1991)

compared rise velocities for bubbles of various sizes (diameter = 20-1000 µm) in three different water types: pure water (4-stage deionised tap water), unfiltered tap water and seawater. Determination of bubble diameters was carried out by holding individual bubbles stationary and sizing them microscopically. For small bubbles < 450 µm in diameter, no difference in the rise velocities was observed. Above 450 µm, rise velocities for bubbles in tap water and seawater agreed but bubbles in pure water had significantly higher rise velocities, almost of a factor of 2. Detsch (1991) attributes this to the contamination with surfactants and particles in sea and tap water, which effectively freeze the bubble's surface. Thus, the bubbles rise as if they were solid spheres. Another factor accounting for reduced rise velocities of seawater bubbles is the increased viscosity due to the presence of salt (Gat and Shatkay, 1991).

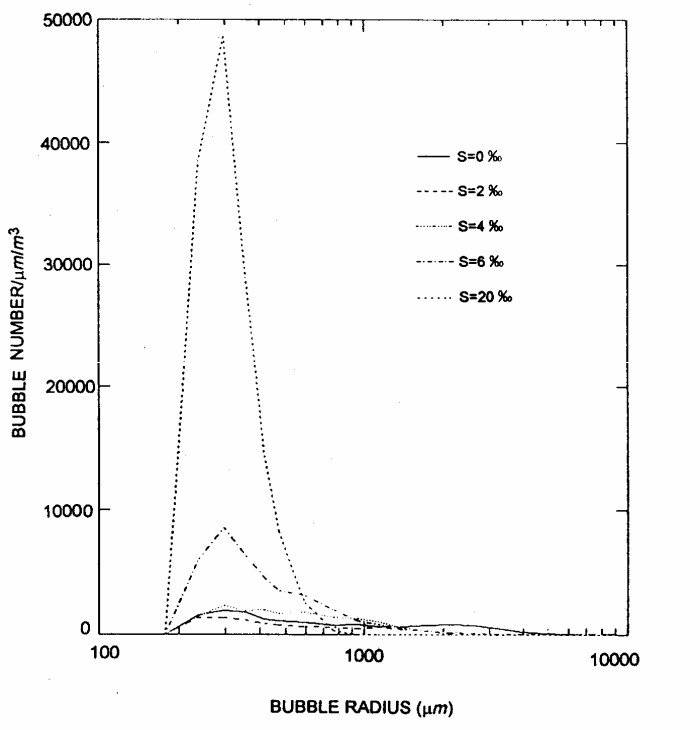

Figure 1.3 Bubble number as a function of radius for different salinities.
Salinities for bubble distribution determination are 0, 2, 4, 6 and 20 at a temperature of 17°C and an O_2 saturation of 100.9% (Carey *et al.*, 1993 in Wang and Monahan, 1995).

1.3.2 Temperature

Water temperature has a significant influence on bubbles both in freshwater and seawater (Thorpe, 1986; Thorpe and Hall, 1987; Hwang *et al*., 1991). Hwang *et al*. (1991) conducted experiments using freshwater (tap water), injected by a water jet into a tank, measuring the entrainment depth of bubbles over a temperature range from 5°C to 40°C with an optical method. They found that small bubbles (diameter of 0.1 mm) were carried to greater depths as the water temperature increased until about 19°C, after which the entrainment depth remained stable (Figure 1.4). These observations are similar to entrainment depths observed in seawater by Thorpe (1986), who used an acoustic method in the ocean and found that bubble entrainment depths during the winter (10.7°C- 11.6°C) were half of the depths in autumn (temperature between 14.7°C and 17°C). Hwang's *et al*. (1991) experiments also showed that the generation of bubbles was hindered at water temperatures lower than 10°C and bubble production increased with increasing temperature between 11°C and 17°C. The hindering of bubble generation, however, could most likely been attributed to the geometry of the experimental set up that was used and should not be generalised. Earlier experiments by Kolovayev (1976) and Johnson and Cooke (1979), discussed by Wu (1992) support the results of Hwang *et al*. (1991). The size spectra of bubbles measured by Johnson and Cooke (1979) at temperatures between 2 and 3°C however were significantly smaller than those measured by Kolovayev (1976) at temperatures averaging 14°C. Another factor that was found to be dependent on water temperature is the rise velocity of bubbles. Leifer *et al*. (2000) and Patro *et al*. (2000) conducted experiments with distilled water, observing the rise velocities of bubbles of various sizes over a range of temperature between 0°C and 20°C. They found that the rise velocity of smaller bubbles (maximum radius of 350 μm) increased with increasing water temperature, whereas for larger, oscillating bubbles, a decrease in rise velocity with increasing temperature was apparent. For small, non oscillating bubbles, the change in rise velocity can be explained by changes in the viscosity. For larger, oscillating bubbles, decreased rise velocities at higher temperatures may be due to a transformation of energy from buoyant rise into horizontal motion and shape oscillation (Leifer *et al*., 2000). However, more recent investigations of Slauenwhite and Johnson (1999) showed converse results. Slauenwhite and Johnson (1999) investigated bubble shattering in filtered seawater and found that significantly more bubbles were produced in seawater at 3°C as opposed to 20°C. A theory developed by Thorpe et al. (1992) could explain this observation that with increased temperature and thus decreased viscosity, the rise velocity of bubbles increases.

An increased rise velocity results in a greater Peclet number, an indicator of gas transfer rate. With higher Peclet number the gas transfer rate increases, resulting in lower bubble concentrations. However, as shown by Leifer *et al*. (2002), the rise velocity is dependent on the size of the bubbles and no linear relationship with temperature exists. The examples discussed here show that there are complex relationships between bubble size spectra, entrainment depths and rise velocities in relation to temperature. Results of different experiments sometimes show good agreement but others contradict. Reasons for this may lie in the different experimental set ups used, however, none of the experiments described has included measurements of gas saturation levels that may have influenced results and could account for the differences in the observations.

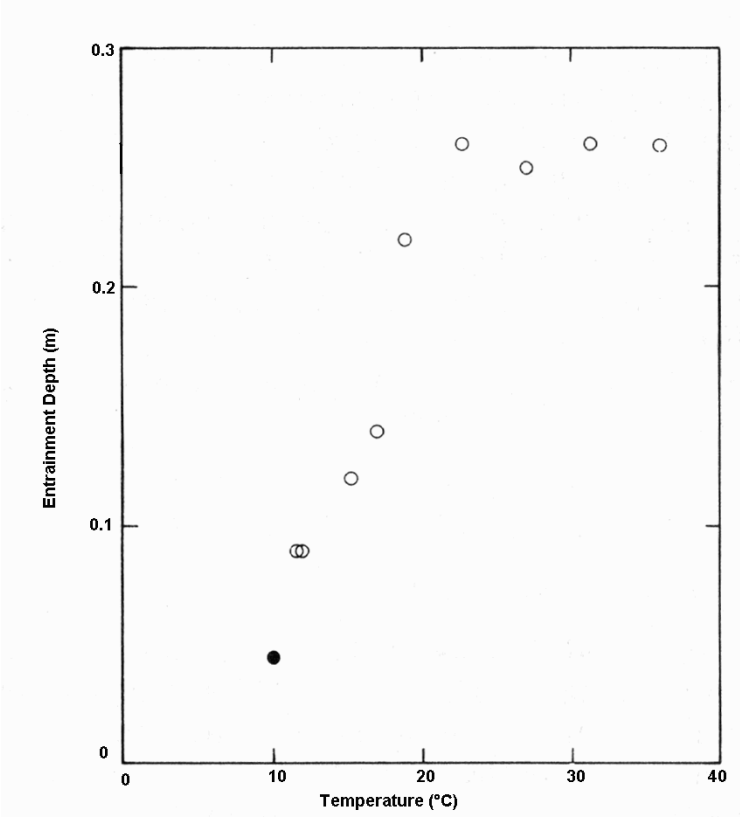

Figure 1.4 Entrainment depth of bubbles produced by a water jet for different temperatures (Hwang *et al*., 1991).

1.3.3 Surfactants

Earlier studies conducted by Garrett (1967) as well as more recent studies by Skop *et al*. (1993) and Slauenwhite and Johnson (1996) show that organics in seawater contribute the largest part to surface active material. Slauenwhite and Johnson (1996) used a method that determined bubble surface tension directly in a phytoplankton culture of *Nitzschia pungens* (*Bacillariophyceae*). They assumed that the lowering of bubble surface tension (from 72-

67 mN m^{-1}) was due to organic exudates produced by the alga although unfortunately, the amount of organic material present in the seawater was not measured. Investigations by Kolaini *et al*. (1994) of bubble production by capillary-gravity waves have shown that significantly more bubbles were produced if the surface tension of water was lowered by various quantities of a surfactant (ethyl alcohol). Thorpe *et al*. (1992) found that the state of a bubble's surface affects the diffusion of gas and particles to and from the bubble, as well as its rise speed and the surface tension. Several authors (Garrett, 1967; Detwiler, 1979; Thorpe *et al*., 1992; Slauenwhite and Johnson, 1996; Leifer *et al*., 2000) have investigated the influence of surfactants on bubble behaviour, with special focus on the rise velocity and their theory and findings show good agreement. The bubble surface is supposed to be initially clean and hydrodynamically mobile but becomes dirty and less mobile as organic molecules and particulates diffuse to the surface (Thorpe *et al.*, 1992). Detwiler (1979) and Patro *et al*. (2000) have described in detail what happens to a bubble in surfactant contaminated water. When a bubble rises in contaminated water, the stress from the upward motion of the bubble convects surfactants towards the downstream hemisphere, creating a gradient in surfactant concentration. This gradient reduces the surface tension, resulting in a tangential force towards the region of higher surface tension. Local surface viscosity is reduced, causing decreased interfacial mobility. This interfacial retardation is called the Marangoni effect, which has been described earlier by Burger and Blanchard (1983) and is caused by the flow from regions of low to high surface tension that develops as a surface tends to equilibrate its surface tension. The accumulation of surfactants at the rear of the bubble leads to the formation of a rigid cap. Patro *et al*. (2000) developed a model to show that bubble rise velocity is dependent on the angle of the rigid cap (Figure 1.5). If the angle is below 30°, their model predicted that bubble rise velocity is largely unaffected, but if the angle is >30° < 45°, rise velocity decreases. Patro's *et al*. (2000) measurements of bubble rise velocity for seawater and lake water bubbles agree with the model (Figure 1.6) as the rising behaviour was different from dirty bubbles, indicating that the bubbles must accumulate sufficient surfactant material for rise velocity to decrease. Smaller bubbles can accumulate surfactants more rapidly due to the smaller surface area and thus show a stronger and faster reduction in rise velocity than larger bubbles.

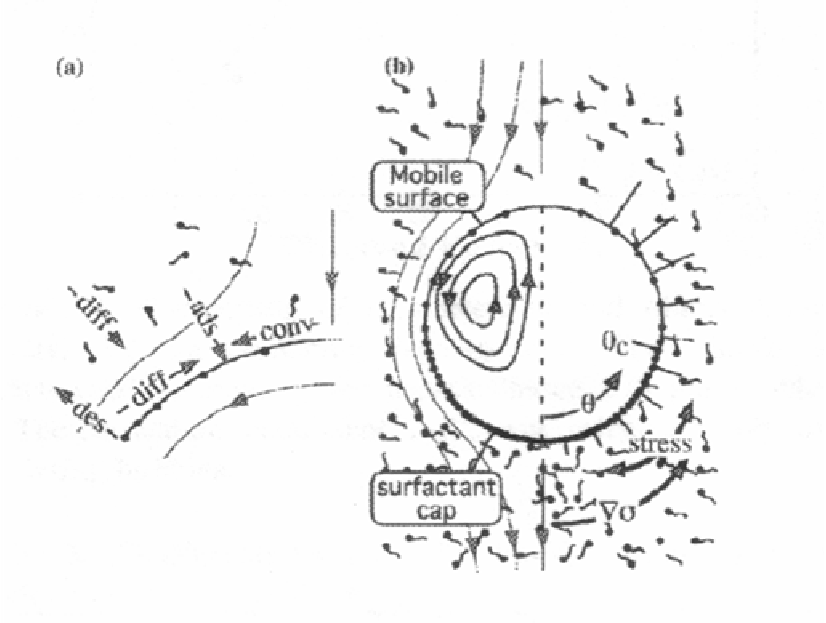

Figure 1.5 Schematic diagram of rigid Cap Model.
(a) transport processes affecting surfactants on a bubble and (b) variation of surface tension, σ, with zenith angle, θ. Key: ads- adsorption, des- desorption, diff- diffusion, conv- convection (Patro *et al*., 2000).

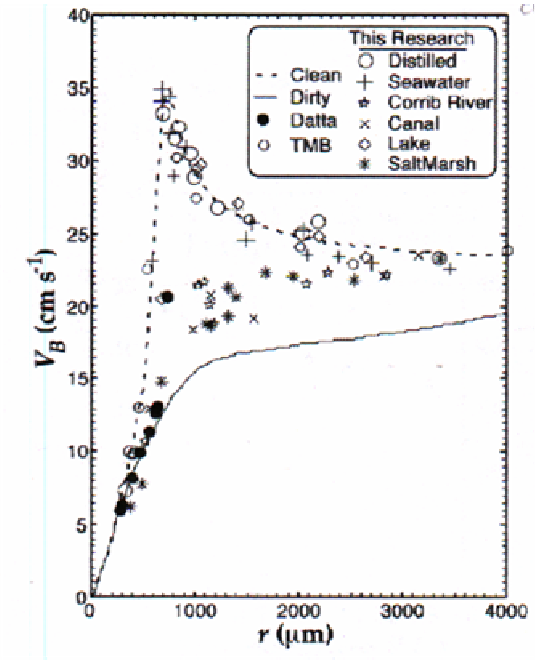

Figure 1.6 Rise velocity (VB) as a function of radius (r) at 20°C from observations, parameterisations and other publications.
Dirty parameterisation from Clift *et al.* (1978), clean parameterisation from Patro *et al*. (2000). Data key: Datta from Datta *et al*. (1950), TMB from Haberman and Morton (1953). Figure taken from Patro *et al*. (2000).

1.3.4 Gas saturation

The level of gas saturation in water has a significant influence on the stable existence, growth or disappearance of bubbles in near surface waters (Ramsey, 1962). Air bubbles dissolve faster at lower air saturations both in seawater and in freshwater, where in freshwater, the dissolution occurs faster than in seawater (Detsch, 1990). Bubbles loose gas by dissolution when the internal bubble pressure exceeds the total gas pressure in the water and they tend to gain gas when the opposite is true. The net tendency for bubbles to grow or contract therefore depends on the dissolved concentrations of major gases O_2 and N_2 (Keeling, 1993). Thorpe (1982) makes the assumption that the gas contained in air bubbles is composed of a mixture of oxygen and nitrogen which are in approximately the ratio 7:26, appropriate to air. The presence of other gases may be negligible, provided they diffuse at rates similar to oxygen and nitrogen. Dissolved oxygen is the only gas normally present in seawater at saturations significant to initiate bubble growth (Ramsey, 1962). This is usually due to biological activity as well as variations in temperature. The solubility of both nitrogen and oxygen decreases by about 2% per °C so if the water temperature increases, it is likely supersaturation will occur (Bowyer and Woolf, 2004). When a bubble rises in saturated seawater, it expands slightly due to the change in hydrostatic pressure. At the same time, gas from inside the bubble is exchanged into the surrounding water via the bubble's surface by molecular diffusion. This exchange of gas counteracts the growth of the bubble and results in slight shrinkage. The change in size as the bubble rises results in a changing degree of gas exchange, thus (i) the exchange of gas across a bubble's surface is nonlinear (Bowyer and Woolf, 2004) and (ii) bubbles can contribute to supersaturation in the oceans (Thorpe and Woolf, 1991). In fact, Thorpe and Woolf (1991) and Keeling (1993) agree that bubbles support supersaturation in the ocean for poorly soluble gases (O_2 and N_2) of typically 1-2% but do not support a globally significant supersaturation of carbon dioxide (soluble gas). Harris and Detsch (1991) conducted experiments to investigate bubble dissolution at 50% and 100% air saturation rates using reagent grade 1 water (4-stage deionised filter system) and seawater with a salinity of ~27. They found that at 100% air saturation, larger bubbles (>60 µm diameter) decreased linearly with time while for smaller bubbles, the decrease was non linear. At 100% saturation, a nonzero dissolution rate was obtained even for larger bubbles. For 50% air saturation, the dissolution was much faster. Seawater bubbles dissolved more slowly than freshwater bubbles. The linear decrease of larger bubbles (diameter > 60 µm) found by Harris and Detsch (1991) contradicts Bowyer and Woolf (2004). However, Bowyer and Woolf (2004)

do not specify if the nonlinearity exists only for smaller bubbles. This may well be the case as for larger bubbles, the gas exchange rate is independent of the dissolved concentrations of the major gases as they rise to the surface at least 10 times faster than they dissolve (Keeling, 1993). The degree of gas saturation also influences the size spectrum of air bubbles and hence their rise velocities. Bowyer (1992) and Stramska *et al*. (1990) found that if the saturation of water increases, the smallest bubbles that can exist in this water show a tendency towards the lower radius. At a saturation of 102%, Bowyer (1992) found a detection threshold for the smallest bubbles at a radius of 32 µm and for a saturation of 114%, the smallest bubbles observed had a radius of 9 µm. If the initial radii of newly formed bubbles are below the threshold, the Laplace pressure causes these to collapse a few seconds after formation. Increasing supersaturation results in faster bubble growth when small bubbles rise, thus resulting in increasing rise velocities for small bubbles.

1.3.5 Biological activity

Not much is known about the relationship between bubbles in seawater and biological activity. A first indication on biological influences on bubbles was made by Ramsey (1962) who investigated the oxygen concentration on a seasonal and diurnal basis in the shallow near-shore waters off Mission Beach, California. He found high surface layer oxygen content at all times during the period of measurements and attributed this to efficient mixing processes as well as the very high biological production during spring, summer and early autumn, which was characterised by large phytoplankton populations. Ramsey concluded that the supersaturation of surface waters with oxygen would lead to the growth of bubbles present in these waters. Ramsey's assumption was confirmed by Sandler *et al*. (1982), who observed a phytoplankton bloom in seawater that was dominated by the diatoms *Thalassiosira nordenskioldii* and *Chaetoceros pseudocrinitus*. They detected an increase in bubble concentrations 10-50 times greater in the area of the bloom as opposed to the background values and suggested that the observations are likely to result from oxygen supersaturation in the areas of increased primary production. Supersaturation leads to stabilisation of gas bubbles due to oxygen diffusion into the bubbles when its partial pressure in water is higher than that inside the bubbles (Zakharkov *et al*., 1991). This process can prolong the lifetime of bubbles and therefore increase the observed concentration of bubbles. They found that the number of bubbles produced in a shattering event in seawater with a phytoplankton culture was significantly greater than the number of bubbles formed in filtered, photo-oxidised seawater. Billard *et al*. (1994)

observed cavitation nuclei in the ocean and correlated these with bioluminescence. They found that in the upper 10 metres of the water column, bioluminescence as well as the nuclei concentration and size are larger than in deeper water below 20 metres, suggesting a possible correlation between the number of nuclei and biological production. Mulhearn (1982) reported diurnal differences in bubble sizes in coastal waters. He found that during daytime, smaller bubbles were produced than at night. This may be the result of diurnal variations in oxygen saturation due to biological activity, resulting in supersaturation during the day and thus the formation of smaller bubbles. Despite the increased concentration of oxygen in seawater with high primary production, another factor that would be conceivable to account for the behaviour of bubbles is the organic exudates, which are released by phytoplankton. Nägeli and Schanz (1991) have found that phytoplankton release surface active organic substances, that can significantly change the surface tension. Organic surfactants released by phytoplankton can accumulate on bubbles, thus changing their rise velocity (see section 1.3.3). A decrease in surface tension would also result in enhanced bubble production (see section 1.3.3).

1.4 Acoustic characteristics of air bubbles

Various investigations of air bubbles in water have been carried out using acoustic rather than optical techniques (Table 1.2). The use of acoustic techniques compared to optical techniques in bubble investigations has several advantages. For one, the ocean is more or less opaque to electromagnetic radiation, except over rather short distances to light (Vagle and Farmer, 1991). Optical techniques sometimes have difficulties in differentiating between small bubbles and particles (McIntyre, 1986 cited in Vagle and Farmer, 1991). Many optical techniques have limitations regarding the resolution of the minimum bubble size that can be detected. The advantage of acoustic techniques is based on the fact that a bubble can resonate. Microbubbles in water possess the requirements of any resonating mechanical oscillator: stiffness and inertia. Therefore, they are capable of resonating in the presence of an incident sound wave (Vagle and Farmer, 1991). At resonance, a maximum oscillation of the bubble develops, and a maximum amount of energy is extracted from the incident sound wave. A portion of this energy is scattered in all directions by the pulsating bubble and the remainder is converted into heat. The oscillating bubble may therefore be viewed as intercepting a portion of the incident sound wave characterized by the extinction cross section σ_e of the bubble and reradiating it as scattered sound in all directions,

characterised by a scattering cross section σ_s, as well as converting it to heat, defined by an absorption cross section σ_a.

The extinction, scattering and absorption cross sections for a single bubble are given by:

$$\sigma_s = \frac{\text{Power scattered over all angles}}{\text{Incident acoustic intensity}} = \frac{4\pi R^2{}_0}{[(\omega_0/\omega)^2 - 1] + \delta^2} \qquad \text{(Equation 1.1)}$$

$$\sigma_a = \frac{\text{Power absorbed by bubble}}{\text{Incident acoustic intensity}} = \sigma_s \times \left(\frac{\delta}{K_0 R_0} - 1 \right) \qquad \text{(Equation 1.2)}$$

$$\sigma_e = \sigma_a + \sigma_s \qquad \text{(Equation 1.3)}$$

where R_0 = resonant bubble radius, ω = angular frequency of incident sound, ω_0 = angular frequency of bubble pulsation at resonance, δ = total bubble damping constant, K_0 = sound propagation constant at bubble resonance frequency (= 1.36×10^{-3} for a clean air bubble). Since δ ranges from 0.067 to 0.15, at resonance, the scattering and absorption cross sections of a bubble can be up to 10^3 times its geometrical cross section and fall off with frequency away from resonance (see Figure 1.7; Medwin, 1970; Clay and Medwin, 1977). Smaller bubbles exhibit strong acoustic resonances in the frequency range 10-400 kHz, corresponding to radii of 8-200 µm. Thus, the frequency-dependent target strengths obtained from multifrequency echo sounders give an indication of the bubble size spectrum of a plume (Trevorrow *et al.*, 1994). The distinctive and exaggerated acoustical cross sections of a single resonant bubble and the narrowness of the resonance curve permit a bubble to be selectively identified in the presence of non-resonant bubbles or of particulate matter or non-bubble-carrying marine animals.

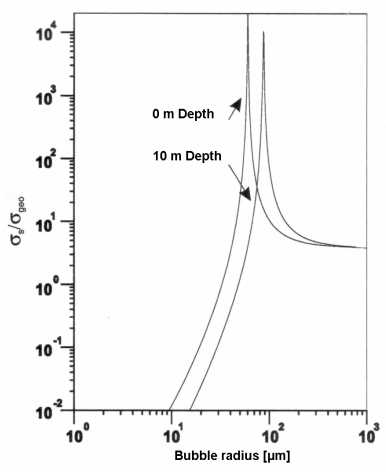

Figure 1.7 Ratio of acoustical to geometrical cross section of an ideal bubble as a function of radius at 50 kHz for two different depths (Clay and Medwin, 1977).

Reference	Study aim	Technique	Results
Thorpe (1982)	Investigate differences of bubble clouds in freshwater (Loch Ness) and seawater (Oban)	Upward looking echo sounder operating at 248 kHz with a pulse length of 0.08 ms and repetition rate of 2.5 Hz; Measurement of acoustical scattering cross section	Bubble clouds penetrate to greater depths with increasing wind speed. The scattering cross section decreases with depth and the scale increases with wind speed.
McConnell (1988)	Investigate role of near surface bubbles in surface backscattering, forward loss and ambient noise at high frequencies	Several acoustic transducers producing a narrow combined beam (beamwidth = 3dB) ranging from 1.2° at 50 kHz to 4.1° at 15 kHz	Bubbles are acoustically observable at wind speeds as low as 3 m sec^{-1}. For wind speeds > 5-6 m sec^{-1} the surface forward loss can become quite large (>10dB).
McDaniel (1988)	To determine dependence of subsurface bubble populations on wind speed, resonant bubble radius, water temperature and vicinity of land.	Short acoustic pulses, narrow beam sources and receivers	Wind speed dependence of bubble densities followed a power law; little dependence of subsurface bubble density on temperature; bubble densities were an order of magnitude higher in coastal seas than in the open ocean at high wind speeds.
Terrill and Melville (2000)	Measuring bubble size distributions at r = 30-800 µm	Sound velocimeter measuring the attenuation and dispersion of a broadband acoustic pulse at 4-100 kHz across a fixed pathlength	Comparison with optical sizing technique supports accuracy of acoustic system in measuring bubble size distributions
Dahl (2000)	Fate of bubbles in the surf zone; effects of bubbles on acoustic propagation	4 upward looking sonars (240 kHz) that measure the acoustic scattering cross section simultaneously	Transport of bubbles via rip currents; increased scattering level of 5 and 10 minutes caused by bubble clouds

Table 1.2 Several acoustic methods of bubble cloud observation, their implications and main outcome.

1.5 Exudation products of phytoplankton and their influence on the physico-chemical characteristics of seawater

1.5.1 Production and composition of dissolved organic matter by phytoplankton

It is well known that primary photosynthetic production by phytoplankton in surface seawater is the greatest source of organic carbon in the marine system and the largest part of organic matter in the sea is present in dissolved form (Hellebust, 1974; Ittekkot, 1982; Lee and Wakeham, 1989). The release of extracellular dissolved organic matter (DOM) is a normal process in healthy phytoplankton and takes place during all phases of growth (Sharp, 1977; Fogg, 1977; Myklestad, 1995). The rate of release, however, may vary depending on environmental factors, species composition and phase of growth. Fogg *et al.* (1965), Hellebust (1965) and Zlotnic and Dubinsky (1989) investigated the effect of light intensity on the release rate of DOM. They found that the release of photoassimilate at very high and very low light intensities was inhibited while it was relatively unaffected by the light intensity if this was at intermediate range. Hellebust (1974) states that rapid changes of temperature often result in high release rates of extracellular DOM, which is species specific with respect to its intensity (Zlotnik and Dubinsky, 1989). Myklestad (1977), Jensen (1984) and Myklestad (1995) found that the composition of the phytoplankton medium influences the rate of exudation of DOM from phytoplankton cells. Not only the absolute concentrations of nutrients are of importance but also the ratio between them, but this is again species specific. Release of DOM by phytoplankton has been observed during all stages of growth and increases with increasing cell density but the absolute rates of exudation are highest in the stationary phase, when the cells become depleted in nitrogen (Nalewajko and Lean, 1972; Myklestad, 1977; Ittekkot, 1982; Brockmann *et al*., 1983; Lee and Wakeham, 1989; Williams, 1990; Norrman *et al*., 1995). Increased production and release of DOM may thus be a result of nutrient stress (Jensen, 1984; Williams, 1990) as well as cell lysis (Ittekkot, 1982; Lee and Wakeham, 1989; Chen and Wangersky, 1996). Among the different substances released by phytoplankton cells are carbohydrates, of which the largest part are polysaccharides (Vieira and Myklestad, 1986), proteins, nucleic acids, lipids and other small molecules, most of which are still unknown (Hellebust, 1974; Fogg, 1983; Myklestad, 1995). Myklestad *et al*. (1972), Jensen (1984), Brockmann *et al.* (1983) and Leppard (1995) state that polysaccharides are a major component of oceanic DOM, especially in surface waters. Many of these polysaccharides are highly sticky and glue-like and are referred to as mucopolysaccharides (Leppard, 1995; Mopper *et al.*, 1995). The molecular weight of these polysaccharides is usually high (> 500 Dalton; Nalewajko

and Lean, 1972; Mopper *et al*., 1995) as much of the low molecular weight fraction is utilised by heterotrophic bacteria (Rosenstock and Simon, 2001; Coffin *et al*., 1993; Möller Jensen, 1993; Larsson and Hagström, 1979). Bacteria also contribute a significant amount of polysaccharides to the oceanic DOM pool (Stoderegger and Herndl, 1998, 1999; Decho, 1990).

1.5.2 Surface activity of dissolved organic material

Polysaccharides are generally quite soluble but contain sufficient hydrophobic groups to be at least weakly surface active and thus influence interfacial processes (Frew *et al*., 1990). Proteins and lipids are less abundant in phytoplankton exudates than carbohydrates but especially lipids are highly surface active (Williams *et al*., 1986; Frew *et al*., 1990). Few studies have been carried out investigating the production of surfactants by phytoplankton and their influence on the surface tension. Mitsuyasu and Bock (2001) found that the surface activity of seawater samples collected off the Delaware Bay increased with longitude towards the coast. They attributed this increase to an increase in nutrient concentration and thus an enhanced primary productivity. Zutic *et al*. (1981) studied the surfactant concentration in cultures of *Skeletonema costatum* (*Bacillariophyceae*) and *Cryptomonas* sp. (*Cryptophyceae*). They detected a distinct increase in surfactant concentration immediately after the exponential growth phase for *Skeletonema costatum*. The surfactant concentration in *Cryptomonas* sp. was higher and showed a more gradual increase than that for *Skeletonema costatum*, even though cell concentration was lower. Their results show that surfactant production is species specific and that it is dependent on the age of the cultures. Comparisons with model surfactants resulted in the assumption that a continuous mixture of surfactants is produced by the algae. Measurements of surfactants carried out in the northern Adriatic Sea over a period of three years (1976-1979) by Zutic *et al*. (1981) revealed high surfactant concentrations with seasonal and annual variation. A covariation between surfactant activity, chlorophyll *a*, oxygen saturation and pH was found. Nägeli and Schanz (1991) investigated the surface pressure (surface pressure = surface tension pure water – surface tension sample) of the freshwater algal cultures *Chlamydomonas rheinhardii* (*Chlorophyceae*) and *Oscillartoria agardhii* (*Cyanophyceae*) over their growth phases (Table 1.3). Even though they found quantitative differences in surface pressure between the two cultures, the qualitative change was very similar. No change in surface pressure was measured during the exponential growth phase, but surface pressure increased temporarily during the stationary phase. At the end of the stationary

phase, the surface pressure was higher than at the start of growth. The higher surface pressures during the stationary phase compare with the observations of surfactant production by Zutic *et al*. (1981). Measurements of surface pressure in Lake Zürich water carried out by Nägeli and Schanz (1991) revealed higher surface pressures when algal extracts of diatoms (*Fragilaria*, *Diatoma*) were added in comparison to the addition of green algal extracts (*Ankistrodesmus*). They attribute the higher surface pressure of diatom extracts to droplet lipids released by diatoms. Furthermore, Nägeli and Schanz (1991) investigated the surface pressure in the water of Lake Zürich and observed strong increases during the spring bloom, dominated by *Chlorophyta*, and during the summer growth period, dominated by *Chlorophyta* and *Dinophyta*. Decreases in surface pressure were observed at the beginning of the spring bloom as well as near its end and after the summer growth maximum. Krägel *et al*. (1995) investigated the surface tension of fulvic acid extracted from seawater samples from the Tyrrhenian Sea during May and July 1993. Surface tension of fulvic acid was measured with a ring tensiometer as well as with a drop volume tensiometer over 10 seconds and a drop in surface tension was detected, which was stronger with increasing concentration of fulvic acid (Table 1.3).

1.5.3 Effect of dissolved organic material on viscosity

As much of the DOM released by phytoplankton is present in colloidal form (Chin *et al*., 1998), this colloidal organic material accumulates on the surface of rising bubbles, changing their surface tension and rise velocity (Kepkay, 1994). The accumulation of colloidal DOM can result in the formation of polymer gels (Chin *et al*., 1998), often referred to as transparent exopolymer particles (TEP, Alldredge *et al*., 1993). These polymers are of various size distribution, from colloidal (1-1,000 nm) to micrometer size. These polymers can significantly alter the rheological properties of seawater, as it has been shown by Jenkinson (1993) and Jenkinson and Biddanda (1995). Jenkinson (1993) investigated the viscoelastic properties of seawater samples from the Mediterranean and the North Sea (German Bight) using a low shear cuette rheometer. He found that the viscosity of Mediterranean seawater samples was 0.71 to 19 times that of the solution viscosity (pure filtered seawater) at a shear rate of 0.0021 s^{-1}. The viscosity for samples taken from the North Sea at the same shear rate, where patchy blooms of *Noctiluca scintillans* (*Dinophyceae*) and *Phaeocystis* (*Haptophyceae*) were present was 0.99 to 127 times that of the solution viscosity. Petkov and Bratkova (1996) measured viscosity of algal cultures. They detected changes in viscosity for *Chlorococcum* and *Scenedesmus*

(*Chlorophyceae*) of varying algal density at temperatures of 25 and 35°C (Table 1.3). Viscosity was generally lower at 35°C than at 25°C which can be attributed to temperature effects. However, the range between minimum and maximum viscosity for different algal densities was greater at 25°C than at 35°C, indicating that environmental conditions such as temperature influence the degree of change in viscosity with changing algal density. This environmental condition seems to be species specific and may be linked to different exudation rates of DOM. Large changes in viscosity were found in cultures of *Porphyridium* (*Rhodophyceae*, Table 1.3) with a range of 1.67 mPa sec for algal densities between 0 g l^{-1} and 5.12 g l^{-1}, showing that the influence of algal density on viscosity is species specific.

Parameter measured	Methodology	Microalgae present	Algal density	Results	Reference
Viscosity (mPa×sec)	Capillary visco-meter V3 Measurement of different algal densities at different temperatures (25-35°C)	*Scenedesmus acutus* *Chlorococcum* sp. *Porphyridium sordidum*	MediumI: 0gl^{-1} 25°C 0gl^{-1} 35°C 2.13gl^{-1} 25°C 2.13gl^{-1} 35°C Medium III: 0gl^{-1} 25+35°C 1.29gl^{-1} 25°C 5.11gl^{-1} 25°C 1.29gl^{-1} 35°C 5.11gl^{-1} 35°C Medium I: 2.53gl^{-1} 25°C 5.04gl^{-1} 25°C 2.53gl^{-1} 35°C 5.04gl^{-1} 35°C MediumV: 0gl^{-1} 25°C 2.76 gl^{-1} 25°C 5.12gl^{-1} 25°C	 0.92 0.75 1.05 0.86 No data 1.02 1.12 0.82 0.90 1.14 1.44 0.93 1.15 0.95 1.86 2.62	Petkov and Bratkova (1996)
Surface pressure (SP) (mN/m) Surface tension (mN/m) was calculated from SP and given in brackets	Krüss interfacial ring tensiometer Measurement of SP over a time period of 56 days on 2 freshwater cultures	*Clamydomonas rheinhardii* *Oscillatoria agardhii*	Cells per litre: 4,200-416,00 416,00-1,9*10^6 1,9*10^6-3,1*10^6 3,1*10^6-6,5*10^6 5-13,800 13,800-33,800 33,800 15,000	 1.4 (71.4) 6.7 (66.1) 4.2 (68.6) 10.3 (62.5) 1.2 (71.6) 4.4 (68.4) 1.5 (71.3) 6.3 (66.5)	Nägeli and Schanz (1991)
Bubble surface tension (BST) with time (mN/m)	Spinning cell in which bubbles deform under well defined conditions. BST is monitored with a microscope (Princen et al. 1967) BST measurement over 15mins	Super Q water Filtered seawater Filtered medium from *Nitzschia pungens*	- - -	72.5 73 - 70.5 72.3 -67	Slauenwhite and Johnson (1996)
Dynamic surface tension (mN/m) over 10 seconds	TD1 ring tensiometer (LAUDA) (10 seconds) Drop volume tensiometer(3.1 seconds)	Fulvic acid (FA) extract	0.5% FA 1.0% FA 0.5% FA 1.0% FA	71-64.5 62- 60 71-69 68.5-62	Krägel *et al.* (1995)

Table 1.3 Summary of methodology, algal species and results of surface tension and viscosity measurements from the literature.

1.6 Thesis Aims and Objectives

Based on the above theory and findings, the aim of this work is to investigate if phytoplankton growth and abundance and their metabolic products of dissolved oxygen and dissolved organic material influence the mean residence times of gas bubbles in seawater. The research objectives are:

• To investigate the effect of phytoplankton abundance on seawater viscosity and surface tension and compare this with bubble residence time (BRT) during the growth of different phytoplankton species in monocultures and natural populations.

• To determine if BRT changes during different growth phases of phytoplankton populations using both monocultures and mixed species in natural seawater.

• To investigate if changes in oxygen saturation produced either naturally by photosynthesis or artificially by changes in water temperature have an effect on BRT.

• To determine the causes of changes in BRT in relation to phytoplankton particle abundance, oxygen production and phytoplankton exudates, that may act as surfactants in seawater.

The hypotheses to be tested are:

(I) "The residence time of gas bubbles in seawater is increased as a result of increased saturation of the seawater with oxygen, reducing bubble dissolution."

(II) "The interfacial properties of the bubbles' surfaces are changed by organic exudates released by phytoplankton, resulting in longer BRT as a result of reduced rise velocities and dissolution rates".

2 Chapter Two. Methodology

2.1 Experimental tank system

The experiments were carried out in a specially designed laboratory experimental tank system (FWG, Figure 2.1). The important feature of this system is that physical parameters such as temperature and salinity can be kept constant and attention can be focused on changes of biological and chemical parameters of the water. The large bubble tank consists of a 200 cm long, transparent plexi-glass tube, 40 cm in diameter. The total water volume in the tank system used for experiments is approximately 200 litres. The water surface of the large bubble tank is covered with small plastic balls (diameter 6 mm), that serve to optimise the acoustic signal reflection from the surface. The plexi-glass tube is held vertical by metal scaffolding. A small water supply tank (volume ca. 7 litres) made of plastic (Nalgene) is mounted on top of the plexi-glass tube. From this small supply tank, a defined water volume (0.8 litres) can be injected into the bubble tank, producing the bubble cloud (Appendix A). The water outlet of the small supply tank is a straight elongated plastic tube (20 cm in length, 5 cm in diameter), pointing vertically into the middle of the bubble tank, producing a water jet. Inside the water outlet, a stroke magnet enables opening and closure of the outlet by lifting a rubber buckler. Another small plastic tank (Nalgene, volume ca. 7 litres) is mounted to the side of the tank system, acting as a water level balancing tank. This balancing tank can either take up excess water from the bubble tank or provide the bubble tank with additional water in order to adjust the water level. The supply tank and the balancing tank are equipped with a float switch to avoid overflow. Both, the supply tank and the balancing tank are connected to the bubble tank via Teflon tubing. Teflon tubing was chosen for two reasons. Firstly, contrary to polyethylene (PE) tubing, Teflon does not release organic compounds such as phthalates, which are used as softeners in, into the water and which may contribute to the DOC signal. Secondly, Teflon tubing is characterised by a smoother surface than PE tubing, preventing heavy accumulation of planktonic and bacterial plaque on the inner linings of the tubes. All Teflon tubing was covered with opaque foam isolation. The tank system is equipped with a cryostat (AQUAMEDIC T-Computer) to maintain a consistent temperature of the water in the bubble tank as well as in the supply tank. A total of 6 membrane pumps (JOHNSON) and 5 solenoid valves enable the circulation of water between the bubble tank, the supply tank and the balancing tank as well as the circulation of water through the cryostat. A water in-and outlet for circulation in the bubble tank are situated at the bottom of the

"bubble tank" (Figure 2.1). The pumps and solenoid valves are operated via a relay matrix by the control software "BRITTA" (Bubble Reverberation In The Tank), developed using the software MATLAB by scientists of FWG. A tungsten fill level sensor in the large tank serves to adjust the water level. A temperature/conductivity sensor (WTW Cond 340i) is positioned at the bottom of the bubble tank for monitoring of temperature (resolution ± 0.1°C) and salinity (resolution ± 0.1). An oxygen sensor (WTW Profi Line Oxi 197) is integrated into the tank system to monitor the dissolved oxygen (resolution ± 0.1%). The oxygen sensor is screwed into a small cylindrical enclosed container which is interlinked to the turbulence and cooling cycle (see section 2.2.1) in order to ensure an incident flow required for the sensor operation. A flow meter (FM, precision = ± 3%, repeat accuracy = >0.25%) is interlinked between the bubble tank and the supply tank in order to recontrol the water volume that is injected into the bubble tank by the water jet. The bubble cloud is monitored using two transmitting hydrophones (ITC-1042 band = 0.01-100 kHz, resonance frequency = 79 kHz and TC 4034 band = 1Hz – 470 kHz, resonance frequency = 300 kHz) and one receiving hydrophone (TC 4014 band = 15 Hz-480 kHz; Appendix B) that are attached to the bottom of the bubble tank. The tank system is also equipped with 12 special plant fluorescent tubes (OSRAM L58 W/77) to stimulate phytoplankton growth, which are fitted on two opposite sides (6 on each side) of the bubble tank, illuminating the whole length of the water column (Appendix C). The fluorescent tubes are operated by a timer and hence switched on and off automatically. The experimental tank system is operated fully automatically via the control software.

2.1.1 Cleaning procedure of experimental tank system

The tank system was thoroughly cleaned after every single experiment. This involved rinsing all tanks and pipes several times with hot (~ 50°C) clean water. The inner walls of the large bubble tank were mopped with a small magnetic mop used for fish tanks until all plaque had been removed. The supply tank and the balancing tank were dismantled from the system and cleaned and wiped thoroughly under hot water. The oxygen electrode and its container were also rinsed and wiped with fresh water. Teflon tubes were checked and exchanged when necessary (if signs of plaque at inner linings). Following this cleaning procedure, the system was filled and rinsed with deionised water and the water was discarded before the system was finally filled with the water type intended for the next experiment.

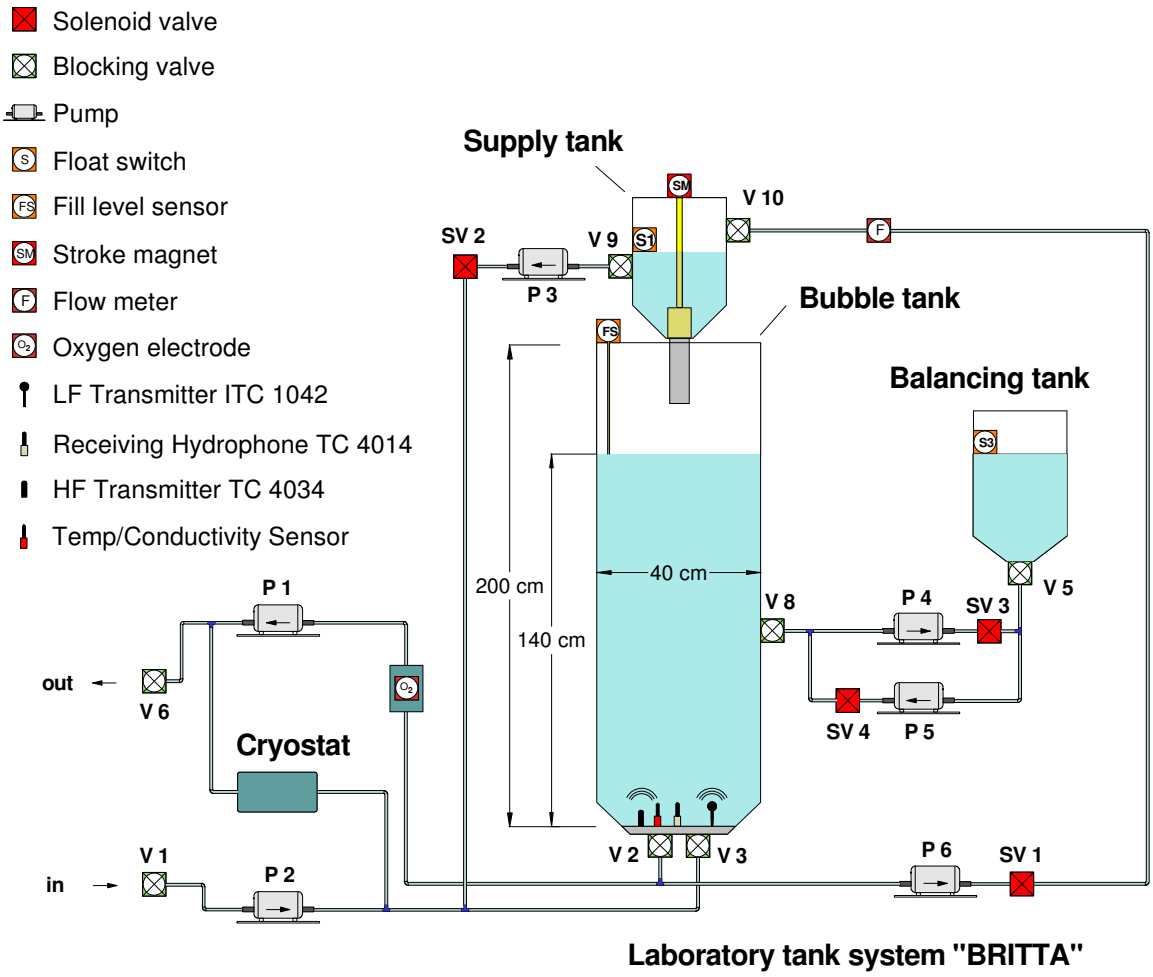

Figure 2.1 Schematic diagram of the laboratory tank system "BRITTA".

2.2 Bubble residence time measurement

2.2.1 Measurement cycle

The measurement cycle is defined as the time interval between successive measurements of bubble residence time. Measurements of bubble residence time are always carried out at constant temperature, which can be specified prior to starting the measurements. The duration of a measurement cycle depends on the difference in pre-selected measurement temperature and room temperature. The greater the difference between measurement and room temperature, the longer the duration of one measurement cycle due to the extended cooling phase. The duration of a measurement cycle varies between 1 and 1.5 hours. The room temperature is maintained with two air-conditioning units. Measurements of bubble residence time are carried out with frequencies ranging from 40 to 400 kHz. These frequencies are subdivided into two frequency bands, one comprises the lower frequencies (LF = 40-180 kHz), the other comprises the higher frequencies (HF = 180-400 kHz). This division is due to the different resonance frequencies and the resulting frequency ranges of the two transmitting hydrophones (see section 2.1). Detailed information on the frequencies used are summarised in Table 2.1. For a measurement cycle only one frequency band can be sampled. Measurements of bubble residence time can be made using both frequency bands interchangeably, hence the same frequency band is sampled every other measurement cycle. Alternatively, only one frequency band can be used, hence the same frequency band is sampled for every measurement cycle. A measurement cycle is subdivided into several steps/phases. All steps of the measurement cycle are conducted via the control software, applying specified temperature, measurement duration and frequency band(s). A measurement cycle begins with the adjustment of the water levels in the different tanks. First, the supply tank is filled until the float switch is activated. The filling of the supply tank is monitored by the flow meter and the impulse count of the flow meter is logged. Secondly, the water level of the bubble tank is adjusted to a set height of 140 cm by either replenishing water from or discharging water to the balancing tank, using the fill level sensor. After the water level has been adjusted in the bubble tank, the water from the supply tank is pumped back into the bubble tank. Then the turbulence-and-cooling phase begins, when the water in the bubble tank is pumped through the cryostat, until the predefined measurement temperature is reached. Phytoplankton cells are re-suspended and re-distributed during this phase. Once the set measurement temperature is reached, the excess water in the bubble tank is pumped back into the supply tank until the fill level sensor registers that the correct water level has been reached. Then a 20 minute quiescent

phase commences, during which any bubbles created during the cooling-and-turbulence phase may dissolve and/or rise. Following the quiescent phase, the acoustic sampling begins. After a 30 second forerun of acoustic sampling the bubble cloud is produced by the water jet. The duration of the water jet is 2 seconds, discharging 0.8 litres of water into the bubble tank. The acoustic sampling then continues for another 19.5 minutes. For every measurement cycle, a new data file is created. Information about the time of measurement, water temperature, salinity, oxygen saturation, water type, illumination, frequency bands, flow meter counts as well as various control parameters of the experimental set-up is logged in a header file for every measurement cycle. For an overview of parameters recorded in the header files, refer to Appendix D.

LF (kHz)	**HF (kHz)**
40	200
50	220
60	240
70	260
80	280
90	300
100	320
120	340
140	360
160	380
180	400

Table 2.1 Frequencies sent out in lower (LF) and higher (HF) frequency bands.

2.2.2 The acoustic signal

In this section, the path of the acoustic signal is described by which the bubble cloud is sampled. The acoustic signal is illustrated by the block diagram shown in Figure 2.2 as well as by Appendix J. As stated in section 2.2.1 the bubble cloud is sampled over a range of different frequencies from 40 kHz to 400 kHz. Before the continuous measurement cycles are started, the waveforms for the different frequencies are generated. The waveform generation is carried out using the calibration curves of the hydrophones which contain information of the different frequencies and the resulting amplitudes of the transmitting hydrophones. The software picks out the frequency-dependent amplitude from the calibration curves of those frequencies that were selected. From each selected frequency, the resulting amplitude of that frequency and the pulse length (125 µs), a waveform is generated which is sent to an arbitrary waveform generator (WAVETEK 296) and saved. The waveform generator comprises three different oscillators which are set off

by an internal trigger. All three oscillators are triggered simultaneously. The first oscillator (oscillator 1) sends out a frequency pulse with an accordant amplitude and voltage. The frequency pulse is amplified by a power amplifier (Brüel & Kjaer 2713) by 20 dB to excite the transmitting hydrophone (RESON TC 4034 and ITC 1042). The pulse is directed by a relay matrix (Rhode & Schwarz) to the corresponding transmitting hydrophone, depending on the frequency band used for the respective measurement cycle. While the acoustic signal (an omni directional pulse) is sent into the water column by the transmitting hydrophone, the receiving hydrophone (RESON DK TG 4014) is deactivated by an electronic time switch. The deactivating of the receiving hydrophone is called "dead time" and it avoids that the extremely strong backscattering level of the transmitting signal that is reflected in the vicinity of the receiver short-circuits the receiver.

Once the frequency pulse has been sent, the receiving hydrophone is reactivated, receiving the backscattering signal from the bubble cloud as well as the reflections of the tank walls and water surface. The receiving hydrophone disposes of an integrated pre-amplifier (voltage level = 26 dB), amplifying the received voltage by a factor of 20. This is done in order to distinguish the backscattering level from the ambient noise and is called dynamic enhancement. The received signal then passes through a highpass filter (Precision 6611 A), where frequencies lower than 20 kHz (i.e. interferences by buzzing of power system or switch impulses) are damped. After the highpass filter, the signal passes a frequency mixer. A frequency mixer converts a highly frequent oscillation to a frequency range that enables a simpler and more effective signal processing. The mixing process results in a frequency translation. The frequency mixer is supplied with two signals of different frequencies – the input (original) frequency (here: 40-400 kHz) and the oscillator frequency, which is generated by the second oscillator of the waveform generator. The mixing product always results in a consistent frequency, which, in this case, is set to 20 kHz. A lowpass filter (KEMO VBF 8) with a cut-off frequency of 30 kHz removes any impurities in the signal produced by the mixing process such as harmonics, before the signal passes through an amplifier in order to adjust the level to the analogue/digital (A/D) converter. The analogue signal is then sampled with a sampling frequency of 80 kHz (factor 4 of the signal's frequency of 20 kHz, Shannon Theorem). The sampling frequency is generated by the third oscillator of the waveform generator. The A/D converter transforms the analogous voltages into digital code and it is triggered 200 times per pulse with a frequency of 80 kHz. The digital data is logged to the computer at a frequency of 50 Hz.

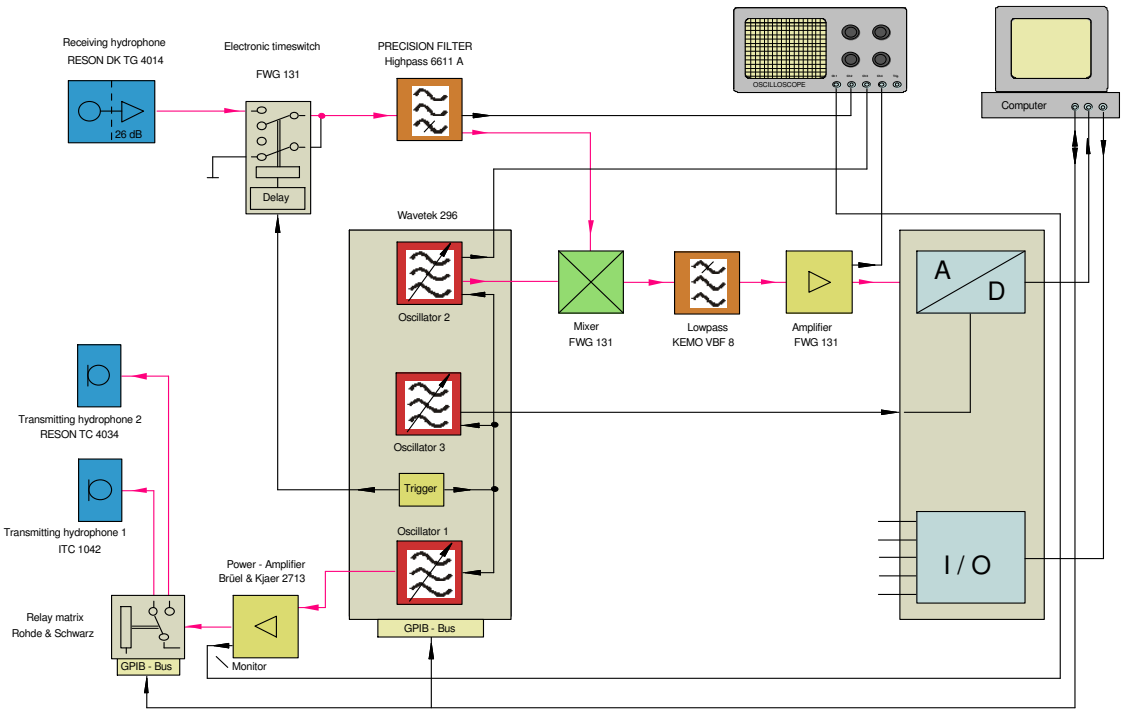

Figure 2.2 Schematic block diagram of the acoustic signal.
This diagram illustrates the path of the acoustic signal from its generation by the waveform generator via transmitting and receiving hydrophones, through several filters, a frequency converter, amplifier, A/D converter to the digital data recording as described in detail in the previous paragraph.

2.2.3 Determination of bubble residence time (carried out by FWG)

The determination of BRT begins with the definition of the reference backscattering level. This reference backscattering level comprises the first 30 seconds of the acoustic measurement phase before the water jet is released and only includes acoustic information about interferences from the tank walls and floor as well as the backscattering signal from the water surface (ambient noise). The reference level is determined from the first 90% of acoustic pings before the water jet is released. The pings are summed up and the mean is calculated over all pings and all 200 samples per ping for every frequency. This results in a reference backscattering level value for every frequency. A standardisation is then carried out for the remaining pings (from the point in time the water jet is released until the end of

the acoustic measurement phase) with the corresponding reference value. A second standardisation is applied using a reference value which is determined after the water jet has been released. As a result of the water jet, the alignment of the small scattering plastic balls on the water surface has changed and a second standardisation compensates for the modified backscattering level of the water surface. The second reference value is determined using the last 20 pings of the acoustic measurement phase. Figure 2.3 shows a 3-dimensional diagram of the standardised backscattering level of an acoustic measurement for a frequency of 120 kHz. The backscattering level is plotted over time and depth. A maximum value for bubble residence time can now be determined by applying a detection threshold. The detection threshold is set in the surface near layer to a level of 3 dB. BRT is then defined as the point in time when the backscattering level near the water surface falls below the detection threshold. All BRT results presented in section 3 are for a frequency of 120 kHz.

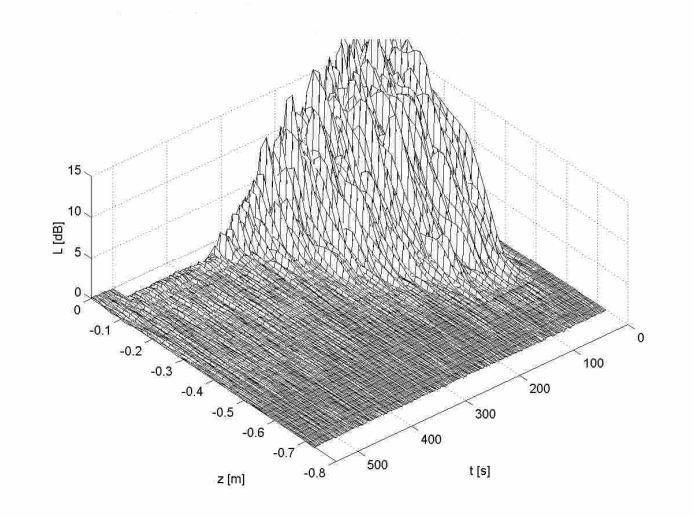

Figure 2.3 Backscattering level of the acoustic signal at 120 kHz over time and for different water depths of the tank system.
Axes key: z = depth from water surface (m), t = time (seconds), L = backscattering level (dB).

2.2.4 Median-filtering of BRT

For all experiments except the reference measurements with deionised water and the first growth experiment with Kiel Firth water, BRT data was median filtered for all further analyses. This was done in order to reduce the amount of scatter in BRT data as well as pointing out certain structures in the data e.g. the light dark fluctuations of BRT during the growth experiments. BRT data is median filtered by applying a one dimensional median filter of the order 4, using the Matlab function “medfilt1”. This calculates the median of

n successive BRT values. For n = 4 and k = number of BRT values

$BRT_{median\text{-}filtered}(k)$ = median of BRT(k-n/2 : k+n/2-1) (Equation 2.1)

Additionally, outliers were eliminated before the median filtering. Details of the Matlab script for median filtering of BRT values are given in Appendix L.

2.3 Sampling

In this section, the sampling procedure is described for all parameters. Table 2.2 indicates which parameters were sampled for the different experiments. Collection of water samples for chemical, biological and physico-chemical parameters was carried out once a day. Samples were drawn from a tap fitted mid way up the bubble tank. Triplicate samples for determination of dissolved oxygen were directly filled into 120 ml volumetric glass bottles, which were rinsed with approximately twice the bottle volume of water. The reagents, 1ml each of manganese (II) chloride and 1 ml of alkaline iodide solution were then added to the sample bottle, the stopper inserted and the bottles shaken for about 30 seconds. The oxygen sample bottles were then kept in the dark for at least 1 hour before titration. A large volume of about 1.5 litres of tank water was filled into a plastic measuring jug for later sub-sampling for dissolved inorganic nutrients, chlorophyll *a*, phytoplankton cell counts, bacteria cell counts, pH measurement and viscosity measurement. A sample for filtration and further analysis of dissolved organic carbon (DOC) was filled directly from the tap into a 500 ml SCHOTT glass flask which had previously been rinsed with the sampling water. The flask was closed with a Teflon-lined lid. A small water sample was directly filled into a 30 ml SCHOTT glass beaker, which had also been rinsed with the sampling water. The beaker was embedded in a styrofoam block for temperature control and surface tension measurement of the sample was carried out immediately.

Exp. No.	Chl *a*	Nutrients	Bacteria cell counts	Phytopl cell counts	DOC	pH	O_2 Winkler	O_2 Probe	Surface tension	Vis-cosity	Surf. Shear Viscos.	Temp.	Sali-nity
1	X	X	-	-	X	-	X	-	-	X	-	X	X
2	X	X	X	X	X	X	X	X	X	X	-	X	X
3	X	X	X	X	X	X	X	X	-	-	-	X	X
4	X	X	X	-	-	X	X	-	X	X	-	X	X
5	X	X	X	-	X	X	X	X	-	X	-	X	X
6	X	X	X	X	X	X	X	X	-	X	-	X	X
7	-	-	-	-	-	-	-	X	-	-	-	X	X
8	-	-	-	-	-	-	-	X	-	-	-	X	X
9	-	-	-	-	-	-	X	X	-	-	-	X	X
10	-	-	-	-	-	-	X	-	-	-	-	X	X
11	-	-	-	-	-	-	X	X	-	-	-	X	X
12	-	-	-	-	-	-	X	X	-	X	-	X	X
13	-	-	-	-	-	-	X	X	X	-	-	X	X

Table 2.2 Parameters analysed during experiments.

2.4 Sample processing

Samples for analysis of chlorophyll *a* were filtered in triplicate through Whatman glass fibre filters (GF/F; diameter 25mm, pore size = 0.8µm) with a vacuum pump (vacuum between 0.2 and 0.3 bar). For experiments 1 and 4 (Table 2.2), 250 ml were filtered for spectrophotometric analysis of chlorophyll a. For experiments 2, 3, 5 and 6, 50 ml were filtered in triplicate for fluorometric chlorophyll a analysis. Filters were deep-frozen at –40°C. The filtrate was filled in triplicate into 100 ml plastic bottles and was deep-frozen at –40°C for later analysis of dissolved inorganic nutrients. A 250 ml sample for phytoplankton cell counts was filled directly from the jug into a clean brown glass bottle and fixed with 5 ml of Lugol iodine (Merck) solution. A 50 ml sample for bacteria cell counts was filled into a clean brown glass bottle and fixed with 1 ml of 37% pre-filtered formaldehyde. 3 ml of the sampled water was pipetted from the jug into a SCHOTT Ostwald glass capillary viscometer. For DOC sample processing (Peltzer, 1996), the sample was filtered through pre-combusted (500°C for 12 hours) Whatman GF/F filters with a pressure filtration system at 0.5 bars. The compressed air was purged through an activated carbon filter. The filtered sample was directly filled into 40 ml pre-combusted glass vials (sample volume approximately 30 ml) in triplicate. The samples were then fixed with 150 µl of 50% H_3PO_4 and closed with Teflon-lined caps, which had been soaked in distilled water twice before use. Figure 2.4 shows a schematic diagram of the pressure filtration system.

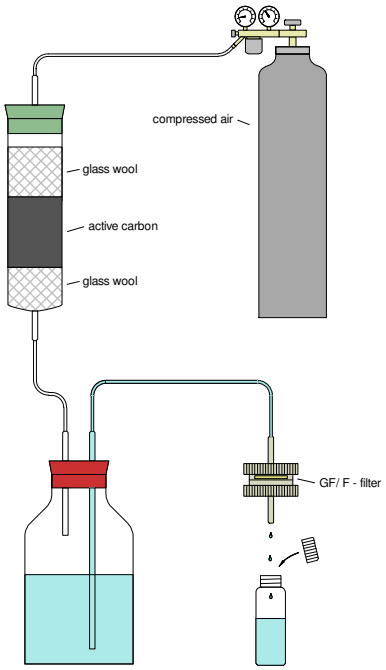

Figure 2.4 Pressure filtration system for DOC.

2.5 Analyses

2.5.1 Chlorophyll a- spectrophotometric analysis

Spectrophotometric analysis of chlorophyll *a* was done by extraction of the pigments from the filter in 5.5 ml of 90% acetone overnight. The filters were placed in 14 ml polypropylene tubes. Filters were then homogenised using a glass bead homogenate. Each filter was layered with 3 g mixed glass beads (2mm and 4 mm in diameter) and homogenised for 3 minutes. After homogenisation, a further 5.5 ml of 90% acetone were added to each tube. To remove cellular debris and filter fibres, the homogenates were centrifuged for 15 minutes at –2°C (5000 rpm) in a cooling centrifuge. The extracts were pipetted into a 5 cm cuvette and absorbance was measured at 750 nm, 665 nm, 647 nm and 630 nm with a HITACHI U2000 spectrophotometer with a spectral bandwidth of 2 nm. Prior to sample measurement, the baseline was adjusted with every new wavelength against 90% acetone. Chlorophyll *a* concentration was then calculated using the following equation of Jeffrey and Humphrey (1975):

$$Chla(\mu g/l) = \frac{(11.85 \times corE_{663} - 1.54 \times corE_{647} - 0.08 \times corE_{630}) \times V}{P \times I} \qquad \text{(Equation 2.2)}$$

where $E_{665} - E_{750} = \text{cor } E_{665}$, $E_{647} - E_{750} = \text{cor } E_{647}$, $E_{630} - E_{750} = \text{cor } E_{630}$,

V=Volume of solvent (ml)

P=filtered volume (l)

I=length of cuvette (cm).

The precision for the determination of chlorophyll *a* was estimated to be 0.006 µg l^{-1} (Humphrey and Wootton, 1966).

2.5.2 Chlorophyll a- fluorometric analysis

Fluorometric chlorophyll *a* analysis was chosen for experiments 2, 3, 5 and 6 as a much smaller sample volume was needed for filtration compared to spectrophotometric analysis, which was considered as an advantage with respect to the limited waver volume available from the tank system.

Preparation of filters for analysis (i.e. extraction in 90% acetone, homogenisation and centrifugation) was done as described in section 2.5.1. 7 ml of supernatant was pipetted into a glass cuvette and the fluorescence measured using a TURNER fluorometer.

Welschmeyer method:

For experiment 2, fluorescence was measured following the method described by Welschmeyer (1994). The total volume of acetone used for this method was 10 ml per filter. The fluorometer (Turner GAT TD10AU) used was equipped with a special blue lamp and optical filters of 436 nm (excitation) and 680 nm (emission). No correction for degradation products of chlorophyll a (phaeopigments) was necessary. 7 ml of extract was pipetted into a glass cuvette and after stabilization of the value, the fluorescence value recorded. The chlorophyll concentration was calculated using the following formula (Welschmeyer, 1994):

$$Chla(\mu g/l) = \frac{F \times V \times C}{P} \qquad \text{(Equation 2.3)}$$

where F = fluorescence reading, V = volume of acetone (10.0ml), C = calibration factor, P = volume of the filtered water sample (l). Calibration of the fluorometer was done by measuring known concentrations of chlorophyll a standards with a spectrophotometer and calculating their concentrations by the following formula:

$$Chla = \frac{(A_{\max} - A_{750nm})}{E * l} * \frac{1000mg}{1g}, \qquad \text{(Equation 2.4)}$$

where Amax = absorption maximum (664nm), A750nm = absorbance at 750nm, E = extinction coefficient for chlorophyll a in 90% acetone at 664nm (87.67 L g^{-1} cm^{-1}), l = cuvette path length (cm).

1mg of chlorophyll *a* standard was diluted into 250ml of 90% acetone, corresponding to a chlorophyll concentration of 4mg l^{-1}. From this standard, 16 different concentrations of chlorophyll were then made up to a volume of 10ml with 90% acetone, ranging from 12 µg Chl *a* l^{-1} to 1200 µg Chl *a* l^{-1} (see Appendix E). The absorbance of the 16 standards was then measured with the spectrophotometer. A calibration factor for the Turner fluorometer was determined by measuring the fluorescence of the chlorophyll standards in the Turner fluorometer and then dividing the spectrophotometric chlorophyll concentration of the standards (in mg l^{-1}) by the Turner readings.

Joint Global Ocean Flux Study (JGOFS) Protocols:

For experiments 3, 5 and 6, the fluorescence was measured as described in the JGOFS Protocols (1994) due to limited equipment availability of the Turner GAT TD10AU. The Turner fluorometer used here was not equipped with optical filters to minimise interferences by phaeopigments. The fluorescence by phaeopigments was corrected for by acidifying the sample, thus converting all of the chlorophyll *a* to phaeopigments. By

applying a measured conversion for the relative strength of chlorophyll and phaeopigment fluorescence, the two values can be used to calculate both the chlorophyll *a* and phaeopigment concentrations. 7 ml of extract was pipetted into a cuvette and fluorescence measured. The sample was then acidified with 100 µl of 0.1 M HCl. Fluorescence was measured again. The concentration of chlorophyll *a* was calculated using the following equation:

$$Chla(\mu g/l) = \left(\frac{F_m}{F_m - 1}\right) \times (F_0 - F_a) \times \left(\frac{vol_{ex}}{vol_{filt}}\right) \qquad \text{(Equation 2.5)}$$

where F_m = acidification coefficient (F_0/F_a) of pure Chl *a*, F_0 = reading before acidification, F_a= reading after acidification, vol_{ex} = extraction volume, vol_{filt} = sample volume. The calibration of the fluorometer was carried out as described for the Welschmeyer method, however each standard solution was also acidified. The acidification coefficient (F_m) is calculated by averaging the ratio of the unacidified and acidified readings (F_0/F_a) of pure chlorophyll *a*.

2.5.3 Dissolved inorganic nutrients

Nitrate

The principle of the method is based on the reduction of the nitrate ions in a sample to nitrite with a cadmium reduction column (Grasshoff *et al.*, 1999). The reduction potential is highly pH-dependent, thus a buffer solution has to be used. The method is specific to nitrate and nitrite. If instructions are followed carefully and reduction is of high efficiency, a yield of reduction of around 95% can be attained. Sample and buffer solution are pumped through the reductor via an arrangement of several tubes and a peristaltic pump. Behind the reductor, the reagents (Appendix F) are added and mixed with the sample using a mixing spiral. The resulting solution is collected and nitrite is determined spectrophotometrically. Before starting the reduction of the samples, the reductor was connected and the reagent tubes were rinsed with the corresponding reagents. The tube carrying the sample was rinsed with distilled water for two pumping intervals. The duration of one pumping interval was 150 seconds, corresponding to an intake of 5 ml of the sample. The reductor was activated using a 100 µmol l^{-1} NO^-_3 solution. After activation, the reductor was washed for at least 3 pumping intervals with distilled water. The analysis was started by pumping the blank, followed by the standards and then the samples. Blanks and all standards were analysed in triplicate. Two intervals were pumped through the reductor for

each blank, standard and sample, where the first interval was always discarded and the second was collected. The extinction was measured after 20 minutes reaction time at 524 nm (HITACHI U2000 spectrophotometer) against deionised water using a 1 cm cuvette. For the concentration and number of standards used for the respective experiments refer to Table 2.3.

Calculation of concentrations

For experiments 1-4, the concentrations of nitrate in the samples were calculated with a proportional factor using the following formulae:

$$\text{Factor}_{St\,X} = \text{Conc}_{St\,X} / (E_{St\,X} - E_{Bl}) \quad \text{(Equation 2.6)}$$

$$\text{Mean Factor} = \Sigma\,\text{Factor}_{St\,Xi} / n \quad \text{(Equation 2.7)}$$

$$\text{Conc}_{sample} = E_{sample} \times \text{Mean Factor} \quad \text{(Equation 2.8)}$$

where:

$\text{Factor}_{St\,X}$ = Factor calculated for corresponding standard

$\text{Conc}_{St\,X}$ = Concentration of corresponding standard ($\mu mol\ l^{-1}$)

$E_{St\,X}$ = Extinction of corresponding standard

E_{Bl} = Extinction of blank

n = Number of standards used

Conc_{sample} = Concentration of nutrient in sample in $\mu mol\ l^{-1}$

E_{sample} = Extinction of sample

For experiments 5 and 6 the concentrations of nitrate in the samples were calculated using the statistical function "FORECAST" of Microsoft EXCEL, which is based on a linear regression of the known concentrations of standards and their respective extinctions. The nitrite concentration measured in the respective sample was subtracted from the nitrate concentration.

Nitrite

In acid solution, sulphanilamide and nitrous acid form a diazonium salt. This is coupled with N-(1-Naphtyl)-ethylendiamine-dihydrochloride (Grasshoff *et al*., 1999). 10 ml of blank (distilled water), standard or sample were pipetted into 14 ml polypropylene tubes. 0.2 ml sulphanilamide solution and 0.2 ml naphtyl-ethylenediamine (Appendix F) were added to the tubes. The tubes were sealed, shaken and the extinction was measured at 542 nm in a 5 cm cuvette against distilled water using a HITACHI U2000 spectrophotometer.

The calculation of sample concentrations was carried out as described for nitrate. Nitrite can be determined with this method for concentrations ranging between 0.01 and 2.5 µmol l^{-1} with a precision of ± 0.02 µmol l^{-1}.

Dissolved inorganic phosphate

Orthophosphate, which is dissolved in seawater, forms a blue heteropoly acid when it has reacted with molybdate ions and can be determined colourimetrically (Grasshoff *et al*., 1999). However, the corresponding reaction with silicic acid (up to 200 µmol l^{-1} Si) does not occur at a pH below 1.0. Hence the reagents (Appendix F) are designed for seawater in a way that the pH adjusts to around 1.0. 10 ml of blank (distilled water), standard or sample were pipetted into 14 ml polypropylene tubes. 0.3 ml of mixed reagent and 0.3 ml ascorbic acid were added, the tubes were sealed and shaken. The extinction was measured at 882 nm against distilled water after 10 minutes reaction time in a 5 cm cuvette using a HITACHI U2000 spectrophotometer. The calculation of phosphate content of the samples was carried out as described for nitrate. The range of the method lies between 0 and 10 µmol PO_4 l^{-1} with a precision of ± 0.02 µmol l^{-1}.

Silicate

Yellow silicomolybtic acid is reduced by means of ascorbic acid to a blue heteropoly acid. In order to suppress interferences caused by high PO_4^{3-} contents, oxalic acid is added. 10 ml of blank, standard or sample were pipetted into 14 ml polypropylene tubes. 0.3 ml of the mixed reagent (Appendix F) was added. After 10 to 20 minutes, 0.2 ml oxalic acid followed immediately by 0.2 ml ascorbic acid were added to the tubes (Appendix F). The tubes were sealed and shaken well. After 30 minutes reaction time, the extinction was measured at 810 nm in 1 cm cuvettes against distilled water. The range of the method lies within 0-80 µmol Si l^{-1}. The precision for low values (up to 4.5 µmol Si l^{-1}) is ± 4%, for intermediate values (up to 45 µmol Si l^{-1}) it is ± 2.5% and for values up to 100 µmol Si l^{-1} it is ± 6%. Calculation of concentrations of silicate in the samples was carried out as described for nitrate.

Experiment No.	NO_3^- (µmol l^{-1})	NO_2^- (µmol l^{-1})	PO_4^{3-} (µmol l^{-1})	Si (µmol l^{-1})
1	0, 150	0, 2	0, 4	0, 50
2	0, 50, 100	0, 1, 2	0, 2, 4	0, 25, 50
3	0, 50	0, 2	0, 4	0, 50
4	0, 50, 100	0, 0.5, 1	0, 5, 10	0, 10, 20
5	0, 10, 20, 50	0, 0.5, 1, 2.5	0, 1, 2, 5	-
6	0, 10, 20, 50	0, 0.5, 1, 2.5	0, 1, 2, 5	0, 10, 20, 50

Table 2.3 Concentrations of standards for nutrient analysis.
Experiment numbers in this Table are assigned to experiment numbers as shown in Table 2.4.

2.5.4 Dissolved organic carbon

Determination of dissolved organic carbon was done by high temperature catalytic oxidation (HTCO; Sharp, 1973). The principle of the analysis is the complete oxidation of organic compounds to carbon dioxide followed by quantitative measurement of the CO_2 produced by non-dispersive infra-red analysis (Grasshoff *et al*., 1999, Dafner and Wangersky, 2002). Removal of interferences by inorganic carbon in the sample was done by sparging with CO_2-free gas after acidification of the sample. Three different instruments were used for the analyses of DOC.

For experiment 1 (Table 2.4), DOC analyses were carried out with a modified DIMATEC TOC 100 analyser (Kaehler *et al.*, 1997). Aliquots of 100 µl of a sample were injected into a quartz tube containing 50 g 5% platinum-on-alumina catalyst heated to 900°C, covered with 0.5 g of platinum wool. The carrier gas was 5% O_2 in argon at a flow rate of 100 ml min^{-1}. Glass tubes filled with zinc and bronze served to scrub HCl and SO_2 from the combustion gas and ice water and $Mg(ClO_4)_2$ traps removed moisture. CO_2 was measured in a "Binos 100" (Rosemount) non-dispersive infra-red detector and the areas of the resulting peaks were determined with a chromatography software ("Boreal", Flowtech). At least four injections were made per sample. The routine precision was typically less than 5% CV or 10µmol l^{-1}. For calibration, three to four standards of Milli-Q water spiked with glucose were used. The concentration of the stock solution was 1 M C. Standards were made up in volumetric flasks rinsed with Milli-Q water and decanted into pre-combusted vials (550°C overnight). Blanks and standards were acidified with 150 µl 50% H_3PO_4. The concentrations of the standards depended on the expected DOC content in the samples and were either 0, 100 and 200 µmol C l^{-1} for culture experiments or 0, 100, 200 and 400 µmol C l^{-1} for Kiel Firth water. A series of standards was run before and after a set

of samples was measured. The DOC content of the samples was calculated by linear regression of the standard series (Appendix G). Further details of the analysis can be found in Peltzer (1994, 1996) and Kaehler *et al*. (1997).

For experiment 2 (Table 2.4), samples were analysed for DOC using a Shimadzu TOC 5000A Organic Carbon Analyser at the National Oceanography Centre, Southampton. This instrument was considered more precise compared to the DIMATEC TOC 100. The range of the instrument lies between ~4 nmol l^{-1} and 333 µmol l^{-1}. The standard deviation of repeatability of the instrument is within 1% of full scale for the range less than 166 µmol l^{-1} , between 166 µmol l^{-1} and 333 µmol l^{-1} the standard deviation is within 2% of the full scale range. Aliquots of 40 µl of a sample were injected into the catalyst (0.5% platinum on alumina) heated to 680°C. At least four injections were made per sample. If the coefficient of variation was > 3.0%, a fifth injection was made. The interval between injections was set to 240 seconds. All inorganic carbon was removed from samples prior to injection by sparging with nitrogen. The carrier gas used was oxygen at a flow rate of 150 ml min^{-1}. Standards were made up from a caffeine stock solution (concentration = 40000 µM C). For the analysis, a blank and two standards were used. The blank was made up from UV-irradiated Milli-Q water. Standards were made up using volumetric flasks that were pre-washed with 10% hydrogen peroxide to a concentration of 200 and 400 µM C. Combusted vials (550°C for 4 hours) were used to decant 10 ml of standard or blank. Blanks and standards were acidified by adding 50 µl 10% HCl. Analysis order began with a blank, followed by the two standards, then followed by the samples. Another blank and set of standards was run at the end of the day. The area under the peaks was integrated using a chromatography software (Class-VP). Concentrations of dissolved organic carbon for the samples were calculated by linear regression of the standards (Appendix G).

For experiments 3, 5 and 6 (Table 2.4), samples were analysed for dissolved organic carbon content using a Shimadzu TOC-V_{CSN} organic carbon analyser with an auto-sampler. This instrument was newly available at Leibniz-Institute of Marine Science in Kiel since October 2004. Acidification of standards and blanks as well as removal of inorganic carbon were carried out automatically by the instrumental set-up. Aliquots of 150 µl of a sample were injected into a quartz tube containing 2% platinum on alumina 203 beads catalyst heated to 720°C. At least three injections were made per sample. If the coefficient of variation was > 2%, a fourth and if necessary a fifth injection was made. The time interval between injections was set to 200 seconds. All inorganic carbon was removed by sparging the sample for 8 minutes with oxygen. The carrier gas used was oxygen at a

flow rate of 130 ml min^{-1}. Standards were made up from a 150 mM C stock solution of potassium hydrogen phthalate. Prior to weighing out, the powder was dried for 1 hour in an oven at 120°C and cooled down in a desiccator. For the stock solution as well as for the preparation of standards, 100 ml volumetric flasks were used. All glassware including volumetric flasks, stoppers, vials and Teflon-lined caps were cleaned prior to use. This involved soaking for 6 hours in 2% DECON® solution, then rinsing three times with UV-irradiated Milli-Q water, followed by soaking for at least 6 hours in 10% HCl, finished with rinsing three times with UV-irradiated Milli-Q water. Volumetric flasks, stoppers and Teflon-lined caps were then stored in clean polyethylene bags. Vials were combusted in the muffle furnance at 450°C for 5 hours. For experiments 5 and 6 (culture experiments), standards of the following concentrations were made up: 30, 60, 90, 120 and 150 µmol C l^{-1}. For experiment 4, standards of 60, 120, 240, 360 and 480 µmol C l^{-1} were prepared. Standards were prepared with UV-irradiated Milli-Q water. Blanks, standards and samples were decanted into pre-combusted vials and placed in the auto-sampler. The measurement order started with two blanks and a series of standards followed by the samples. To ensure the quality of the measurements, standard deep sea water references with known DOC concentrations, as well as low carbon water samples and a mid-concentration standard were measured in between groups of samples. Salt crystals from the seawater samples were removed by regular injection of samples containing 2 M HCl. Blanks, standards, low carbon water samples and deep sea references were acidified with 0.1 M HCl, the amount added being 2% of the sample volume. Another calibration series of standards was run after approximately two thirds of the total samples. The area under the peaks was determined by the instrument and the DOC concentration of the samples was calculated by the linear regression equation from the standards (Appendix G).

2.5.5 Total bacteria number

Water samples from the tank system for bacteria counts were filtered through black polycarbonate filters (Nuclepore, pore size = 0.2µm, diameter = 25 mm) with a maximum vacuum of 0.2 bar. To ensure that cells were evenly distributed on the filter, an underlying cellulose-acetate filter (pore size = 0.2 µm, Sartorius) was used. The filter was then treated with 1 ml of a pre-filtered acridine orange solution (30 mg acridine orange were previously dissolved into 100 ml distilled water, Hobbie *et al.*, 1977). The filtered volume was dependent on bacterial density and ranged from 0.1 ml up to 10 ml. The filter was embedded in immersion oil on a slide, enclose with a cover glass and deep frozen at –

18°C. Determination of bacterial numbers and volumes was carried out with a Zeiss Axioplan epifluorescence microscope with HBO 50 mercury vapour light and a blue-filter 450 – 490 nm. Cells were counted and measured using a 1000-fold magnification and a New Porton G12 counting grid (Graticules LTD, UK). A minimum number of 400 cells were counted corresponding to approximately 20 grids. The standard deviation for the tank samples typically ranged between 25-30%. For the determination of cell volume, 50 cells were measured in length and width using the circular structure of the grid. The diameters of the circles were used to determine length and width of coccoid-and bacillary bacteria. The circumference of the circles enabled determination of length of vibrios and spirilles. The total bacteria number (TBN) was calculated using the following formula:

$$TBN = \frac{\sum SC}{N_G \times V} \times F \qquad \text{(Equation 2.9)}$$

where: TBN = Total bacteria number (l^{-1})

ΣSC = Sum of cells counted

N_G = Number of grids

V = filtered volume (l)

and: F = Effective area of filter / Area of grid.

Cell volume was calculated using an EXCEL spreadsheet. The carbon content of the cells was determined after Simon and Azam (1989):

$$Gp = 88{,}6 \times V^{0.59} \qquad \text{(Equation 2.10)}$$

$$G_K = G_P \times 1.04878 \qquad \text{(Equation 2.11)}$$

Where: Gp = Protein content of cell

V = Volume of cell

GK = Carbon content of cell

The total bacterial biomass (TBB) was calculated from the mean carbon content (MCC ; fg C $cell^{-1}$) of the measured cells and the total bacteria number (TBN):

$$TBB = MCC \times TBN \qquad \text{(Equation 2.12)}$$

2.5.6 Phytoplankton cell counts

Before the preparation of a phytoplankton cell sample, the brown glass sample bottle was rotated in all directions for five minutes in order to ensure that an evenly distributed suspension of particles was achieved. Depending on the concentration of phytoplankton

cells, either 10 ml, 20 ml or 50 ml were prepared in a sedimentation counting cell chamber (Hydro Bios). For the sedimentation of the particles, 24 hours were allowed for 10- and 20 ml samples and 48 hours for 50 ml samples. After sliding off the sedimentation tube and replacing it with a cover slip, the phytoplankton cells were counted using a Zeiss IM 35 inverted microscope (Utermöhl, 1958). The counting mode depended on the density of the phytoplankton cells. Either one or several transects were counted, or for large cell densities a grid was counted using a 25-fold magnification. At least 50 cells of the more frequent species and 100 cells of the dominant species were counted for mixed samples (Kiel Firth water), corresponding to an error of ± 50% and ± 24% respectively. For monocultures, at least 400 cells were counted, giving an error of ± 10%. The phytoplankton cells at the bottom of the counting chamber correspond to the cell content of the prepared water volume. Cell numbers per litre were calculated using the following formulae:

$$F = \frac{A_C(mm^2)}{A_{S/G}(mm^2)} \times \frac{1000/x}{N} \qquad \text{(Equation 2.13)}$$

where:

F = Factor
A_c= Area of counting chamber (for Hydro Bios counting chambers = 530.93 mm2)
$A_{S/G}$ = Area of transect or grid
X = Prepared water volume
N = number of transects or grids counted

Cell number/litre = cells counted × F/ N (Equation 2.14)

2.5.7 Dissolved oxygen

Dissolved oxygen was determined by titration following the Winkler method described by Grasshoff et al. (1999). This is based on the oxidation of iodide to iodine which is divided into several oxidation steps using manganese compounds as a transfer medium. As already described in section 2.3, the reagents Mn(II) and and alkaline KI- solution were added to the water sample, forming Mn (II)-hydroxide

$$Mn^{2+} + 2\ OH^- \rightarrow Mn(OH)_2$$

which was oxidised forming Mn(III)-hydroxide by the molecular dissolved oxygen.

$$2\ Mn(OH)_2 + ½\ O_2\ H_2O \rightarrow 2\ Mn(OH)_3$$

Once the precipitate had settled (after approximately 60 minutes), sulphuric acid was added to the sample bottle, resulting in an oxidation of iodide to iodine by Mn(III) (unsTable in acidic medium). The Mn(III) was reduced to Mn(II).

$$2\ Mn(OH)_3 + 2\ I^- + 6\ H^+ \rightarrow 2\ Mn^{2+} + I_2 + 6\ H_2O$$

The iodine was reduced to iodide by sodium thiosulfate, where the thiosulfate was reduced quantitatively, forming tetrathionate.

$$2\ S_2O_3^{2-} + I_2 \rightarrow S_4O_6^{2-} + 2\ I^-.$$

Measurement of dissolved oxygen was carried out after the following procedure:
Approximately 60 minutes after the reagents had been added to the sample bottle (section 2.3). 2ml of 50% $H_2\ SO_4$ were carefully added to the sample bottle, without dispersing the precipitate. The stopper was inserted into the sample bottle and the bottle shaken vigorously for 20 seconds. The sample was then poured into a 150 ml glass beaker, while the sample bottle and the stopper were rinsed with distilled water. The iodine was titrated with a 0.02 M sodium thiosulfate solution using a Hydro Bios oxygen titration stand and a 10 ml glass burette linked to an electrically driven meter (Metrohm). Shortly before the disappearance of the yellow iodine colour, 1 ml of starch solution was added to the sample, resulting in a blue colour. The sample was then titrated until it was colourless (end point).
The thiosulfate solution was calibrated approximately every 4 days using a 0.01 M iodate standard solution after the following procedure:
2 ml of 50% H_2SO_4 were added to 50 ml of distilled water and, while stirring, 1 ml of alkaline iodide solution and 1 ml of Mn(II) solution were added. 10 ml of iodate standard solution were added with a calibrated pipette and the solution was titrated as described above. For reagent recipes refer to appendix H.
Oxygen concentration was calculated using:

$$O_2(mg\ /\ litre) = \frac{a \times f \times 8 \times 1000}{50(b-2)} \qquad \text{(Equation 2.15)}$$

where

a = amount of thiosulfate added (ml)

b = volume of sample bottle (ml)

f= factor of thiosulfate solution

V = amount of thiosulfate added during calibration (ml)

and

$$f = \frac{5}{V}$$

The range of the method lies between 0 – 15 mg $O_2\ l^{-1}$ with a precision of ± 0.02 mg $O_2\ l^{-1}$.

2.5.8 Measurement of surface tension

For determination of the surface tension of the water sample, a SITA t60 science line bubble pressure tensiometer was used. This instrument measures the dynamic surface tension of a fluid. As a result of the attraction between the molecules of a liquid, air bubbles within a liquid are also subject to these forces i.e. a bubble formed within a liquid is being compressed by the surface tension. The resulting pressure rises with the decreasing bubble radius. This increase in pressure as opposed to the pressure outside the bubble is used to measure surface tension. An air-flow is induced through a capillary into a liquid. This creates a bubble whose surface bulges, thus resulting in a continuous decrease of the bubble radius. During this process the pressure rises to a maximum when the bubble radius reaches its minimum. This radius corresponds to the radius of the capillary, forming a hemisphere. After passing this point the bubble bursts and breaks away from the capillary. A new bubble then forms at the capillary. During this process, a characteristic change of pressure can be measured in the bubble. From this characteristic pressure change the surface tension (σ) can be calculated by the Laplace relationship:

$$\sigma = \frac{r_K}{2}\Delta p \qquad \text{(Equation 2.16)}$$

where r_k is the radius of the capillary and p is the pressure.
The instrument has a resolution of ± 0.1 mN m^{-1}. The precision of the instrument is 0.1% CV or 0.1 mN m^{-1}. The instrument can be operated in two different measurement modes. The online mode produces bubbles of equal lifetime (bubble lifetime = 655 mseconds) at a frequency of 1 Hz. The auto-mode produces bubbles of different lifetimes, ranging from 31 mseconds to 60000 mseconds at frequencies of 11.628-0.012 Hz.

2.5.9 Measurement of viscosity

Kinematic viscosity of tank water was determined with a SCHOTT Ostwald glass capillary viscometer (capillary diameter = 0.4mm). The principle of this method is based on time it takes for a fluid to pass a distance through a small capillary and this is used to calculate the kinematic viscosity of the fluid. Kinematic viscosity (υ) is calculated using:

$$\nu = K \times t \qquad \text{(Equation 2.17)}$$

where *K* is the capillary constant (0.01 for a capillary with diameter = 0.4 mm) and t is the time (in seconds) it takes for the fluid to pass a certain distance of the capillary. The viscosity measurements were made in a temperature controlled water bath (LAUDA) at 12

or 18°C ±0.01°C, depending on the water temperature for the respective experiment. 10 repetitive measurements were made of every sample. The CV of this method is less that 0.1%.

2.5.10 Measurement of surface shear viscosity

Surface shear viscosity was measured using an interfacial shear rheometer (ISR-1 Sinterface Technologies Berlin). The method has been described in detail by Krägel *et al*. (1994). The measurement principle of the ISR is based on a ring with a sharp edge (measurement body) hanging from a torsion wire. The torsion wire is fixed to a deflection drive (a stepper motor). The interval of the deflection angle can be selected within 0.5°-3° with a resolution of < 0.01°. By an instantaneous movement of the torsion head a torque is applied to a measurement body touching the interface of a planar fluid surface in a measuring vessel. A shear field is built up between the inner wall of the measuring vessel and the outer part of the measurement body. The tension of the shear field is recorded by the ISR. During the measurement, a pendulum performs damped harmonic oscillations with a damping factor α and a radian frequency β. The angular position of the measuring body is registered via a mini laser and a position-sensitive photosensor. The circular movement of the measuring body can be measured with an accuracy of 0.01° at deflection angles of 2°. The registered oscillation curve is then fitted and the damping factor α and the radian frequency β of the torsion oscillation are determined. From the difference of the values for the two variables compared with those for the oscillation in the pure solvent (i.e. water), the rheological parameters are calculated using the following formulae:

$$\eta_s = 2H_S I_r(\alpha-\alpha_0) \qquad \text{(Equation 2.18)}$$

$$G_S = H_S I_r(\alpha^2-\alpha_0^2+\beta^2-\beta_0^2) \qquad \text{(Equation 2.19)}$$

where

η_S = surface shear coefficient of viscosity

G_S = surface shear modulus of rigidity

H_s = apparatus constant which depends on the slit geometry

I_r = moment of inertia of the measurement system.

The ISR was set up in a way that a measurement was performed every 20 minutes. The duration of a measurement was 40 seconds. Measurements of surface shear viscosity were carried out in a temperature controlled room at 20°C in half-light with a deflection angle of 2°. Surface shear viscosity measurements of a seawater or algal culture sample were

carried out for several hours, so that the adsorption or desorption of surface active substances to or from the fluid interface could be monitored. Before starting the measurements with a fresh sample, the measuring vessel and the measurement body were soaked for approximately 20 minutes in 98% H_2SO_4 and then rinsed several times with distilled water. Gloves were worn while handling the measurement equipment and the sample. Before the start of measurements, a layer of liquid on the sample surface was carefully removed with a clean pipette tip connected to a vacuum pump in order to remove any surface active substances already accumulated at the interface. The time was registered and set to 0 immediately after removal of the interface. Time "zero" is then the point in time when adsorption (or desorption) of substances to or from the interface began.

2.6 Reference measurements

2.6.1 Reference measurements at 12°C

For the first reference experiment with deionised water at 12°C, the water was filled into the tank system 3 days before the start of BRT measurements. For the second reference experiment, the same water was used as for the previous reference water experiment at 12°C. A measurement break of 1 day existed between the experiments, when the water rested in the tank system and no measurements were made. For the third reference experiment with deionised water at 12°C, water was filled into the tank system 3 days prior to the beginning of BRT measurements. Oxygen saturation was recorded for each BRT measurement with the oxygen electrode.

2.6.2 Reference measurements at 18°C

For the first reference experiment at 18°C, deionised water was filled into the tank system 20 hours before the beginning of measurement. Reference measurements for the second experiment at 18°C were carried out with deionised water that had been contained in the tank system for 2 weeks prior to the beginning of measurement. For the third reference water experiment, BRT measurements started immediately after the filling of the tank system with deionised water. The fourth reference experiment at 18°C was carried out using deionised water that had been kept in the tank system for 7 days at 12°C. For all BRT reference measurements at 18°C, oxygen saturation was measured simultaneously with the oxygen electrode.

2.7 Phytoplankton growth experiments

2.7.1 First eutrophic Kiel Firth water experiment

300 litres of Kiel Firth water were pumped into plastic containers in March 2002 on board the research vessel "Polarfuchs" using the on-board seawater pump. All plastic containers had previously been rinsed with 10% HCl and several times with deionised water. The water was filled into the tank system and measurements of BRT were made for several days (data not included) at a temperature of 12°C. This water was then enriched with 25 ml of each stock solution of F/2 nutrient medium (Guillard and Ryther, 1962, see section 2.11.1). The fluorescent tubes were operated on a 12/12 hour light/dark cycle just after addition of nutrients. Only 6 fluorescent tubes (3 each side) were used. Acoustic measurements of BRT were made for 12 consecutive days. The parameters that were sampled/recorded during the experiment are indicated in Table 2.2.

2.7.2 Second eutrophic Kiel Firth water experiment

300 litres of Kiel Firth water were pumped into plastic containers (containers had been previously rinsed with deionised water) in January 2004 at the Kiel lighthouse on board the research vessel "Polarfuchs". A JOHNSON membrane pump was used to pump the water from approximately five metres below the surface. The water was filled into the tank system on the same day it was sampled and the measurement software was started. The temperature of water in the tank was set to 12°C. The fluorescent tubes were operated on a 12/12 hour light/dark cycle (only 6 tubes were illuminating). However, the water jet was purposely suppressed for a period of two days to let the water degas. After two days of degassing, the jet was switched on and bubble residence time measurements began. After four measurement cycles, 50 ml of each stock solution of F/2 nutrient medium were added to the water and BRT measurements were carried out for 13.5 consecutive days. Samples were taken from day 0.5.

2.7.3 Third eutrophic Kiel Firth water experiment

300 litres of Kiel Firth water were sampled using a membrane pump during March 2004 at Heikendorf Bay approximately 5 metres below the water surface. The water was filled into the tank on the same day it was sampled and acoustic measurements of BRT were started at 12°C. However, for the first 24 hours of measurement, the small plastic balls were removed from the water surface to enable a more effective degassing of the water. The

lights were operated from the beginning of measurement on a 12/12 hour light/dark cycle. 50 ml of each stock solution of F/2 medium were added on day 4. Samples were taken daily from day 3.3 for the parameters listed in Table 2.2. Measurements were carried out after nutrient addition for a further 9 days.

2.7.4 Growth experiment with Chaetoceros muelleri

Aged filtered (GF/F) North Sea water was filled into the tank system in June 2003 and measurements of BRT were started immediately for 7 days at a temperature of 18°C. An initial sample for all parameters (see Table 2.2 for parameters sampled) was taken on the first day. The tank was not illuminated during this period. On day 7.5, 25 ml of each stock solution of F/2 medium were added to the water as well as 10 litres of a dense monoculture of the diatom *Chaetoceros muelleri*. Sampling began on day 7.5. From that point in time, lights were operated on a 12/12 hour light/dark cycle and BRT and all other parameters were measured for a further 11 days.

2.7.5 Growth experiment with Phaeocystis

Filtered (GF/F) aged North Sea water was filled into the experimental tank in June 2004 and left to rest for 5 days in the dark before measurements of BRT were started at a temperature of 18°C. One day after the beginning of measurements (day 1.5), 50 ml of $NaNO_3$, 50 ml of Na_2HPO_4, 250 ml Vitamin-Mix and 25 ml of each metal stock solution of F/2 nutrient medium were added to the tank together with 10 litres of a dense monoculture of *Phaeocystis*. Samples were taken from day 1.5. Six fluorescent tubes were operated on a 12/12 hour light/dark cycle. Measurements of BRT as well as sampling for all other parameters (see Table 2.2) were carried out for 14 consecutive days.

2.7.6 Growth experiment with Nitzschia closterium

Filtered (GF/F) aged North Sea water was filled into the tank in October 2004 and measurements of BRT were started immediately at 18°C with the fluorescent tubes switched off. After one day (day1.5), 40 ml $NaNO_3$, 40 ml Na_2HPO_4 and 40 ml Na_2SiO_3 stock solution as well as 135 ml of Vitamin Mix and 20 ml of each metal stock solution of F/2 nutrient medium were added to the tank followed by 10 litres of a dense monoculture of the diatom *Nitzschia closterium*. Samples were taken from day 1.5. After addition of the

culture, six fluorescent tubes were operated on a 12/12 hour light/dark cycle and measurements of BRT as well as sampling for all other parameters (Table 2.2) were carried out for a further 22 days. From day 12 to day 14, the light/dark interval of the fluorescent tubes was changed to 24 hours and it was set back to 12 hours from midday on day 14 until the end of the experiment.

2.8 Experiment with a model polysaccharide "Xanthan Gum"

The tank system was filled with deionised water and BRT measurements were started at a temperature of 18°C. After four days, a polysaccharide solution of Xanthan Gum (SIGMA) was added to the water, resulting in a concentration of approximately 0.008 g Xanthan Gum l^{-1}. After one day, the concentration of Xanthan Gum was increased to approximately 0.08 g l^{-1}. Kinematic viscosity of the tank water was measured several times throughout the experiment. After the second addition of Xanthan Gum, measurements of BRT were carried out for a further six days.

2.9 Experiment with a surfactant "Triton X 100"

Deionised water which had already been in the tank for a previous experiment was set to a measurement temperature of 18°C and measurements of BRT were carried out for two days, followed by the addition of the surfactant Triton X 100 (SIGMA) to an approximate concentration of 10^{-6} mol l^{-1}. Bubble residence time measurements continued for one more day, then the concentration of Triton X 100 was increased to approximately 5×10^{-5} mol l^{-1}. After a further three days, the concentration of Triton X 100 was increased to approximately 2.5×10^{-4} mol l^{-1}. Measurements continued for two more days. Measurements of surface tension were carried out daily.

2.10 Gas saturation experiments

2.10.1 First saturation experiment

Deionised water was filled into the tank system, and measurements of BRT were made at 12°C for five consecutive days. The temperature was then set to 18°C and BRT measurements were carried out at this temperature for 3.5 days. After the water was cooled down to 12 °C again and BRT measurements were carried out for 2 days at 12°C, it was bubbled with air using a pump via a piece of lime-tree wood for approximately one hour.

Measurements of BRT were then continuously carried out at 12°C. After three days, the water was again bubbled with air for approximately 0.5 hours. After one day, the water temperature was set to 18°C in order for the tank water to slowly warm up while BRT measurements continued. Oxygen saturation was recorded for every measurement of BRT with the oxygen electrode and several control samples were collected for Winkler determination of oxygen saturation. After a further 3 days, the water was again bubbled with air for approximately 1 hour at 18°C. After 2 days, the water was bubbled with oxygen from a pressure bottle for 2 minutes, until a supersaturation of 170% (value of oxygen electrode) was reached. After 2 days, the tank water was bubbled with nitrogen from a pressure bottle until the oxygen saturation had declined to 39%. Measurements of BRT as well as measurements of oxygen saturation continued for another 1.6 days.

2.10.2 Second saturation experiment

Measurements of BRT with deionised water were carried out at a temperature of 12°C for three days. Measurements were then interrupted for one day (malfunction of tank system). When measurements were started again, the circulation was slightly modified in a way that the water inlet, usually located at the bottom of the tank, was linked to a long tube and water was pumped back into the tank (during the turbulence phase) through the top of the tank. The tube was placed in the middle of the large tank, approximately 15 cm above the water surface. Measurements of BRT were carried out for a further three days. After that, the water inlet was changed back to the initial set up (see Figure 2.1) and measurements continued at 12°C. After a further day, the temperature of the tank water was set to 23°C and BRT measurements continued for nine more days. Samples for determination of dissolved oxygen by the Winkler method were drawn once every day.

2.10.3 Third saturation experiment

The tank system was already filled with deionised water from the previous saturation experiment. Measurements of BRT were started at 12°C. After four days, the circulation was modified as described in the previous paragraph, when the water inlet was placed over the top of the large tank. Measurements of BRT continued for another day, until the circulation was changed back and both water in-and outlet to and from the large tank were located at the bottom. After a further day of BRT measurements at 12°C, the water temperature was increased to 23°C. Measurements of BRT were carried out at 23°C for 13

days. After that, the water was cooled down to 12°C and measurements continued for three days at 12°C. During the experiment, oxygen % saturation was measured with the electrode for every measurement cycle of BRT. Winkler controls were taken on a daily basis.

Experi-ment No.	Date	Description	Salinity	Temperatue (°C)	Frequency bands sampled	Duration (days)
Growth experiments in seawater						
1	04/2002	Growth experiment eutrophic Kiel Firth water (FW)	14.5	12	LF + HF	11.8
2	01/2004	Growth experiment with eutrophic FW	16.6	12	LF + HF	24.6
3	03/2004	Growth experiment with eutrophic FW	16.0	12	LF + HF	12.9
Growth experiments with monocultures						
4	06/2003	Growth experiment with *Chaetoceros muelleri*	31.0	18	LF + HF	18.7
5	06/2004	Growth experiment with *Phaeocystis*	31.0	18	LF	8.5
6	10/2004	Growth experiment with *Nitzschia closterium*	31.0	18	LF	23.3
Reference water experiments						
7	11/2004	3 reference measurement series with deion. water	0	12	LF	3.9
8	08/2004	4 reference measurement series with deion. water	0	18	LF	4.0
Gas saturation experiments						
9	04/2004	Gas saturation variation (O_2, N_2, air)	0	12 + 18	LF	30.8
10	11/2004	Gas saturation variation through temperature variation	0	12 + 23	LF	16.7
11	12/2004	Gas saturation variation through temperature variation	0	12 + 23	LF	20.6
Model substances						
12	08/2004	Measurements with Gum Xanthan	0	18	LF	10.9
13	12/2004	Measurements with Triton X 100	0	18	LF	7.9

Table 2.4 Summary of experiments carried out with the experimental tank system.

2.11 Preparation of algal cultures for phytoplankton growth experiments

2.11.1 F/2 nutrient medium stock solutions

Preparation of stock solutions were carried out using the recipe of Guillard and Ryther (1962, Appendix I). The metal stock solution of the recipe was modified in a way that the metal components were made up separately as no Na_2EDTA was used.

2.11.2 Chaetoceros muelleri

A non-axenic stock culture sample of *Chaetoceros muelleri* (originating from CCMP, Scotland) was subcultured into five 100 ml sterile glass flasks, filled with F/10 nutrient medium. F/10 nutrient medium was made up from filtered (GF/F), sterile seawater spiked with F/2 nutrient components (Guillard and Ryther, 1962). To get an F/10 concentration, 200µl of $NaNO_3$, 200 µl of Na_2HPO_4, 200 µl of Na_2SiO_3 stock solutions as well as 200 µl of vitamin stock solution and 20 µl of each metal stock solution of F/2 medium were added to 1 litre of filtered, sterile seawater (salinity 31). The initial ratio of stock culture and F/10 nutrient medium was approximately 1:10. All flasks were sealed with sterile cellulose stoppers and aluminium foil. They were kept in the laboratory at room temperature (approximately 20°C) by the window sill and were additionally illuminated by fluorescent tubes for 12 hours a day. The cultures were left to grow for seven days, until they showed a distinct, slightly brownish colouring. The cultures were then transferred into five 300 ml sterile glass flasks and filled up with fresh F/10 nutrient medium. Cultures were again left to grow for approximately seven days, until they showed distinct colouring. The cultures from the 300 ml flasks were then transferred into two sterile 6 litre glass flasks, each containing 5 litres of fresh F/10 nutrient medium. The cultures were then left to grow until they showed a distinct brownish colouring. To avoid agglutinating of the cells and to enhance growth, the cultures were gently bubbled with air, using a small aquarium air pump (Tetra-Pond). Sterile glass tubes were inserted into the culture flasks. They were linked to the air pump via sterile silicone tubing and a sterile washing flask filled with cotton was interlinked between the pump and the culture flasks to filter the air. The culture flasks were sealed with sterile cellulose stoppers and aluminium foil.

2.11.3 Phaeocystis

Subculturing and growth of a non-axenic culture of *Phaeocystis* was carried out as described in the previous paragraph for *Chaetoceros muelleri*. However, F/10 nutrient

medium was made up using only 200 µl of $NaNO_3$ and 200 µl of Na_2HPO_4 stock solutions as well as 1 ml of vitamin mix stock solution and 100 µl of each metal stock solution for 1 litre of seawater (salinity 31). Cultures were grown in a temperature controlled room at 18°C and were illuminated for 12 hours per day by fluorescent tubes. Cultures of *Phaeocystis* were not bubbled with air but the culture flasks were gently rotated once every day.

2.11.4 Nitzschia closterium

Subculturing and growth of a non-axenic culture of *Nitzschia closterium* was carried out as described for *Chaetoceros muelleri*. The culture was grown in F/10 nutrient medium. 200 µl of $NaNO_3$, Na_2HPO_4 and Na_2SiO_3 stock solution were added with 1 ml of vitamin mix stock solution and100 µl of each metal stock solution to 1 litre of sterile (salinity 31), filtered seawater. Cultures were grown in a temperature controlled room at 18°C and were illuminated 12 hours per day by fluorescent tubes. The cultures were not bubbled with air but the culture flasks were rotated once every day.

2.12 Surface shear viscosity measurements with several phytoplankton monocultures

The aim of this laboratory culture experiment was to investigate if different phytoplankton cultures have an effect on the surface shear viscosity and thus a likely influence on the surface characteristics of air bubbles and to investigate the change in surface shear viscosity at different stages of the growth phase for cultures that have a positive effect. The surface shear viscosity measurements were carried out independently of the tank experiments in July 2004 at the Max-Planck Institute of Colloid and Interface Science with the ISR1 shear rheometer, using four different phytoplankton monocultures, *Thalassiosira rotula*, *Thalassiosira punctigera*, *Nitzschia closterium* and *Phaeocystis*. Phytoplankton cultures were grown in a temperature controlled room at 20°C. All cultures were illuminated by fluorescent tubes for 14 hours per day. All cultures were kept in sterile 2 litre glass flasks. The culture flasks were sealed with sterile cellulose stoppers and aluminium foil. For the three diatom cultures, the 2 litre cultures were set up with F/2 nutrient medium.1 ml of each $NaNO_3$, Na_2HPO_4, Na_2SiO_3 and vitamin stock solution and 100 µl of each metal stock solution were added to 1 litre of sterile filtered seawater with a salinity of 31. 200 ml of stock culture were inoculated into 1.8 litre F/2 medium. For

Phaeocystis, 200 ml of stock culture were inoculated to F/20 nutrient medium. F/20 medium was made up by adding 200 µl of $NaNO_3$ and Na_2HPO_4 stock solutions as well as 1 ml of vitamin stock solution and 100 µl of each metal stock solution to 1 litre of sterile and filtered seawater (salinity 31). Before drawing a sample for phytoplankton cell counting, the culture flasks were rotated to evenly distribute cells. Samples were taken with a sterile glass pipette. An initial sample was taken for cell counting after the cultures were set up. Adjacent samples for cell counts were drawn once a day for 10 consecutive days except days 5 and 6, when no samples were taken. Determination of phytoplankton cell numbers was carried out with a Zeiss microscope using a 100 fold magnification. Cells were counted on a Fuchs-Rosenthal (Brand) counting chamber with a total area of 0.0625 mm^2 and a depth of 0.2 mm and a Sedgewick Rafter Cell S50 microlitre (Graticules) counting chamber. A minimum of 400 cells were counted for every sample, corresponding to an error of ~ ± 10%. Measurements of surface shear viscosity were carried out as described in section 2.5.10. Table 2.5 summarises date and duration of surface shear viscosity measurements for a particular culture.

Date	**Sample measured**	**Starting time**	**Duration (minutes)**
12.07.2004	*Nitzschia closterium* stock culture	13:39	1092
13.07.2004	*Phaeocystis* stock culture	09:45	313
13.07.2004	*Thalassiosira rotula* stock culture	16:16	918
14.07.2004	F/2 nutrient medium	08:55	194
14.07.2004	*Thalassiosira punctigera* stock culture	13:16	155
14.07.2004	*Nitzschia closterium* diluted culture	16:38	915
15.07.2004	F/2 nutrient medium	09:10	251
15.07.2004	*Nitzschia closterium* diluted culture	15:53	940
16.07.2004	Filtered sterile seawater salinity 31	09:24	215
16.07.2004	*Nitzschia closterium* diluted culture	14:19	1521
19.07.2004	*Thalassiosira punctigera* diluted culture	08:48	376
19.07.2004	*Nitzschia closterium* diluted culture	16:04	919
20.07.2004	*Nitzschia closterium* stock culture	09:09	291
20.07.2004	*Nitzschia closterium* filtered (GF/F) stock culture	15:19	972
21.07.2004	*Phaeocystis* diluted culture	10:23	1293

Table 2.5 Surface shear viscosity measurement timetable.

2.13 Viscosity experiment

Bulk water viscosity was determined for several chlorophyll concentrations using a stock culture of the diatom *Chaetoceros muelleri*. Several dilutions were made of the stock culture and viscosity was determined of these dilutions (Table 2.6). For each sample, 10 individual measurements of viscosity were made.

Number	Dilution of stock culture
1	Stock culture (undiluted)
2	2:1
3	1:1
4	1:2
5	Filtered seawater

Table 2.6 Dilutions of *Chaetoceros muelleri* stock culture.

3 Chapter Three. Results

3.1 Reference measurements with deionised water

Results for three reference measurement series with deionised water (for experimental description refer to section 2.6.1) at a temperature of 12°C are shown in Figure 3.1 a and their corresponding oxygen saturations are shown in Figure 3.1 b. Mean BRT values (no median filter for BRT was applied for reference measurements) including standard deviations as well as mean oxygen saturations and standard deviations are summarised in Table 3.1. The BRT at 12°C remained consistent with increasing measurement number (Figure 3.1 a) for all three measurement series with standard deviations ranging from 6.4% to 8% (Table 3.1). The duration of 12°C reference measurement series was approximately 2.6 days for each series with a time interval of 0.06 days between the BRT measurements. Single reference values for series two and three for 12°C reference measurements overlap (Figure 3.1a) and their mean values are similar (109 ± 7 seconds and 110 ± 9 seconds, Table 3.1). The water was undersaturated with oxygen at all times, where the saturations for series two and three were almost identical. Oxygen saturation increased slightly with time for all three reference measurement series at 12°C (Figure 3.1 b) consistent with saturation slowly approaching ~100% through gas exchange. The Kruskal-Wallis test of BRT reference measurements at 12°C shows that there is a significant difference between at least two median values (p-value = 0.000; test statistic (H) = 41.17; degrees of freedom (DF) = 2; $\chi^2_{(2/0.01)} = 9.21$), as indicated by the test statistic H. If H is greater than the theoretical χ^2 value, the difference between one or more population medians (here between median BRT) is statistically significant. The Kruskal-Wallis test of series two and three indicates that their median BRT values do not differ significantly (p-value = 0.720; H = 0.13; degrees of freedom = 1; $\chi^2_{(1/0.01)} = 6.64$). BRT for series one at 12°C has the highest mean value (125 seconds) and the lowest mean oxygen saturation (74.3%). Reference measurement series for 18°C reference measurements were carried out for approximately 2.0 days (Figure 3.1 c), except series 18-1, which was carried out for 1 day. The time interval between subsequent BRT measurements was ~ 0.04 days. For reference measurement series with deionised water at a temperature of 18°C (for experimental description refer to section 2.6.2), mean BRT values reveal much larger differences than mean BRT values for reference measurements at 12°C. Generally, absolute mean values of BRT were higher for reference measurements at 18°C than absolute mean values for 12°C reference measurements (Figure 3.2). All initial values of reference measurements at 18°C

differ significantly (Figure 3.1 c) from each other. Standard deviations are slightly higher than for reference measurements at 12°C (Table 3.1) ranging from 7.5 to 12.5%. The deionised water was undersaturated with oxygen for all measurement series at 18°C, with slight increases in oxygen saturation occurring with time as the saturation was slowly approaching ~100% as a result of gas exchange (Figure 3.1 d). Oxygen saturation for reference experiment number 4 was significantly higher than for the remaining experiments. This was most likely due to the lower temperature that the water was kept at prior to starting the measurements. The first 8 values of oxygen saturation show a more distinct increase than later values. This increase occurred simultaneously for the first 8 data points of BRT, when BRT started from a lower initial value but equilibrated rapidly (Figure 3.1 c). The Kruskal-Wallis test of 18°C reference measurements confirms that significant differences between the median BRT exist ($p < 0.000$, $H = 84.27$, $DF = 4$; $\chi^2_{(2/0.01)} = 13.28$).

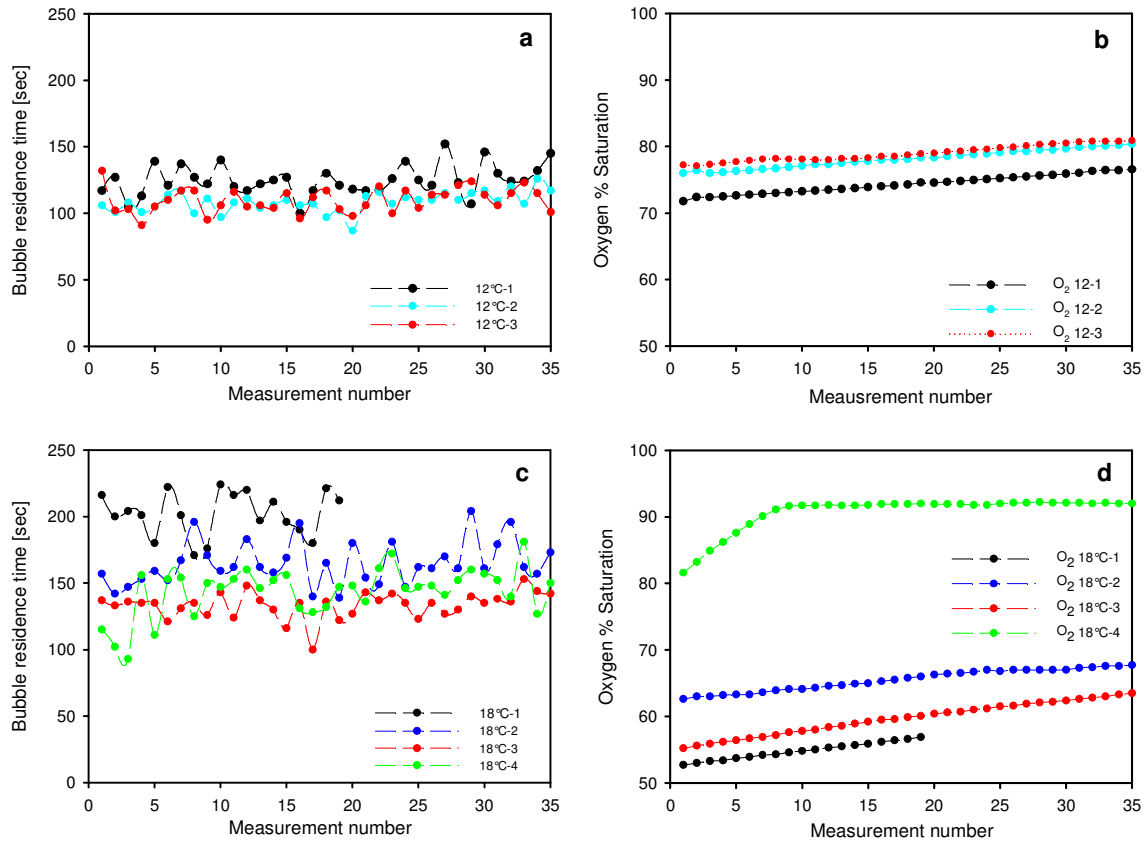

Figure 3.1 BRT and oxygen saturation with increasing measurement number for 12°C and 18°C reference measurement series with deionised water.
a) BRT with measurement number for 12°C reference measurements; b) oxygen saturation with measurement number for 12°C reference measurements
c) BRT with measurement number for 18°C reference measurements; d) oxygen saturation with measurement number for 18°C reference measurements.

Measurement series	Mean BRT (sec)	Stand. deviation BRT	Mean O_2 saturation (%)	Stand. deviation O_2
12°C-1	125	±11	74.3	±1.4
12°C-2	109	±7	78.1	±1.4
12°C-3	110	±9	78.9	±1.2
18°C-1	202	±16	54.8	±1.2
18°C-2	165	±16	67.6	±3.5
18°C-3	133	±10	61.1	±3.1
18°C-4	144	±18	91.0	±2.3

Table 3.1 Mean BRT, standard deviation and mean oxygen saturation for reference measurement series with deionised water at 12 and 18°C.

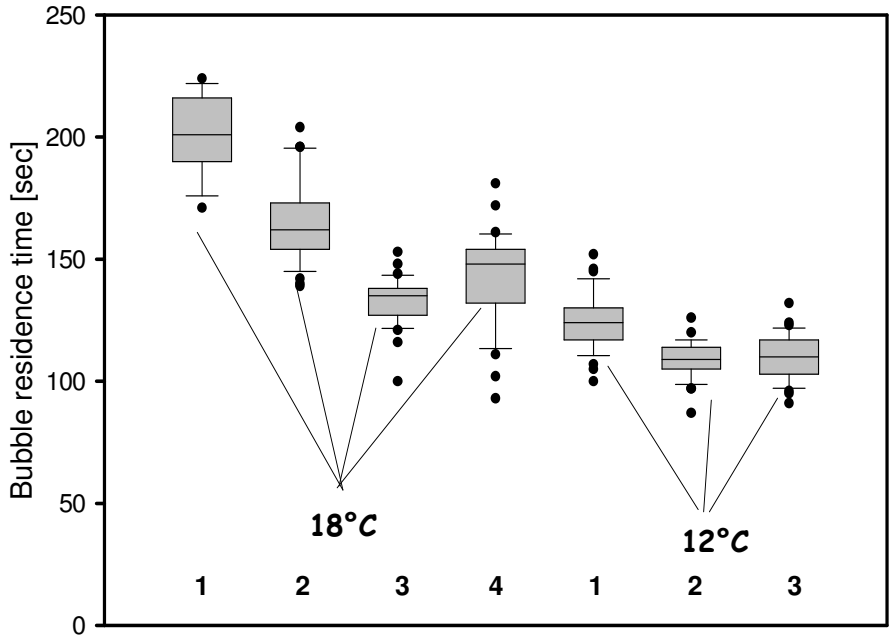

Figure 3.2 Boxplot of BRT reference measurements with deionised water at 18°C and 12°C
Boxes are in the same order as measurement series shown in Figure 3.1. Upper box boundary: 75th percentile; lower box boundary: 25th percentile. Whiskers below and above boxes show the 10th and 90th percentiles. Black dots show outliers and the black solid lines within the boxes represent the median value.

3.2 Kiel Firth water growth experiments

3.2.1 First eutrophic Kiel Firth water experiment

The aim of this preliminary experiment was to investigate if phytoplankton growth of a natural population from Kiel Firth could be initiated in the tank system and if BRT would change as a result of phytoplankton growth. Following the addition of the nutrients on day 0.5, the chlorophyll *a* concentration in the tank began to increase exponentially for three days from an initial concentration of 0.54 $\mu g\ l^{-1}$ to a maximum of 7.6 $\mu g\ l^{-1}$ (Figure 3.3) on day 3.5. This indicates that the tank system supported good phytoplankton growth. Changes in inorganic nutrient concentration (NO_3^-, PO_4^{3-} and Si) are shown in Figure 3.3 and indicate a PO_4^{3-} concentration decrease to 0.13 $\mu mol\ l^{-1}$ and a decrease in silicate to 2.0 $\mu mol\ l^{-1}$ on day 2.5, when the maximum chlorophyll concentration occurred. The nutrient removal ratio of 67 from days1.5-2.5 indicates that the system became limited in phosphate (Table 3.2). During days 6.4-10.5, the phytoplankton became limited in silicate and the chlorophyll concentration decreased to 4 $\mu g\ l^{-1}$ on day 10.5. The phytoplankton in the tank system were dominated by diatoms, the major species that could be identified on the first day of the experiment were *Stephanopyxis turris*, *Nitzschia closterium* and *Asterionella japonica*. However, for this experiment, no phytoplankton cell count data was available as samples were not collected. Figure 3.4 also shows the temporal variation in oxygen saturation with the light and dark phases of illumination of the tank system indicated. With increasing chlorophyll concentration in the tank system, the oxygen saturation increased from 90% on day 0.5 to a maximum of 158% on day 6.4, when the chlorophyll concentration had already started to decline. Oxygen saturation then decreased to just over 130% on day 10.5. Concurrently with increasing chlorophyll concentration an increase in BRT occurred from an initial value of approximately 150 seconds to maximum values of 350 seconds on days 5 and 6 (Figure 3.5). Chlorophyll *a* concentration then decreased to 3.9 $\mu g\ l^{-1}$ between days 6.4 and 10.5, and BRT decreased to its initial value of 150 seconds over the same period. BRT data was not median-filtered for this experiment as the diurnal changes were clearly detectable in the raw data. With the onset of oxygen saturation increase, changes in BRT correlated with the light-dark cycle with higher values measured when the tank system was illuminated and lower values during dark phases (Figure 3.5). In Figure 3.6, only the last datum point for BRT for each light and dark phase is shown, indicating clearly the higher values of BRT following a period of illumination. A fast Fourier transform of 512 interpolated data points (see Appendix L for method of interpolation) of BRT (Figure 3.7) shows a distinct peak located at a frequency of 1 per

day. Figure 3.5 indicates that distinct changes in BRT synchronised with the light-dark changes only occurred once the oxygen saturation had exceeded 100% at the beginning of phytoplankton growth. During the chlorophyll decline phase after day 3.5, the water in the tank remained supersaturated with oxygen, however, BRT decreased to its initial value and the light-dark changes are not so obvious. The increase in BRT covaried with an increase in oxygen saturation and as the oxygen saturation declined towards the end of the phytoplankton growth period, BRT also decreased. A regression analysis of chlorophyll and mean daily BRT shows a linear statistically significant relationship with an r^2 of 0.74 and a p-value of 0.003, giving a level of significance (α-level) of = 0.01 (Figure 3.8). The Spearman's correlation coefficient is r=0.854 with a p-value=0.002 for n = 9. A significant correlation also exists between mean daily BRT and oxygen saturation (Figure 3.9). With a correlation coefficient r=0.929 and p=0.000 for n = 9, the correlation is significant at α = 0.01.

Changes in DOC concentration did not show any obvious trend in relation to chlorophyll *a* content of the water (Figure 3.10) although some indication of increase over time exists with values ranging from a minimum of 271 µmol l^{-1} on day 2.5 to a maximum value of 396 µmol l^{-1} on day 9.5. During the exponential growth phase, no increase in DOC occurred but as the cells entered the stationary phase (after day 3.5) and the decline phase (after day 6.4), DOC showed some increase. No relationship was obvious between chlorophyll *a* concentration and bulk water viscosity (Figure 3.11) and DOC and viscosity. Bulk water viscosity showed no trend over time with viscosity values ranging from 1.18 mm^2 sec^{-1} to 1.20 mm^2 sec^{-1} ± 0.009 mm^2 sec^{-1} with a range of 0.067 mm^2 sec^{-1} (Figure 3.11).

Results from this experiment suggested that oxygen saturation and chlorophyll concentration may be co-factors influencing BRT. It was attempted to therefore estimate BRT using chlorophyll concentration and oxygen saturation as predictors. Equation 3.1 best fitted the data of daily mean BRT:

$$BRT = BRT_0 + 0.25 \times chl(O_2 - [O_2]_{critical}) \qquad \text{(Equation 3.1)}$$

with BRT_0 (offset of BRT) = 140 seconds and O_2 critical = 100%.

As shown in Figure 3.12, the model closely predicts the mean daily BRT, indicated by the 1:1 ratio. The correlation between predicted BRT and mean daily BRT is statistically significant with r = 0.996 and p <0.000.

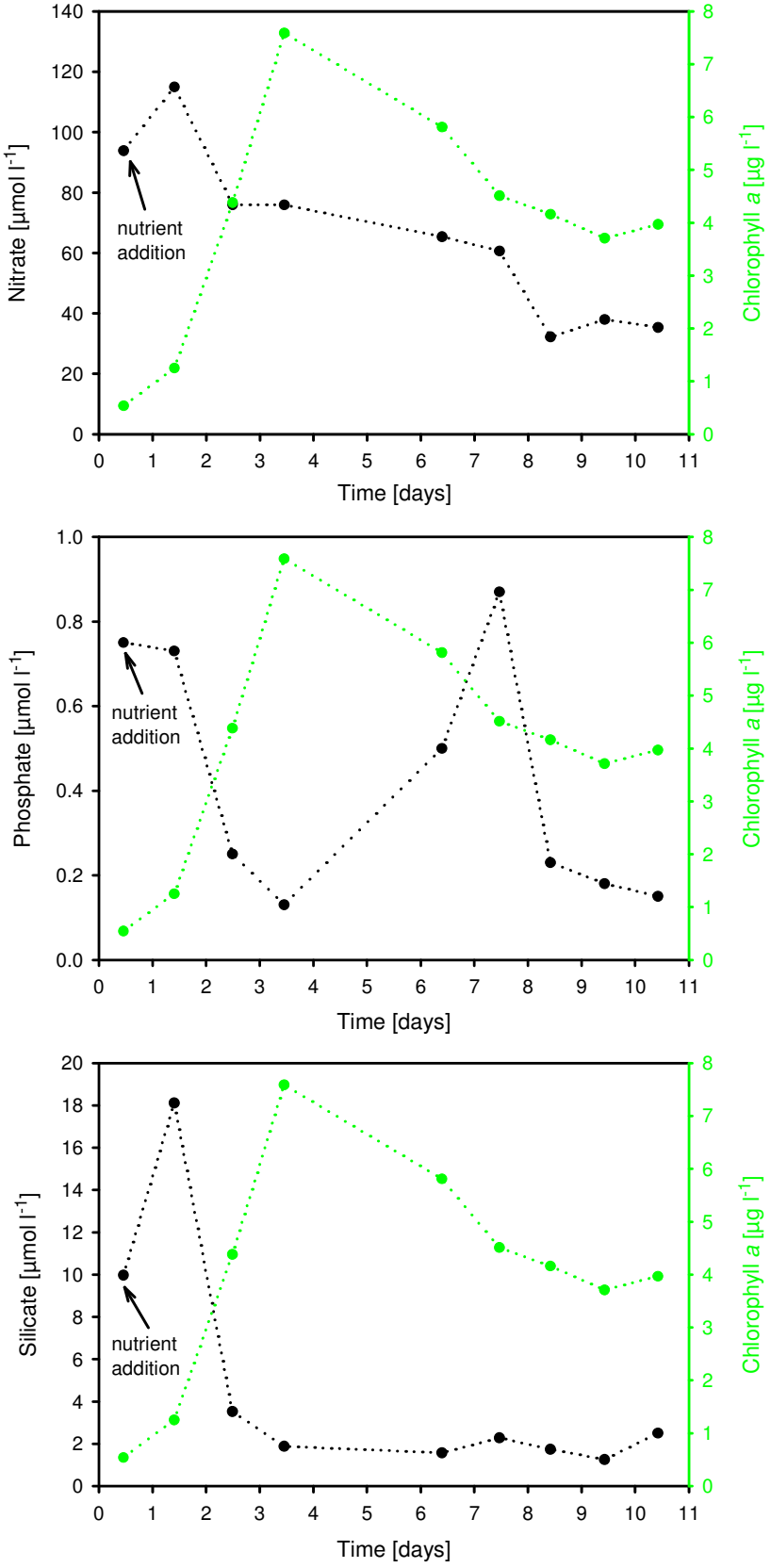

Figure 3.3 Changes in nitrate, phosphate, silicate and chlorophyll concentrations with time for experiment 1.
No error bars exist because only discrete samples were taken for this experiment.

Day No.	Δ NO_3^- (µmol l^{-1})	Δ PO_4^{3-} (µmol l^{-1})	Δ NO_3^-/ΔPO_4^{3-}	Δ Chlorophyll *a* (µg l^{-1})
0.5-1.4	+21.1	-0.02	-	+0.71
1.5-2.5	-38.9	-0.58	67	+3.13
2.5-3.5	-0.1	-0.12	0.8	+3.21

Table 3.2 Nitrate and phosphate uptake, nutrient removal ratios and change in chlorophyll concentration during the exponential growth phase for experiment 1.

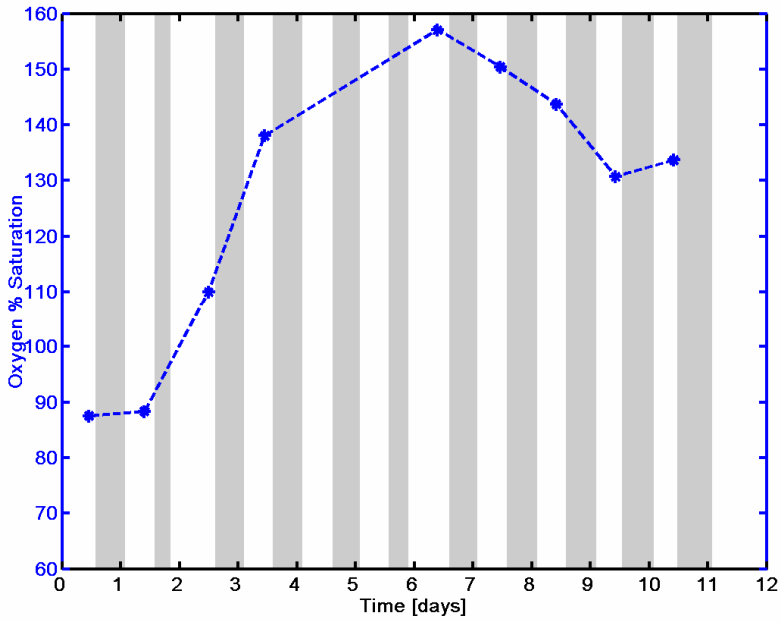

Figure 3.4 Changes in oxygen saturation with time for experiment 1.
Grey shaded areas: illumination off; white areas: illumination on. The unequal light-dark phases during days 1.5 and 2.6 resulted from a timing error of the light switch.
No error bars exist because only discrete samples were taken for this experiment.

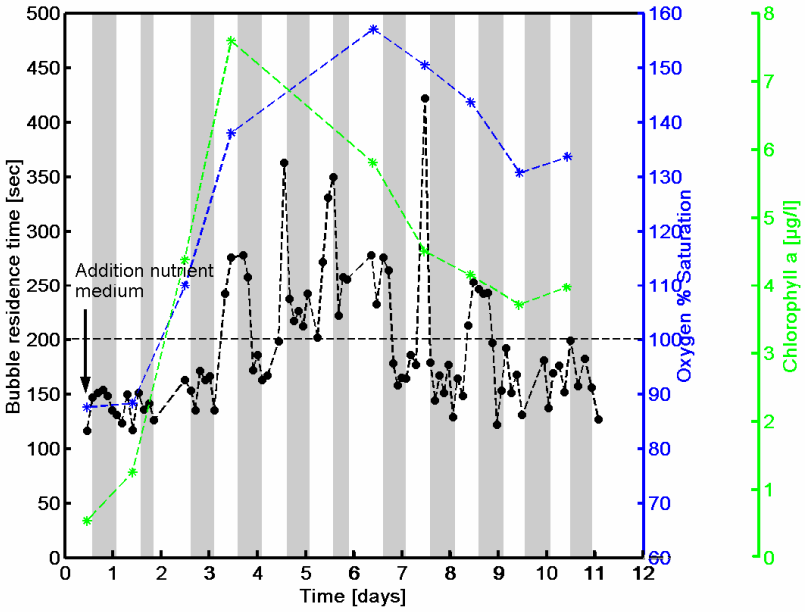

Figure 3.5 Changes in BRT, oxygen saturation and chlorophyll concentration with time for experiment 1.
Grey shaded areas: illumination off; white areas: illumination on. The unequal light-dark phases during days 1.5 and 2.6 resulted from a timing error of the light switch. Dashed black line: 100% oxygen saturation threshold. No error bars exist because only discrete samples were taken for this experiment.

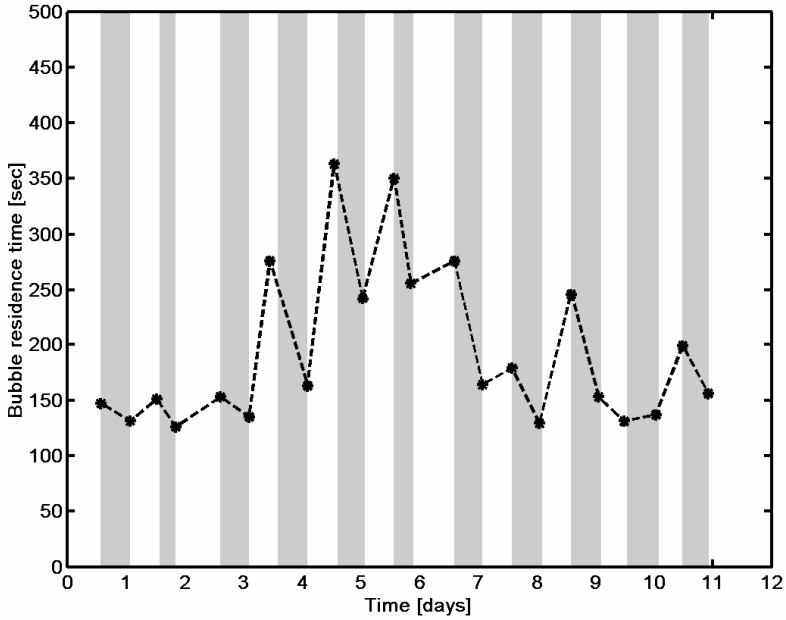

Figure 3.6 Changes in BRT- last data points of light and dark phase for experiment 1.
Grey shaded areas: illumination off; white areas: illumination on. The unequal light-dark phases during days 1.5 and 2.6 resulted from a timing error of the light switch.

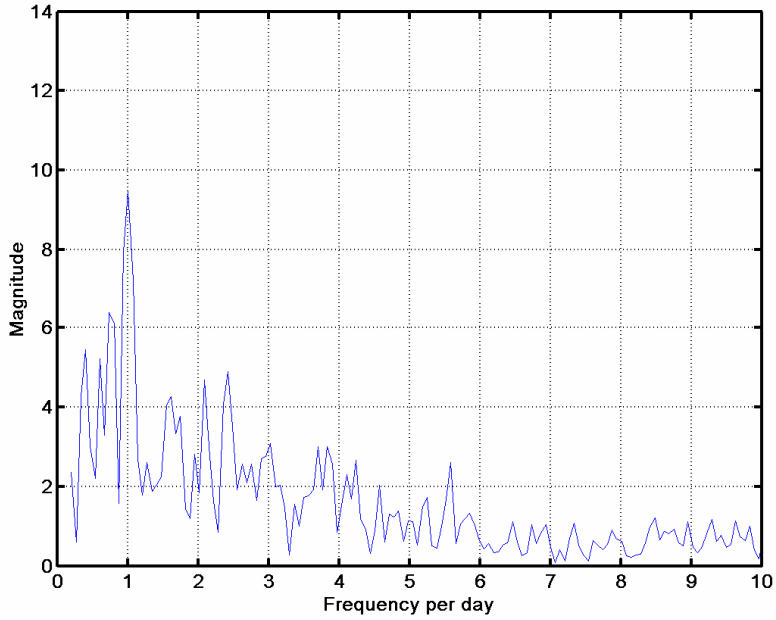

Figure 3.7 Fourier analysis of BRT data for experiment 1.
The distinct peak at frequency 1 (per day) indicates that the fluctuations in BRT data occurred at regular intervals corresponding to the light-dark cycle of the tank system.

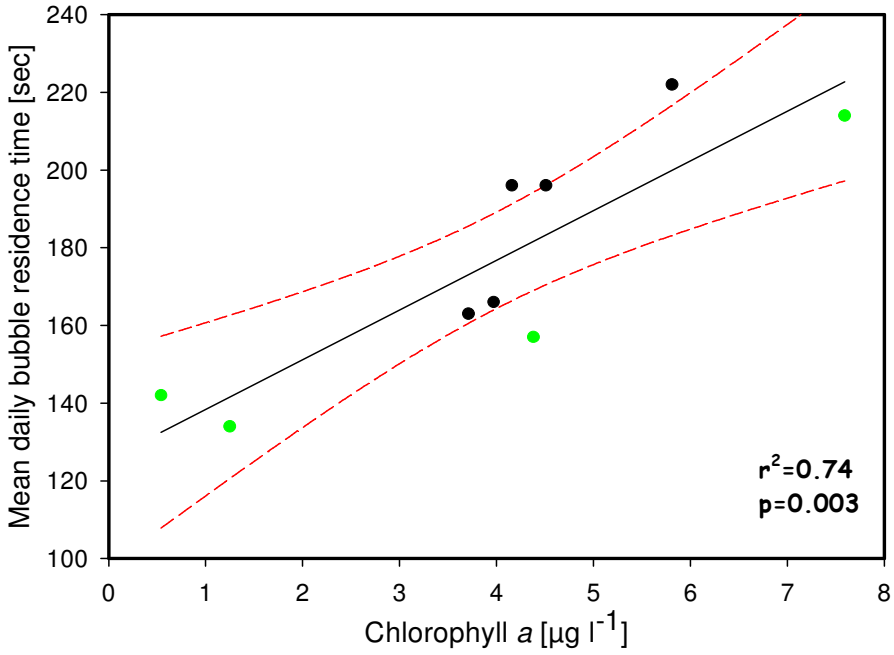

Figure 3.8 Chlorophyll versus mean daily BRT for experiment 1.
Black solid line = linear regression; red dashed lines = 95% confidence intervals; green symbols = data points during chlorophyll increase; black symbols = data points during chlorophyll decrease.

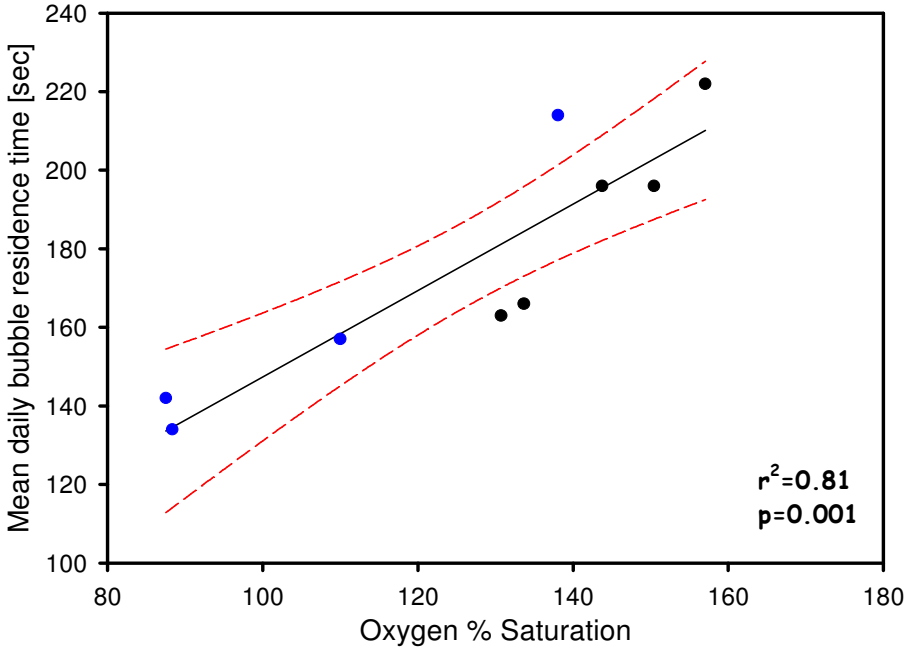

Figure 3.9 Oxygen saturation versus mean daily BRT for experiment 1.
Black solid line = linear regression; red dashed lines = 95% confidence intervals; blue symbols = data points during oxygen increase; black symbols = data points during oxygen decline.

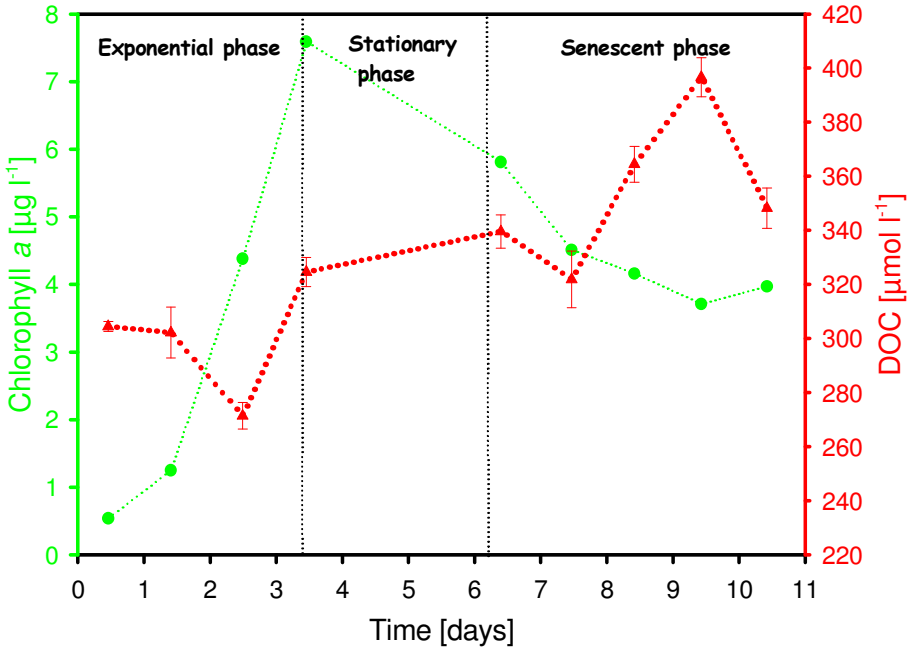

Figure 3.10 Changes in DOC and chlorophyll concentration with time for experiment 1.
DOC error bars: ~ ± 5 µmol l^{-1}.
No error bars exist for chlorophyll data points because only discrete samples were taken for this experiment.

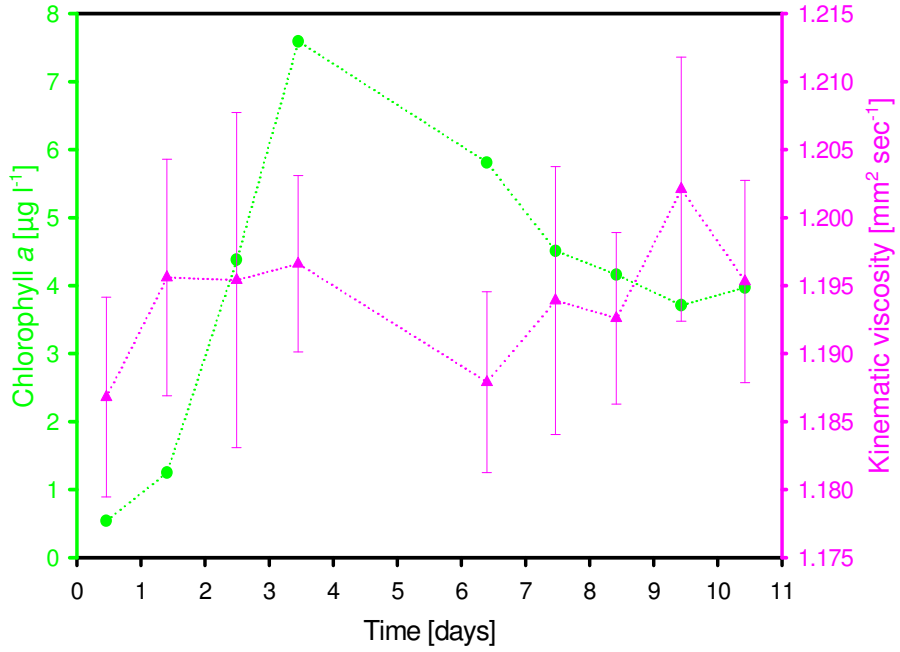

Figure 3.11 Changes in bulk water viscosity and chlorophyll concentration with time for experiment 1.
Viscosity error bars: ± 0.006-0.01 mm^2 sec^{-1}.
No error bars exist for chlorophyll data points because only discrete samples were taken for this experiment.

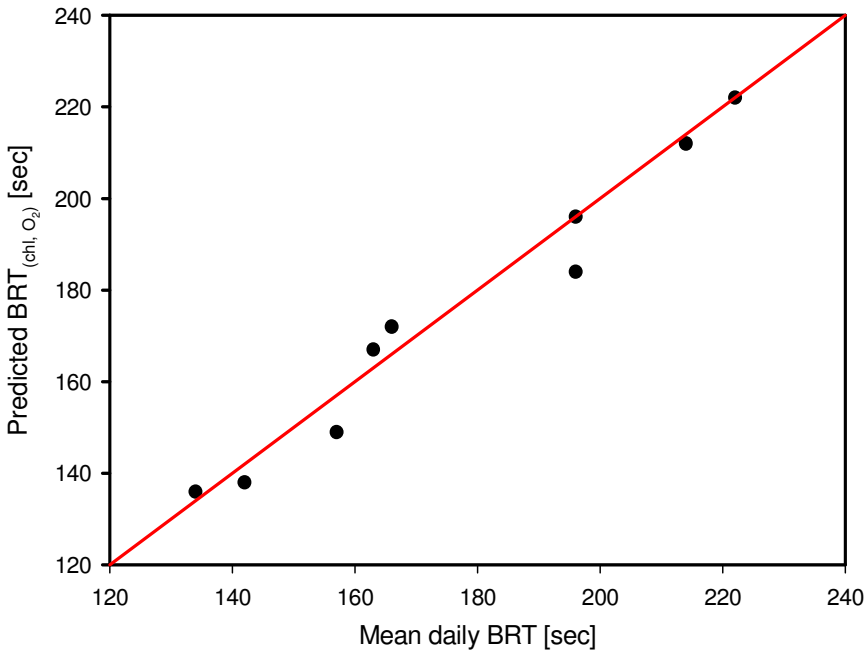

Figure 3.12 Predicted BRT versus mean daily BRT for experiment 1.
Red line = 1:1 ratio.

3.2.2 Second eutrophic Kiel Firth water experiment

Water was collected from Kiel Firth on the day the experiment was started with the aim of investigating if an increase in BRT could be observed following the growth of a natural phytoplankton population. Addition of nutrient medium was made on day 0.7 as indicated on Figure 3.13. The chlorophyll *a* concentration in the tank increased exponentially from 1.7 µg l^{-1} to a maximum of 26.7 µg l^{-1} on day 5.5 (Figure 3.13) indicating that the system supported good phytoplankton growth. After day 5.5, the chlorophyll concentration decreased again until day 10.5 to 6.9 µg l^{-1}, followed by another slight increase to 10.5 µg l^{-1} on day 12.5. The standard deviation of mean chlorophyll concentration calculated from the triplicate samples was usually below 10%, most values have a standard deviation of around 4 % (see appendix M). The nutrient data in Figure 3.13 show that phytoplankton growth in the tank depleted silicate to 2 µmol l^{-1} by day 7.5 of the experiment, while nitrate had only slightly decreased from 200 µmol l^{-1} to 150 µmol l^{-1} and showed a slight increase after day 7.5, possibly resulting from mixing of remineralised nitrate. Phosphate concentration decreased gradually from 12 µmol l^{-1} to 6 µmol l^{-1} between days 0.7 and 13.5. Nutrient removal ratios are shown in Table 3.3.

The phytoplankton were dominated by diatoms, with the most abundant species being *Thalassionema nitzschioides*, *Skeletonema costatum*, *Thalassiosira* sp. and *Nitzschia closterium*. The composition of the phytoplankton is summarised for three selected days in Table 3.4. On day 0.5, the most dominant species was *Thalassionema nitzschioides* (2.7×10^5 cells l^{-1}) followed by *Skeletonema costatum* (1.0×10^5 cells l^{-1}), *Thalassiosira* sp. (3.8×10^4 cells l^{-1}) and *Nitzschia closterium* (1.7×10^4 cells l^{-1}). The highest specific growth rate during the exponential phase was found for *Skeletonema costatum* (1 division per day between days 0.5-4.5), accordingly its fraction increased while the fractions of *Thalassionema nitzschioides*, *Nitzschia closterium* and *Thalassiosira* sp. decreased as their specific growth rates were lower.

The increase in chlorophyll concentration was accompanied by a rapid increase in oxygen saturation of the water from an initial supersaturation of 110% to a maximum of 190% on day 5.5, when the chlorophyll concentration was highest (Figure 3.15). The accuracy of the oxygen data from the electrode was monitored by Winkler titrations and the data show good agreement to the 1:1 ratio (Figure 3.14). The light and dark changes in oxygen saturation as shown on Figures 3.15 and 3.17 vary by a difference of 10% between the dark phase minimum and the light phase maximum at the beginning of the phytoplankton growth period to a maximum difference of approximately 40% between days 4.0 and 6.0,

when chlorophyll concentrations were highest. Once the chlorophyll concentration started to decline from day 6.5, the oxygen supersaturation decreased and light-dark differences diminished, with the light-phase rate of increase in oxygen saturation being less than the rate of decline during dark phase. After 13 days, the oxygen saturation had reduced back to its initial value of just over 100%. BRT data showed much scatter (Figure 3.16), therefore only the median filtered (refer to section 2.2.4 for method of median filtering) BRT data (mf BRT) are shown.

During the first two days of the experiment, when chlorophyll concentrations were still low (~2 $\mu g\ l^{-1}$) mfBRT decreased from 450 seconds to just less than 300 seconds (Figure 3.17). This decrease may have resulted from mixing and equilibration of the freshly filled seawater with the tank system. During days 2.0 to 4.0, mfBRT increased to 400 seconds during light phase and decreased to 300 seconds during dark phase, indicated by the shaded areas in Figure 3.17. From day 4.0, when chlorophyll was high (25 $\mu g\ l^{-1}$), oxygen supersaturation increased rapidly and the rate of increase during light phase was high, mfBRT increased to a maximum value of over 620 seconds on day 5.0, followed by a decline on the same day to 500 seconds and a further increase between days 6.0-8.0. Between days 4.0 and 9.0, when the water was highly supersaturated with oxygen, no light and dark cycle was observed in mfBRT data. From days 9.0-10.5, when chlorophyll concentration and oxygen saturation both declined to 6 $\mu g\ l^{-1}$ and~105% respectively, mfBRT decreased to 200 seconds. Between days 9.0-11.0, when oxygen saturation and mfBRT declined, mfBRT followed the light and dark phases indicated by the grey and white shaded areas on Figure 3.17. Figure 3.18 shows the last datum point of mfBRT for every light and dark phase over the experiment, indicating that mfBRT shows little covariation with the light-dark phase. The Fourier analysis of 512 interpolated mfBRT data points (Figure 3.19) confirms this observation as no distinct peak is visible at a frequency of 1. Chlorophyll concentration and daily mean mfBRT do not show a strong correlation with a correlation coefficient $r = 0.481$, a p-value of 0.041 and $n = 14$, the correlation is significant at an α-level of 0.05. Chlorophyll concentration and mfBRT are linearly related for a significance level of $\alpha = 0.05$, with $r^2 = 0.44$, $p = 0.01$ (Figure 3.20). MfBRT did show a general covariation with oxygen saturation and a regression analysis of oxygen saturation and mfBRT (Figure 3.21) indicates a linear relationship between the two parameters ($r^2 = 0.66$ and a p-value = 0.000). Also, mfBRT and oxygen saturation show a good correlation ($r = 0.691$; p-value = 0.000; $n = 77$; α-level = 0.01).

DOC remained fairly constant during the exponential growth phase with values around 260-270 µmol l^{-1} (Figure 3.22). As the chlorophyll concentration reached its maximum on day 5.5 and then began to decrease, the DOC concentration in the tank increased steadily up to 340 µmol l^{-1} on day 13.5. DOC concentration did not show any obvious trend with mfBRT.

Bulk water viscosity did not show a detectable change over time during the experiment (Figure 3.23).

Results of daily measurements of water surface tension (auto-mode, Figure 3.24) did not show any significant changes over the period of the experiment. All values range between 73 mN m^{-1} and 74 mN m^{-1} and no decrease in surface tension occurred with increasing bubble lifetime (refer to section 2.5.8).

The total bacteria number per ml doubled between days 0.7 and 2.5 of the experiment (Figure 3.25) from 2.7×10^{6} cells ml^{-1} to 5.4×10^{6} cells ml^{-1}. A 3-fold increase occurred on day 6.5 with 1.7×10^{7} cells ml^{-1}. After that, the total bacteria number decreased again to 7.0×10^{6} cells ml^{-1} on day 12.5. The standard deviation of bacteria cell counts varied between ± 12% - ± 30%.

Estimation of mfBRT by applying equation 3.1 to chlorophyll and oxygen data obtained in this experiment (Figure 3.26) shows that the equation is not valid for mfBRT prediction for this experiment and that predicted BRT values are much higher than measured daily mean mfBRT.

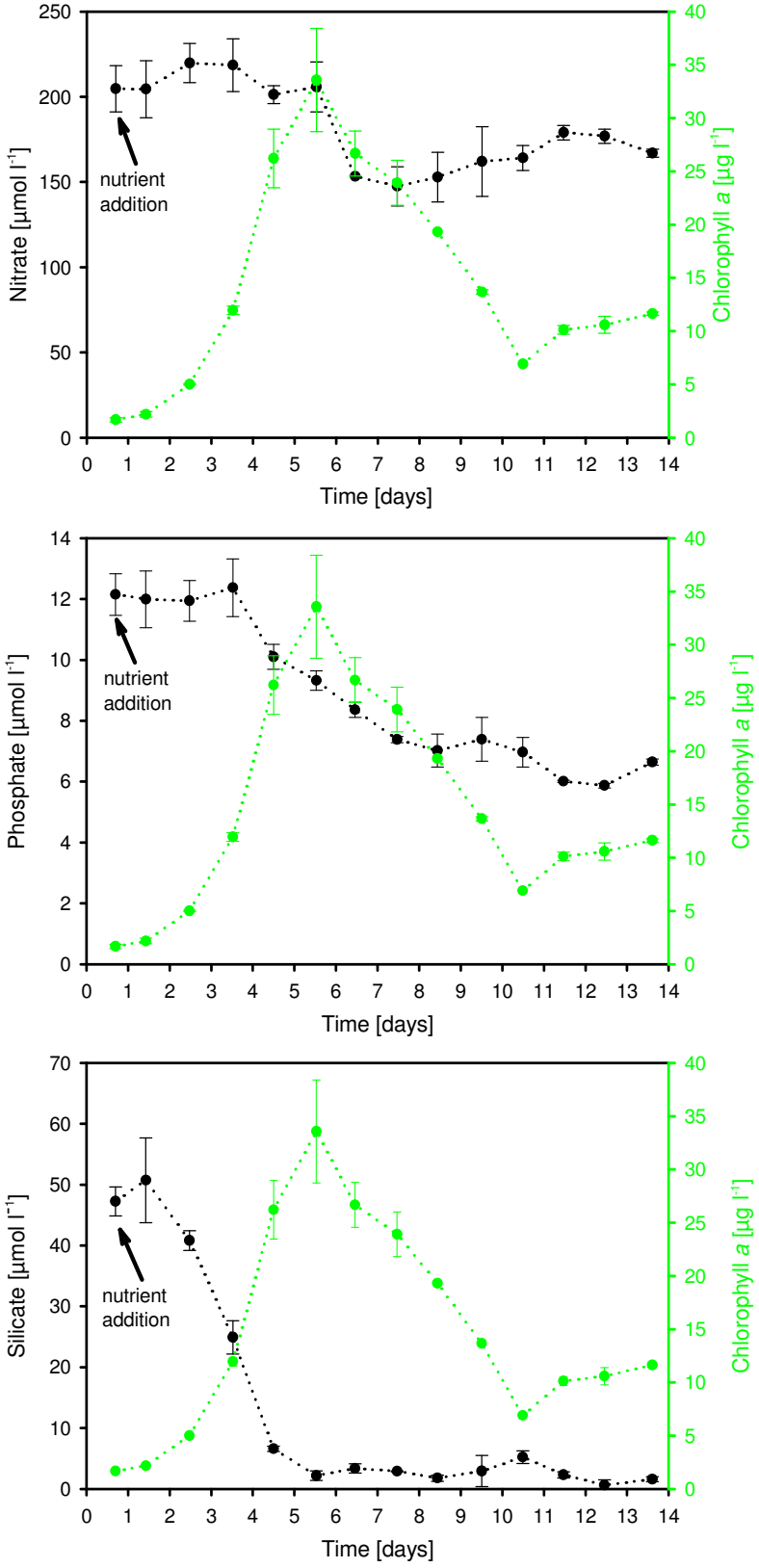

Figure 3.13 Changes in nitrate, phosphate, silicate and chlorophyll concentrations with time for experiment 2.
NO_3^- error bars: ± 4-13 µmol l^{-1}; PO_4^{3-} error bars: ± 0.01-0.9 µmol l^{-1}; Si error bars: ± 0.2-6 µmol l^{-1}; chlorophyll error bars: ± 0.2-2.8 µg l^{-1}.

Day No.	Δ NO_3^- (µmol l^{-1})	Δ PO_4^{3-} (µmol l^{-1})	Δ $NO_3^-/\Delta PO_4^{3-}$	Δ Chlorophyll *a* (µg l^{-1})
0.7-1.5	0	-0.3	-	+0.5
1.5-2.5	+15	0	-	+2.38
2.5-3.5	-1	-0.5	2	+6.94
3.5-4.5	-17	-2.3	7.4	+14.26
4.5-5.5	+4	-0.8	-	+7.36

Table 3.3 Nitrate and phosphate uptake, nutrient removal ratios and change in chlorophyll concentration during the exponential growth phase for experiment 2.

	Day 0.5		Day 4.5		Day 5.5			
Species	**Cell no. l^{-1}**	**% of total cells**	**Cell no. l^{-1}**	**% of total cells**	**Cell no. l^{-1}**	**% of total cells**	**Specific growth rate days 0.5-4.5**	**Specific growth rate days 4.5-5.5**
Thalassionema nitzschioides	2.7×10^5	62.9	2.8×10^6	39.3	4.0×10^6	35	0.6	0.3
Nitzschia closterium	1.7×10^4	4.1	1.0×10^5	1.4	1.3×10^5	1.2	0.4	0.3
Thalassiosira sp.	3.8×10^4	8.8	2.9×10^5	4.1	4.3×10^5	3.8	0.5	0.4
Skeletonema costatum	1.0×10^5	24.1	3.9×10^6	55.3	6.9×10^6	60.1	1	0.6

Table 3.4 Phytoplankton cell numbers, percentages of total cells counted and specific growth rates for three selected days for experiment 2.

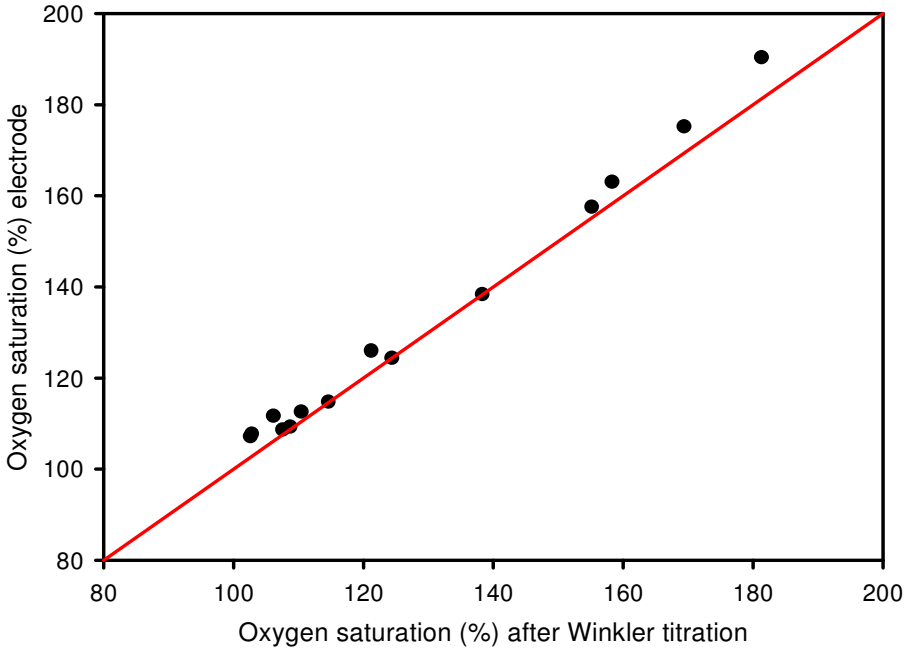

Figure 3.14 Oxygen saturation determined by Winkler titration versus oxygen saturation measured by electrode for experiment 2.
Key: red line = 1:1 ratio.

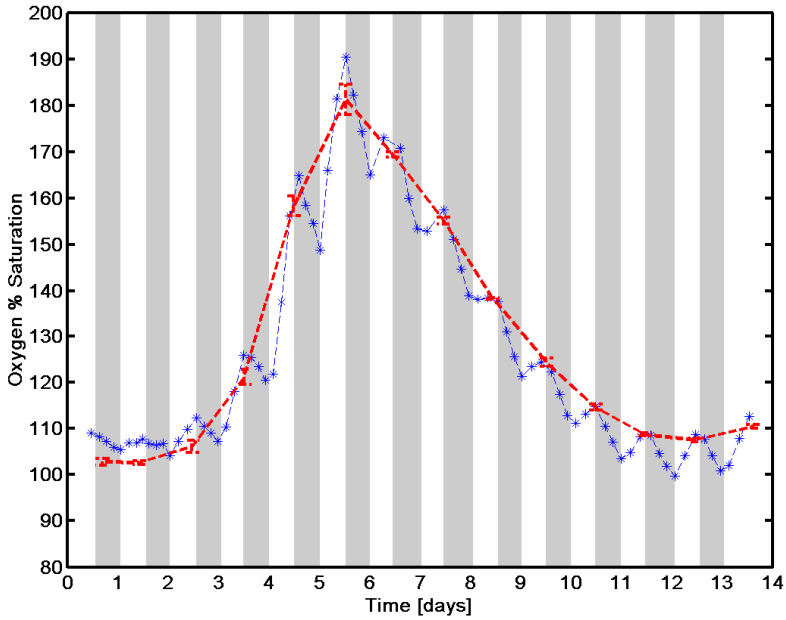

Figure 3.15 Changes in oxygen saturation with time for experiment 2.
Grey shaded areas: illumination off; white areas: illumination on; blue symbols: oxygen saturation$_{electrode}$; red symbols: oxygen saturation$_{Winkler}$; error bars: ± 0.4-3%.

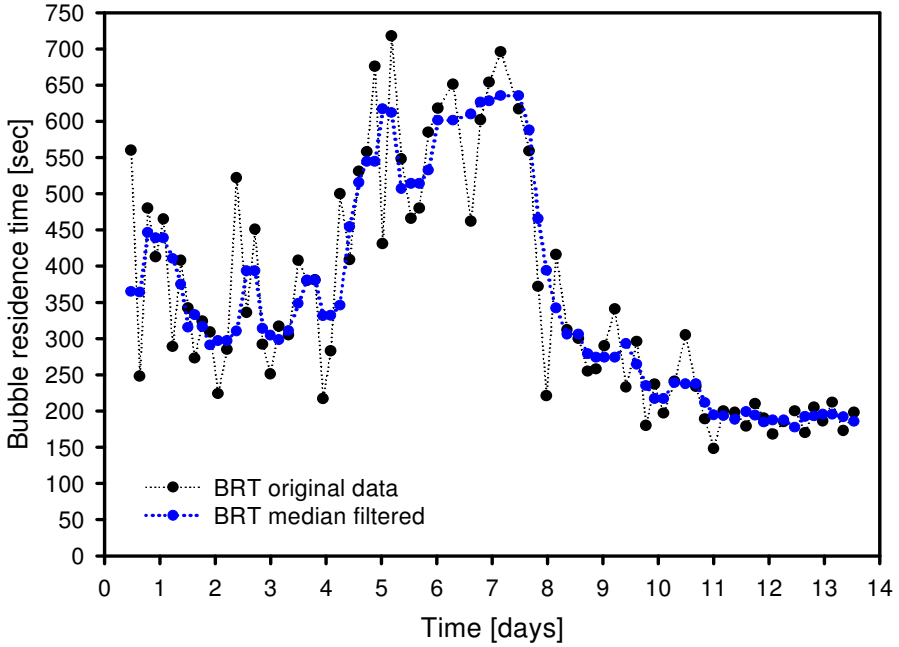

Figure 3.16 Comparison of BRT and median filtered BRT with time for experiment 2.

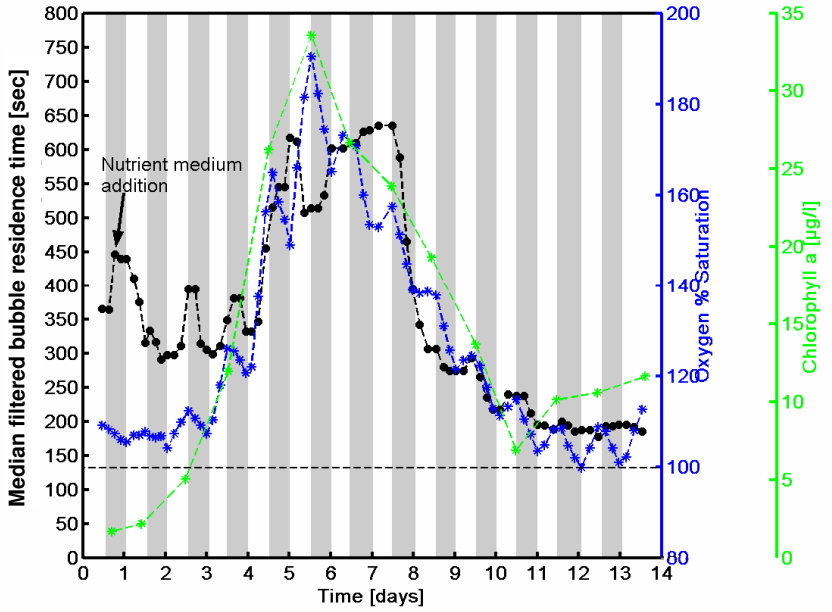

Figure 3.17 Changes in mfBRT, oxygen saturation and chlorophyll concentration with time for experiment 2.
Grey shaded areas: illumination off; white areas: illumination on.

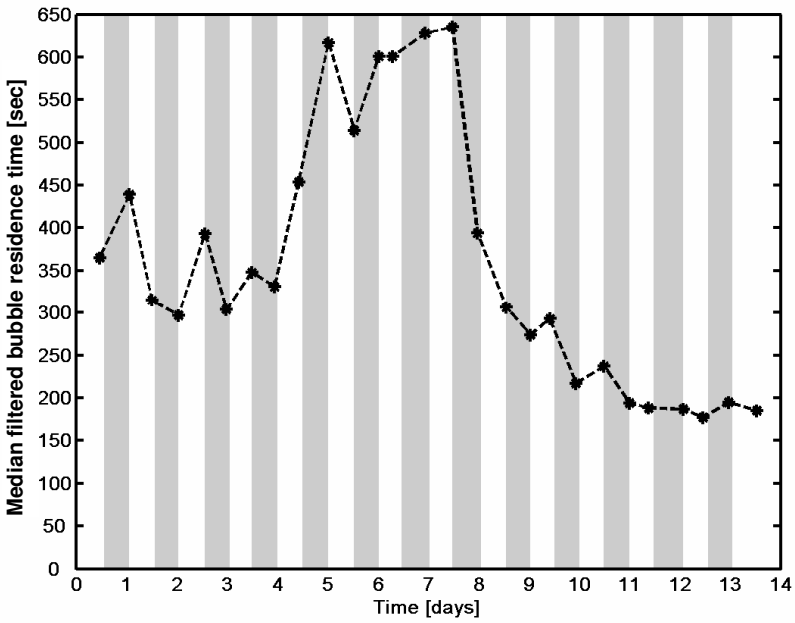

Figure 3.18 Changes in mfBRT - last data points of light and dark phase for experiment 2. Grey shaded areas: illumination off; white areas: illumination on.

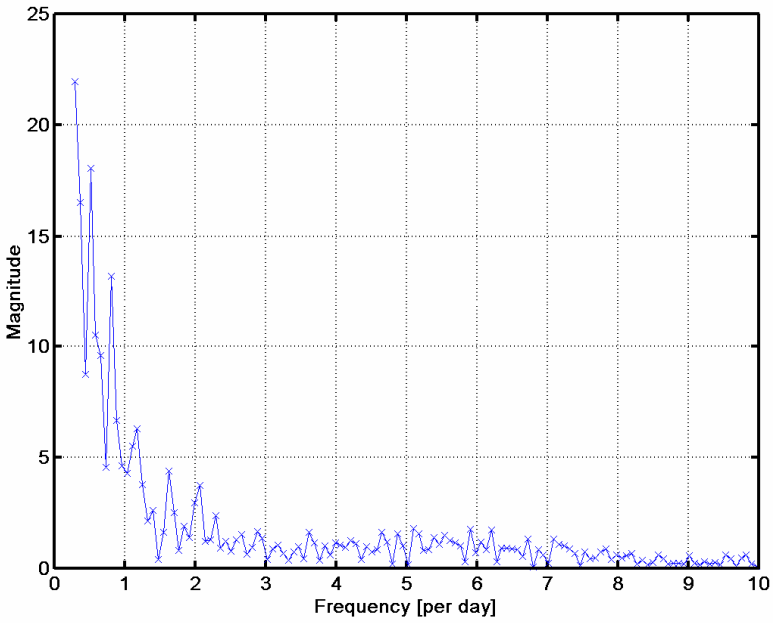

Figure 3.19 Fourier analysis of mfBRT data for experiment 2.
No distinct peak visible at frequency 1 indicating no light-dark dependency of mfBRT.

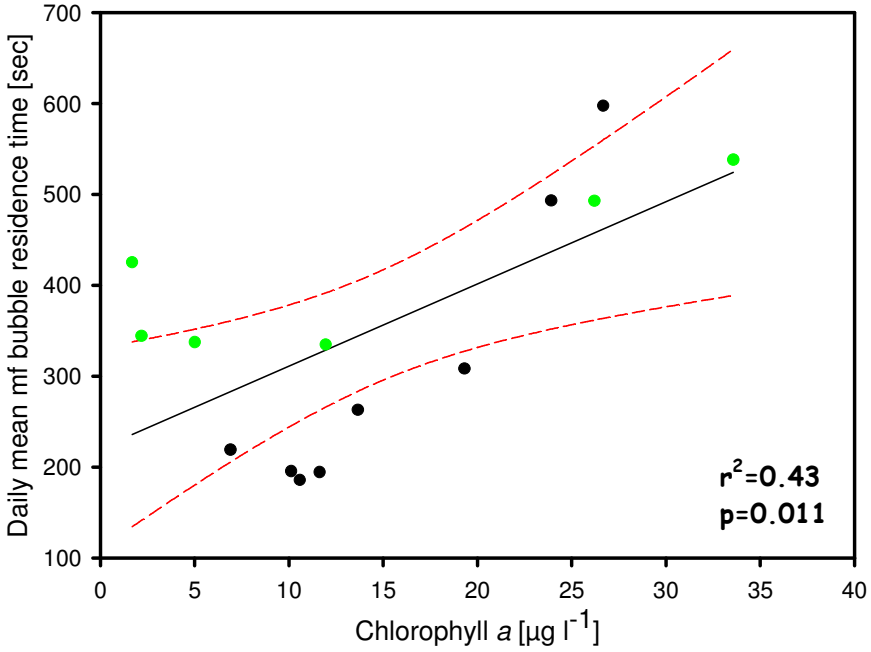

Figure 3.20 Chlorophyll concentration versus mean daily mfBRT for experiment 2. Black solid line = linear regression; red dashed lines = 95% confidence intervals; green symbols = data points during chlorophyll increase; black symbols = data points during chlorophyll decrease.

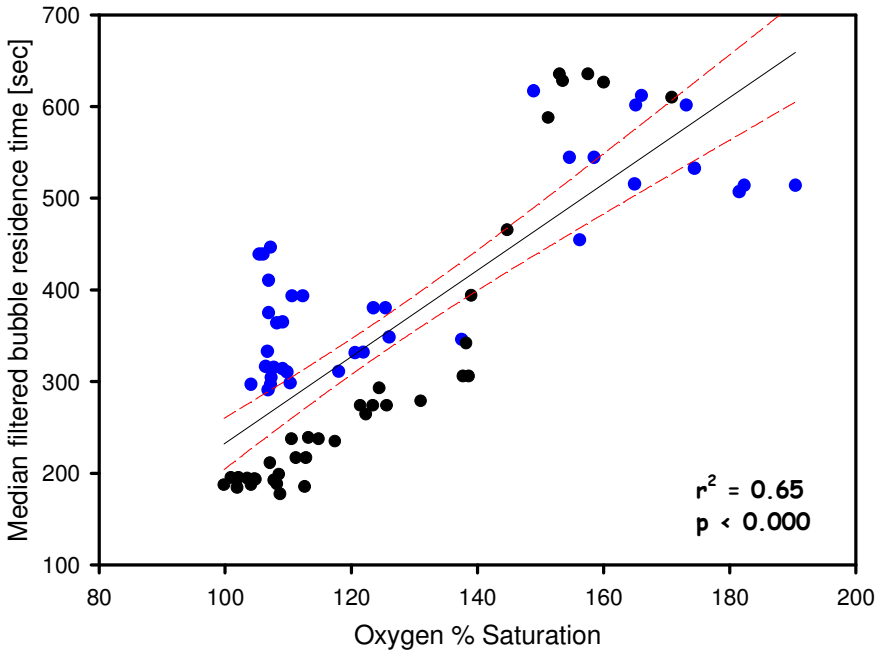

Figure 3.21 Oxygen saturation versus mfBRT for experiment 2. Black solid line = linear regression; red dashed lines = 95% confidence intervals; blue symbols = data points during oxygen increase; black symbols = data points during oxygen decline.

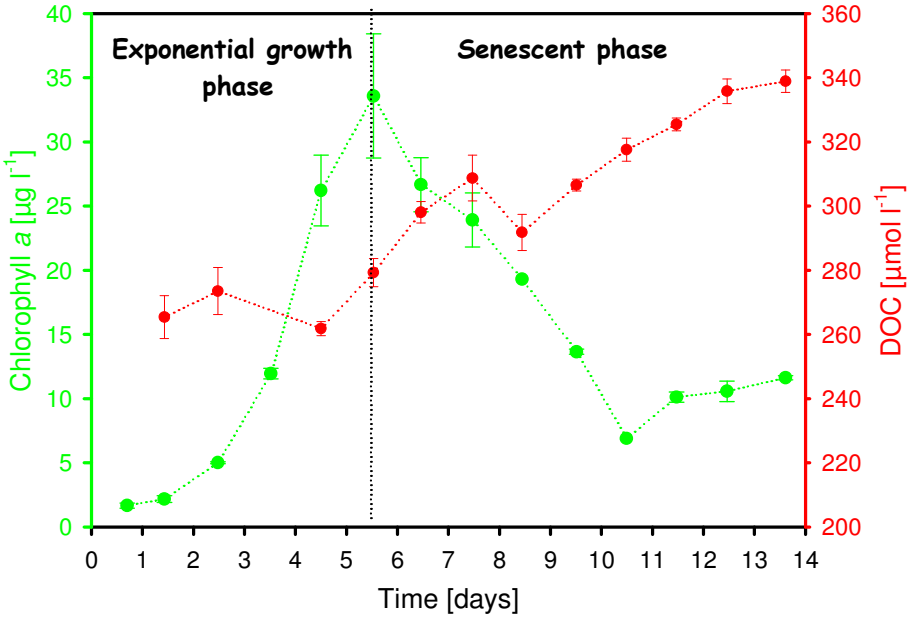

Figure 3.22 Changes in DOC and chlorophyll concentration with time for experiment 2. DOC error bars: ± 0.2-11 µmol l^{-1}.

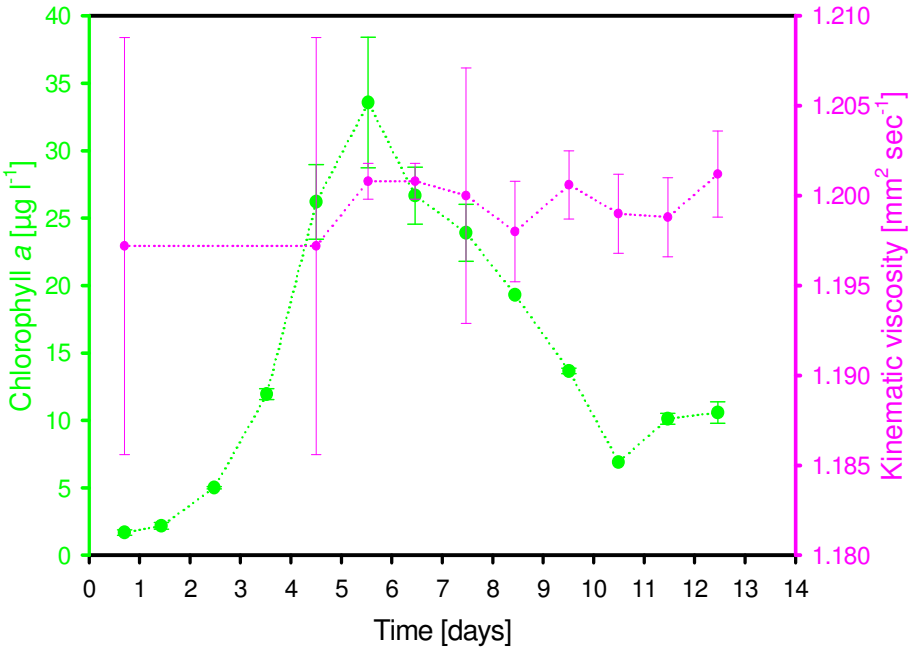

Figure 3.23 Changes in bulk water viscosity and chlorophyll concentration with time for experiment 2. Viscosity error bars: ± 0.001-0.01 mm^2 sec^{-1}.

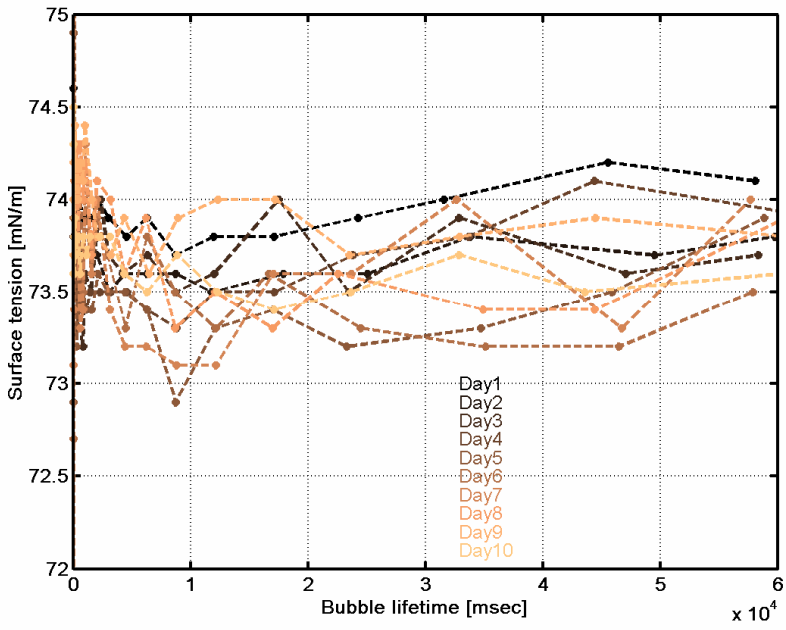

Figure 3.24 Changes in surface tension with time and for different bubble lifetimes for experiment 2.

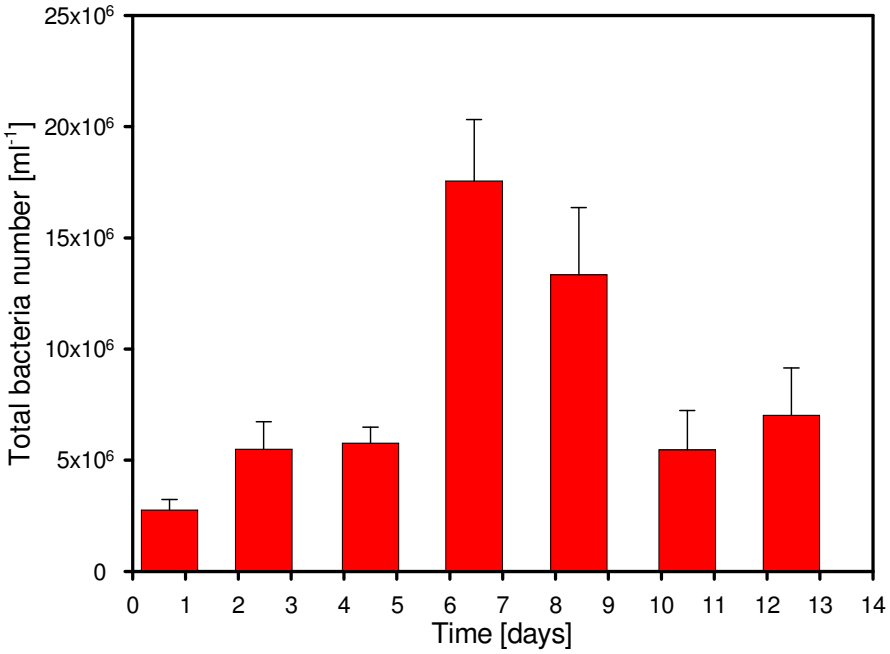

Figure 3.25 Changes in total bacteria numbers with time (per ml) for experiment 2. The bar middle is located at the point in time when the sample was taken from the tank. Error bars: ± 4.7×10^5 - 3.0×10^6 cells ml^{-1}.

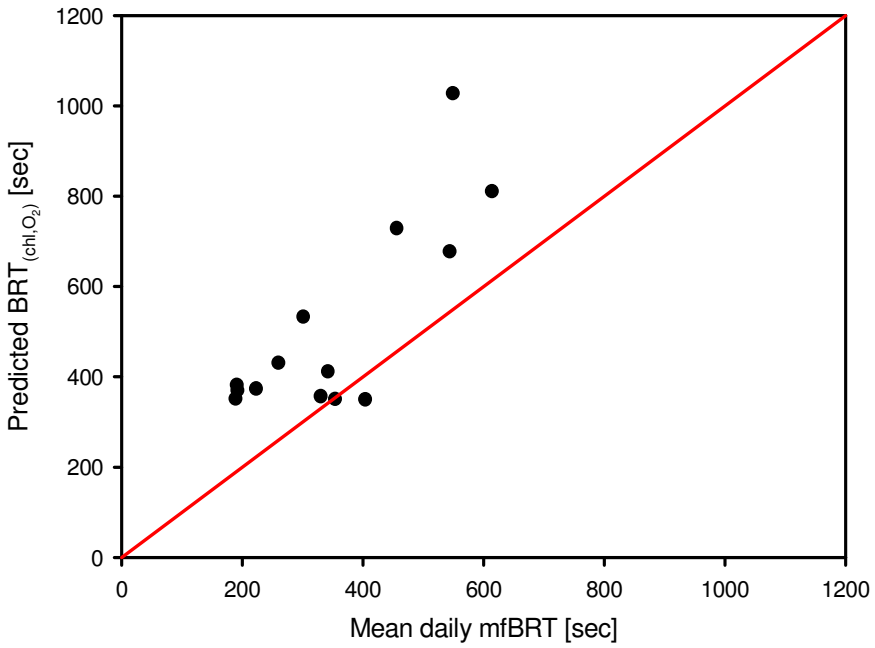

Figure 3.26 Predicted BRT versus mean daily mfBRT for experiment 2 using relationship from experiment 1 (see page 60). Red line = 1:1 ratio.

3.2.3 Third eutrophic Kiel Firth water experiment

This experiment was conducted to investigate further the effect of growth of a natural phytoplankton population collected in March 2004 from Kiel Firth, on BRT. BRT measurements were carried out for 3 consecutive days before the addition of inorganic nutrients due to the high initial BRT on day 0.5. During this time a short but rapid increase on day 0.5-1 was followed by a decrease in BRT between days 1.0 and 5.0 from 430 seconds to 180 seconds (Figure 3.30). It is unclear what might have caused this initial elevated value of BRT, as Winkler oxygen samples were only taken from day 3.5. Possibly, the high BRT values at the beginning of measurement may have been related to the water equilibrating with the tank system.

Inorganic nutrients were added on day 3.4 and initiated an increase in chlorophyll concentration between days 4-7 from 4.8 µg l^{-1} to 39 µg l^{-1}. Between days 8-13.5 the chlorophyll concentration declined to 7.6 µg l^{-1}. The nutrient data (Figure 3.27) show that nitrate and phosphate were available in sufficient quantities throughout the experiment and decreased only gradually with time. The nutrient removal ratio was below the Redfield ratio of 16:1 for days 3.4-4.4, indicating that nitrate was removed more rapidly than phosphate (Table 3.5). Between days 5.4 and 6.4 however, the nutrient removal ratio of 95.6 shows that phosphate was removed more rapidly than nitrate. Between days 6.4-7.5, when the chlorophyll concentration already declined, nutrients (mostly nitrate) were still removed (Table 3.5). Silicate became depleted on day 5.4, followed by a major increase on day 6.4 and another decline on days 7.5 and 8.5. Due to the large standard deviation of silicate on day 6.4 (silicate concentration = 8.8 µmol l^{-1}, standard deviation = 2.73 µmol l^{-1}) it is highly likely that this value is in error.

Cell numbers of the most abundant phytoplankton species in the tank system, *Skeletonema costatum*, *Thalassionema nitzschioides* and *Nitzschia closterium* are summarised in Table 3.6 for 5 selected days of the experiment. On day 3.5, *Skeletonema costatum* represented the largest fraction of the total phytoplankton with 1.4×10^7 cells l^{-1}. However, the specific growth rates during the exponential growth phase (days 3.5-6.5) was highest for *Thalassionema nitzschioides* (1.5 divisions per day) and for *Nitzschia closterium* (1 division per day), while the fraction of *Skeletonema costatum* decreased (0.6 divisions per day). By the end of the experiment, the fractions of *Thalassionema nitzschioides* and *Nitzschia closterium* had increased to 12 and 6% respectively. With increasing chlorophyll concentration in the tank, the oxygen saturation (determined by Winkler titration only for

this experiment) increased from days 3.5-8 from ~110% to 240 %, followed by a decline to ~130% on day 13.5 (Figure 3.28).

Due to the scatter in BRT data, a median filter (see section 2.2.4) was applied (Figure 3.29) and only median filtered BRT is used for further analysis. With increasing chlorophyll concentration and oxygen saturation in the tank, mfBRT increased from 180 seconds on day 5.0 to a maximum of 540 seconds on day 6.3, when the chlorophyll concentration in the tank was highest (58 $\mu g\ l^{-1}$) and the tank water was strongly supersaturated with oxygen (238%, Figure 3.30). Between days 6.3 -7.8, when chlorophyll concentration began to decline, oxygen saturation and mfBRT remained high. During the dark phase of day 7, mfBRT decreased from 540 seconds to 450 seconds and increased again during both the light and dark phases on day 8 to 550 seconds. When the oxygen saturation started to decrease on day 9, mfBRT declined as well until day 11.0. After day 11.0 the decrease in mfBRT was only small. On day 13.5, mfBRT had reached approximately 200 seconds, this being roughly equal to values of mfBRT just before nutrient addition. No consistent dark-light dependent variation can be seen in mfBRT (Figure 3.31), except for days 11.0-13.0, when mfBRT values were higher during light phase and lower during dark phase. The lack of light-dark consistent changes in mfBRT for this experiment is also supported by the fast Fourier transform of mfBRT data (Figure 3.32), which does not show a peak at frequency 1 per day. Despite the reasonable correlation between mfBRT and chlorophyll ($r = 0.782$, p-value = 0.002, $n = 11$, $\alpha = 0.01$) as well as mfBRT and oxygen % saturation ($r = 0.727$, p-value = 0.006, $n = 11$, $\alpha = 0.01$), the linearity of the relationship of chlorophyll and mfBRT as well as oxygen and mfBRT is not quite as strong (Figures 3.33 and 3.34) but still statistically significant. For chlorophyll concentration and mfBRT, linear regression gives $r^2 = 0.66$ with a p-value of 0.002. The linear relationship between oxygen saturation and mfBRT is also significant with $r^2 = 0.65$ and $p = 0.003$.

DOC concentration remained constant at 291 $\mu mol\ l^{-1} \pm 4\ \mu mol\ l^{-1}$ between days 3.4-5.4 wile the cells grew exponentially. DOC began to increase to 321 $\mu mol\ l^{-1}$ (Figure 3.35) during the chlorophyll maximum and increased further to 370 $\mu mol\ l^{-1}$ on day 13.5 as the chlorophyll concentration in the tank system declined. The standard deviation of triplicates for DOC was below 5 %, most triplicates had a coefficient of variation of 1%. DOC concentration showed no covariation with mfBRT.

The total bacteria number in the tank water samples decreased from 1.1×10^7 cells ml^{-1} ($\pm$ 2.0×10^6 cells ml^{-1}) on day 3.4 of the experiment, when the first sample was taken to 3.3×10^6 cells ml^{-1} ($\pm$ 1.0×10^6 cells ml^{-1}) on day 6.4 (Figure 3.36). Between days 7.5 and

9.4, the bacteria number increased again to 6.7×10^6 cells ml^{-1} ($\pm$ 2.0×10^6 cells ml^{-1}), followed by another decrease between days 10.4 and 13.5 to 3.7×10^6 cells ml^{-1} ($\pm$ 1.2×10^6 cells ml^{-1}). The change of bacterial cell numbers over time does not show a similar trend to mfBRT.

The application of equation 3.1 to chlorophyll and oxygen data of this experiment results in predicted BRT values that are much higher than the measured mean daily mfBRT values (Figure 3.37) and shows that the model does not fit the data from this experiment.

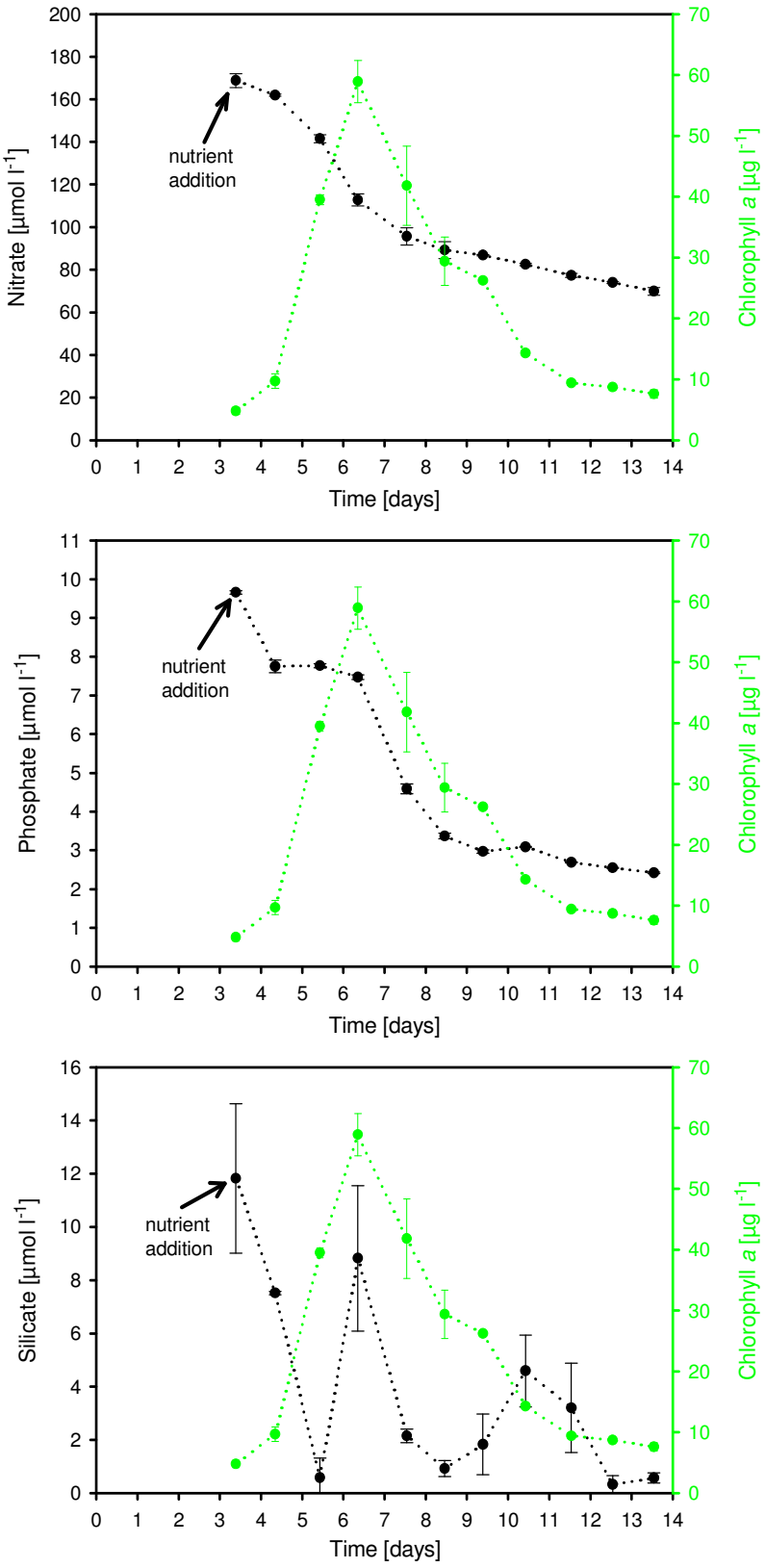

Figure 3.27 Changes in nitrate, phosphate, silicate and chlorophyll concentrations with time for experiment 3.
NO_3^- error bars: ± 0.3-4 µmol l^{-1}; PO_4^{3-} error bars: ± 0.01-0.1 µmol l^{-1}; Si error bars: ± 0.1-2.8 µmol l^{-1}; chlorophyll error bars: ± 0.4-6 µg l^{-1}.

Day No.	Δ NO_3^- (µmol l^{-1})	Δ PO_4^{3-} (µmol l^{-1})	Δ NO_3^-/ΔPO_4^{3-}	Δ Chlorophyll *a* (µg l^{-1})
3.4-4.4	-6.9	-1.9	3.6	+4.9
4.4-5.4	-20.4	0	-	+29.8
5.4-6.4	-28.7	-0.3	95.6	+19.4
6.4-7.5	-17.4	-2.9	6.0	-17.1

Table 3.5 Nitrate and phosphate uptake, nutrient removal ratios and change in chlorophyll concentration during the exponential growth phase for experiment 3.

	Day 3.5		Day 6.5		
Species	**Cell no. l^{-1}**	**% of total cells**	**Cell no. l^{-1}**	**% of total cells**	**Specific growth rate days 3.5-6.5**
Skeletonema costatum	1.4×10^7	95.7	9.3×10^7	66.1	0.6
Thalassionema nitzschioides	5.2×10^5	3.4	4.3×10^7	31.0	1.5
Nitzschia closterium	1.5×10^5	1.0	4.1×10^6	2.9	1

	Day 8.5		Day 11.5		Day 13.5	
Species	**Cell no. l^{-1}**	**% of total cells**	**Cell no. l^{-1}**	**% of total cells**	**Cell no. l^{-1}**	**% of total cells**
Skeletonema costatum	7.9×10^7	97.5	7.1×10^6	84.1	2.2×10^6	82.4
Thalassionema nitzschioides	1.7×10^6	2.1	1.0×10^6	12.3	3.2×10^5	12.0
Nitzschia closterium	3.0×10^5	0.4	3.0×10^5	3.6	1.4×10^5	5.5

Table 3.6 Phytoplankton cell numbers, percentages of total cells counted and specific growth rates for five selected days for experiment 3.

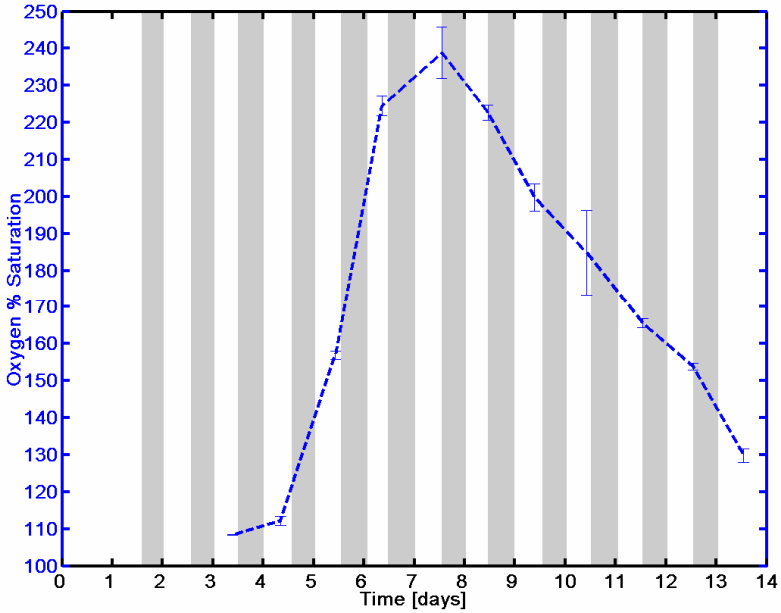

Figure 3.28 Changes in oxygen saturation (Winkler titration) with time for experiment 3. Grey shaded areas: illumination off; white areas: illumination on. Error bars: ± 0.1-11%.

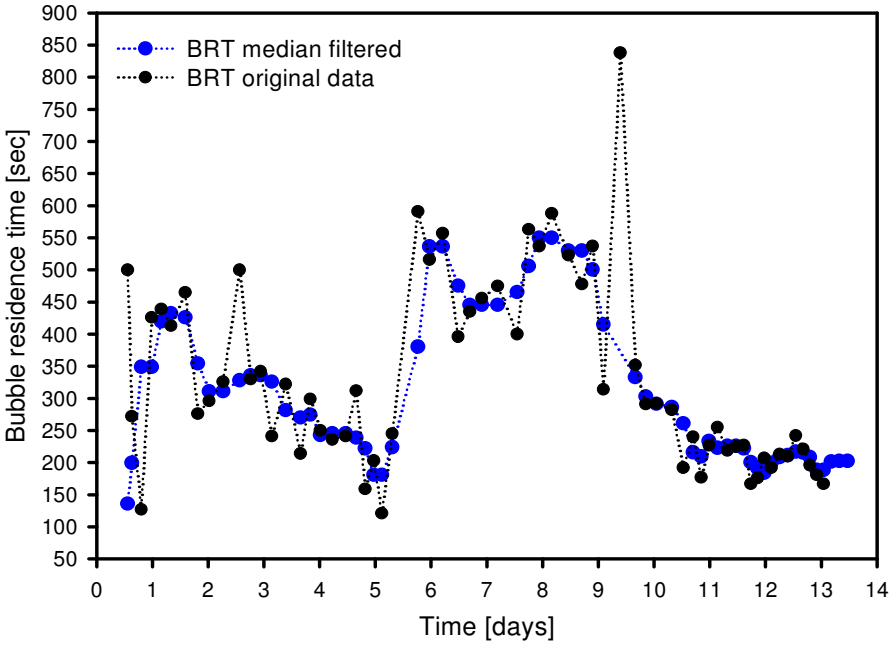

Figure 3.29 Comparison BRT and median filtered BRT with time for experiment 3.

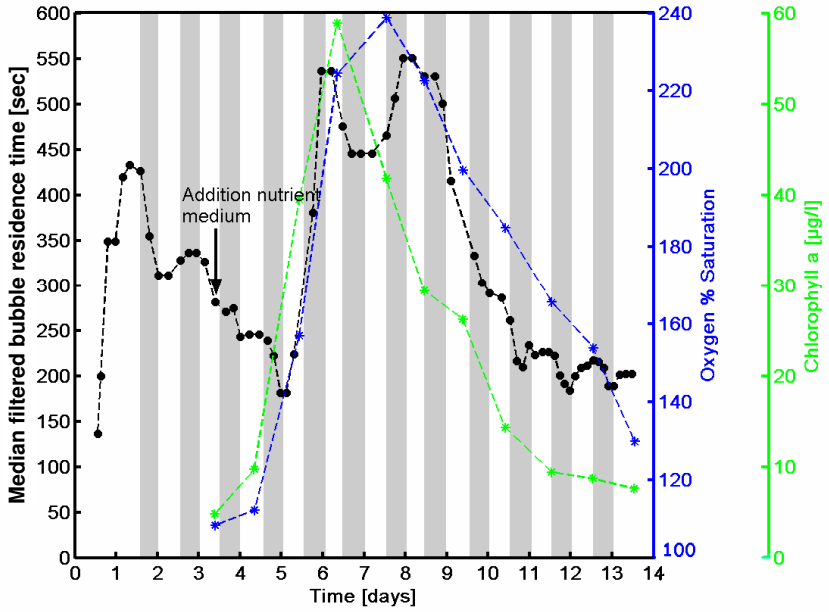

Figure 3.30 Changes in mfBRT, oxygen saturation and chlorophyll with time for experiment 3. Grey shaded areas: illumination off; white areas: illumination on. Samples were taken from day 3.3.

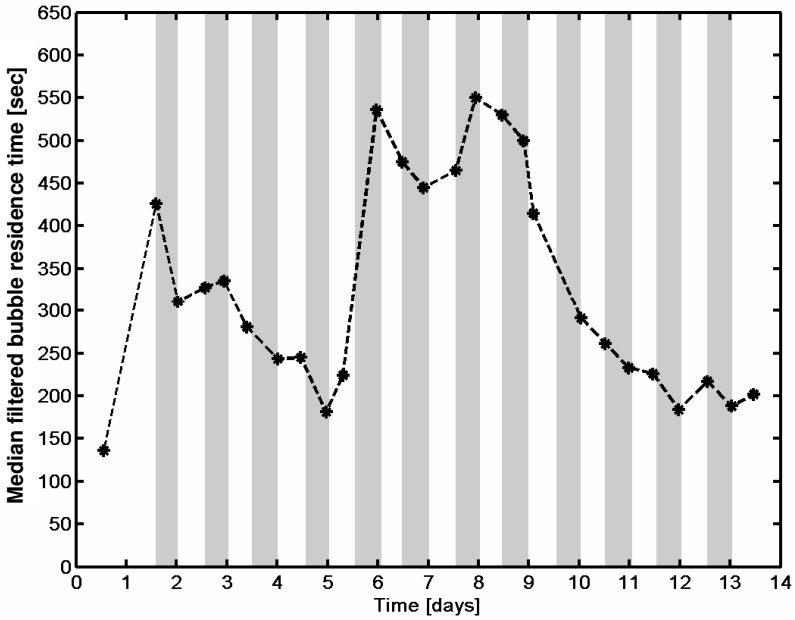

Figure 3.31 Changes in mfBRT with time - last data points of light and dark phase for experiment 3. Grey shaded areas: illumination off; white areas: illumination on.

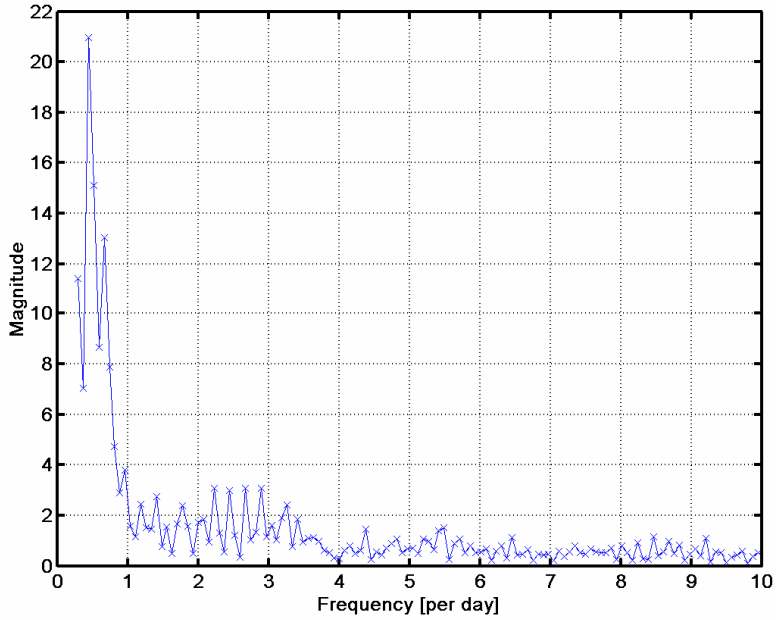

Figure 3.32 Fourier analysis of mfBRT data for experiment 3.
No distinct peak visible at frequency 1 indicating no light-dark dependency of mfBRT.

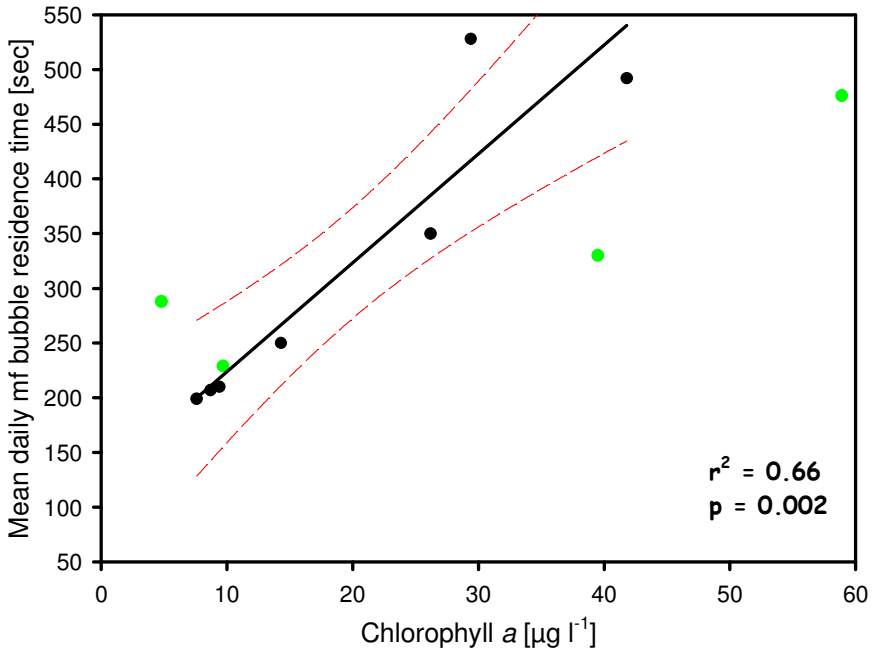

Figure 3.33 Chlorophyll concentration versus mean daily mfBRT for experiment 3.
Black solid line = linear regression; red dashed lines = 95% confidence intervals; green symbols = data points during chlorophyll increase; black symbols = data points during chlorophyll decrease.

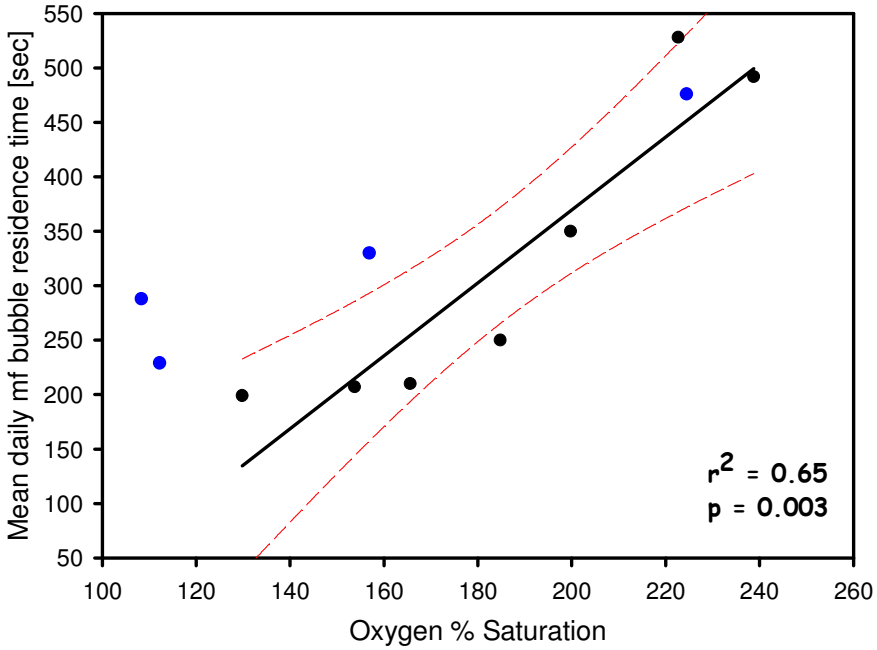

Figure 3.34 Oxygen saturation versus mean daily mfBRT for experiment 3.
Black solid line = linear regression; red dashed lines = 95% confidence intervals; blue symbols = data points during oxygen increase; black symbols = data points during oxygen decline.

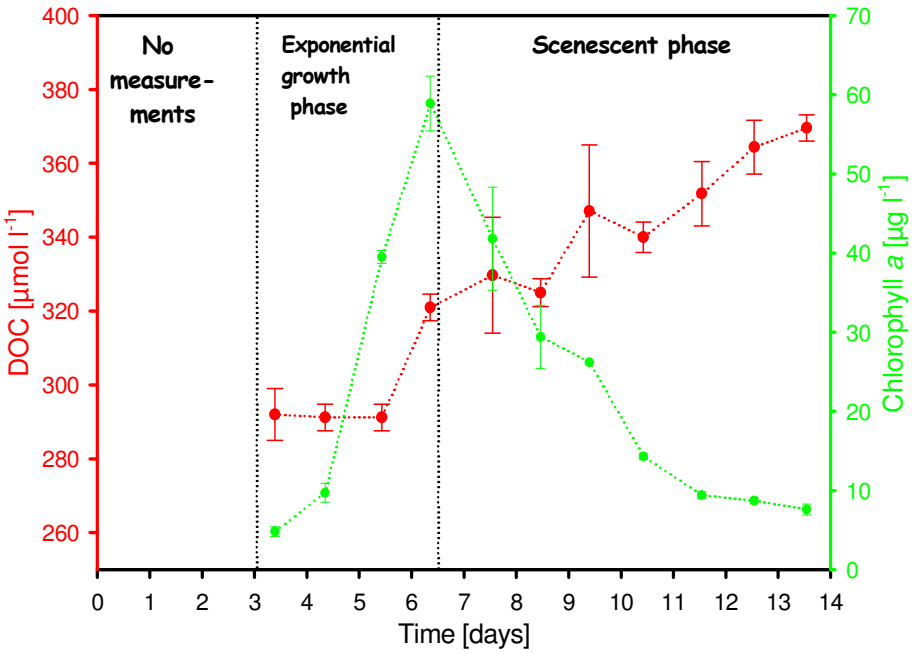

Figure 3.35 Changes in DOC and chlorophyll concentration with time for experiment 3.
DOC error bars: ± 3.6-18 µmol l^{-1}.

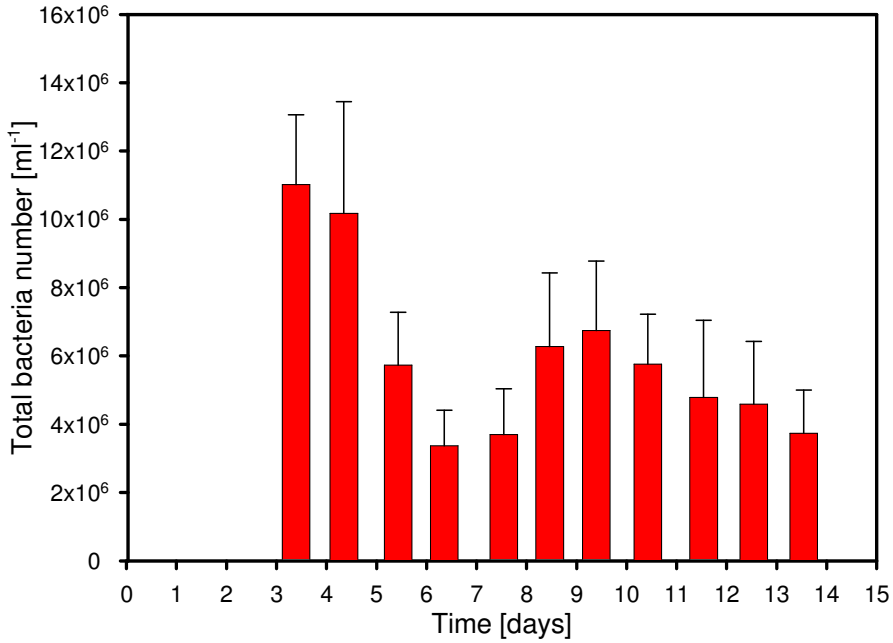

Figure 3.36 Changes in total bacteria numbers with time (per ml) for experiment 3. Error bars: ± 1.0×10^6 – 3.2×10^6 cells ml^{-1}.

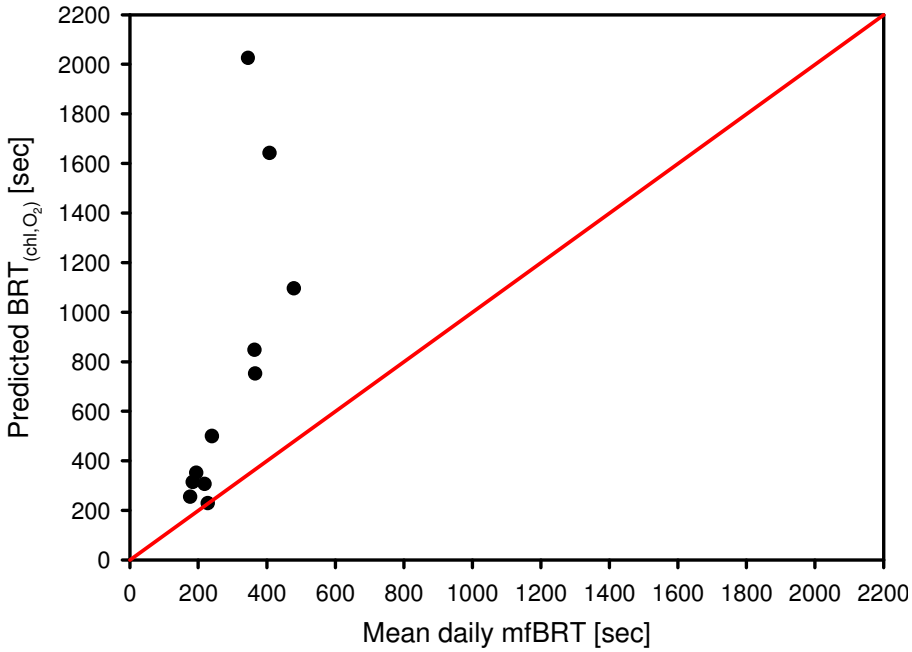

Figure 3.37 Predicted BRT versus mean daily mfBRT for experiment 3 using relationship from experiment 1 (see page 60). Red line = 1:1 ratio.

3.3 Monoculture growth experiments

3.3.1 Growth experiment with Chaetoceros muelleri

The aim of this experiment was to investigate the influence of a diatom monoculture on BRT measured in the tank system. Prior to the addition of nutrient medium and culture to the water, BRT measurements were made for 8 days with filtered North Sea water (GF/F filter pore size = 0.8 µm) as mfBRT values started at a higher level (240 seconds) just after the filling of the tank system with the seawater. Measurements of BRT were made for 8 days prior to nutrient and algae addition, while mfBRT decreased from 240 seconds to 150 seconds (Figure 3.42). Simultaneously, the oxygen saturation decreased from 87% to 39% between days 0.5 and 5.5. MfBRT increased marginally between days 4.5 to 5.5 and then remained constant at a mean value of 156 seconds until the addition of algae and nutrient medium on day 7.6.

Following the addition of nutrients and algae to the water, chlorophyll concentration remained constant between days 7.5-9.5 at ~ 17 µg l^{-1} (Figure 3.38). Between days 10.5-13.5, the chlorophyll concentration in the tank system increased to 70 µg l^{-1}. Nitrate concentration decreased consistently during days 7.5- 18.5 from 282 to 48 µmol l^{-1} (Figure 3.38). Phosphate decreased from 9.7 µmol l^{-1} to 0.1 µmol l^{-1} during days 7.5-14.5. The ratio of nitrate to phosphate uptake was 20 between days 10.5-11.5, 16 between days 11.5-12.5 and 14 between days 12.5-13.5, indicating that phytoplankton growth was balanced and nutrients were removed close to the Redfield ratio (Table 3.7). Silicate declined from an initial concentration of 33 µmol l^{-1} on day 7.5 to 0.5 µmol l^{-1} on day 16.5. Chlorophyll concentration in the tank system declined from 70 µg l^{-1} on day 15.5 to 46 µg l^{-1} on day 18.5 (Figure 3.38).

Oxygen saturations as measured by the electrode versus Winkler controls are shown in Figure 3.39. The relationship between oxygen $saturation_{electrode}$ and oxygen $saturation_{Winkler}$ is linear, however, as shown by the 1:1 ratio, the $oxygen_{Winkler}$ values are slightly higher than the $oxygen_{electrode}$ values. Therefore, the oxygen saturation values measured by the electrode were corrected, applying equation 3.2:

$$O_2\,\%\,\text{saturation}_{\text{corrected}} = 2.35 + 1.04 \times O_2\,\%\,\text{saturation}_{\text{electrode}} \qquad \text{(Equation 3.2)}$$

The relationship between oxygen $saturation_{Winkler}$ and oxygen $saturation_{electrode}$ had an r^2 of 0.995. Change in oxygen saturation over time is shown in Figure 3.40. Oxygen saturation decreased from ~95% on day 0.5 to 44% on day 6.5, followed by an increase to 52% on

day 7.5. Following the addition of nutrients and culture, the oxygen saturation decreased to 25% on day 9.0. From day 9.0 onwards, the oxygen saturation showed light phase increases and dark phase decreases. At the beginning of light dark changes (days 9.0-13.0), the saturation increase during light phase was approximately 15%, while the decrease at darkness was smaller (~10%). Oxygen saturation reached a maximum on day 12.5 with 78%. This maximum in oxygen saturation occurred one day before the chlorophyll maximum. The oxygen saturation increase during light phase was about 30%. Between days 13.5 and 19.5, the oxygen saturation decreased again until a minimum value of ~10% during dark phase and 20% during light phase on day 19.5.

To reduce scatter, BRT data were median filtered (see section 3.43) and only the median filtered data are used for further analyses (Figure 3.41). Following the addition of nutrients and algae to the tank system, mfBRT increased slightly to a mean value of 182 seconds and then decreased again to 152 seconds between days 8.0 and 10.0 when the oxygen saturation declined to 22% (Figure 3.42). BRT data is missing between days 9.9 11.5 (malfunction of tank system). Between days 9.5 and 12.0, a slight increase in mfBRT occurred from 152 seconds to a mean value of 180 seconds, when chlorophyll concentration and oxygen saturation increased. Between days 12.0 and 14.0, when the oxygen saturation was at maximum and chlorophyll concentrations were high, mean mfBRT remained constant at 172 seconds, but small increases (between 10-30 seconds) occurred during light phase and small decreases were found during dark phase. The light and dark phase dependency of mfBRT (Figure 3.43) occurred from day 12.0 to day 17.0 and was strongest during days 13 and 14 with increases of 24 seconds during light phase and decreases of 18 seconds during dark phase. The Fourier analysis (Figure 3.44) of mfBRT shows the light dark dependency of mfBRT with a distinct peak at frequency 1. Between days 13.5 and 19.5, when the oxygen saturation declined, mfBRT decreased fractionally to a mean value of 150 seconds (Figure 3.42). Performance of a Kruskal-Wallis test on mfBRT between days 8.0 and 19.5, to investigate if one or more daily median values of mfBRT differed significantly, resulted in a test statistic H = 40.33 and a p-value = 0.000 at 9 degrees of freedom. As $\chi^2_{(9/0.01)}$=21.67, this result shows that one or more mean daily values of mfBRT differ significantly from one another at $\alpha = 0.01$. With r = 0.21, n = 11 and p = 0.268, no statistically significant correlation was found between chlorophyll concentration and mean daily mfBRT (Figure 3.45). Despite the marginal increase in mfBRT during phytoplankton growth, when the oxygen saturation increased, a statistically significant correlation exists between mfBRT and oxygen saturation (Figure

3.46). A correlation coefficient of r = 0.745 with p = 0.000 for n = 145 was calculated, indicating that the two variables are correlated at the 0.01 significance level. DOC samples were not analysed for this experiment due to limited equipment availability.

Measurements of bulk water viscosity did not reveal any covariance with the chlorophyll concentration of the water although on day 12.5, viscosity was significantly higher (1.285 $mm^2\ sec^{-1}$) compared to all other days (Figure 3.47).

Surface tension values ranged between 73.3 mN m^{-1} and 73.7 mN m^{-1} (Figure 3.48) and did not show a significant trend with time or an obvious covariation with chlorophyll concentration. The total bacteria number showed a strong increase between days 0.5 and 5.5 from 9.7×10^5 cells ml^{-1} to 4.3×10^6 cells ml^{-1} (Figure 3.49). The bacteria number decreased again until day 7.5 to 1.1×10^6 cells ml^{-1} just before the addition of algae and nutrient medium. After addition, the number increased to 2.4×10^6 cells ml^{-1}. Until day 16.5, total bacteria number increased, reaching a maximum of 5.8×10^6 cells ml^{-1} on day 16.5. Between days 16.5 and 18.5, the bacteria number increased again to 4.6×10^6 cells ml^{-1}. The mean standard deviation of the total bacteria number was approximately ± 35%.

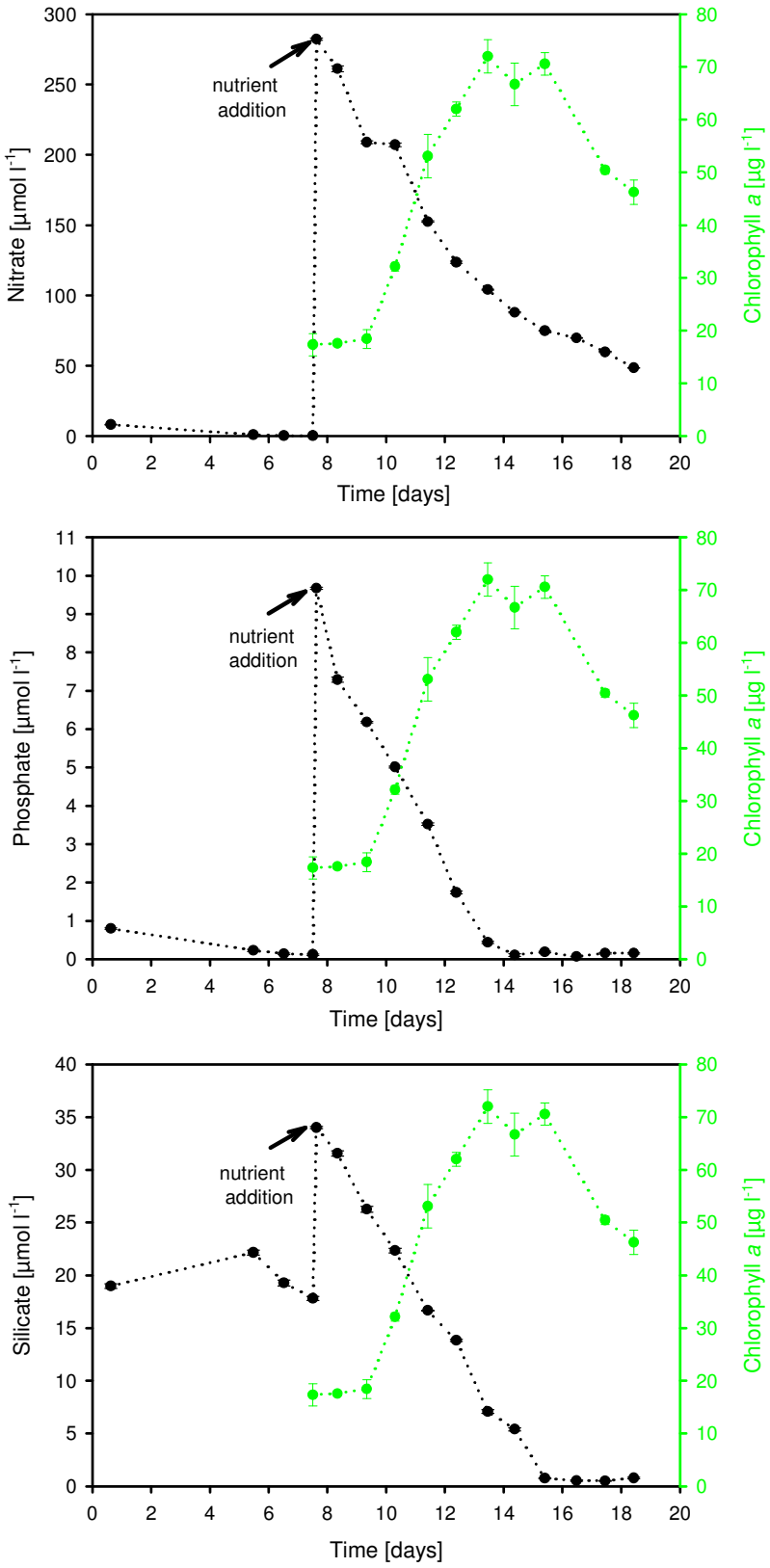

Figure 3.38 Changes in nitrate, phosphate, silicate and chlorophyll concentrations with time for experiment 4.
NO_3^- error bars: ± 0.07-2.1 µmol l^{-1}; PO_4^{3-} error bars: ± 0.02-0.07 µmol l^{-1}; Si error bars: ± 0.02-0.28 µmol l^{-1}; chlorophyll error bars: ± 0.7-4.1 µg l^{-1}.

Day No.	Δ NO_3^- (µmol l^{-1})	Δ PO_4^{3-} (µmol l^{-1})	Δ NO_3^-/ΔPO_4^{3-}	Δ Chlorophyll *a* (µg l^{-1})
7.5-8.5	-21	-2.3	9.1	+0.25
8.5-9.5	-53	-1.1	48.2	+0.83
9.5-10.5	-1	-1.2	0.8	+13.69
10.5-11.5	-55	-2.7	20	+21
11.5-12.5	-29	-1.8	16	+8.9
12.5-13.5	-19	-1.3	14	+10

Table 3.7 Nitrate and phosphate uptake, nutrient removal ratios and change in chlorophyll concentration during the exponential growth phase for experiment 4.

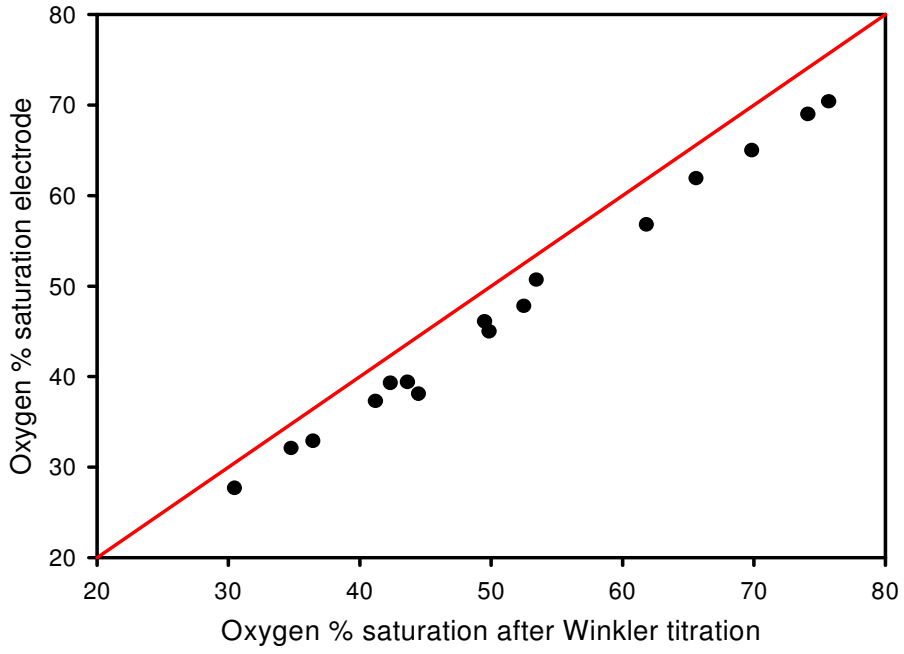

Figure 3.39 Oxygen saturation determined by Winkler titration versus oxygen saturation measured by electrode for experiment 4.
Key: red line = 1:1 ratio.

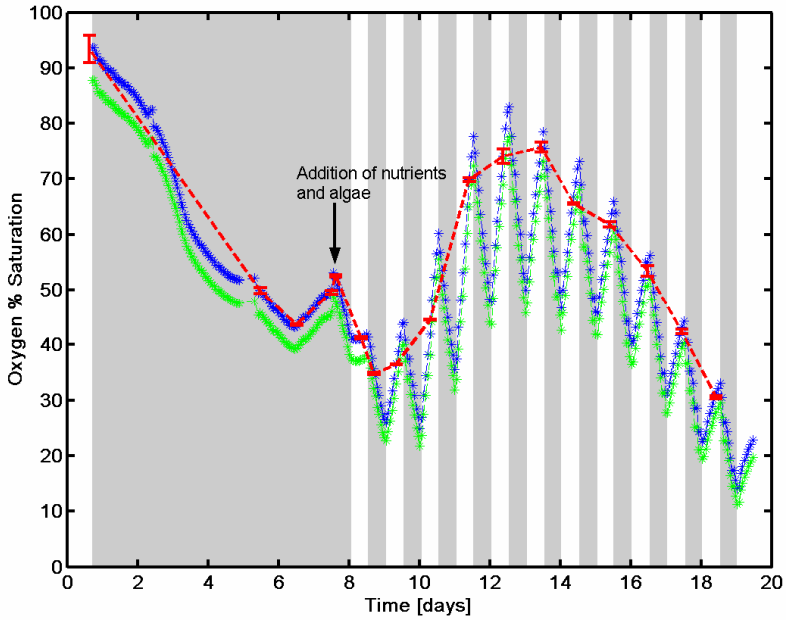

Figure 3.40 Changes in oxygen saturation with time for experiment 4.
Key: green data points: oxygen saturation measured by electrode; red data points: oxygen saturation Winkler controls (errorbars = +/- 0.4-2 %); blue data point: corrected oxygen saturation electrode; grey shaded areas: illumination off; white areas: illumination on.

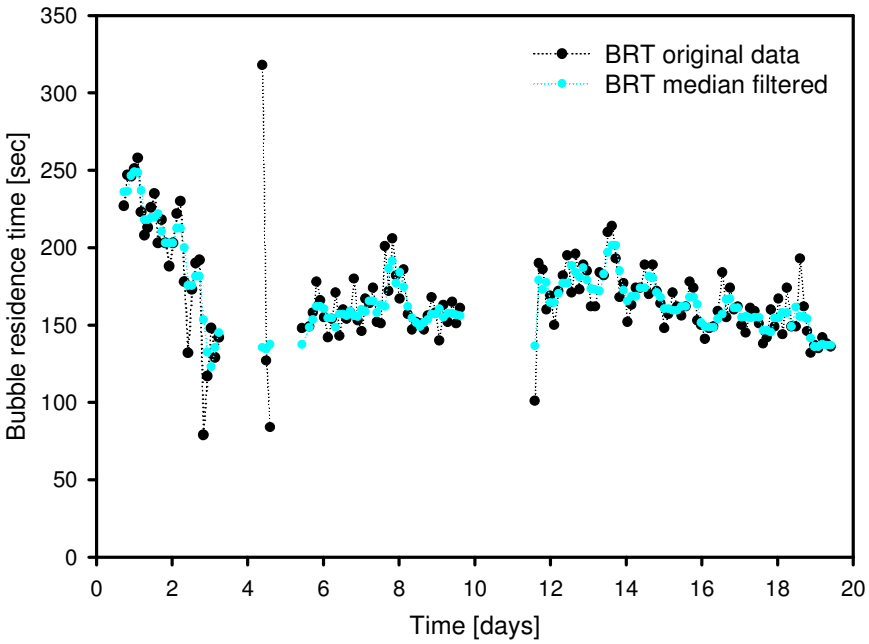

Figure 3.41 Comparison of original BRT and median filtered BRT for experiment 4.

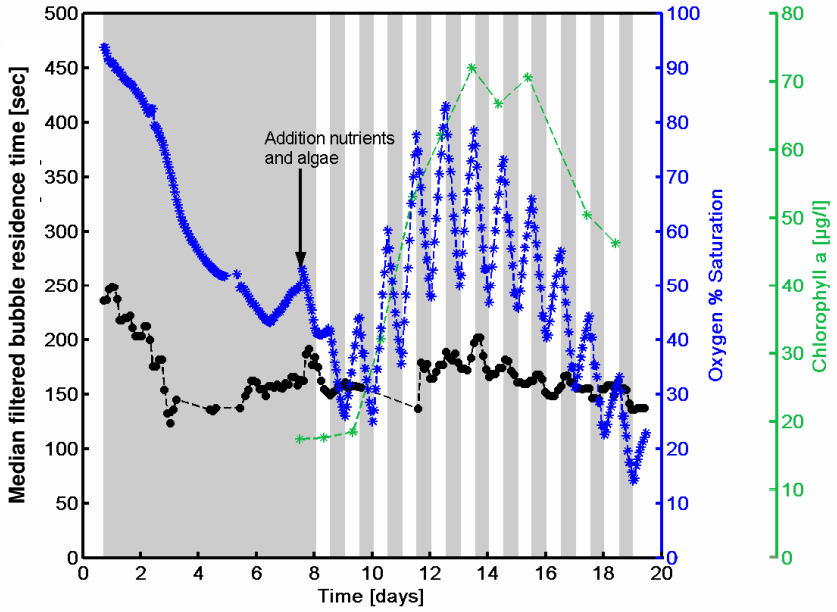

Figure 3.42 Changes in mfBRT, oxygen saturation and chlorophyll concentration with time for experiment 4.
Grey shaded areas: illumination off; white areas: illumination on.

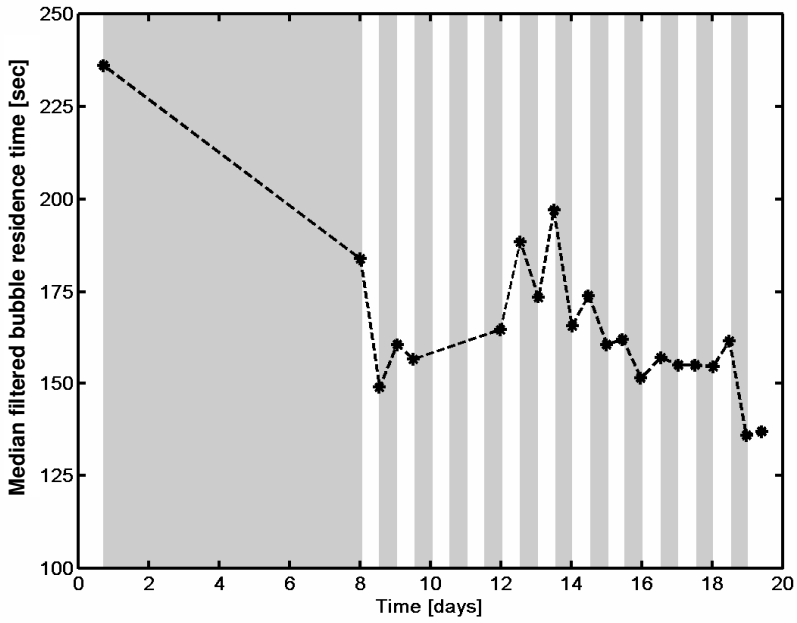

Figure 3.43 Changes in mfBRT with time - last data points of light and dark phase for experiment 4.
Grey shaded areas: illumination off; white areas: illumination on.

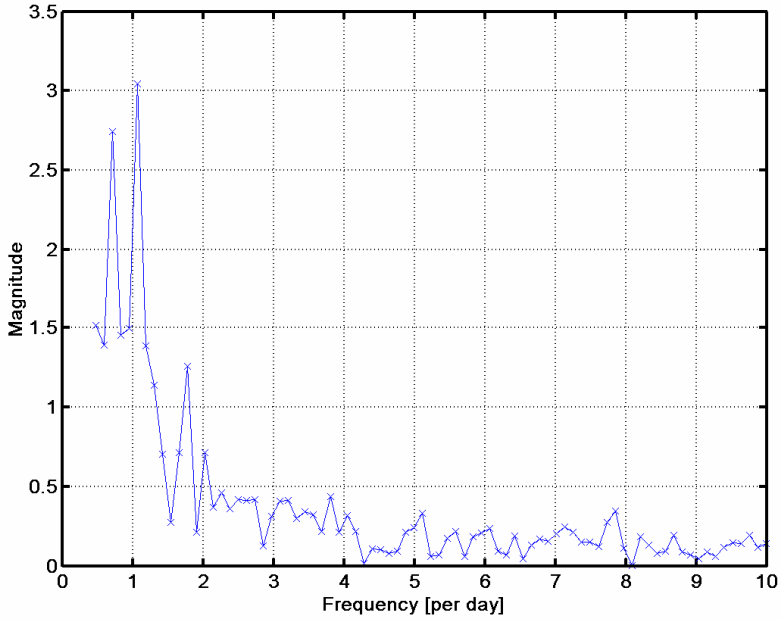

Figure 3.44 Fourier analysis for mfBRT data for experiment 4.
Highest peak at frequency 1 indicates light-dark change dependency of mfBRT.

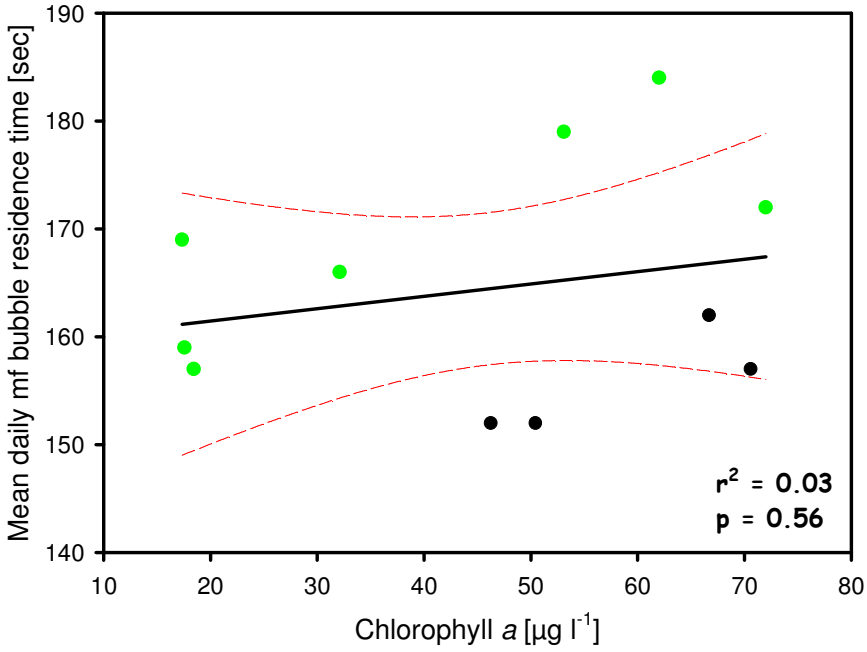

Figure 3.45 Chlorophyll concentration versus mean daily mfBRT for experiment 4.
Black solid line = linear regression; red dashed lines = 95% confidence intervals; green symbols = data points during chlorophyll increase; black symbols = data points during chlorophyll decrease.

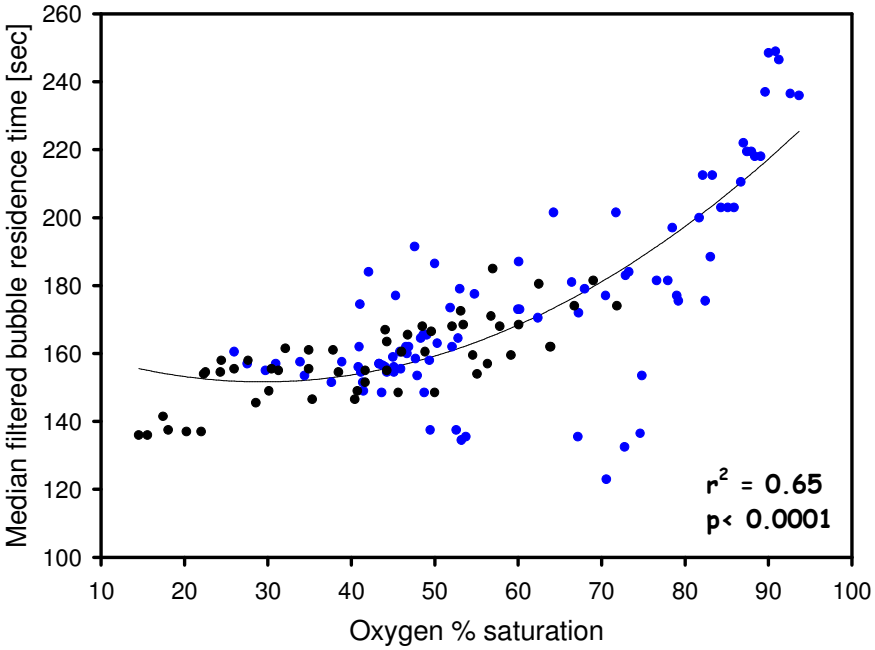

Figure 3.46 Oxygen saturation versus mfBRT for experiment 4.
Black solid line = Quadratic regression; red dashed lines = 95% confidence intervals; blue symbols = data points during oxygen increase; black symbols = data points during oxygen decline.

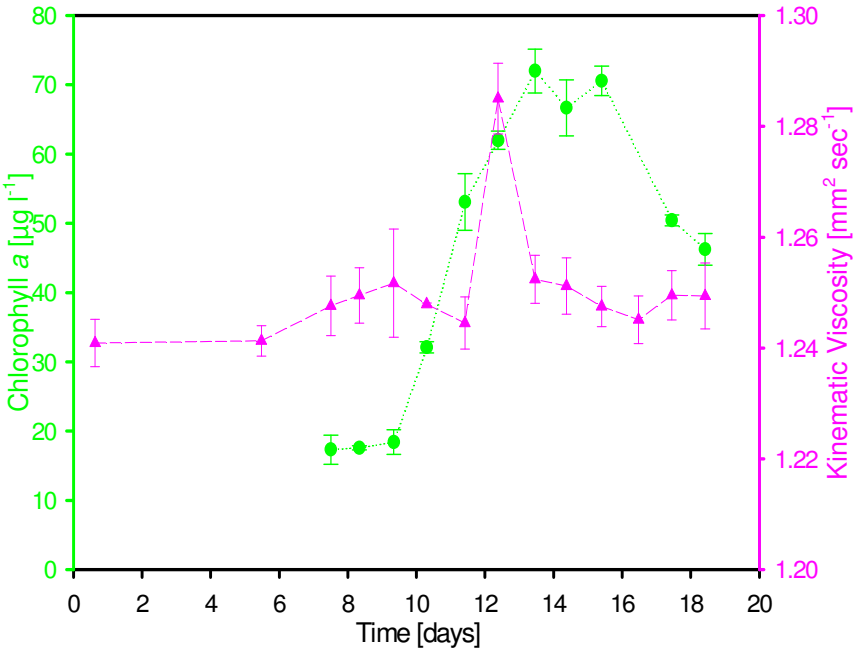

Figure 3.47 Changes in bulk water viscosity and chlorophyll concentration with time for experiment 4.
Viscosity error bars: ± 0.002-0.009 mm^2 sec^{-1}.

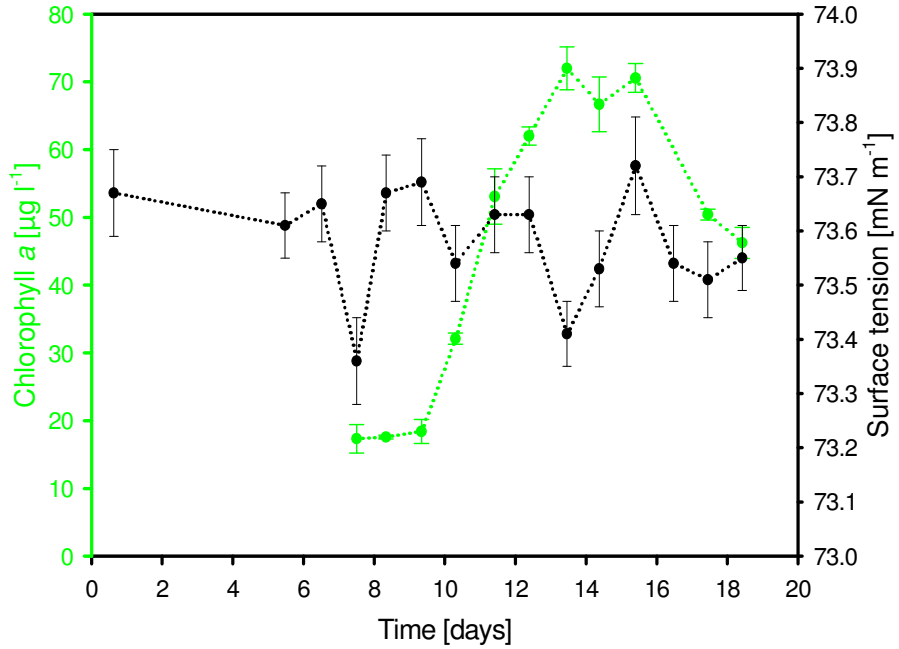

Figure 3.48 Changes in surface tension and chlorophyll concentration with time for experiment 4. Surface tension error bars: ± 0.06-0.09 mN m^{-1}.

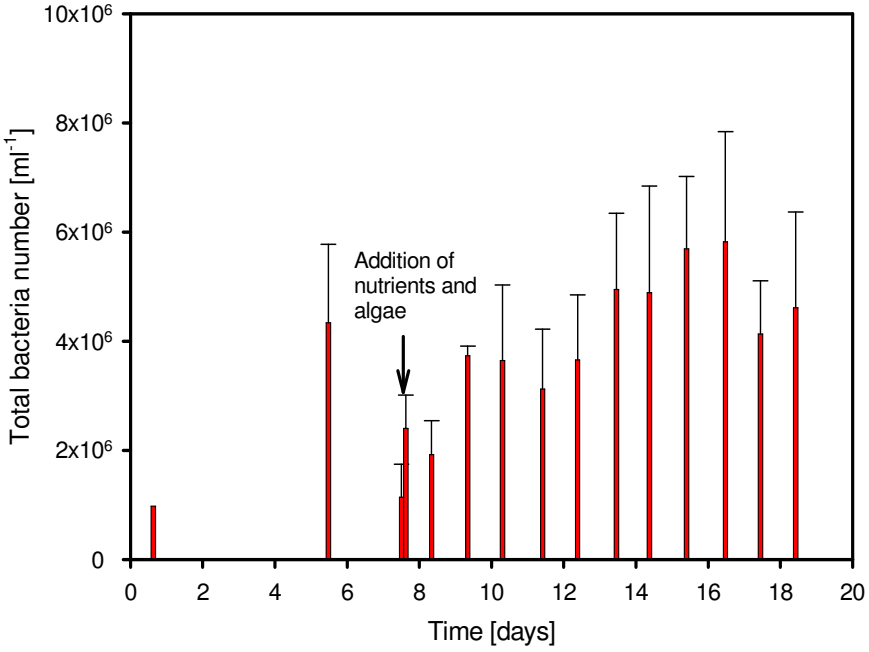

Figure 3.49 Changes in total bacteria numbers with time (per ml) for experiment 4. Error bars ± 2.0×10^5 - 2.0×10^6 cells ml^{-1}.

3.3.2 Growth experiment with Phaeocystis

The aim of this experiment was to investigate the influence of the colony-forming *Phaeocystis* sp. on BRT, which is known to release large amount of polysaccharides and causes foam phenomena regularly in the German Bight (Lancelot, 1994). Nutrient medium and culture were added on day 1.5 of the experiment. Chlorophyll concentration began to increase after day 2.5 from 1.2 to 4 µg l^{-1} on day 5.5 (Figure 3.50). Chlorophyll concentration then remained fairly constant between days 5.5 to 9.5 at approximately 4 µg l^{-1} (± 0.8). Chlorophyll concentration declined to 0.9 µg l^{-1} on day 12.5. The nutrient data (Figure 3.50 and Table 3.8) show that the *Phaeocystis* culture was not depleted in either nitrate or phosphate when growth ceased on day 9.5. Nitrate concentration declined between days 2.5 and 7.5 from 293 µmol l^{-1} to 231 µmol l^{-1}. On day 8.5, the nitrate increased again to 331 µmol l^{-1} (standard deviation of 25% on day 9) and declined slightly until day 11.5 to 308 µmol l^{-1}, followed by a further increase to 452 µmol l^{-1} on day 12.5. Phosphate concentration varied between 8 and 10 µmol l^{-1} between days 2.5 and 11.5 and increased to 13.28 µmol l^{-1} on day 12.5 (Table 3.8). Nitrite revealed an increasing trend throughout the whole experiment from 0.14 µmol l^{-1} to 0.49 µmol l^{-1} between days 1.5-12.5.

Comparison of the oxygen saturation data measured by the electrode to Winkler controls is shown in Figure 3.51. The data do not lie directly on the 1:1 line, however, O_2 % saturation $_{electrode}$ correlates significantly with O_2 % saturation $_{Winkler}$ ($r = 0.721$, $p = 0.006$ and $n = 11$). The oxygen electrode data were corrected using equation 3.3 ($r^2 = 0.96$):

$$O_2\ \%\ \text{saturation}_{corrected} = -6.73 + 1.11 \times O_2\ \%\ \text{saturation}_{electrode} \qquad \text{(Equation 3.3)}$$

Oxygen saturation increased from 86% on day 0.5 to 88.5% just after the addition of nutrients and culture to the tank water (Figure 3.52). With increasing chlorophyll concentration, oxygen saturation increased until day 6.5, when it reached 108%, showing increases in saturation during light phase and decreases during dark phase. Oxygen saturation remained at approximately 108% at the end of the illumination period between days 6.5 to 8.5. Increases in oxygen saturation during illumination were approximately 5% and decreases were approximately 6% during dark phase at the saturation maximum (days 6.5-8.5). When the chlorophyll concentration declined after day 8.5, oxygen saturation started to decrease to 96% at the end of the dark phase on day 11.0. Between days 11.0 and 11.5 oxygen saturation increased slightly to 98% and then declined continuously between days 12.5-14.5 to 81.5%.

Figure 3.53 shows a comparison of original BRT data and less scattered median filtered BRT data. Only median filtered BRT data are further described.

At the start of the experiment, mfBRT was approximately 175 seconds (Figure 3.54). The initial decline in mfBRT observed for the previous monoculture growth experiment (experiment 4) did not occur, possibly because no severe oxygen consumption took place as a result of less bacterial activity compared to experiment 4, before mfBRT measurements began (see section 2.7.5). With the addition of nutrient medium and the *Phaeocystis* culture (initial chlorophyll concentration in the tank = 1.26 µg l^{-1}) on day 1.5 and the first short illumination period, mfBRT increased slightly to 190 seconds while the oxygen saturation increased from 85 to 88%. Between days 2.0 and 4.5, when chlorophyll concentration and oxygen saturation increased to 3.2 µg l^{-1} and 104 % (on day 4.5), mfBRT remained constant at about 200 seconds, with small fluctuations that did not show any obvious phase changes with the light-dark periods of the tank system. From day 5.5 onwards, when the oxygen saturation reached 106 % during light phase, small increases in mfBRT of approximately 20 seconds were found during light phase and decreases of about 20 seconds occurred during dark phase. The light-dark phase changes of mfBRT are illustrated in Figure 3.55, where only the last datum point of each light and dark phase is shown. The Fourier analysis of mfBRT data shows several peaks at frequencies 1, 1.5 and 2 (Figure 3.56), indicating that there was significant scatter in mfBRT data and that mfBRT did not always follow the light dark changes in oxygen saturation. However, the peak with the highest magnitude at frequency 1 indicates that the light dark changes were strongest as opposed to the smaller fluctuations. The chlorophyll maximum occurred between days 7.5 and 8.5 with 4.4 µg l^{-1} and on the same days, oxygen saturation reached its maximum with 108 and 109% respectively during light phase. Mean daily mfBRT increased from ~ 200 seconds (day 4.5) to 217 and 219 seconds during the chlorophyll maximum. Day and night fluctuations in mfBRT were less clearly marked between days 8.0 and 10.0 as the daily mean oxygen saturation and chlorophyll concentration began to decrease. Mean daily mfBRT also decreased slightly to 206 seconds during this period. Between days 11.0 and 14.5, the tank was illuminated constantly, however, this did not result in any increase of oxygen saturation or mfBRT. On the contrary, oxygen saturation declined to 81% and mfBRT decreased to a mean daily value of 186 seconds. Despite the very small increase in mfBRT with increasing oxygen saturation, a correlation exists between the two parameters with $r = 0.694$, $p = 0.000$ and $n = 271$ and is significant at $\alpha = 0.01$ (Figure 3.58). Correlation between mean daily mfBRT and chlorophyll concentration

was not as strong but with r = 0.624, p = 0.020 and n = 11 the correlation was statistically significant at α= 0.05 (Figure 3.57).

Mean DOC concentration (Figure 3.59) declined slightly during the exponential growth phase from 155 µmol l^{-1} to 145 µmol $l^{-1}$and remained constant during the stationary phase (days 5.5-9.5). During the decline phase (days 9.5-12.5), a slight increase in DOC occurred from 142 µmol l^{-1} to 167 µmol l^{-1}. The standard deviation for DOC triplicates was always below 10%, most standard deviations were about 5%.

Bulk water viscosity showed no obvious covariation with chlorophyll concentration (Figure 3.60) with values ranging between 1.06 and 1.08 mm^2 sec^{-1}. Viscosity remained fairly constant during most of the experiment except from day 1.5 to day 2.5, when it increased from 1.06 mm^2 sec^{-1} to 1.08 mm^2 sec^{-1}.

Total bacteria number showed little variation between days 1.5 and 4.5 with approximately 8.6×10^5 cells ml^{-1} (Figure 3.61). Between days 4.5 and 7.5, the number increased to 3.3×10^6 cells ml^{-1}. The maximum in the total bacteria number on day 7.5 corresponds to the chlorophyll maximum. Total bacteria number decreased again to 9.1×10^5 cells ml^{-1} on day 10.5. Between days 11.5 and 12.5, a slight increase occurred again to 1.5×10^6 cells ml^{-1}. The standard deviation of total bacteria numbers was approximately ± 30%.

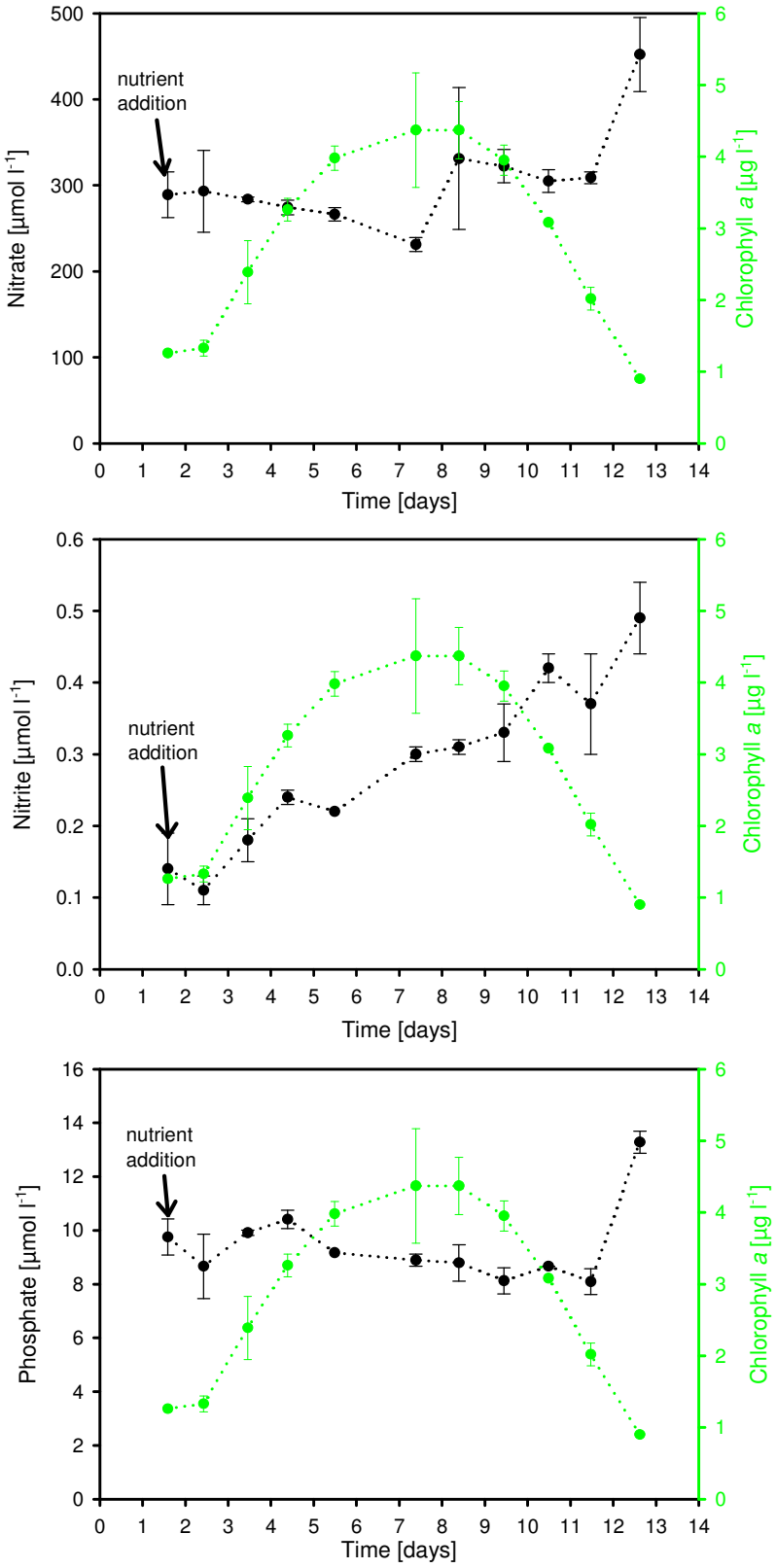

Figure 3.50 Changes in nitrate, phosphate, nitrite and chlorophyll concentrations with time for experiment 5.
NO_3^- error bars: ± 2-82 µmol l^{-1}; PO_4^{3-} error bars: ± 0.01-1.2 µmol l^{-1};
NO_2^- error bars: ± 0.01-0.07 µmol l^{-1}; chlorophyll error bars: ± 0.04-0.8 µg l^{-1}.

Day No.	Δ NO_3^- (µmol l^{-1})	Δ PO_4^{3-} (µmol l^{-1})	Δ $NO_3^-/\Delta PO_4^{3-}$	Δ Chlorophyll *a* (µg l^{-1})
1.5-2.5	+4	-1.1	-	+0.07
2.5-3.5	-10	+1.25	-	+1.07
3.5-4.5	-9	+0.5	-	+0.86
4.5-7.5	-8	-1.25	6.4	+0.72
7.5-8.5	-32	-0.27	118	+0.39

Table 3.8 Nitrate and phosphate uptake, nutrient removal ratios and change in chlorophyll concentration during the exponential growth phase for experiment 5.

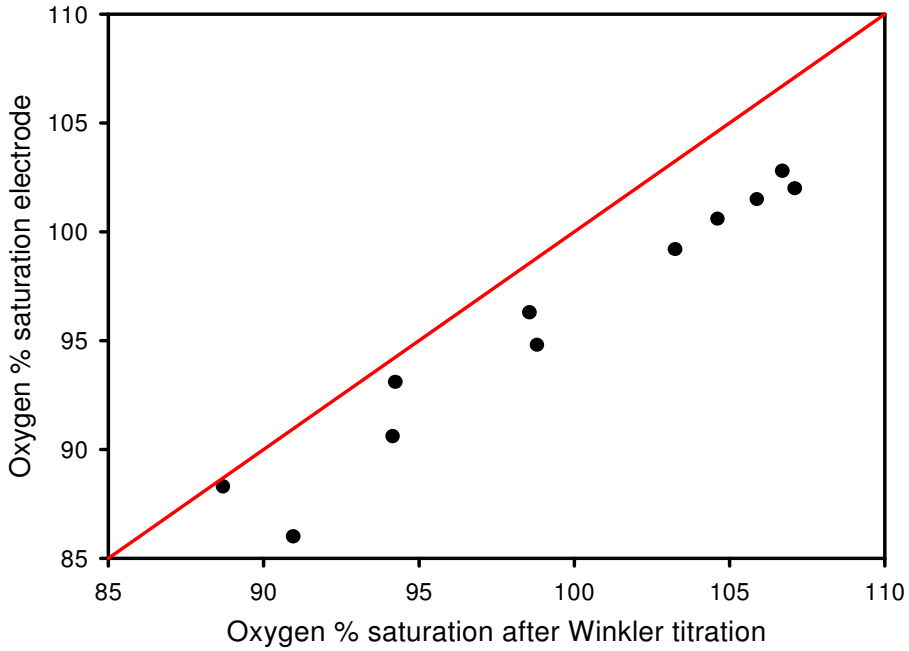

Figure 3.51 Oxygen saturation determined by Winkler titration versus oxygen saturation data measured by electrode for experiment 5.
Key: red line = 1:1 ratio.

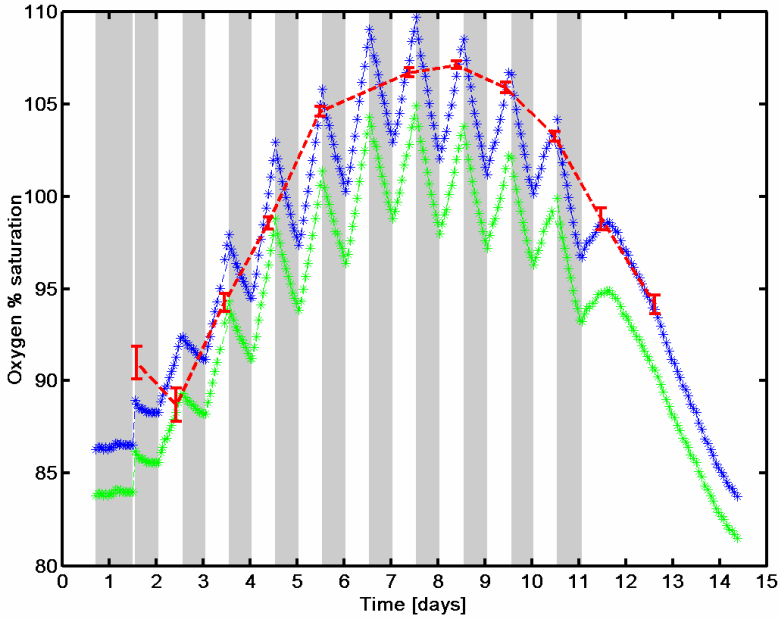

Figure 3.52 Changes in oxygen saturation with time for experiment 5.
Key: green data points: oxygen saturation measured by electrode; red data points: oxygen saturation Winkler controls (errorbars = ± 0.2-0.9 %); blue data point: corrected oxygen saturation electrode; grey shaded areas: illumination off; white areas: illumination on.

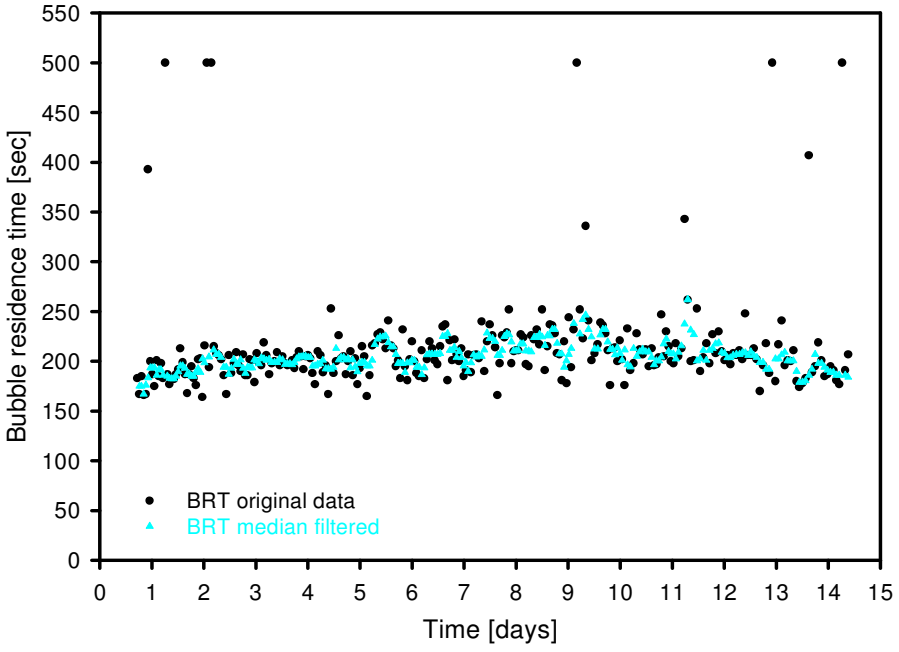

Figure 3.53 Comparison of BRT and median filtered BRT for experiment 5.

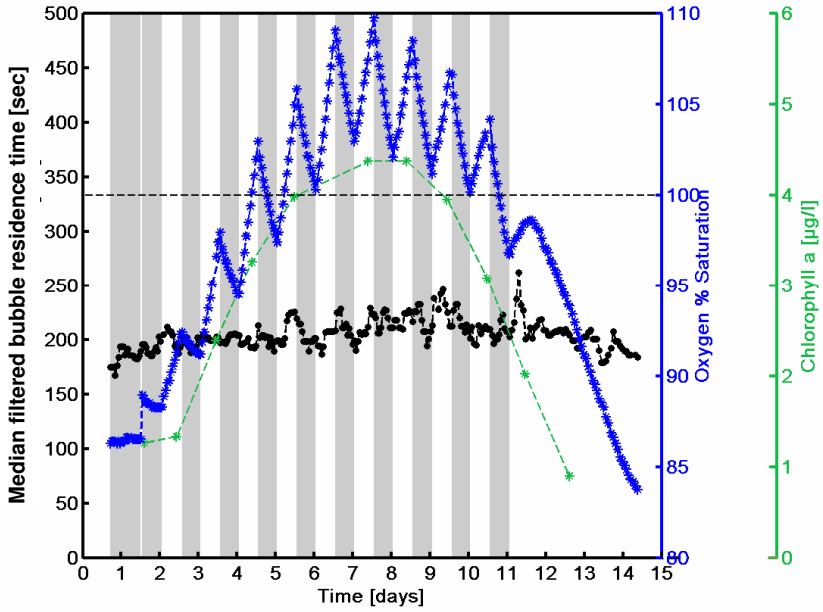

Figure 3.54 Changes in mfBRT, oxygen saturation and chlorophyll concentration with time for experiment 5.
Grey shaded areas: illumination off; white areas: illumination on; dashed line: 100% saturation threshold.

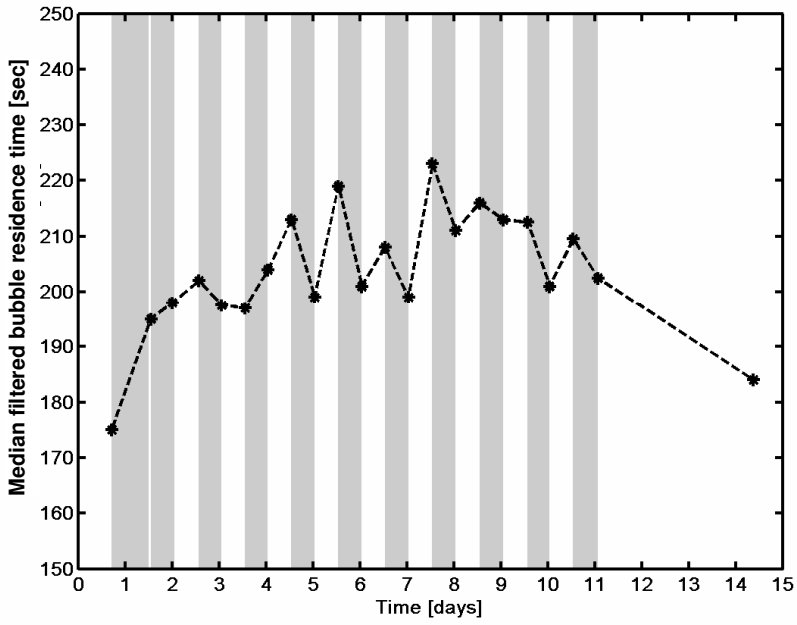

Figure 3.55 Changes in mfBRT with time - last data points of light and dark phase for experiment 5.
Grey shaded areas: illumination off; white areas: illumination on.

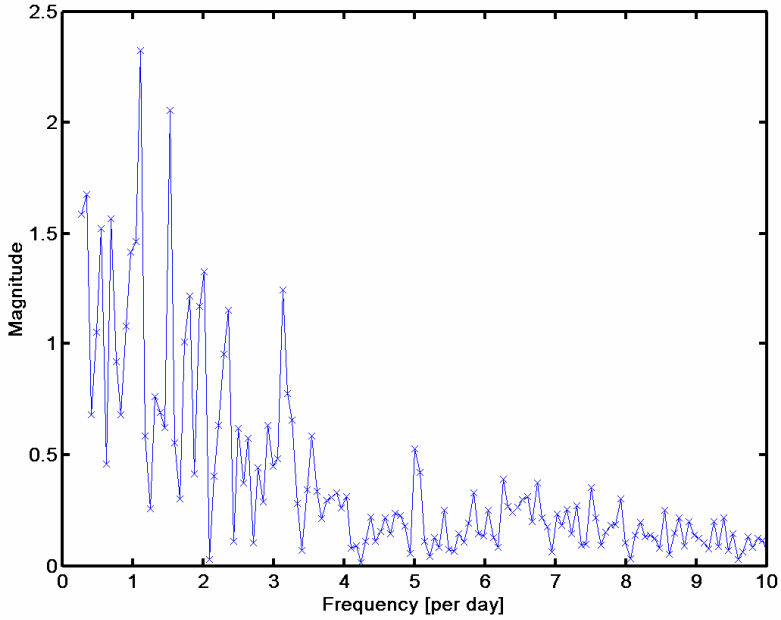

Figure 3.56 Fourier analysis for mfBRT data for experiment 5.
Peak at frequency 1 indicates some light-dark dependency of mfBRT.

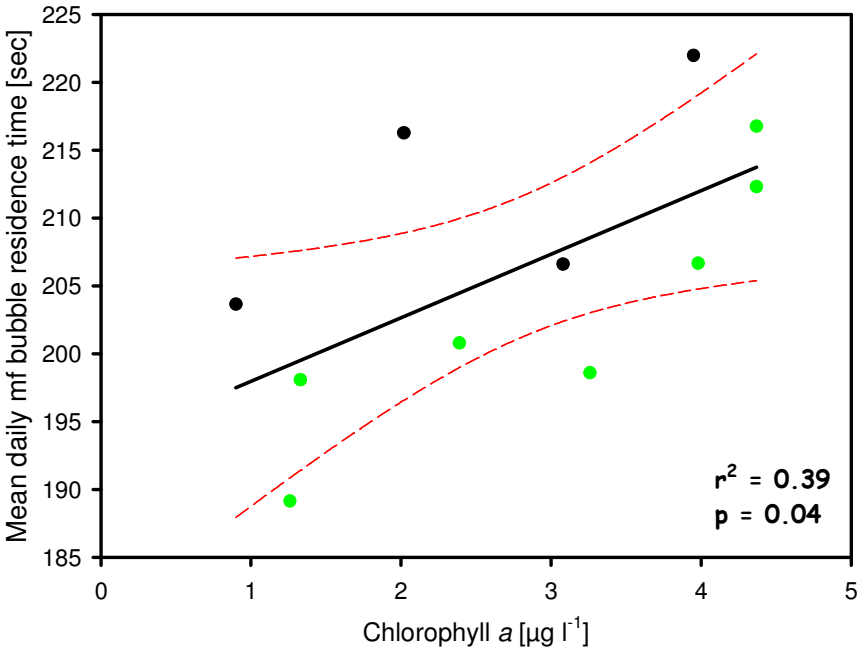

Figure 3.57 Chlorophyll concentration versus mean daily mfBRT for experiment 5.
Black solid line = linear regression; red dashed lines = 95% confidence intervals; green symbols = data points during chlorophyll increase; black symbols = data points during chlorophyll decrease.

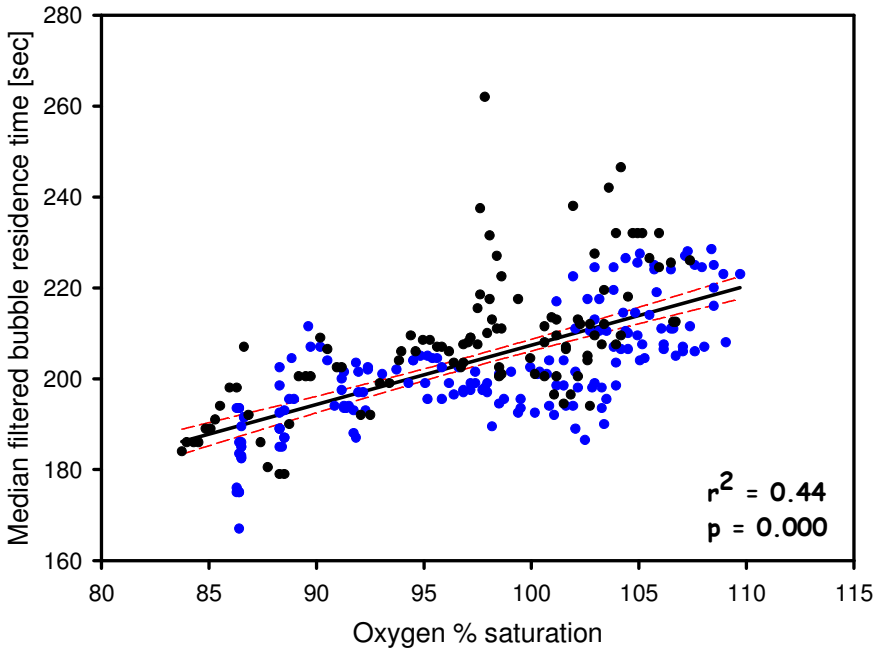

Figure 3.58 Oxygen saturation versus mfBRT for experiment 5.
Black solid line = linear regression; red dashed lines = 95% confidence intervals; blue symbols = data points during oxygen increase; black symbols = data points during oxygen decline.

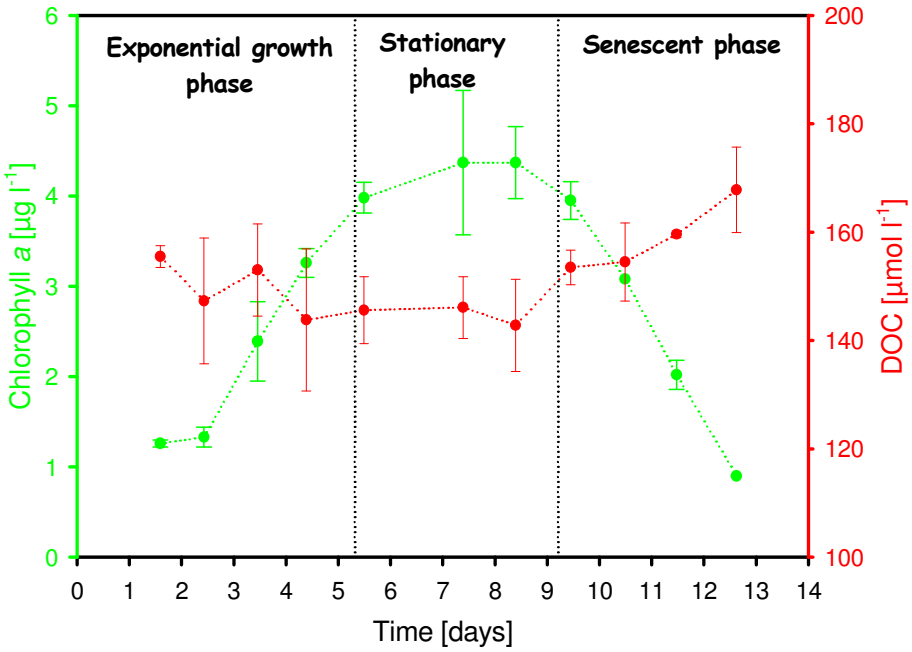

Figure 3.59 Changes in DOC and chlorophyll concentrations with time for experiment 5.
DOC error bars: ± 0.6-13 µmol l^{-1}.

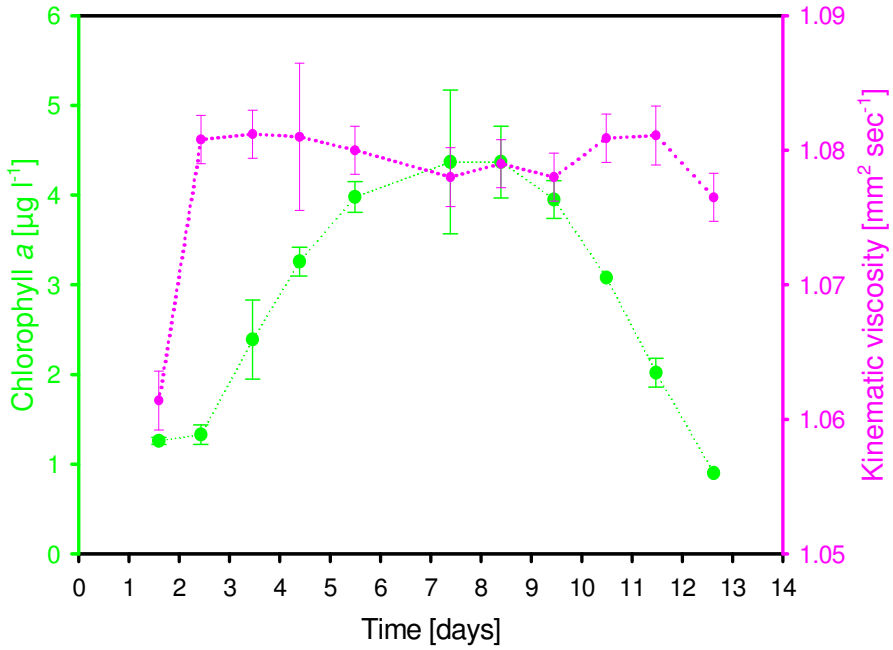

Figure 3.60 Changes in bulk water viscosity and chlorophyll concentration with time for experiment 5. Viscosity error bars: ± 1.7×10^{-3}-5.4×10^{-3} mm^2sec^{-1}.

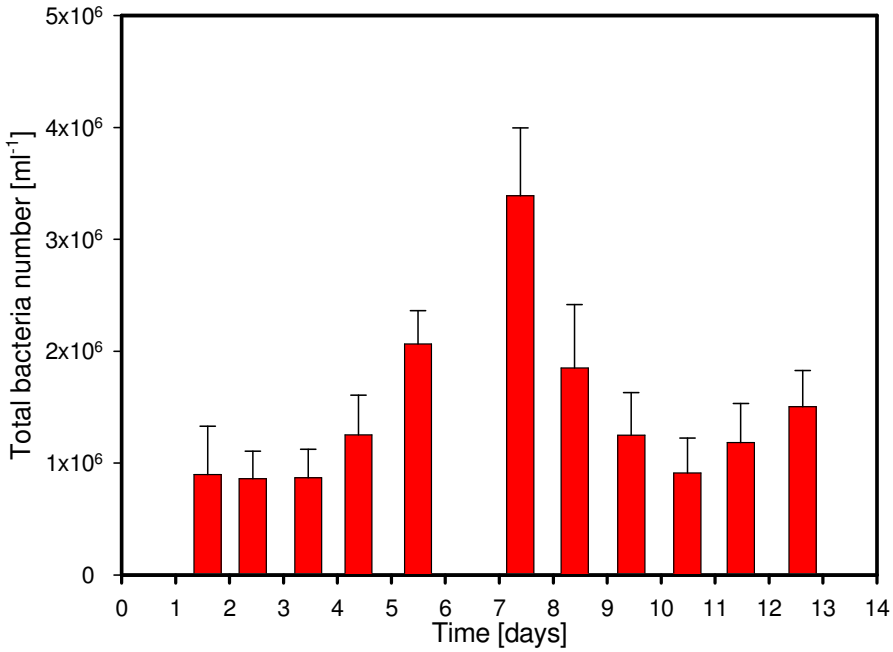

Figure 3.61 Changes in total bacteria numbers with time (per ml) for experiment 5. Error bars: ± 2.4×10^5 – 6.0×10^5 cells ml^{-1}.

3.3.3 Growth experiment with Nitzschia closterium

The aim of this experiment was to investigate the influence of *Nitzschia closterium* growth on BRT in the tank system. This species is known to be responsible for the mucilage phenomena in the Northern Adriatic Sea and its production of extracellular material (Revelante and Gilmartin, 1991). Nutrients and algae were added to filtered North Sea water on day 1.5 of the experiment. Chlorophyll concentration declined from an initial concentration of 21 µg l^{-1} to 10 µg l^{-1} between days 1.5 and 2.5 (Figure 3.62) due to sedimentation of some cells to the tank floor. Between days 2.5 and 9.5, the chlorophyll concentration increased to 24 µg l^{-1}. Between days 9.5 and 12.5, chlorophyll concentration remained fairly constant at approximately 25 µg l^{-1} (± 2; Figure 3.62). A drop in chlorophyll concentration to 17.4 µg l^{-1} (± 1) occurred on day 13.5 followed by an increase to 23 µg l^{-1} on day 14.5. Chlorophyll concentration began to decline from day 16.5 to 1.4 µg l^{-1} on day 21.5. The nutrient data (Figure 3.62) revealed that the algae were not limited in inorganic nutrients throughout the experiment. Nitrate decreased gradually from an initial concentration of 319 µmol l^{-1} (day 1.5) just after the addition of nutrient medium to 222 µmol l^{-1} on day 21.5. Phosphate showed a similar gradual decrease as nitrate from an initial concentration of 11 µmol l^{-1} (day 1.5) to 5.8 µmol l^{-1} (day 21.5). The nutrient removal ratio was close to Redfield from days 1.5-2.5 (~11) and days 3.5-4.5 (15, Table 3.9). Between days 2.5-3.5, nitrate was removed more rapidly than phosphate (nutrient removal ratio of ~ 6). Silicate concentration increased between days 1.5 and 2.5 from 25 to 28 µmol l^{-1} and then remained constant until day 6.5. On day 7.5, the silicate had decreased to 17 µmol l^{-1} and then increased again to 21 µmol l-1 on day 10.5. After day 10.5, silicate concentration remained constant for the remaining period of the experiment.

Oxygen saturation measured by the electrode and Winkler oxygen data show good agreement (Figure 3.63) and are close to the 1:1 ratio. Before the addition of nutrients and culture, oxygen saturation of filtered North Sea water was 96% between days 0.5 and 1.5. Shortly after the addition of nutrients and the *Nitzschia closterium* culture (from day 2.5), oxygen saturation began to increase, showing distinct light phase increases and dark phase decreases (Figure 3.64). Between days 2.0 and 6.5, oxygen saturation increases from 96% to a maximum of 150%. Saturation increased approximately by 22% during light phase and decreased by 11% during dark phase. Saturation remained constant during days 6.5-11.5 (maximum of 150% during light phase, minimum of 132 during dark phase). Between days 11.5-12.5, when the tank illumination was off for a period of 24 hours, oxygen saturation decreased from 150% to 118%. Between days12.5-13.5, when the tank system was

illuminated for 24 hours, saturation increased again to142%. From days 13.5 to 16.5 (again 12/12 hour light dark cycle), oxygen saturation declined slightly from a maximum of 142% to 135%, still showing distinct light-dark changes. From day 17.5, the light dark changes became much smaller until they ceased completely from days 18.0 to 23.5, when saturation declined to a minimum of 63%.

BRT data for experiment 6 showed much more scatter (Figure 3.65) than for most other experiments although it is unclear why this should be. Plotting both original BRT and median filtered BRT with an offset (Figure 3.65) indicates that some of the peaks/very low values of BRT may be attributed to real variability at maximum/minimum oxygen saturation just before the change of light/dark phase. However, as median filtered BRT shows the transition between light and dark phase more clearly, median filtered BRT data were used for all further analysis. Following the filling the tank with filtered North Sea water on day 0.5, mfBRT decreased from 240 to 220 seconds during the first day (Figure 3.66). Then with the addition of algae and nutrient medium, mfBRT stabilised at about 220 seconds. With increasing chlorophyll concentration and oxygen saturation, mfBRT increased consistently from 220 to 350 seconds on day 5.5 (Figure 3.66). From days 4.0 to 18.0, mfBRT showed light-dark fluctuations with increases during light period, when the oxygen saturation increased, and decreases during darkness, when the saturation decreased (Figure 3.67). Differences in the mfBRT values between dark phase and light phase were about 80 seconds at the chlorophyll and oxygen saturation maximum (~25 $\mu g\ l^{-1}$ and 150% respectively) during days 8.0 to 12.0, when mfBRT reached maximum values of 420 seconds during light phase. Fourier analysis of mfBRT data (Figure 3.68) shows a distinct peak at a frequency of 1, clearly indicating the light-dark dependency of mfBRT. On days 11.5 and 12.5, when the light dark cycle was changed to 24 hours, the strong decrease in oxygen saturation during dark phase (150-117%), covaried with a strong decline in mfBRT from 400 to 225 seconds (Figure 3.66). During the following 24 hour light phase, the increase in oxygen saturation was accompanied by an increase in mfBRT to 400 seconds by the end of the light phase. The change of the light/dark cycle to 24 hours was supposed to show that mfBRT would drop/rise consistently even if the duration of the light/dark phase was changed. From days 14.0-17.0, the oxygen saturation declined slightly as did mfBRT, however, the light dark fluctuations were still visible until day 18.0. Between days 18.0 and 23.5, when chlorophyll concentration and oxygen saturation declined rapidly, mfBRT decreased to a mean value of approximately 170 seconds. MfBRT and oxygen saturation correlate strongly with a correlation coefficient of $r = 0.928$ with a p-value of

0.000 and n = 507. The relationship between oxygen saturation and mfBRT can be described by quadratic regression (Figure 3.70) with $r^2 = 0.96$. Chlorophyll concentration and daily mean mfBRT also showed good correlation with r = 0.757, p = 0.000 and n = 21 and Figure 3.69 shows that both variables are linearly related.

DOC values did not change significantly during the exponential growth phase (~135 µmol l^{-1}, Figure 3.71). During the stationary phase (days 7.0-17.0), DOC increased to 195 µmol l^{-1} and continued to increase during the senescent phase (days 17.0-21.5) to 245 µmol l^{-1}.

Bulk water viscosity shows some increase (0.905 mm^2 sec^{-1} to 0.910 mm^2 sec^{-1}) during the exponential growth phase between days 1.5 and 7.0 as chlorophyll concentration increased (Figure 3.72). Another increase in viscosity occurred between days 7 and 13 (increase to 0.915 mm^2 sec^{-1}). However, the range of viscosity values is very small (0.905 mm^2 sec^{-1} – 0.915 mm^2 sec^{-1}) and the standard deviations are large compared to the small range of values ($\pm 1.8\times10^{-3}$ - 8.2×10^{-3} mm^2 sec^{-1}).

The total bacteria number per ml in the tank water increased between days 1.5 and 5.5 from 3.4×10^6 cells ml^{-1} to 9.3×10^6 cells ml^{-1}, followed by a decrease between days 6.5 and 8.5 to 1.2×10^6 cells ml^{-1} (Figure 3.73). From day 9.5 to day 13.5, another increase in the total bacteria number occurred to 5.5×10^6 cells ml^{-1}. Between days 15.5 and 18.5, a further increase to 9.8×10^6 cells ml^{-1} was followed by another decline (days 19.5 and 20.5) to 3.6×10^6 cells ml^{-1}. The standard deviation of total bacteria number was ~ ± 25% on average.

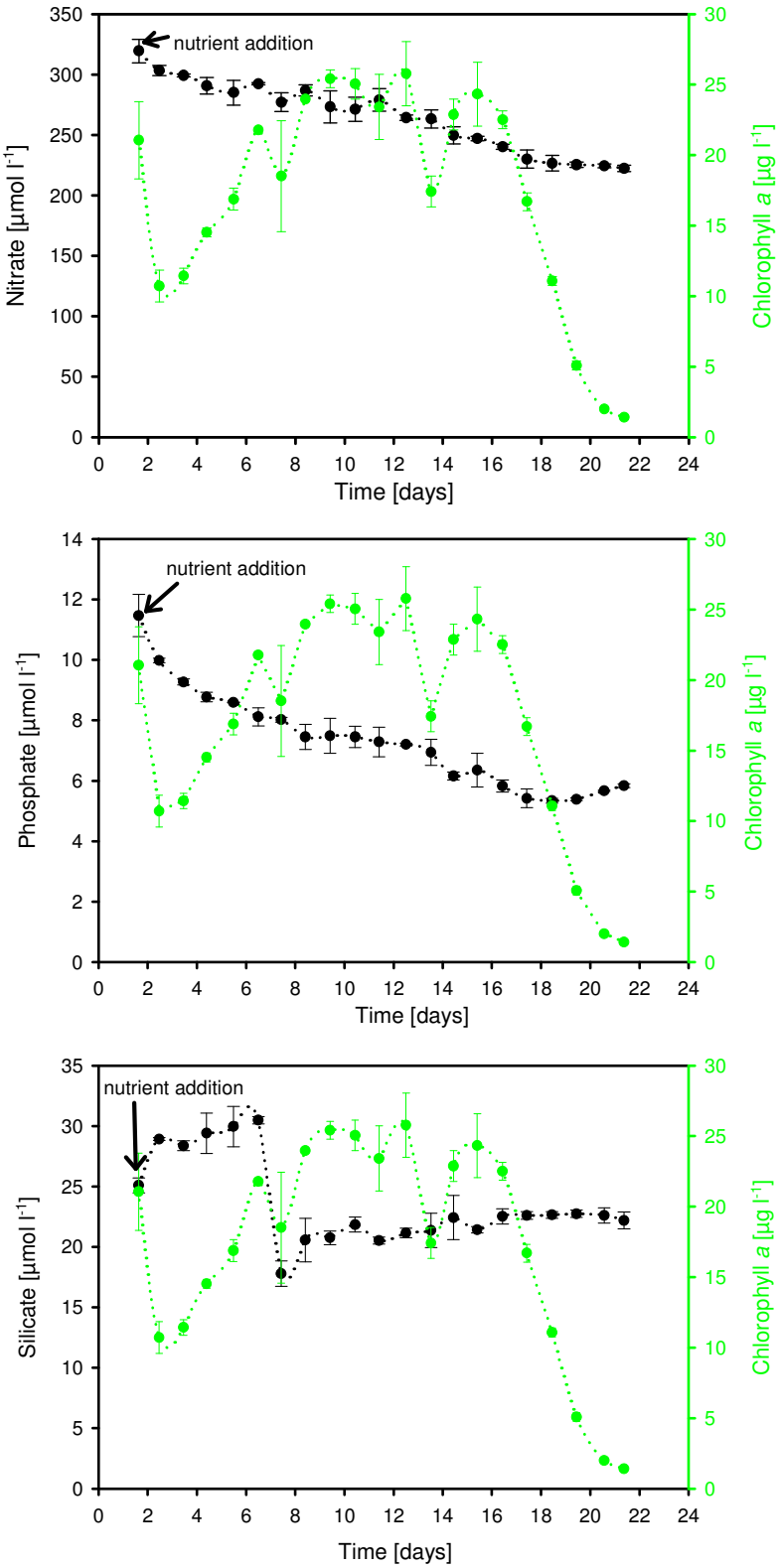

Figure 3.62 Changes in nitrate, phosphate, silicate and chlorophyll concentrations with time for experiment 6.
NO_3^- error bars: ± 1-13.2 µmol l^{-1}; PO_4^{3-} error bars: ± 0.02-0.7 µmol l^{-1}; Si error bars: ± 0.1-1.8 µmol l^{-1}; chlorophyll error bars: ± 0.1-2.7 µg l^{-1}.

Day No.	Δ NO_3^- (µmol l^{-1})	Δ PO_4^{3-} (µmol l^{-1})	Δ NO_3^-/ΔPO_4^{3-}	Δ Chlorophyll *a* (µg l^{-1})
1.5-2.5	-16	-1.5	10.6	-11
2.5-3.5	-4	-0.7	5.7	+0.7
3.5-4.5	-9	-0.6	15	+3.1
4.5-5.5	-5.5	-0.1	55	+2.3
5.5-6.5	-15	-0.5	30	+5
6.5-7.5	+9	-0.1	-	-3.3
7.5-8.5	-13	-0.5	26	+5.5

Table 3.9 Nitrate and phosphate uptake, nutrient removal ratios and change in chlorophyll concentration during the exponential growth phase for experiment 6.

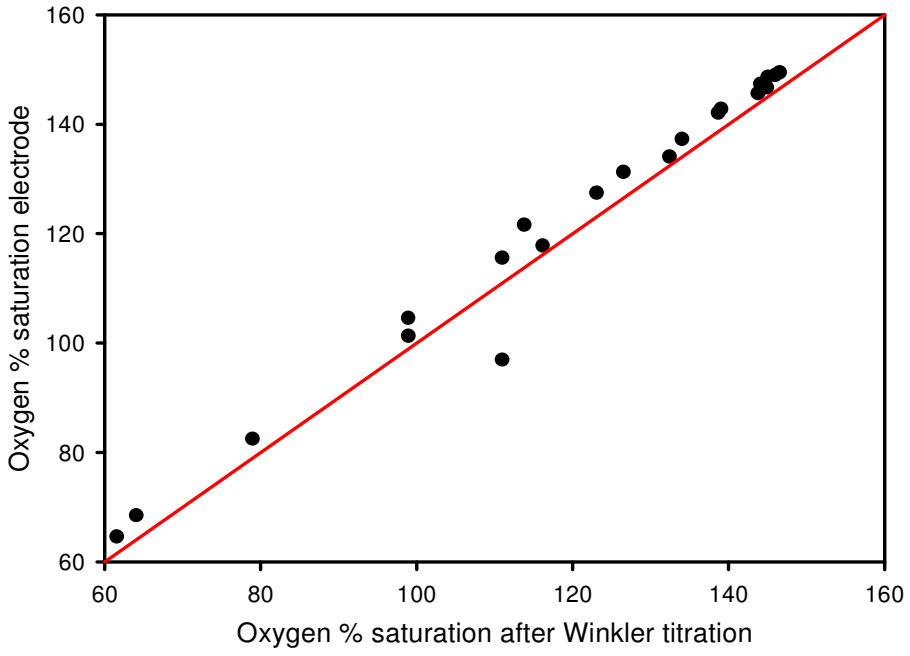

Figure 3.63 Oxygen saturation determined by Winkler titration versus oxygen saturation data from electrode for experiment 6.
Key: red line = 1:1 ratio.

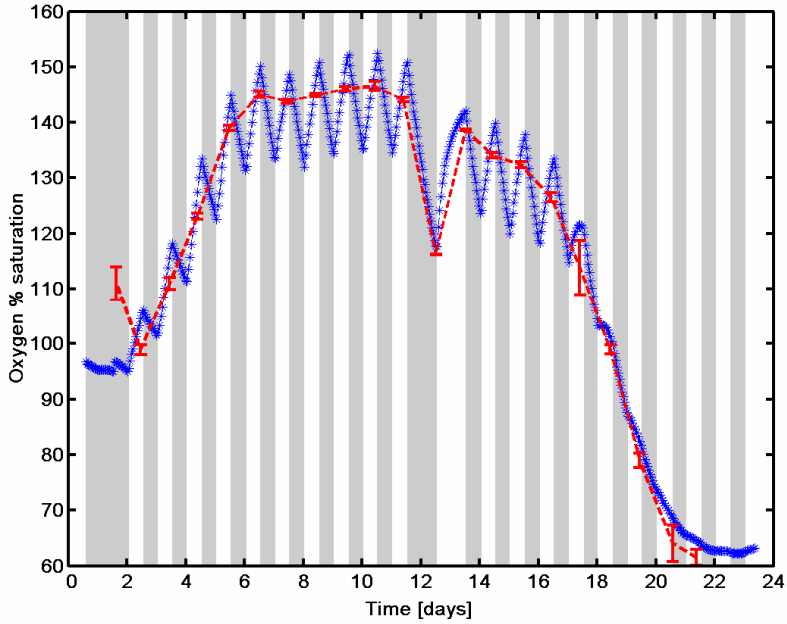

Figure 3.64 Changes in oxygen saturation with time for experiment 6.
Grey shaded areas: illumination off; white shaded areas: illumination on;
Red symbols: oxygen saturation$_{Winkler}$; blue symbols: oxygen saturation$_{electrode}$; error bars: ± 0.1-3.3 %.

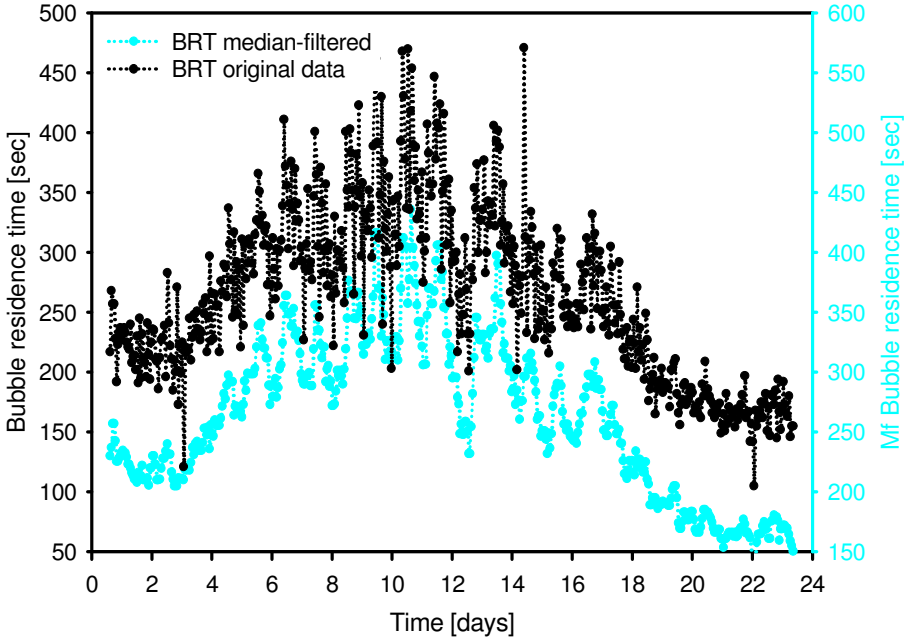

Figure 3.65 Comparison of BRT and median filtered BRT for experiment 6.

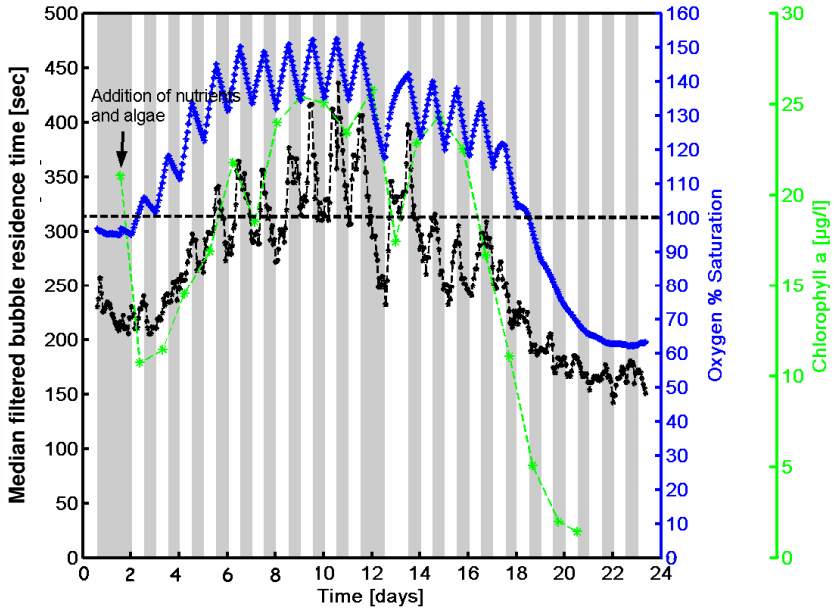

Figure 3.66 Changes in mfBRT, oxygen saturation and chlorophyll concentration with time for experiment 6.
Grey shaded areas: illumination off; white areas: illumination on.

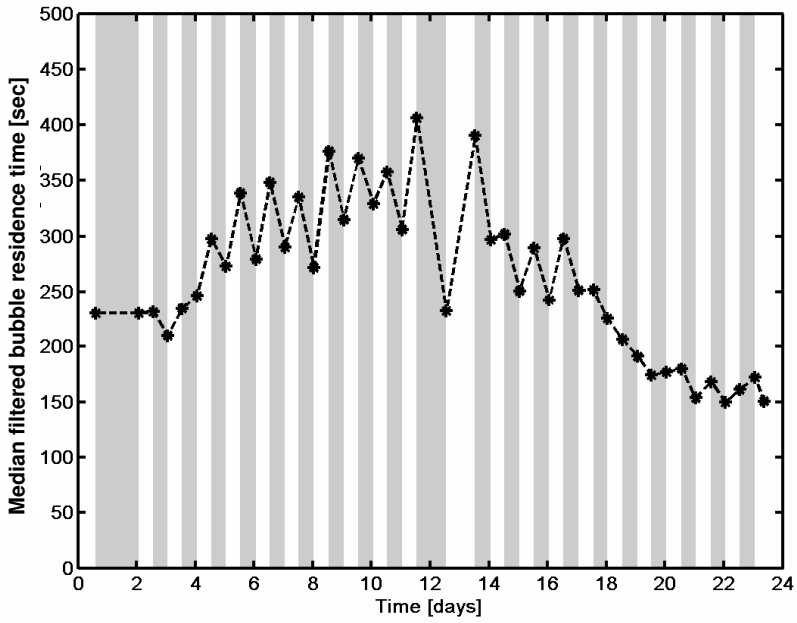

Figure 3.67 Changes in mfBRT with time - last data points of light and dark phase for experiment 6.
Grey shaded areas: illumination off; white areas: illumination on.

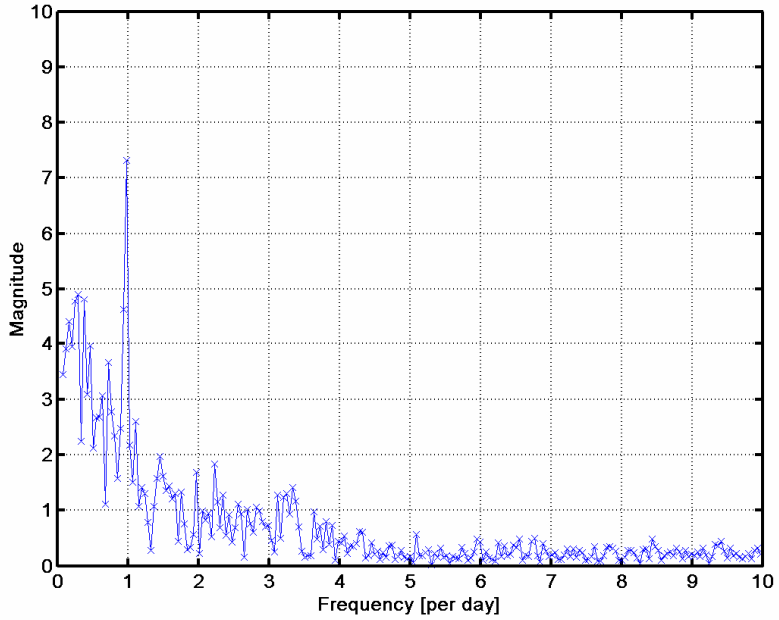

Figure 3.68 Fourier analysis of mfBRT for experiment 6.
The distinct peak at frequency 1 indicates that the fluctuations in mfBRT data occurred at regular intervals corresponding to the light-dark cycle of the tank system.

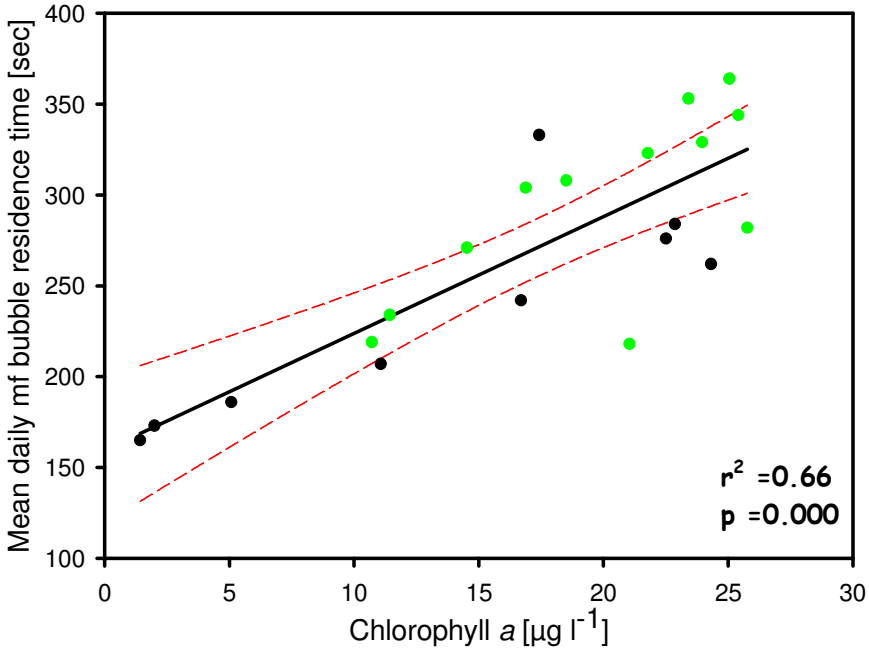

Figure 3.69 Chlorophyll concentration versus mean daily mfBRT for experiment 6.
Black solid line = linear regression; red dashed lines = 95% confidence intervals; green symbols = data points during chlorophyll increase; black symbols = data points during chlorophyll decrease.

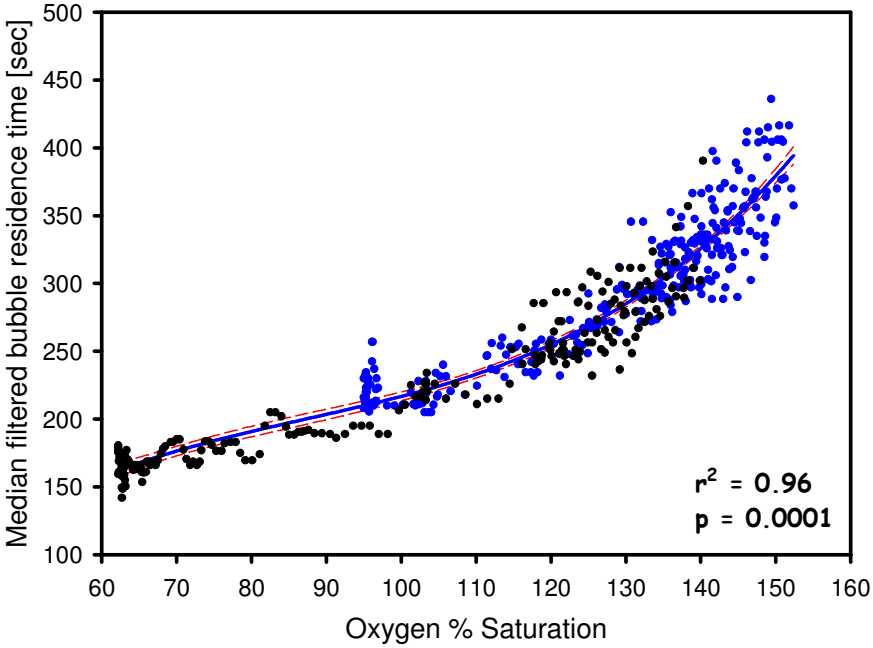

Figure 3.70 Oxygen saturation versus mfBRT for experiment 6.
Black solid line = quadratic regression; red dashed lines = 95% confidence intervals; blue symbols = data points during oxygen increase; black symbols = data points during oxygen decline.

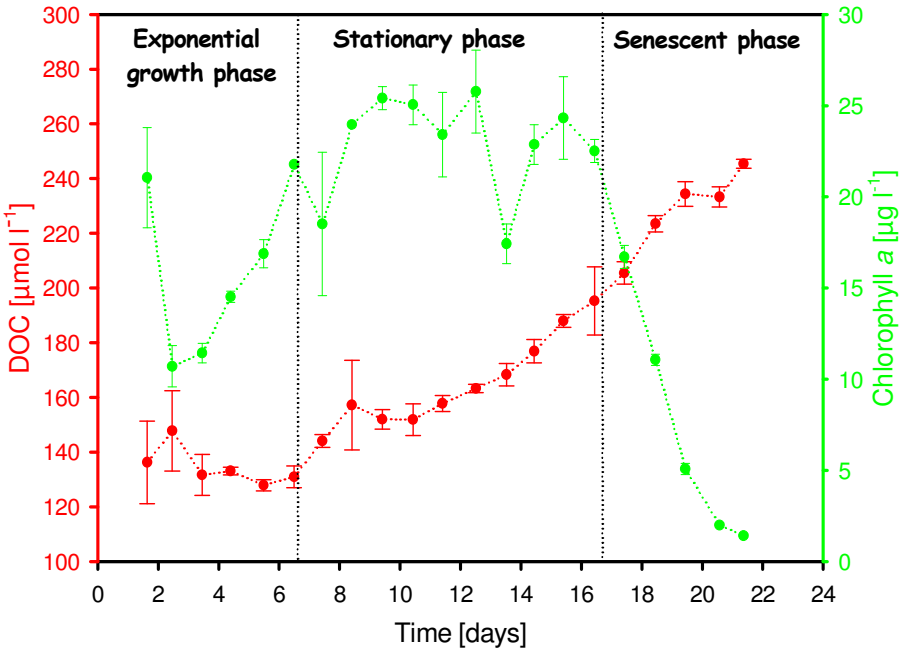

Figure 3.71 Changes in DOC and chlorophyll concentrations with time for experiment 6.
DOC error bars: ± 1.4-16.4 µmol l^{-1}.

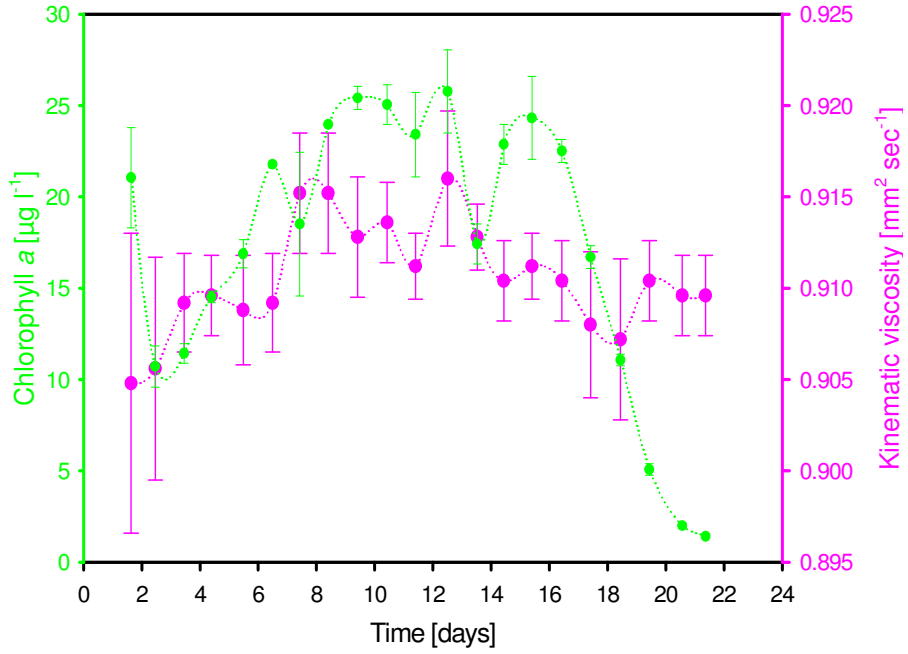

Figure 3.72 Changes in bulk water viscosity and chlorophyll concentration with time for experiment 6. Viscosity error bars: ± 1.8×10^{-3}-8.2×10^{-3} mm^2 sec^{-1}.

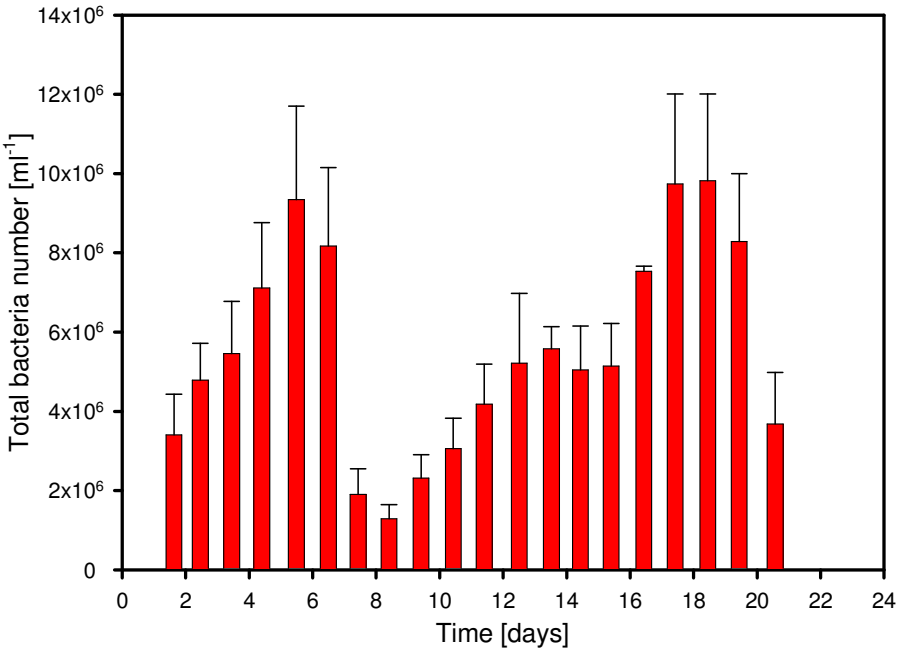

Figure 3.73 Changes in total bacteria numbers with time (per ml) for experiment 6. Error bars: ± 8.3×10^{5}-6.7×10^{6} cells ml^{-1}.

3.4 Gas saturation experiments

3.4.1 First saturation experiment

BRT and oxygen saturation

Results from the phytoplankton growth experiments described in sections 3.2 and 3.3 have shown that the main influence on BRT appears to be the degree of oxygen saturation of the water as a result of phytoplankton photosynthesis and that organic exudates appear to matter little as no direct correlation was found between DOC concentration and BRT. To verify the influence of oxygen saturation on BRT, it was attempted to physically change the oxygen saturation of water in the absence of phytoplankton. A number of gas saturation experiments were carried out to investigate the influence of oxygen saturation by bubbling deionised water with oxygen and nitrogen and by water temperature changes. Deionised water was used as this was easily produced and would minimise the effect of salt and other organic substances on BRT. Details of the experimental procedure are given in section 2.10.

For the first gas saturation experiment, median filtered BRT data is used (for comparison of original BRT data and median filtered data see Figure 3.74) to reduce the amount of scatter. During the first 5 days of mfBRT measurement, a slight decline in mfBRT occurred from 190 seconds to 170 seconds, while the oxygen saturation of the tank water increased slightly from 70% to 80% (Figure 3.75). On day 4.5, the water temperature was increased from 12°C to 18°C and mfBRT increased simultaneously to a maximum of 400 seconds when the temperature reached 18°C. While the temperature remained at 18°C, mfBRT declined immediately after its maximum value of 400 seconds and reached 190 seconds after 4.4 days. With the increase of water temperature to 18°C, the oxygen saturation increased from 80% to 90% and then declined slowly to 88% during the 18°C period. Given that oxygen solubility decreases by 2% per °C, one would have expected a theoretical oxygen saturation of 92% after the 6°C temperature increase. The water temperature was then reduced to 12°C again on day 8.5 and oxygen saturation was reduced to 79% and mfBRT decreased further from 150 to 140 seconds. When the tank water was first bubbled with air on day 10.5, oxygen saturation increased to 105% with a coincident increase in mfBRT to 250 seconds. Both oxygen saturation and mfBRT then declined gradually again after the bubbling had ceased to 96% saturation and 198 seconds respectively. When the tank water was bubbled again on day 13.5, the oxygen saturation increased again to 103% and mfBRT increased to 215 and then to 230 seconds. Saturation and mfBRT gradually declined further until the water temperature was increased to 18°C

on day 14.5, which resulted in an increase in oxygen saturation to 107% and an increase in mfBRT to a maximum of 473 seconds. Again, the expected increase due to changing oxygen solubility would have been slightly higher (110%) than the observed (107%). Once the temperature had reached 18°C, mfBRT and oxygen saturation started to decline again. MfBRT reached a consistent value of approximately 200 seconds 2 days after the temperature increase while the oxygen saturation declined gradually until the next air bubbling was carried out (96.8%). On day 17.5, the water was again bubbled with air and the oxygen saturation increased to 101% and mfBRT increased to 220 seconds. Both mfBRT and oxygen saturation declined once the bubbling stopped. The bubbling of tank water with pure oxygen for 2 minutes on day 20.5 resulted in an oxygen supersaturation of 170%. Saturation then gradually declined with time. However, no significant change in mfBRT occurred, while the water was highly supersaturated with oxygen. Bubbling of tank water with nitrogen for approximately 2 minutes on day 21.5 of the experiment resulted in a reduction of oxygen saturation from 132% to 40%. MfBRT showed an increase from 166 seconds to 220 seconds immediately following the bubbling period. MfBRT declined gradually after ceasing the nitrogen bubbling to approximately 176 seconds and oxygen saturation increased slowly from 40% to 60% within the next 1.6 days.

Theoretical calculation of nitrogen saturation

As the warming and cooling of the deionised water as well as the bubbling with oxygen and nitrogen did not only affect the oxygen saturation but the total gas saturation of the water, which mainly consists of oxygen and nitrogen, an attempt was made to reconstruct the theoretical nitrogen saturation of the water. It is assumed that at the start of the experiment, nitrogen and oxygen were present at equal saturations. As the oxygen saturation at the start of the experiment was 75%, it is assumed that the nitrogen saturation of the tank water was also at 75%. It is further assumed that nitrogen began to equilibrate with the atmosphere across the tank surface during days 0.5-4.5 of the experiment similarly to oxygen. As the solubility of nitrogen with temperature is similar to that of oxygen (~ -2% per °C), warming of the water by 6°C on day 4.5 resulted in a nitrogen saturation of approximately from 79% to 91%. Cooling by 6°C on day 8.5 resulted in a nitrogen saturation of ~ 79%. Bubbling with air from a depth z =1 m, nitrogen saturation should have increased to 105%, given that there was an increase in saturation of ½ % per 0.1 m and that the average depth of air bubbles was z/2 as:

% saturation at z/2 = 100+5z (Equation 3.4)

where z = depth of bubbling in metres.

If it is assumed that nitrogen saturation after bubbling was similar to oxygen saturation, then this calculation is correct as oxygen saturation was ~105% following air bubbling on day 10.5. Bubbling with oxygen on day 20.5 replaced a significant fraction of the nitrogen in the deionised water by oxygen. Eventually, by bubbling with oxygen, the partial pressure of oxygen at 1 m bubbling depth should be 1.05 atmospheres, while the partial pressure of nitrogen should reach 0 when equilibrium is reached. This would mean that the tank water would theoretically be saturated by 525%. However, as the oxygen saturation of the tank water was only 170%, the nitrogen saturation of the water can be calculated as follows:

$p\_O_2 + p\_N_2 = 1.05$ atmospheres and (Equation 3.5)

$p\_O_2 = O_2$ Saturation/100 × $p_O_2$atmosphere (Equation 3.6)

N_2 saturation (%) = p_N_2/p_N_2atmosphere × 100 (Equation 3.7)

where p_O_2 and p_N_2 are the partial pressures of oxygen and nitrogen after bubbling with oxygen and $p_O_2$atmosphere and $p_N_2$atmosphere are the partial pressures of oxygen and nitrogen in 1 atmosphere of air (~0.2 and 0.8 atmospheres respectively).

This gives a theoretical nitrogen saturation of ~ 88% after bubbling with oxygen.

Using equations 3.5, 3.6 and 3.7, the theoretical nitrogen saturation after bubbling with nitrogen would have been approximately ~ 121%.

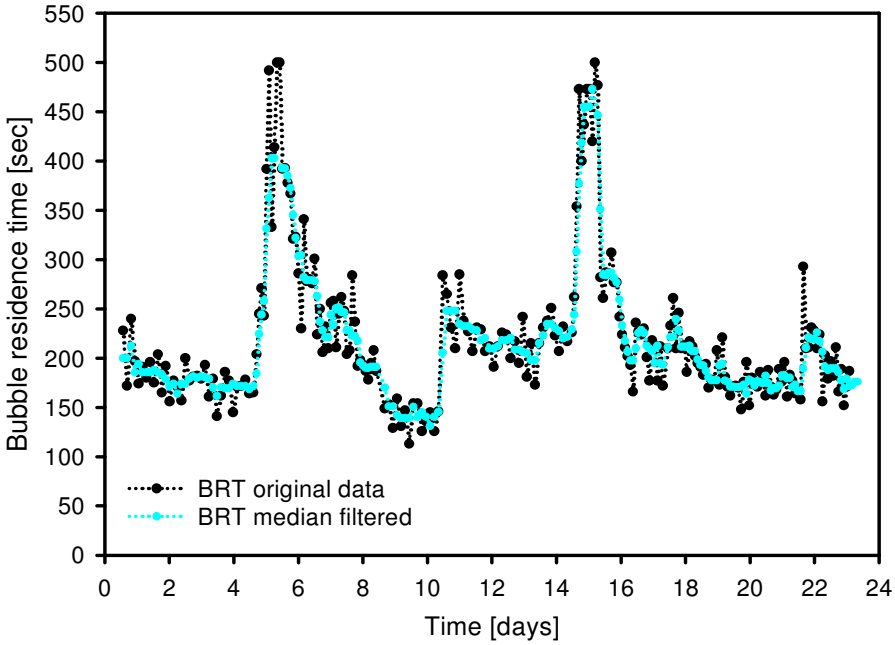

Figure 3.74 Comparison of original BRT data and median filtered BRT data for experiment 9.

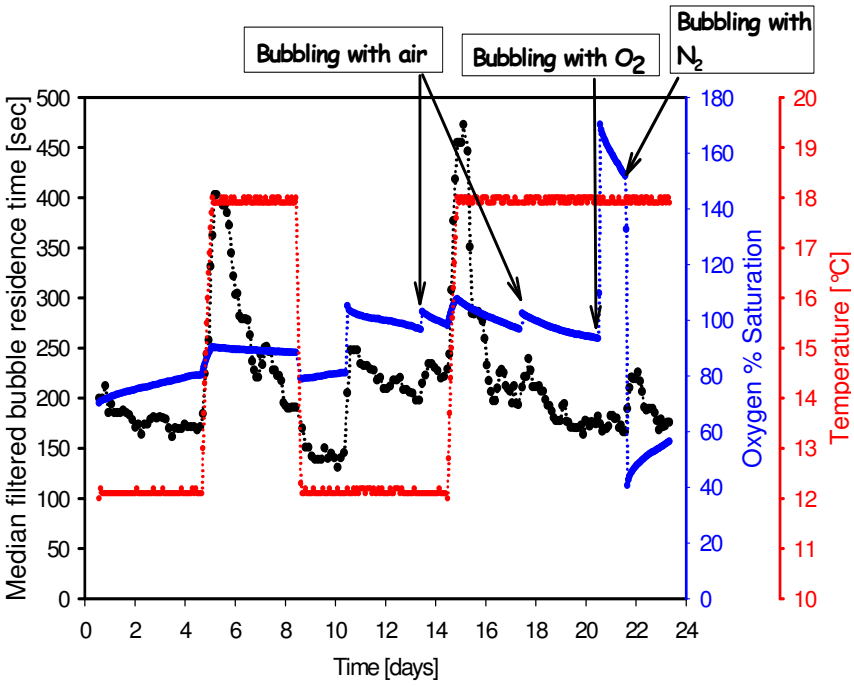

Figure 3.75 Changes in mfBRT, oxygen saturation and water temperature with time for experiment 9.

3.4.2 Second saturation experiment

The previous gas saturation experiment described in section 3.4.1 showed that oxygen saturation could only be increased via bubbling with air or changes in water temperature. Therefore another gas saturation experiment was conducted to investigate changes in oxygen saturation through changing the water temperature and the effects on BRT in order to further investigate the role of oxygen saturation with respect to BRT. Oxygen saturation was recorded continuously by the electrode but samples for Winkler determination of oxygen saturation were taken during several occasions of the experiment. Oxygen saturations determined by the electrode show very good agreement with the Winkler samples (Figure 3.77).

To reduce scatter of BRT data, a median filter was applied (see section 2.2.4). MfBRT (for original BRT data refer to Figure 3.76) increased slightly during the first 3.5 days of the experiment from 111 seconds to 135 seconds (Figure 3.78). During this time, the oxygen saturation increased gradually from an initial value of 72% to 78.2% after 3.5 days. Following a brief measurement interruption between days 3.5 and 4.5, the oxygen saturation of the tank water had increased further to 85.2% and mfBRT had increased to 160 seconds. Between days 4.5 and 7.5, when the water inlet was fitted on top of the tank system, the oxygen saturation increased more steeply from 85% to 98.5%. MfBRT increased slightly from 160 to 218 seconds over this period. When the water inlet was changed back to the bottom of the tank system, this resulted in a slight decrease in oxygen saturation to 97% between days 7.5 and 8.5 and mfBRT declined to 190 seconds. When the water temperature was increased on day 8.5 from 12°C to 23°C, the oxygen saturation increased simultaneously to 110.7% while mfBRT increased to 450 seconds. The maximum saturation was reached before the water temperature had reached its maximum of 23°C. The theoretical oxygen saturation should have increased by approximately 22% for the temperature increase of 11°C to a saturation of 119%, so the actual oxygen saturation after warming of the water was lower. Between days 9.0 and 10.5, mfBRT remained high at approximately 450 seconds, while the oxygen saturation had already declined gradually. Between days 10.5 and 11.0, a decrease in mfBRT occurred to 300 seconds, followed by another increase to 400 seconds on day 11.5. Between days 11.5 and 12.0, mfBRT declined rapidly to 230 seconds and then declined more gradually to approximately 200 seconds for the remaining days of the experiment. Oxygen saturation declined continuously to 92% until day 13.5. On day 14.5, another small increase in oxygen saturation occurred to 94.5% followed by a further decrease for the last day of the

experiment to 90%. MfBRT and oxygen saturation correlate strongly with each other, the Spearman's correlation coefficient was 0.903 with a p-value of < 0.0001 and n = 255 the correlation is significant at $\alpha = 0.01$. Figure 3.79 shows that oxygen saturation and mfBRT appear to fit a quadratic regression with $r^2 = 0.85$ and $p < 0.0001$.

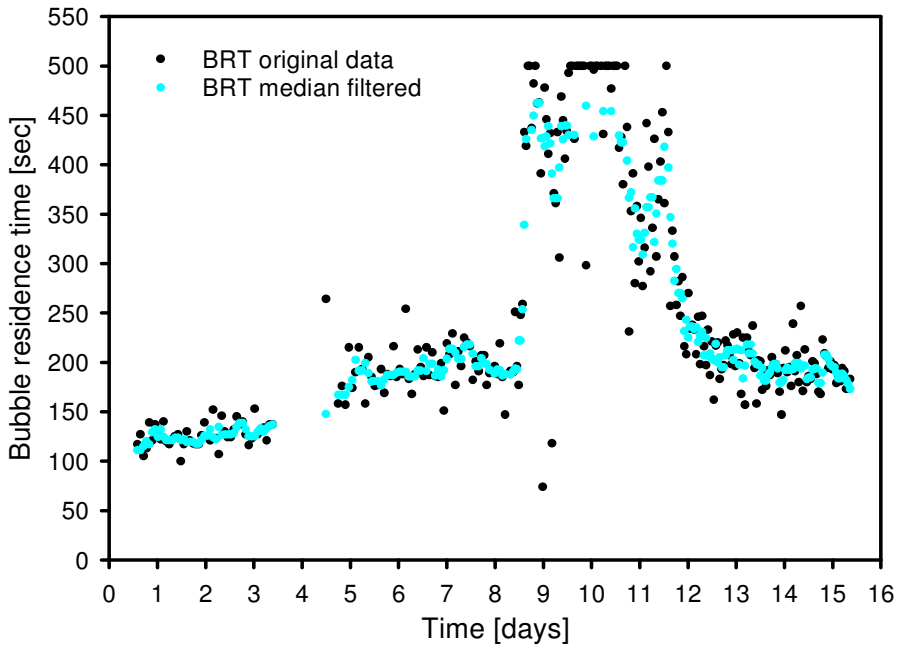

Figure 3.76 Comparison of original BRT data and median filtered BRT data for experiment 10.

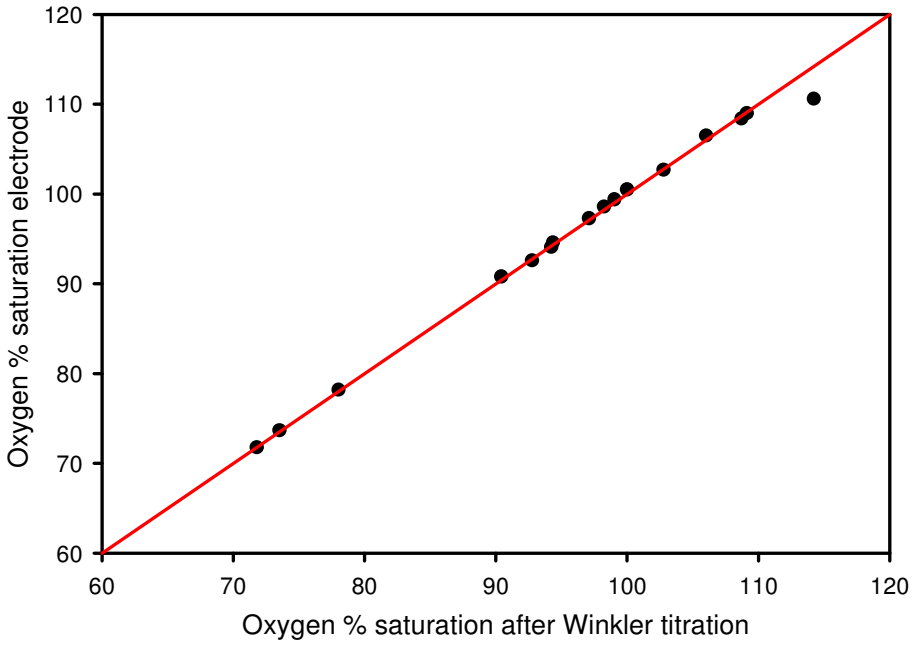

Figure 3.77 Oxygen saturation determined by Winkler titration versus oxygen saturation measured by electrode for experiment 10.

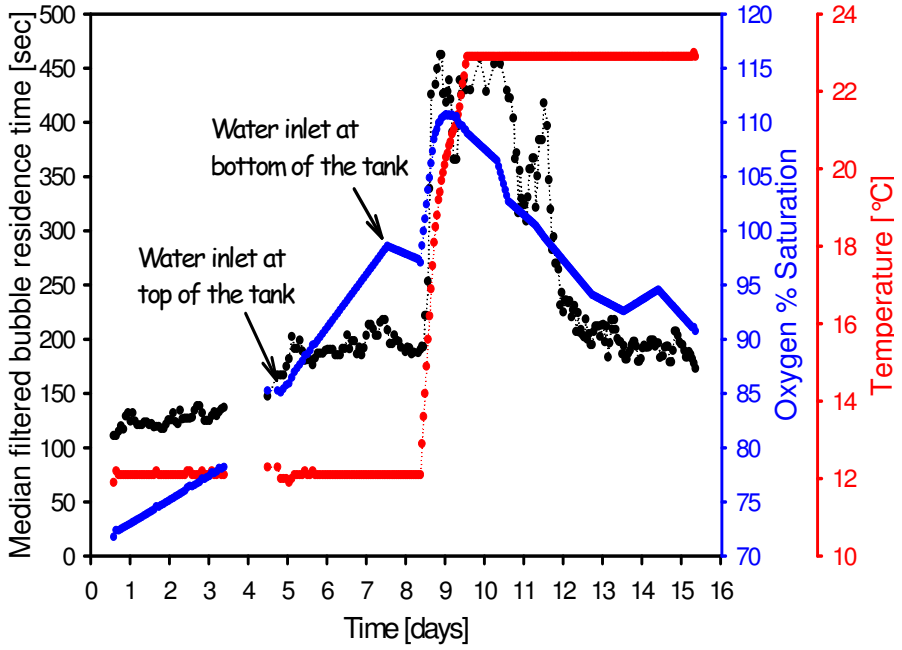

Figure 3.78 Changes in mfBRT, oxygen saturation and water temperature with time for experiment 10.

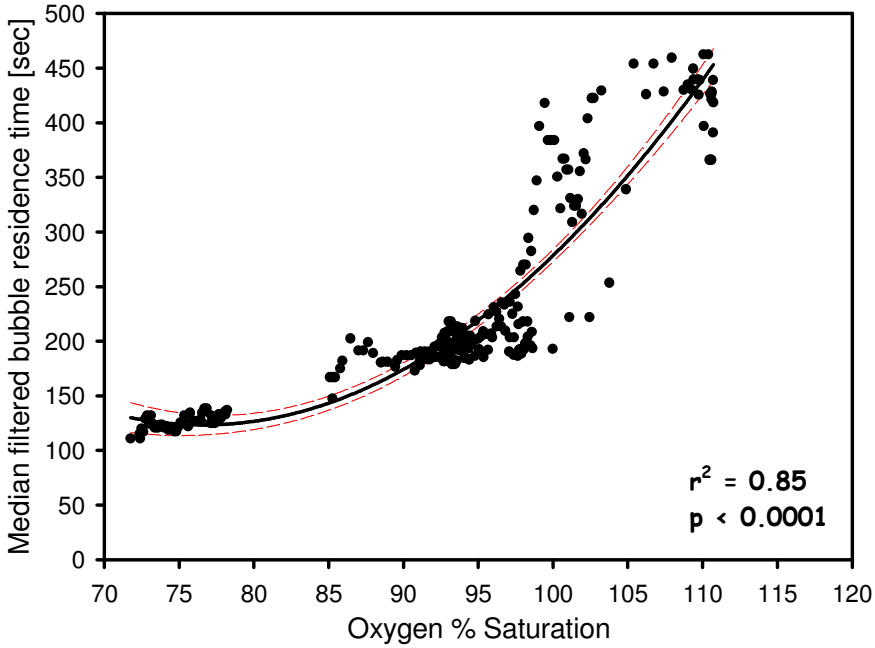

Figure 3.79 Oxygen saturation versus mfBRT for experiment 10.
Black solid line shows that the data fit a quadratic regression. Red dashed lines show the 95% confidence intervals.

3.4.3 Third saturation experiment

The aim of the third saturation experiment was to verify the results of the second saturation experiment described in section 3.4.2 and to investigate if a repetition of the experiment would lead to changes in oxygen saturation and BRT of a similar order of magnitude compared to the second saturation experiment. Oxygen saturation was recorded continuously by the electrode but samples for Winkler determination of oxygen saturation were taken on several occasions of the experiment. Figure 3.81 shows that the oxygen saturations measured by the electrode were slightly higher than the Winkler samples. The relationship between oxygen saturation$_{electrode}$ and oxygen saturation$_{Winkler}$ is approximately linear ($r^2 = 0.96$), thus the oxygen saturation$_{electrode}$ values were corrected by equation 3.8:

$$O_2\ \%\ \text{saturation}_{corrected} = -9.06 + 1.06 \times O_2\ \%\ \text{saturation}_{electrode} \qquad \text{(Equation 3.8)}$$

During the first 4 days of BRT measurement at 12°C, mfBRT (for original BRT data see Figure 3.80) increased slightly from 103 seconds to 130 seconds, while the oxygen saturation of the tank water increased from 73% to 81% (Figure 3.82). After 4.5 days, when the water circulation was modified as described in section 2.10.3, the oxygen saturation increased rapidly from 81% to 101% within one day. During the same period mfBRT increased from 130 seconds to approximately 190 seconds. When the tank circulation was changed back to the original state (as described in section 2.10.3), oxygen saturation as well as mfBRT declined slightly for the next day to 97% and 158 seconds respectively. On day 6.5, when the water temperature was increased to 23°C, oxygen saturation and mfBRT increased simultaneously with both, oxygen saturation and mfBRT reaching maximum values of 113% and 450 seconds respectively as the temperature reached its maximum. The theoretical oxygen saturation after warming of the water by 11°C should have been approximately 118.5%. While the temperature remained constant at 23°C for the following 13 days, oxygen saturation and mfBRT declined. During days 7.5-11.0, the decline was more rapid and mfBRT showed large fluctuations. After day 12.0, both parameters declined more gradually until constant values of 88% saturation and 155 seconds were reached on day 17.0. The temperature reduction to 12°C on day 19.0 resulted in a rapid decrease in oxygen saturation to 72% and a decrease in mfBRT to 102 seconds. For the last 2 days of the experiment, when the temperature remained at 12°C, oxygen saturation increased again to 77% and mfBRT increased slightly to approximately 115 seconds. Oxygen saturation and mfBRT show a strong correlation with the Spearman's

correlation coefficient calculated to be 0.927 with a p-value of 0.000 (n = 419). The correlation is significant at $\alpha = 0.01$. Figure 3.83 shows that the relationship between oxygen saturation and mfBRT is well described by quadratic regression with $r^2 = 0.85$ and $p = <0.0001$. Comparison of oxygen saturation versus mfBRT for experiments number 10 and 11 (Figure 3.84) shows that the data as well as the regression lines show very good agreement. The increase in mfBRT with increasing oxygen saturation for both experiments was gradual until saturation of the tank water was reached. As soon as the tank water became supersaturated with oxygen, mfBRT increased almost exponentially.

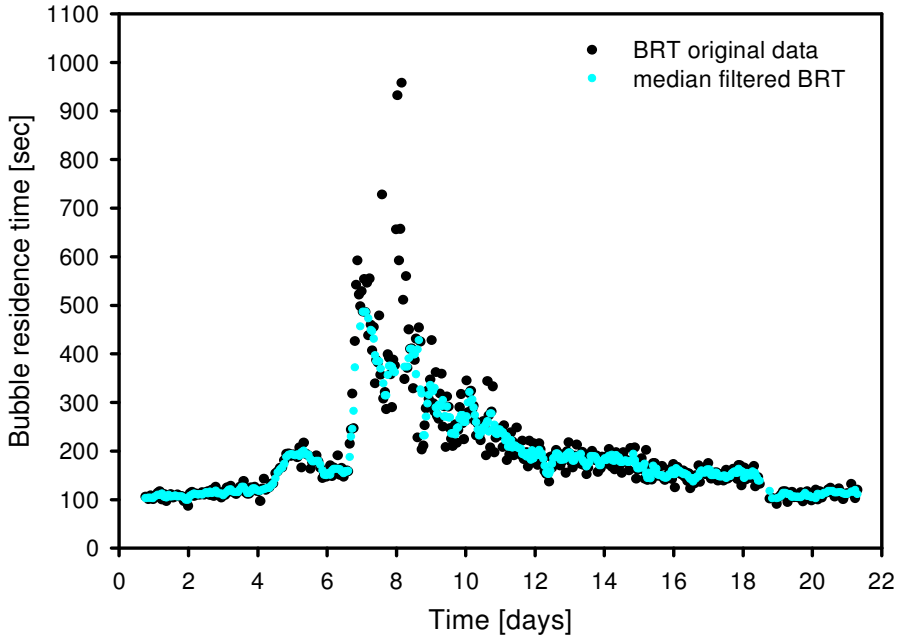

Figure 3.80 Comparison of original BRT data and median-filtered BRT data for experiment 11.

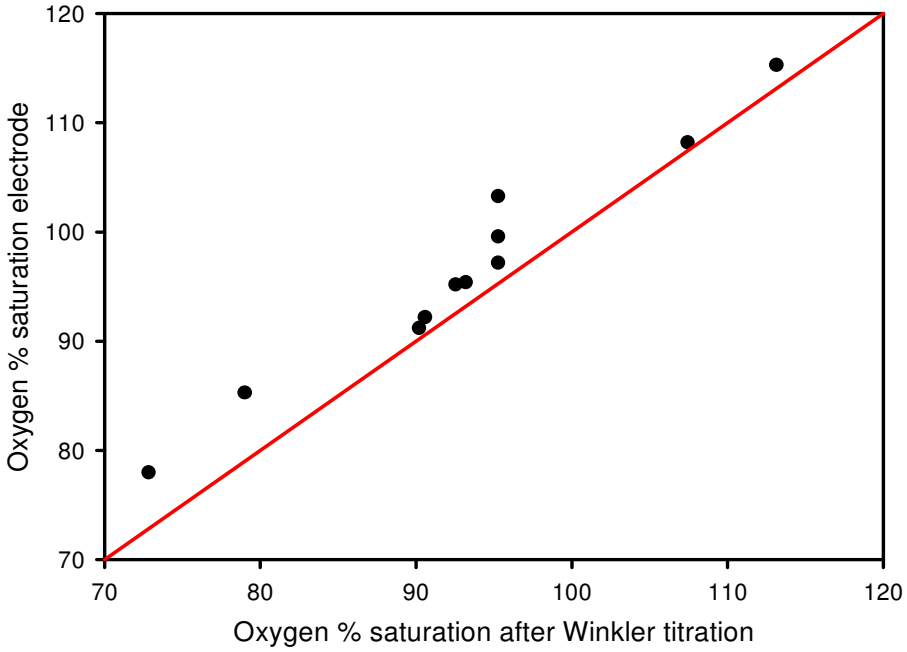

Figure 3.81 Oxygen saturation determined by Winkler titration versus oxygen saturation measured by electrode for experiment 11.
Red line: 1:1 ratio.

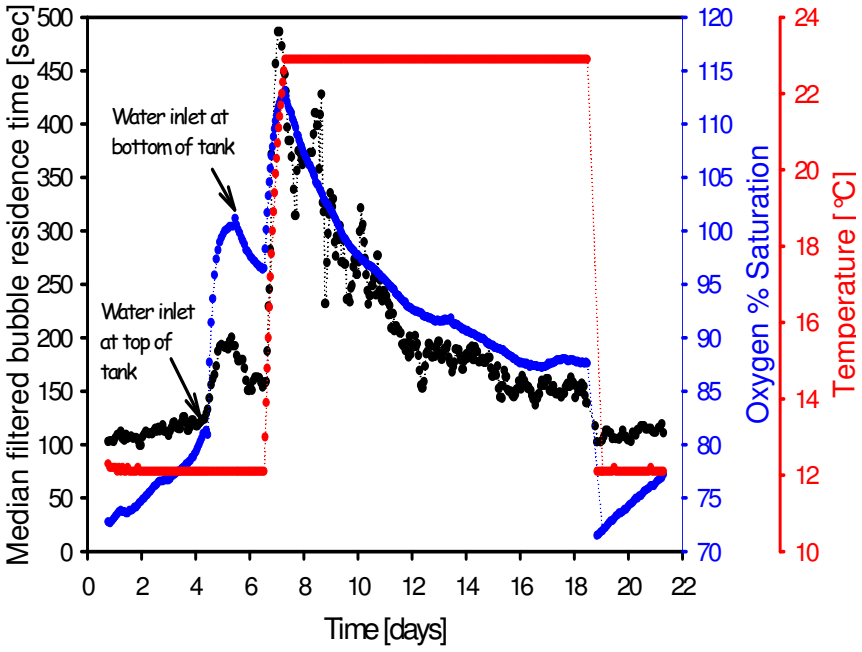

Figure 3.82 Changes in mfBRT, oxygen saturation and water temperature with time for experiment 11.

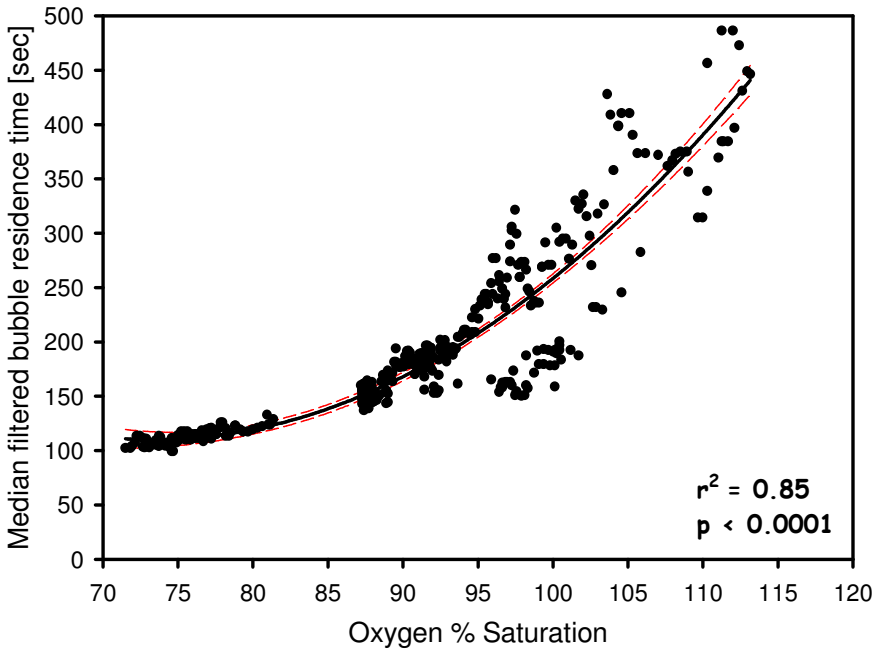

Figure 3.83 Oxygen saturation versus mfBRT for experiment 11.
Black solid line: quadratic regression; red dashed lines: 95% confidence intervals.

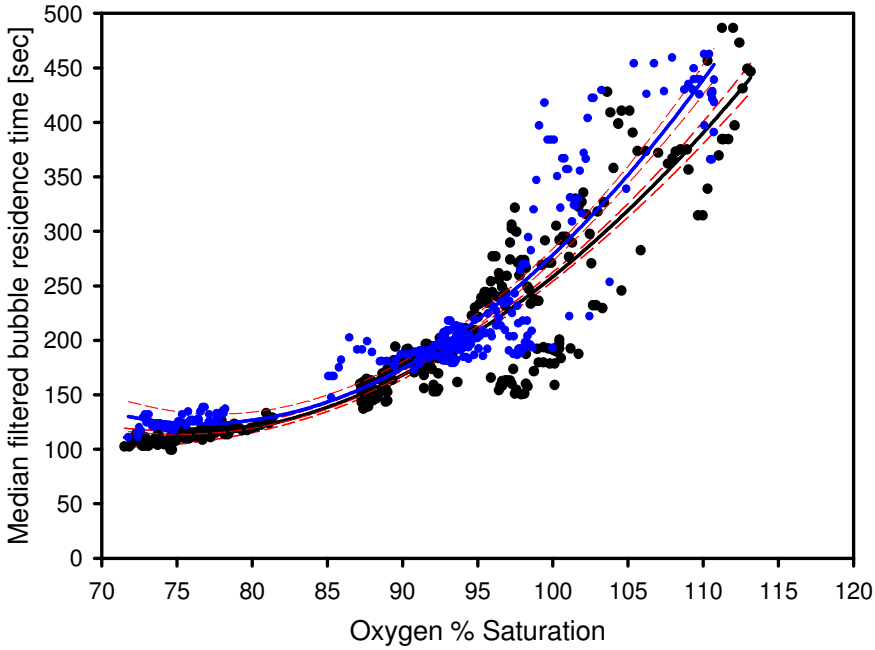

Figure 3.84 Oxygen saturation versus mfBRT for experiments 10 and 11.
Blue dots: data points for experiment 10; blue solid line: quadratic regression for experiment 10; black dots: data points for experiment 11; black solid line: quadratic regression for experiment 11; red dashed lines: 95 % confidence intervals.

3.5 Experiment with a model polysaccharide "Xanthan Gum"

By using high concentrations of a model polysaccharide (Xanthan Gum serves as a thickening agent in nutrition), it was aimed to create solutions of elevated viscosity to investigate if increases in viscosity would result in increased BRT and of what order of magnitude this increase would be. To reduce scatter in BRT data, a median filter was applied (Figure 3.85). During the first four days of the experiment, mean mfBRT of deionised water was 136 seconds with a standard deviation of ± 5 (Figure 3.86). Bulk water viscosity had a value of 0.8680 $mm^2\ sec^{-1}$ (Figure 3.88; ± 0.001). With the addition of Gum Xanthan to a concentration of approximately 0.008g l^{-1}, mean mfBRT increased slightly to 145 seconds (standard deviation of 4) and bulk water viscosity increased to 0.900 $mm^2\ sec^{-1}$. No measurements of surface shear viscosity were made for this Gum Xanthan concentration. The Kruskal-Wallis test, comparing the medians of mfBRT for the concentrations 0 g l^{-1} and 0.008 g l^{-1} Gum Xanthan gave a test statistic H = 11.66 and a p-value = 0.001 for 1 degree of freedom ($\chi^2_{(1/0.01)} = 6.64$). This confirms that the mean mfBRT for the two concentrations are statistically different from each other at a significance level $\alpha = 0.01$ as shown in Figure 3.87. An approximate 10-fold increase of Gum Xanthan concentration in the tank water to 0.08g l^{-1} on day 5.7 resulted in a quite distinct increase of mean mfBRT to 237 seconds (standard deviation of 24) immediately after addition of the model polysaccharide and an increase in bulk water viscosity to 1.272 $mm^2\ sec^{-1}$ (Figure 3.86). Surface shear viscosity measurements of a 0.08 g l^{-1} Gum Xanthan solution over a period of 1246 minutes (carried out by Max Planck Institute of Colloids and Interfaces) indicate that at the start of measurements, the surface viscosity was high (53-54 $\mu N\ s\ m^{-1}$) and it declined with time to 23.3 $\mu N\ s\ m^{-1}$ after 1246 minutes (Figure 3.88). The time span of the decline in surface shear viscosity temporally compared with the rapid decline in mfBRT from 280 seconds to 210 seconds between days 5.8 to 6.6. Results of the Kruskal-Wallis test of the median mfBRT values of concentrations 0.008g l^{-1} and 0.08g l^{-1} Gum Xanthan give a test statistic H = 47.14 and a p-value of 0.000 for 1 degree of freedom.

As $\chi^2_{(1/0.01)} = 6.64$, the null hypothesis can be rejected, indicating that there is a statistically significant difference between the means of the two concentrations as shown in Figure 3.87. Figure 3.86 shows that mfBRT for 0.08g l^{-1} Gum Xanthan did not remain at a consistent level but began to decline very soon after the addition of the model polysaccharide, and reached a mean value of approximately 185 seconds on day 11.5 of the experiment. Bulk water viscosity declined slightly to 1.240 $mm^2\ sec^{-1}$ on day 11.5.

Spearman's rank correlation of viscosity and mfBRT gave a correlation coefficient of 1.0 for n = 4 and a p-value of 0.000. Thus the correlation is statistically significant at α= 0.01.

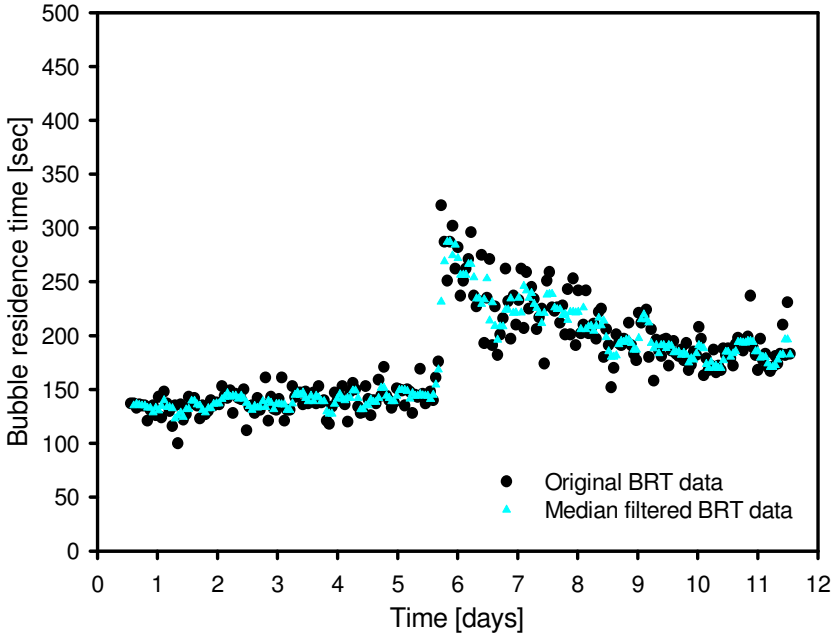

Figure 3.85 Comparison of original BRT data and median filtered BRT data for experiment 12.

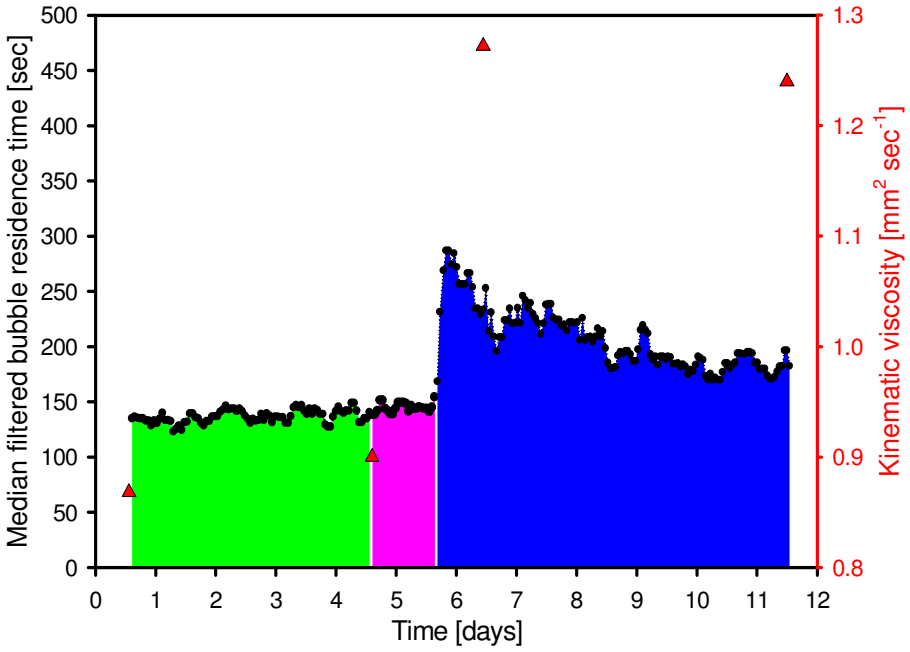

Figure 3.86 Changes in mfBRT and viscosity with time for different Gum Xanthan concentrations. Green area fills: deionised water; red area fills: ~0.008 mg ml^{-1} initial Gum Xanthan concentration; blue area fills: ~0.08 mg ml^{-1} initial Gum Xanthan concentration; red symbols; bulk water viscosity; error of viscosity: ± 0.002 mm^2 sec^{-1}.

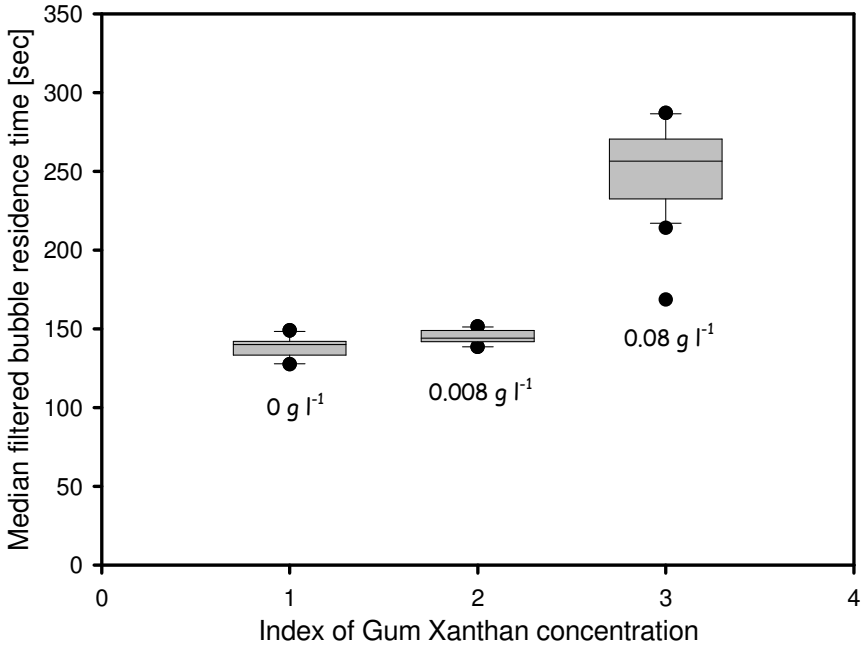

Figure 3.87 Boxplot of mfBRT for different Gum Xanthan concentrations.
Upper box boundary: 75th percentile; lower box boundary: 25th percentile. Whiskers below and above boxes show the 10th and 90th percentiles. Black dots show outliers and the black solid lines within the boxes represent the median value.

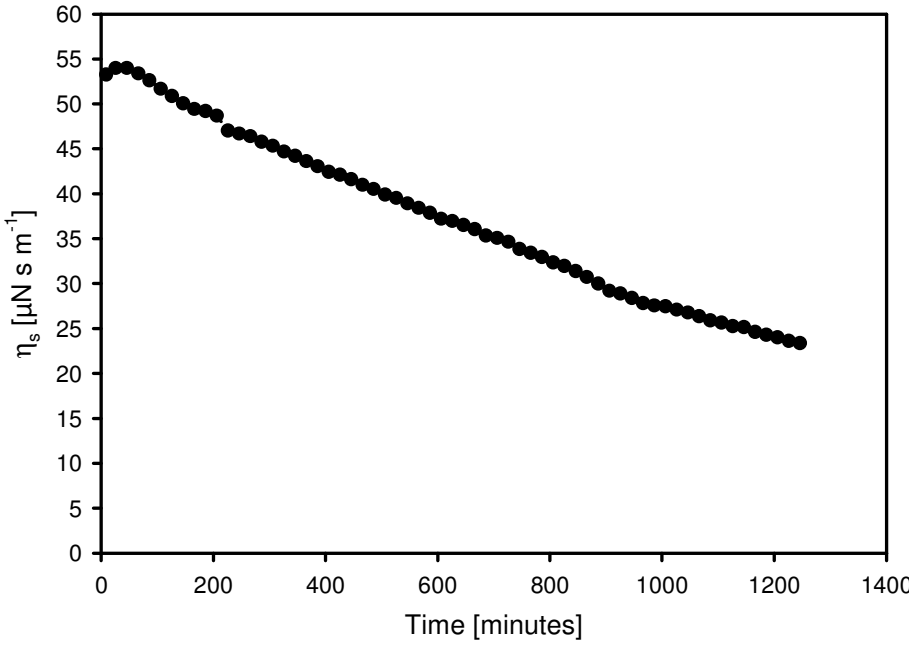

Figure 3.88 Changes in surface shear viscosity with time for a 0.08 g l^{-1} Gum Xanthan solution.

3.6 Experiment with the model surfactant Triton X 100

This experiment aimed to investigate whether a strong reduction in surface tension would result in increased BRT. To significantly reduce the surface tension of deionised water, a model surfactant Triton X 100 was added to make up 3 different concentrations. Median filtered BRT data is used for all analyses of results from this experiment. For comparison between original BRT data and mfBRT data refer to Figure 3.89. Mean mfBRT of deionised water at 18°C before the addition of the surfactant was 148 seconds with a standard deviation of 7 (Figure 3.90). The surface tension of deionised water was approximately 72.8 mN m^{-1} for all bubble lifetimes of the SITA f60 tensiometer (Figure 3.91). The addition of Triton X 100 to a concentration of approximately 10^{-6} mol l^{-1} resulted in an increase of mean mfBRT to 171 seconds, with a standard deviation of 7 (Figure 3.90). The Kruskal-Wallis test, comparing the median values of mfBRT for the two concentrations 0 and 10^{-6} mol l^{-1} gives a test statistic H = 45.01 with p = 0.000 at 1 DF. As $\chi^2_{(1/0.01)} = 6.64$, the test shows that the addition of Triton X 100 significantly changed the mean mfBRT. However, surface tension did not change significantly after the addition of Triton X 100 (Figure 3.91) and remained approximately 72.8 mN m^{-1}. A further increase of the Triton X 100 concentration to approximately $5x10^{-5}$ mol l^{-1} resulted in a further increase in mean mfBRT to 196 seconds with a standard deviation of 8 (Figure 3.90). Comparison of the median mfBRT values of the concentrations 10^{-6} mol l^{-1} and $5x10^{-5}$ mol l^{-1} by the Kruskal-Wallis test gives a test statistic H = 53.6 with p = 0.000 at 1 DF. Comparing H with $\chi^2_{(1/0.01)} = 6.64$, this indicates that the median mfBRT values for the two different concentrations of Triton X 100, 10^{-6} mol l^{-1} and $5x10^{-5}$ mol l^{-1} differ significantly from each other. For $5x10^{-5}$ mol l^{-1} Triton X 100, surface tension decreased significantly with increasing bubble lifetime from 72.5 mN m^{-1} at a bubble lifetime of 0.58 sec to 55.4 mN m^{-1} at a bubble lifetime of 58 seconds (Figure 3.91). A further increase of the Triton X 100 concentration to $2.5x10^{-4}$ mol l^{-1} resulted in a further increase of mean mfBRT to 223 seconds (standard deviation of ± 14). The test statistic H = 72.99 shows that the median mfBRT values of the Triton X 100 concentrations 5×10^{-5} mol l^{-1} and 2.5×10^{-4} mol l^{-1} are significantly different. The surface tension for Triton X 100 concentration of $2.5x10^{-4}$ mol l^{-1} was significantly lower than for the two higher Triton X 100 concentrations and for deionised water. Surface tension was 71.0 mN m^{-1} for a bubble lifetime of 0.41 seconds and decreased to 37.8 mN m^{-1} for a bubble lifetime of 57 seconds.

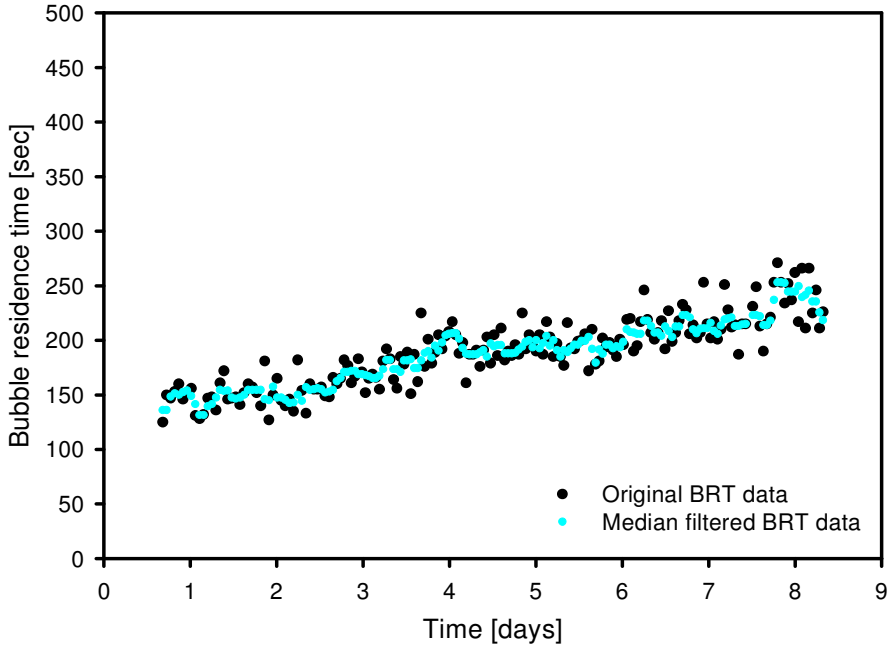

Figure 3.89 Comparison of original BRT data and median filtered BRT data for experiment 13.

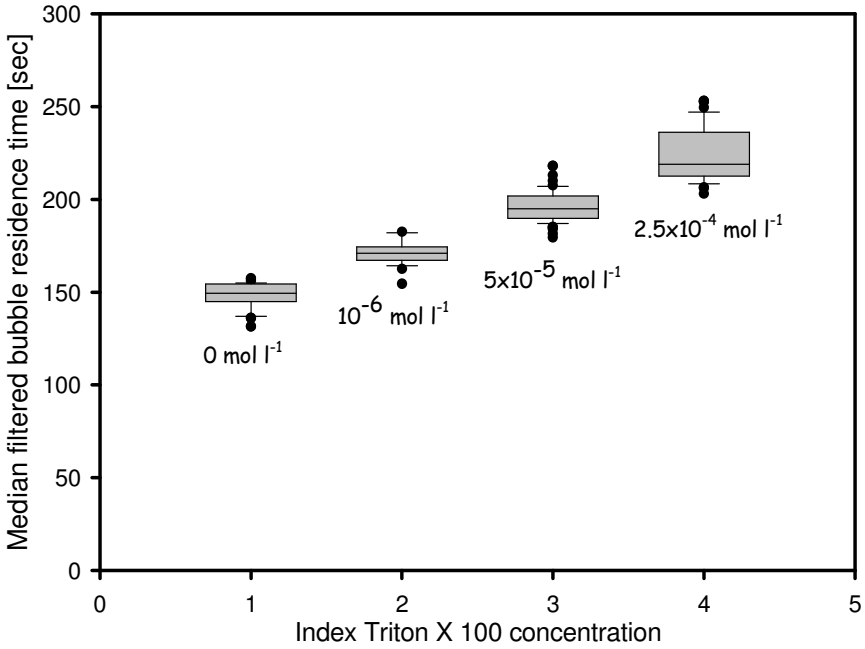

Figure 3.90 Boxplot of mfBRT for different concentrations of Triton X 100.
Upper box boundary: 75th percentile; lower box boundary: 25th percentile. Whiskers below and above boxes show the 10th and 90th percentiles. Black dots show outliers and the black solid lines within the boxes represent the median value.

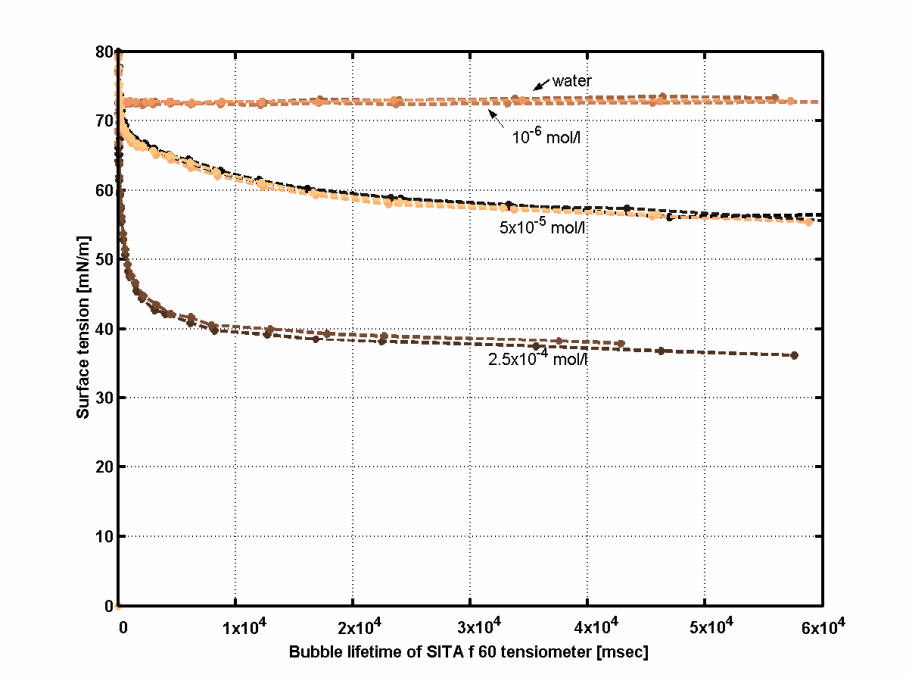

Figure 3.91 Surface tension versus bubble lifetime for different concentrations of Triton X 100.

3.7 Surface shear viscosity measurements with phytoplankton monocultures

Results of surface shear viscosity measurements for the concentrated stock cultures of *Thalassiosira rotula*, *Thalassiosira punctigera*, *Phaeocystis* and *Nitzschia closterium* are presented in Figure 3.92. Cell numbers per ml of these stock cultures are given in Table 3.10. Cultures were measured for a range of durations, however, an increase in surface shear viscosity with adsorption time was only detected for *Nitzschia closterium*. The increase occurred over the first 300 minutes from 11 μN s m^{-1} to 31 μN s m^{-1}. Following that, the surface shear viscosity remained constant until approximately 650 minutes from the start of measurements. During the remaining 500 minutes, surface shear viscosity decreased from 31 μN s m^{-1} to 21 μN s m^{-1}. For all other cultures, surface shear viscosity decreased from the beginning of measurement and showed similar behaviour to F/2 nutrient medium (green symbols on Figure 3.92). Seawater, for comparison had a surface shear viscosity of 1 μN s m^{-1}, which remained constant with measurement time. As the surface shear viscosity of these other cultures did not reveal any significant increases, surface shear viscosity measurements were predominantly carried out with *Nitzschia closterium* and only these results are presented. Surface shear viscosity of a diluted, nutrient enriched culture of *Nitzschia closterium* showed different behaviour at several stages of the growth phase (Figure 3.94). On day two of the growth experiment, surface shear viscosity showed no distinct increase with time. At the beginning of the surface shear viscosity measurement period a slight decrease similar to that detected in *Phaeocystis*, *Thalassiosira rotula* and *Thalassiosira punctigera* cultures (Figure 3.92) occurred. Towards the end of surface shear viscosity measurement, a negligible increase was detected between 600 and 900 minutes from 1 to 2 μN s m^{-1}. On days 3 and 4 of the growth experiment, when the cells were growing exponentially (Figure 3.93; cell numbers were 1.7×10^5 and 3.6×10^5 cells ml^{-1} respectively), the surface shear viscosity increased markedly with increasing measurement time to 26.6 μN s m^{-1} on day 3 and 24 μN s m^{-1} on day 4. On day 7, when cell numbers already declined to 1.8×10^5 cells ml^{-1} (Figure 3.93), surface shear viscosity showed no increase, only a slight decrease with measurement time from

5 μN s m^{-1} to 0 μN s m^{-1} occurred during the first 450 minutes. Results from a filtered and unfiltered stock culture of *Nitzschia closterium* (Figure 3.95) show that the surface shear viscosity increased when cells were present in the sample and a decrease occurred for the filtrate.

Name of stock culture	Cell number of stock culture (ml^{-1})	Standard deviation
Nitzschia closterium	2.27×10^{6}	$\pm 0.34\times10^{6}$
Phaeocystis	0.12×10^{6}	$\pm 0.041\times10^{6}$
Thalassiosira rotula	9.8×10^{3}	$\pm 1.5\times10^{3}$
Thalassiosira punctigera	11.4×10^{3}	$\pm 1.4\times10^{3}$

Table 3.10 Cell numbers of stock cultures for surface shear viscosity determination.

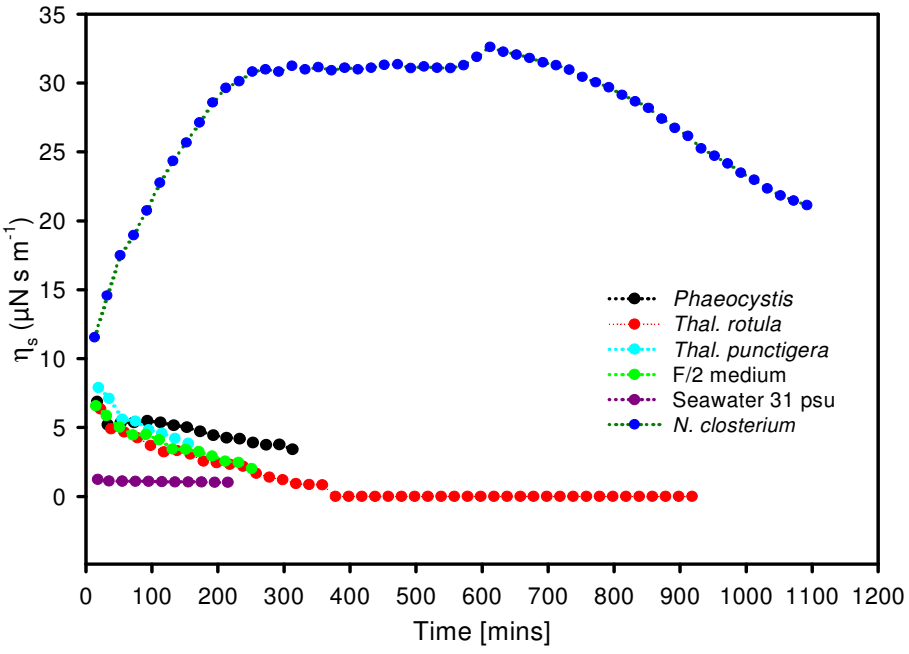

Figure 3.92 Surface shear viscosity of algal stock cultures, F/2 medium and seawater.

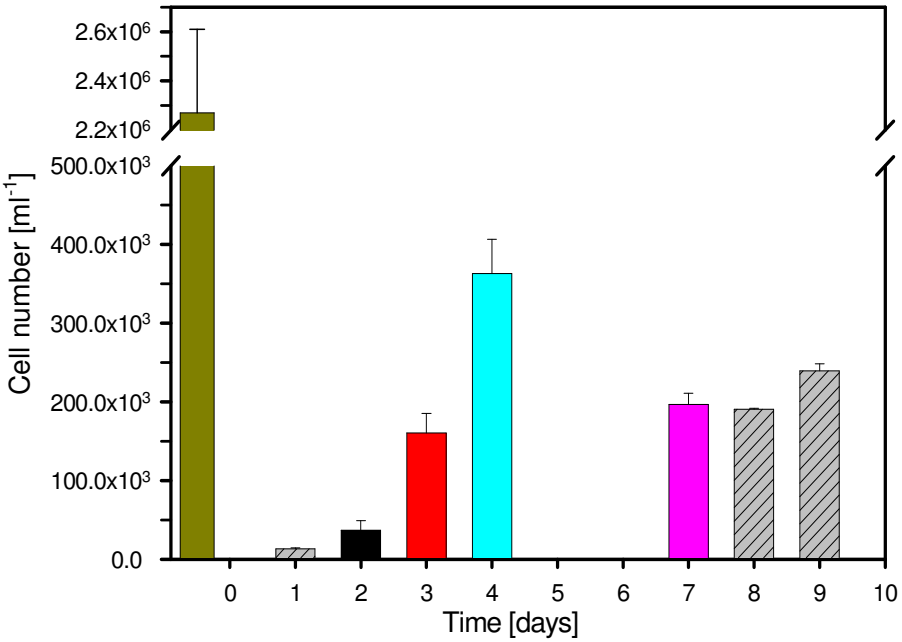

Figure 3.93 Cell numbers per ml of *Nitzschia closterium*.
Coloured bars indicate cell numbers for respective surface shear viscosity measurements shown in Figure 3.94. Grey bars with coarse pattern indicate days without surface shear viscosity measurements. Brown bar shows cell concentration of the *Nitzschia closterium* stock culture (see also Table 3.10).

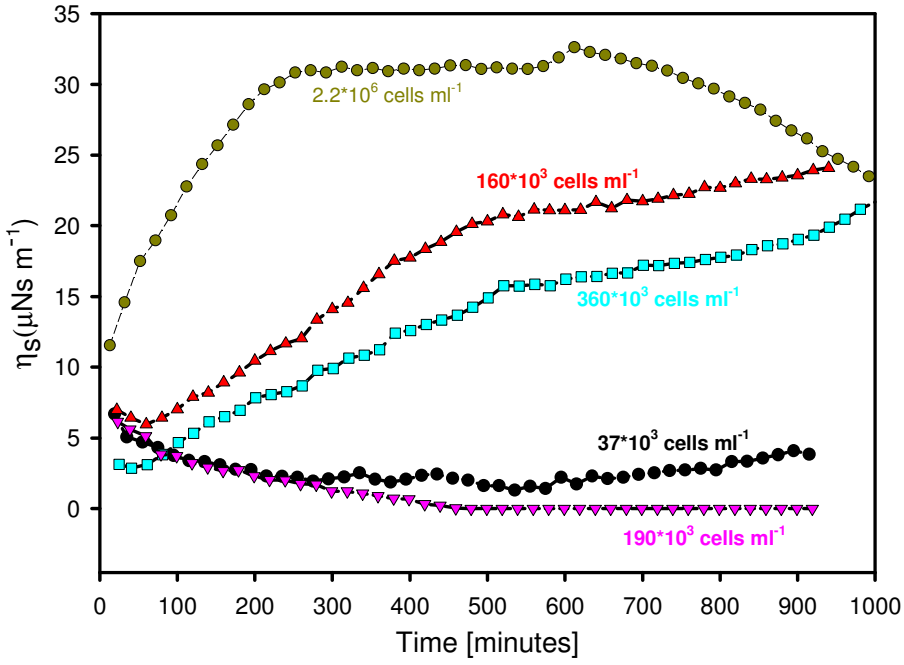

Figure 3.94 Surface shear viscosity of *Nitzschia closterium*.
Coloured bars indicate surface shear viscosity measurements for respective days of experiment and cell numbers (see also Figure 3.93).

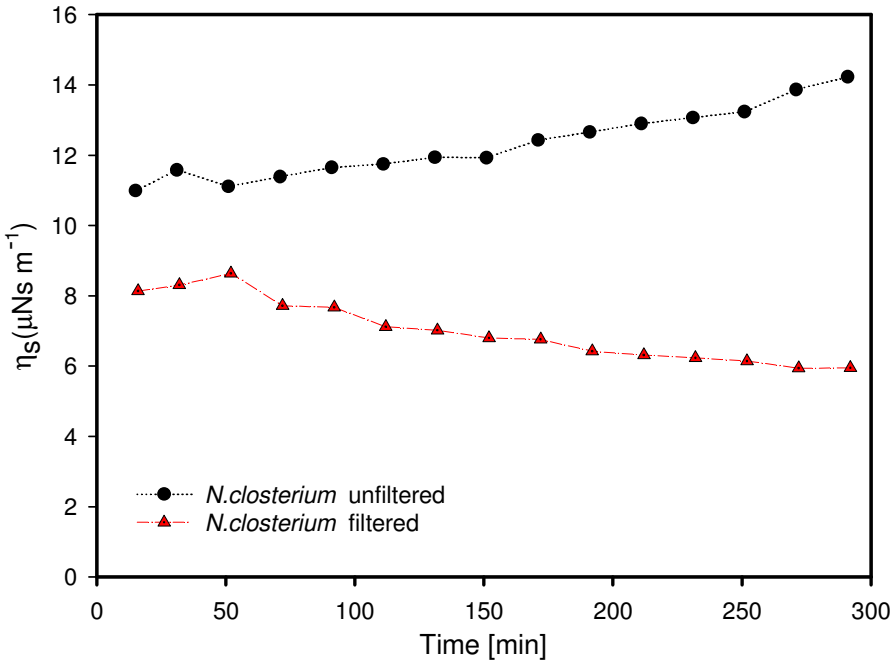

Figure 3.95 Surface shear viscosity of an unfiltered stock culture of *Nitzschia closterium* and its filtrate.

3.8 Viscosity experiment

Bulk water viscosity of different chlorophyll concentrations using a culture of *Chaetoceros muelleri* were made to investigate the dependency of viscosity on the concentration of phytoplankton cells. Results of the viscosity experiment show that bulk water viscosity is approximately linearly related to chlorophyll concentration at a significance level of $\alpha = 0.05$ (Figure 3.96). Viscosity increased with increasing chlorophyll concentration, however, the increase was only detected when the chlorophyll concentration was sufficiently high (>150 µg l^{-1}). Even at very high chlorophyll concentrations, the overall increase in viscosity was relatively small ranging from 1.048 mm^2 sec^{-1} to 1.071 mm^2 sec^{-1}.

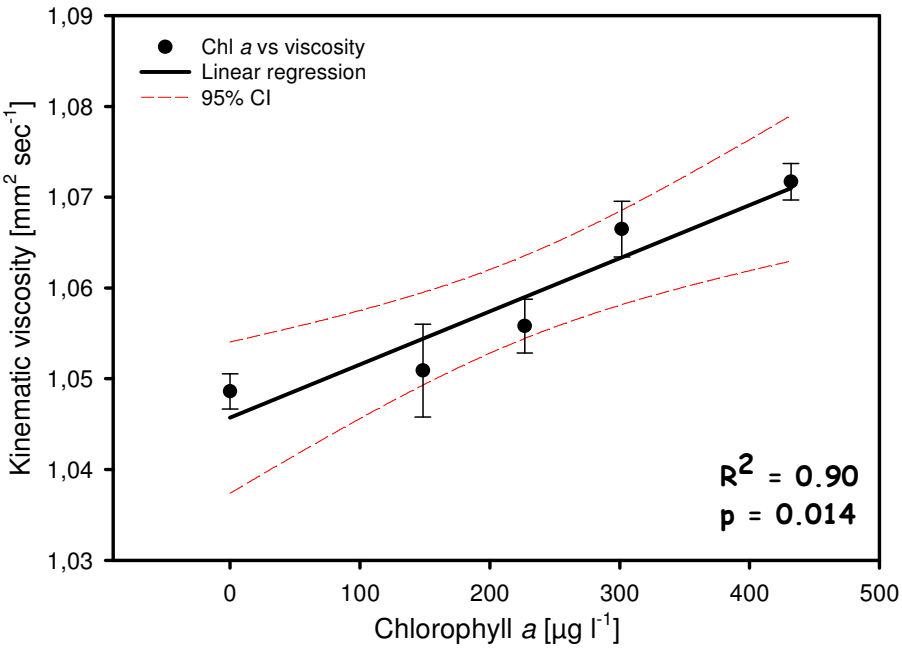

Figure 3.96 Bulk water viscosity of different chlorophyll concentrations of a *Chaetoceros muelleri* culture.

4 Chapter Four. Discussion

4.1 "Bubble residence time"- the limitations of the acoustic measurement method

The advantages of an acoustic technique for the investigation of air bubbles in water originate from the specific acoustical characteristics of a bubble. Air bubbles have large acoustical cross sections, as described and discussed by Medwin (1970) and Clay and Medwin (1977), which enable the identification of a bubble in the presence of particles such as phytoplankton cells and detritus. However, the use of an acoustic technique in an enclosed tank system also implies disadvantages. The presence of tank walls and tank bottom cause interferences that strongly disturb the acoustic backscattering level. Even though most of the interferences through tank bottom and walls were eliminated by subtracting the reference backscattering level from the bubble cloud backscattering (see determination of bubble residence time, section 2.2.3), interferences were still caused by the bubble cloud scattering signal. The special set-up of transmitting and receiving hydrophones at the bottom of the tank system enabled vertical sampling of the bubble cloud, determining the BRT as the point in time when the backscattering level from this bubble cloud in the near surface layer falls below a detection threshold. Therefore, an increase in BRT can have three causes. Firstly, increasing BRT may result from a larger number of bubbles produced. This could imply that bubbles did not necessarily reside longer in the water, if the values for BRT increased, but simply a greater volume of bubbles (hence a greater void fraction) was produced by the jet as a result of strong oxygen supersaturation. Secondly, increased BRT can result from reduced rise velocity of bubbles. A decrease in bubble rise velocity can be caused by an increase in water viscosity as well as through accumulation of surfactants on the bubbles' surfaces. This was described by Thorpe (1982) and Patro *et al*. (2000), who found that the rise velocity of bubbles changed when they became dirty and surfactants had started to accumulate. A third factor that could have resulted in increased BRT would be through decelerated bubble dissolution. However, as the acoustic method used in this study only determined BRT via the backscattering level, a distinction between the possible causes accountable for increased BRT is not possible. Unfortunately, the acoustical method used could not provide information about the rise velocity of bubbles. To investigate the dissolution and the rise velocity of air bubbles and to actively observe the accumulation of material on the surfaces of individual bubbles, a highly sensitive optical technique as used by Detsch (1991) and Patro *et al*. (2000) would be needed. These authors determined rise velocities of bubbles of

different sizes and over different temperatures. To conclude, there is a possibility that increased BRT was not only a result of reduced rising of bubbles or decelerated bubble dissolution but could also have resulted from the creation of a greater number of bubbles with consistent residence time throughout the duration of an experiment.

4.2 Advantages and disadvantages of the mesocosm tank system

Mesocosm systems have been used by various researchers, to investigate particular objectives under controlled conditions, attempting to simulate the real environment. The great advantage of the mesocosm tank system used in this study was that a number of parameters could be kept constant and experimental conditions controlled and therefore repeated as opposed to *in situ* experiments. This feature was vital in gaining detailed information on the changes and interrelations of particular, selected parameters, for instance the chlorophyll concentration, oxygen saturation and corresponding BRT. Experiments were carried out under temperature controlled conditions, salinity was kept constant and these parameters could be varied whenever this was considered necessary. Time intervals between BRT measurements were fairly consistent and the duration of particular phases of a measurement cycle (see section 2.2.1) as well as various system control parameters could be defined. Especially for phytoplankton growth experiments, the mesocosm tank system could be optimised with respect to illumination intervals and the amount of nutrient supply, to exaggerate real environmental conditions and to produce intense phytoplankton blooms. Several growth specific biological and chemical parameters could be monitored more easily on self-selected intervals. One of the great advantages of this particular laboratory tank system was its automated operation via software enabling continuous measurements of BRT during day and night. However, several disadvantages accompany this particular mesocosm tank system, that are discussed in the following paragraphs.

Tubes, valves and pumps

The tubes, valves and pumps integrated in the tank system were an important means to enable water circulation within the large tank and between the different tanks. However, they were extremely difficult to clean between experiments and were therefore always a potential source of contamination. Bacterial plaque settled on the inner lining of the tubes and inside the valves and pumps which in turn influenced the numbers of bacteria counts. Circulation of phytoplankton cells through pumps and valves may lead to the destruction

of cells, even though membrane pumps were used to minimise stress and damage for phytoplankton. Damage of phytoplankton was especially observed for the *Phaeocystis* culture in the tank system (experiment 5, Table 2.4), where colonies were disrupted most likely by the narrow valves.

Dimensions, material and arrangement of the tank system

The complex experimental set-up did not allow phytoplankton growth experiments to be conducted under axenic conditions. Thus, the extent of phytoplankton influence and bacterial influence on parameters such as BRT, DOC content and oxygen saturation could not be rigorously quantified.

Mixing and water circulation in the tank

In a pelagic system at natural turbulence levels, aged phytoplankton cells sediment out of the system to the sea floor. Due to the slightly stronger degree of turbulence in the tank system, a certain amount of senescent cells were re-suspended and consequently influenced phytoplankton standing stock. However, determinations of chlorophyll concentrations as well as visual observations of the tank system during experiments revealed that when cells entered senescence, a significant amount sank to the bottom of the tank and mixing in the tank was too weak to re-suspend the cells.

Bubble cloud injection

The approach of using a water jet creating the bubble cloud in the large tank was selected in order to simulate the breaking of a wave into the ocean. Despite a constant water volume released and constant opening time of the stroke magnet, the injection of the bubble cloud into the large tank was a stochastic event and the composition of the bubble could was never totally homogenous. The jet created an undefined number of bubbles of undefined size. This in turn resulted in enhanced scattering of values for BRT.

4.3 The problem of standardisation of the tank system indicated by reference measurements with deionised water

Results of four reference measurement series with deionised water (see section 3.1) at 18°C showed that despite a consistent water temperature as well as apparent consistency for all other tank parameters including duration of acoustic measurement phase, quiescent phase, water volume injection and duration of the jet, initial BRT at the start of

measurement as well as mean BRT values differ significantly, ranging from a mean value of 200 seconds (18°C-1 experiment on Figure 3.1 c) to 140 seconds (18°C-4 experiment, refer to Figure 3.1 c in results section). The mean oxygen saturations (Table 3.1) indicate that this parameter was not the main cause for the observed differences for the reference measurements, as the highest mean BRT (202 seconds) occurred when mean oxygen saturation was lowest (54.8%). However, oxygen saturation has some influence on BRT as it is shown by the lower BRT of the first 8 measurement indices (Figure 3.1 c.) for the 18°C-4 measurement series and its rapid equilibration that occurred simultaneously with an increase in oxygen saturation (Figure 3.1 d). The differences in oxygen saturation for the 18°C measurement series can be mainly explained by the different residence times of the deionised water in the tank system prior to the beginning of measurements. The higher oxygen saturation for 18°C-4 and the increase in saturation during the first 8 measurements can be accounted for by a saturation increase resulting from warming of the water, which had previously been kept in the tank system at a temperature of 12°C. Similarly, the intermediate oxygen saturation of 62% to 65% of series 18°C-2 can be accounted for by the longer residence time of the water in the tank system (2 weeks prior to the beginning of measurements, see section 2.6.2 for preparation of experiments). For series 18°C-1 and 18°C-3 BRT measurements were started soon after the filling of the tank system. Despite similar oxygen saturations for 18°C-1 and 18°C-3 series, mean BRT values were very different. It is possible that nitrogen saturation was higher for 18°C-1 than for 18°C-3, causing the higher BRT. However, as nitrogen saturation was not measured and the methodological preparation of the two reference experiments were similar, certain conclusions about nitrogen saturation causing the higher BRT for 18°C-1 cannot be made.

Reference measurements with deionised water at a temperature of 12°C show much smaller differences in mean BRT between the three different measurement series, however, differences still exist and these differences also do not correlate with oxygen saturation. However, it can be noted that the use of newly filled water (series 12°C-1, refer back to Figures 3 a and b) resulted in a slightly higher mean BRT whereas two measurement series using the same water (series 12°C-1 and 12°C-3) showed nearly identical mean BRT and oxygen saturation. This suggests that the differences in BRT are not a result of changing factors of the tank system but can rather be attributed to different characteristics of the water used for the various reference experiments. One possibility is that the differences in mean BRT of reference water experiments resulted from some sort of contamination (see

section 4.2) of the water, which is likely to have occurred as the water in the tank system is susceptible to contamination by bacterial and planktonic plaque from tube and valve linings, as discussed in section 4.2. As measurements could not be carried out under sterile conditions, bacteria were present in the water, converting particulate organic carbon (POC) to DOC. This may also explain the smaller differences in mean BRT for reference measurements at 12°C, when bacterial activity was presumably lower than at 18°C. As deionised water is not buffered as well as seawater, it reacts more sensitively to contamination. Thus, it is possible that different degrees of contamination could have led to the differences in BRT between different reference water experiments. This assumption is supported by the findings of Detwiler (1979), who states that bubble rise speed is directly affected by the concentration and adsorption dynamics of surface active contaminants onto the bubble surface and that the contaminant concentrations only need to be on the order of a few parts per million or less to alter bubble rise speed.

Mean BRT was also found to have been lower for reference measurements at 12°C than for 18°C reference measurements. This would agree with the findings of Leifer *et al*. (2000) and Patro *et al.* (2000), who detected reduced rise velocities of small air bubbles at lower temperature due to decreases in bulk water viscosity. However, as discussed in section 4.1, it could not be distinguished between increases in BRT resulting from decelerated rise velocity and increases in BRT resulting from the production of a greater number of bubbles with the acoustic measurement method applied. Thus, the slightly higher mean BRT values for measurements at 18°C could be accounted for by enhanced bubble production, which was observed by Hwang *et al*. (1991) to occur for increasing temperatures between 11 and 17°C. Retrospectively, the use of artificial seawater (deionised water with artificial sea salt) as reference water would have been more advisable as the carbonate system of seawater acts as a buffer. However, comparison of the initial values of BRT of natural filtered seawater (without nutrient medium and algal cultures), that was used for the three growth experiments with monocultures (Figure 4.1 a) also show differences in BRT ranging from mean values of 157 seconds, 184 seconds and 228 seconds respectively. For seawater reference measurements, oxygen saturation covaried with BRT (Figure 4.1 b). Thus, if contamination influence was reduced as a result of the buffering capacity of seawater, the changes in BRT could be accounted for by changes in oxygen saturation. These results lead to several possible conclusions. It is likely that BRT is extremely sensitive to contamination especially in deionised water. This assumption would agree with

the findings of Detwiler (1979), Thorpe (1992) and Patro *et al*. (2000), who state that the bubble's surface is initially clean but becomes dirty within a few seconds after formation. They found that the accumulation of colloidal substances on the bubbles' surfaces led to surface tension gradients and thus to reduced rise velocity. It is also possible that a combination of contamination effects as well as gas saturation effects of the deionised water may have occurred.

4.3.1 Equilibration of seawater in the tank system

The high initial mfBRT values followed by a decline in BRT that occurred during the second and third Kiel Firth water growth experiments and during the growth experiment with *Chaetoceros muelleri* further demonstrate the problem of standardisation of the tank system. For these experiments, BRT measurements were started directly after filling the water into the tank system. For experiment 4 (*Chaetoceros muelleri*), the initial decrease in mfBRT covaried with the decrease in oxygen saturation (Figure 4.3 d) whereas for experiment 2 (second Kiel Firth water growth experiment), the initial decrease in mfBRT did not show much covariation with oxygen saturation (Figure 4.3 b). For experiment 3 (third Kiel Firth water experiment), oxygen saturation was not measured during the first 3.5 days, therefore it cannot be stated that the mfBRT decline covaried with oxygen saturation. For experiment 6, oxygen saturation covaried with the small initial decline in mfBRT (Figure 4.3 f). However, the decline in initial mfBRT for experiment 6 was much weaker than for experiment 2 despite the same water type used (aged North Sea water). The constant initial mfBRT values for experiment 5 (*Phaeocystis,* Figure 4.3 e) and the initial BRT of the first Kiel Firth water growth experiment (experiment 1, Figure 4.3 a), where the water was left to equilibrate within the system for several days prior to the beginning of BRT measurements (refer to sections 2.7.1 and 2.7.5) further demonstrate that the water needed some time to equilibrate within the tank system. These results suggest that equilibration and mixing effects of the water with the tank system play an important role and may take several days. However these effects seem to be specific to the various types of water used in this study and cannot be generalised. Freshly filled Kiel Firth water showed much higher initial BRT and more time was needed for the water to equilibrate with the tank system compared to aged and filtered North Sea water used for the monoculture growth experiments. Reasons for the differences may be varying degrees of gas saturation, differences in dissolved and particulate substances present in the

water and different lengths of storage of aged North Sea water used in monoculture growth experiments.

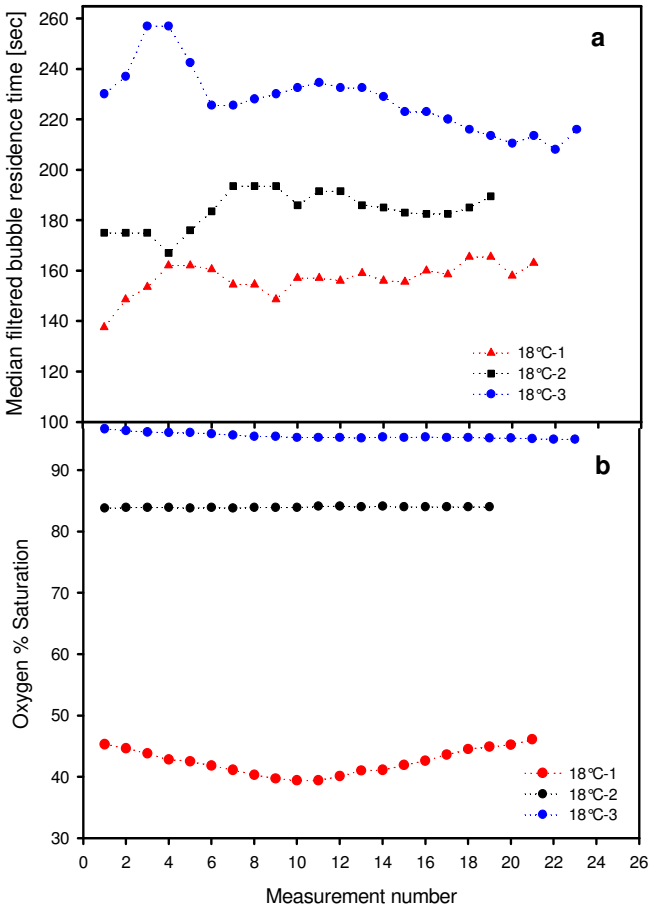

Figure 4.1 Changes in BRT (a) and oxygen saturation (b) with increasing measurement number for filtered seawater at 18°C.

4.4 Air bubble residence time in relation to phytoplankton growth parameters:

4.4.1 Chlorophyll concentration

Note: For the remaining general discussion of BRT in relation to other parameters, the term BRT is used instead of both, BRT and mfBRT, except if actual numbers are involved in the discussion. For exact differentiation between BRT and mfBRT for the respective experiments refer to chapter 3.

A significant correlation between chlorophyll concentration and BRT was found in a majority of experiments (experiments 1, 2, 3 and 6) but for two experiments (experiments 4 and 5), no correlation between the two parameters was detected (Table 4.2). The order of magnitude of chlorophyll concentrations for the different experiments varied greatly, especially with respect to the maximum chlorophyll concentrations detected (Table 4.1 and Figure 4.3). Reasons for the variation in maximum chlorophyll concentration can be found with respect to the different species compositions for the different experiments, as well as to different strengths in the nutrient media, leading to different growth intensities. In the case of *Phaeocystis*, the low chlorophyll concentrations were not a consequence of nutrient limitation as results have shown that nutrient concentrations were available in sufficient quantities. The low chlorophyll concentrations more likely resulted from the physical features of the tank system leading to the disruption of *Phaeocystis* colonies. For Kiel Firth water experiments with natural phytoplankton populations, the maximum chlorophyll concentrations correlated with the maximum oxygen saturations (7.5 µg l^{-1} to 155%; 35 µg l^{-1} to 190%; 55 µg l^{-1} to 240%, Table 4.1). Maximum BRT/mfBRT however (400 seconds, 600 seconds and 550 seconds respectively) does not compare so well with the maximum chlorophyll concentrations showing that the order of magnitude of chlorophyll concentration is not a direct indicator for the respective order of magnitude of BRT. This indicates that changes in BRT were not only a matter of increasing numbers of particles and their possible accumulation on the surfaces of the bubbles as it has been described by Kepkay, (1994), Slauenwhite and Johnson, (1996) and Patro *et al*. (2000). However, it is likely that the increasing particle concentrations represented by increases in chlorophyll concentration were a co-factor of increased BRT, possibly by means of a reduction in rise velocity as has been described by Thorpe (1982) and Patro *et al*. (2000). However, it is more likely that the chlorophyll concentration is an indicator of other phytoplankton-growth related processes and conditions that changed simultaneously and that needed to be satisfied in order for BRT to change.

Exp. No.	Dominant algae	Water temperature (°C)	Salinity	Initial O_2 % saturation (day Number)	O_2 % saturation following growth phase (day number)	Initial chl *a* ($\mu g\ l^{-1}$) (day number)	Chl *a* ($\mu g\ l^{-1}$) following growth phase (day number)	Initial BRT (seconds) (day number)	Maximum BRT (sec.) following growth phase (day number)
Natural algal populations in Kiel Firth water									
1	*Stephanopyxis turris; Rhizosolenia* sp.*; Asterionella japonica; Nitzschia closterium*	12°C	14.5	87.5 (day 0.5)	157 (day 6.5)	0.5 (day 0.5)	7.5 (day 6.5)	140 (day 0.5)	360 (day 6.5)
2	*Thalassionema nitzschioides; Skeletonema costatum; Thalassiosira* sp.*; Nitzschia closterium*	12°C	16.6	102.8 (day 0.5)	195 (day 5.5)	1.7 (day 0.5)	33.6 (day 5.5)	~ 400 (day 0.5) mf BRT	620 (day 5.5) mf BRT
3	*Skeletonema costatum*; *Thalassionema nitzschioides; Nitzschia closterium*	12°C	16.0	108.4 (day 3.5)	240 (day 7.5)	4.8 (day 3.5)	59 (day 7.5)	218 (day 3.5) mf BRT	540 (day 7.5) mf BRT
Monoculture growth experiments									
4	*Chaetoceros muelleri*	18°C	31.0	35 (day 7.5)	75.7 (day 13.5)	17.3 (day 7.5)	72 (day 13.5)	150 (day 9.0) mf BRT	200 (day 13.5) mf BRT
5	*Phaeocystis* sp.	18°C	31.0	90.9 (day 1.5)	107.1 (day 8.5)	1.3 (day 1.5)	4.4 (day 8.5)	189 (day 1.5) mf BRT	225 (day 8.5) mf BRT
6	*Nitzschia closterium*	18°C	31.0	100 (day 2.5)	150 (day 9.5)	10.7 (day 2.5)	25.5 (day 9.5)	219 (day 2.5) mf BRT	400 (day 9.5) mf BRT

Table 4.1 Summary table of minimum and maximum chlorophyll concentrations, oxygen saturations and BRT for phytoplankton growth experiments. mf BRT in the last two columns indicates if BRT values were median filtered.

Experiment number	Correlation chlorophyll concentration versus BRT	Correlation oxygen saturation versus BRT
1	r = 0.854 p = 0.002 n = 9	r 0 0.929 p = 0.000 n = 9
2	r = 0.481 p = 0.041 n = 14	r = 0.691 p = 0.000 n = 77
3	r = 0.782 p = 0.002 n = 11	r = 0.727 p = 0.006 n = 11
4	r = 0.210 p = 0.268 n = 11	r = 0.745 p = 0.000 n = 145
5	r = 0.624 p = 0.020 n = 11	r = 0.694 p = 0.000 n = 271
6	r = 0.757 p = 0.000 n = 21	r = 0.928 p = 0.000 n = 507

Table 4.2 Summary table of Spearman's rank correlation coefficients, p-values and sample size of BRT and chlorophyll concentration and BRT and oxygen saturation for phytoplankton growth experiments. The Spearman's correlation coefficients were computed using SPSS. The non-parametric Spearman's rank correlation coefficient was selected as the variables were not normally distributed. For experiments 2-6, correlation coefficients were calculated using mfBRT values.

4.4.2 Oxygen saturation

BRT and oxygen saturation in phytoplankton growth experiments

The measured parameter that correlates best with BRT is oxygen saturation (Table 4.2), which is in turn linked to the rate of net phytoplankton production. For all phytoplankton growth experiments (Kiel Firth water as well as monoculture experiments), correlations between oxygen saturation and BRT were highly significant (Table 4.2). For those experiments where BRT increased significantly with increasing chlorophyll concentration and thus with increasing oxygen saturation, the absolute saturation values reveal that it was necessary for the tank water to be sufficiently supersaturated with respect to oxygen for major changes in BRT to occur. This corresponds well with the findings of Keeling (1993), who discussed that the tendency of bubbles to grow or contract depends on the concentration of dissolved oxygen in seawater. The results showed that a certain threshold in oxygen saturation needed to be reached, ranging from 110-140% for the different experiments, until significant increases in BRT became apparent (Figure 4.3). The variation of this threshold between different phytoplankton growth experiments may be explained by several factors. First, it is likely that among the different growth experiments, bubbles of slightly different sizes were created. From the findings of Wang and Monahan (1995) and Monahan (2001) the different bubble sizes may be attributed to differences in salinity for the various experiments (see Table 4.1). The amount and composition of organic surfactants produced by the different phytoplankton species may have changed the surface curvature of the bubbles and thus their sizes to different degrees, as has been

discussed by Woolf and Thorpe (1991). If smaller bubbles were created in the tank, they should have dissolved faster than larger bubbles as described by Harris and Detsch (1991). Therefore, smaller bubbles would need different degrees of supersaturation in order to inhibit bubble dissolution and to initiate bubble growth. Thirdly, dissolved and colloidal organic substances produced by the different algal species may have inhibited the exchange of gas from bubbles to the surrounding water at different degrees, depending on the effectiveness of the substances to form a more or less impermeable cover on the bubble surface (Woolf, personal communication, Krägel, personal communication). The dependency of BRT on oxygen saturation was further concluded as the maximum values of BRT temporally occurred with the maximum oxygen saturation of the tank water. Declines in BRT during the senescent phases of the phytoplankton growth cycle corresponded to decreases in oxygen saturation. The dependency of BRT on the oxygen saturation of the water becomes apparent especially for experiments 1 and 6, where, additionally to changes in oxygen saturation and BRT with increasing phytoplankton biomass, diurnal changes in BRT during photosynthesis (i.e. when the tank system was illuminated and positive net production occurred) and during respiration (no illumination) covaried strongly with diurnal oxygen saturation as indicated by the distinct peaks in the Fourier analyses of BRT at a frequency of 1 (Figures 3.7 and 3.68). The two remaining Kiel Firth water experiments (experiments 2 and 3) only revealed these diurnal changes in BRT when oxygen supersaturation did not exceed 150%. At oxygen supersaturations > 150%, this diurnal fluctuation in BRT was not apparent (Figure 4.3). This could have been due to the production of oxygen bubbles by degassing of photosynthetically produced oxygen, resulting in higher BRT. Furthermore, the reduction in oxygen saturation for experiments 2 and 3 during respiration was not strong enough to result in lower BRT, thus it was most likely still leading to the formation of oxygen bubbles as a result of high supersaturation. In comparison to those experiments where the tank water was supersaturated with oxygen (experiments 1, 2, 3 and 6), saturation to ~ 100% as well as undersaturation of the tank water did not result in major changes of BRT, as shown by the results of experiments 4 and 5. This is the main difference compared to the remaining growth experiments, when the tank water was highly supersaturated with oxygen and BRT changed significantly with time. From these comparisons, it becomes evident that it is a precondition for the tank water to be sufficiently supersaturated with oxygen for major changes in BRT to occur. This can be explained by the net diffusive flux of gases across the air bubble - water interface, which is proportional to the concentration gradient driving this flux, as explained

by Woolf and Thorpe (1991), trying to achieve equilibrium between the gas pressure inside an air bubble and the surrounding water. Bowyer (1992) described that for a certain degree of gas saturation, the initial radius of a bubble is important with respect to its lifetime. If this initial radius is below a certain threshold, the bubble will collapse immediately after formation as a result of the Laplace pressure. In order for bubbles not to dissolve immediately after their formation but to grow, gas must diffuse into the bubble from the surrounding water (Bowyer, 1992). As the exchange of gas is always from high to low concentration, gas, respectively oxygen will diffuse into the bubble only if the water is supersaturated with oxygen. This will then result in stabilisation and growth of the bubble, enabling it to reside in the water for a longer period of time. However, as stated by Bowyer and Woolf (2004) the processes of bubble gas dynamics are non-linear, and interdependencies exist between the exchange of gas across a bubble's surface, its resulting size and further gas exchange. If the water is undersaturated with respect to oxygen, as was the case for experiment 4 (*Chaetoceros muelleri*) and for most of experiment 5 (*Phaeocystis*), higher oxygen concentrations of atmospheric level inside the bubble lead to an adjustment of the equilibrium by diffusion of oxygen into the surrounding, undersaturated water. This in turn, will result in rapid dissolution of small bubbles and short BRT. Nevertheless, this process may be accelerated during respiration and may proceed slightly slower during net production, thus explaining why slight day-night fluctuations are still recognisable for experiments 4 and 5.

The regression models investigating the relationship between oxygen saturation and BRT show that for some experiments, the relationship is modelled more accurately by using a quadratic regression, while for other experiments, the relationship is best described by linear regression (Figure 4.2). This finding together with the differences of the regression line slopes as well as the differences in absolute oxygen saturation and BRT for the different experiments indicate that despite the importance of oxygen saturation, BRT in phytoplankton enriched seawater is not only a function of oxygen saturation. The presence of different types and concentrations of algae most likely play an important role with respect to BRT, even though the different degrees of supersaturation of seawater with oxygen are the major influence on BRT. This becomes apparent when referring back to experiment 4 with *Chaetoceros muelleri*, where despite very high chlorophyll concentrations and thus a high number of particles as well as presumably organic exudates present in the water, no major changes in BRT occurred as a result of consistent undersaturation of the seawater with oxygen. The undersaturation despite high net

productivity during this particular experiment resulted from the very low oxygen saturations at the start of the growth phase, which, in turn, originated from the long residence time of the seawater in the tank system before the addition of the algal culture, following enhanced bacterial activity and thus oxygen consumption.

BRT and oxygen saturation in gas saturation experiments

The first gas saturation experiment showed a very important result i.e. increasing the saturation of oxygen on its own by bubbling deionised water with pure oxygen has no effect on BRT. The bubbling of deionised water in the tank system with pure oxygen has been repeated on several occasions at other times to verify this result and has never caused a significant change in BRT. From this it follows that despite the strong correlations between oxygen saturation and BRT for the phytoplankton growth experiments, oxygen saturation on its own is not the only factor responsible for the observed increases in BRT. It demonstrates that sufficient oxygen saturation is a prerequisite for increased BRT but that the increases in BRT are linked to the presence of phytoplankton cells and/or the production of organic exudates as well. Nitrogen saturation, however, seems to have a greater influence on BRT than oxygen saturation, even though the effect of increasing the nitrogen saturation on BRT is not comparable in order of magnitude to the increases observed during most of the phytoplankton growth experiments. However, this implies that oxygen does not play an exceptional role with respect to BRT but that it is rather the overall gas saturation that needs to be sufficient for bubbles to grow. This is also confirmed by the bubbling with air (i.e. bubbling with both nitrogen and oxygen), where increases in BRT were noticeable but small (between 30 and 100 seconds), depending on the saturation prior to bubbling. From the results of bubbling with pure oxygen and nitrogen, it follows that most likely nitrogen saturation was the dominant factor that caused the increases in BRT when bubbling with air.

The variation of gas saturation through temperature changes produced significant increases in BRT that showed strong correlation with oxygen saturation and good agreement of results between the two (second and third gas saturation experiment) experiments. Nitrogen saturation should have increased by the same order of magnitude as oxygen saturation, given that the initial saturations were equal, as both gases have a saturation increase of ~ 2% per °C. However, as the absolute values of oxygen saturation and thus most likely nitrogen saturation resulting from temperature increase were only slightly higher compared to the oxygen saturation values determined after bubbling with air, the

large increase in BRT cannot be attributed to increasing gas saturation alone. It is more likely a result of varying two parameters (gas saturation and temperature) simultaneously. The reference measurements described in section 3.1 have shown that mean BRT is slightly higher for 18°C reference measurements than for 12°C reference measurements. Coupled with rapid changes in gas saturation, these temperature differences of BRT could be more pronounced, thus accounting for the high BRT observed during the second and third saturation experiment.

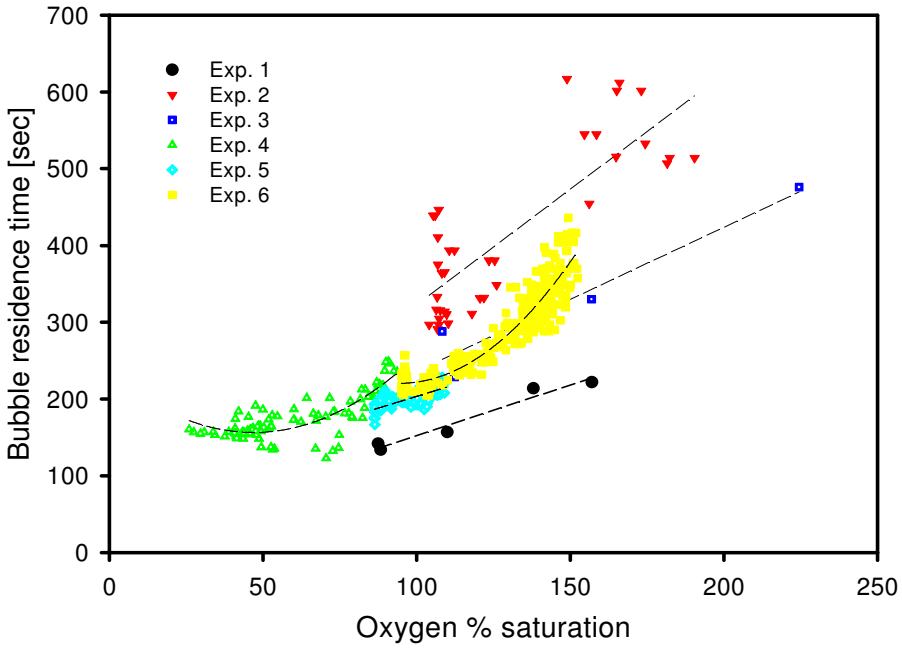

Figure 4.2 Oxygen saturation versus BRT for all phytoplankton growth experiments. The dashed lines are lines of best fit for the respective experiments. For experiments 2-6, mfBRT values were used.

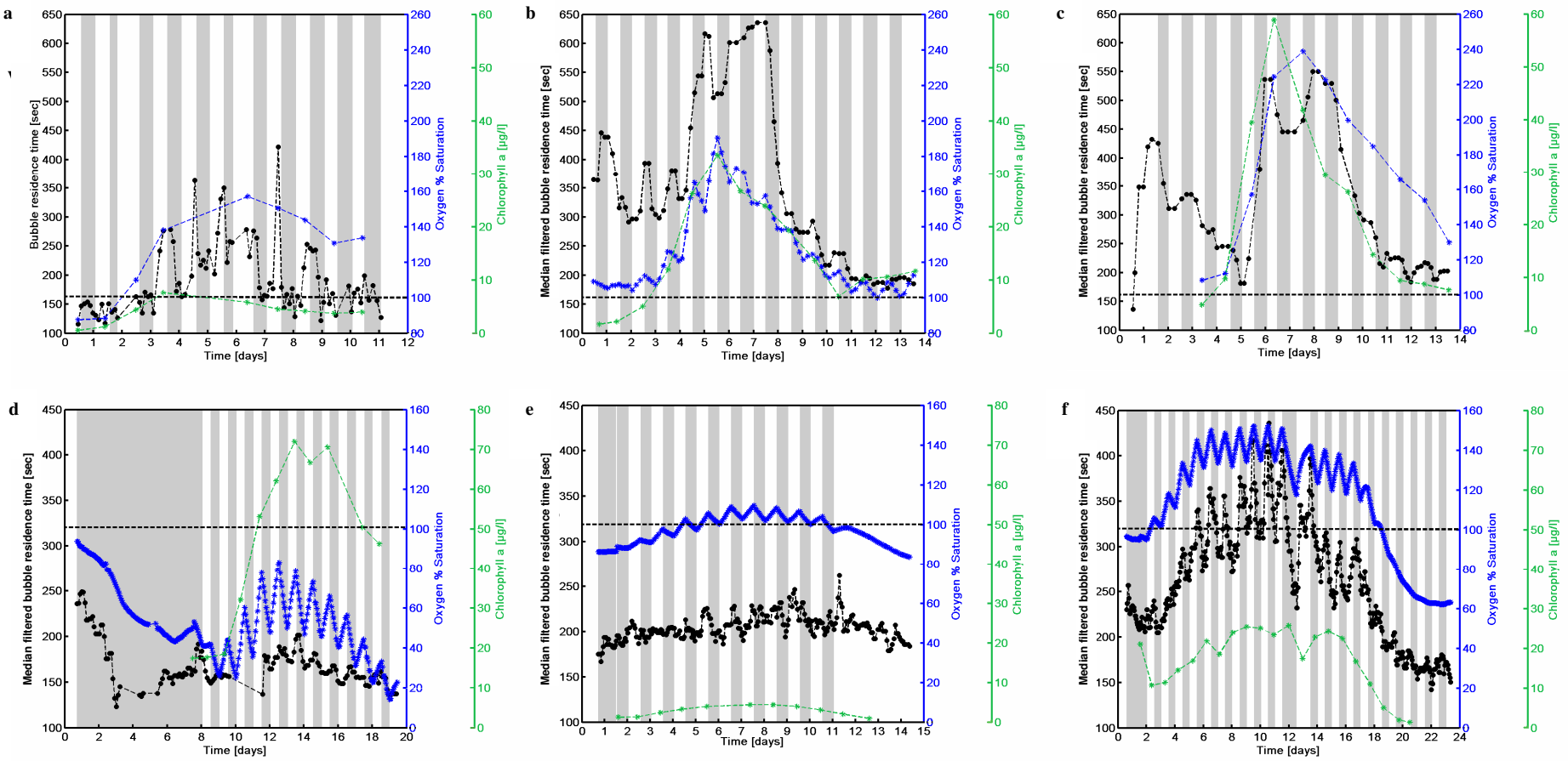

Figure 4.3 Changes in BRT(Exp. 1)/mfBRT(Exp. 2-6), chlorophyll concentration and oxygen saturation with time for all phytoplankton growth experiments.
a)Exp. No.1; b) Exp. No.2; c)Exp. No.3; d) Exp. No.4; e) Exp. No.5; f) Exp. No.6. Dashed black line: 100% oxygen saturation mark.

4.4.3 Prediction of BRT via chlorophyll concentration and oxygen saturation

Prediction of BRT using chlorophyll concentration and oxygen saturation (equation 3.1) proved successful for experiment 1 (first Kiel Firth water growth experiment, see Figure 4.4 a). However, for experiments 2 and 3, prediction of BRT using equation 3.1 was not successful, showing that BRT is not just a function of chlorophyll concentration and oxygen saturation (Figures 4.4 b and c). As shown in Table 4.1, the relationship between maximum chlorophyll concentration, maximum oxygen saturation and maximum BRT was not proportional and for experiment 3, maximum BRT was lower compared to experiment 2 despite higher chlorophyll concentration and oxygen saturation. In all probability this can be attributed to species specific influences on BRT, that cannot be expressed simply via chlorophyll concentration and oxygen saturation but most likely involve other secondary parameters such as the DOC concentration, bacterial activity and interfacial properties. Unfortunately, it was not possible to define the particular influences of these parameters on BRT adequately due to methodological limitations as well as the fact that parameters were interlinked. In order to establish a more accurate prediction of BRT, clarification is needed of which parameters (except chlorophyll concentration and oxygen saturation) are responsible for increased BRT during the growth experiments and how these parameters are interlinked. This will need further detailed experimental investigation as well as modifications and improvement of the methodological approach.

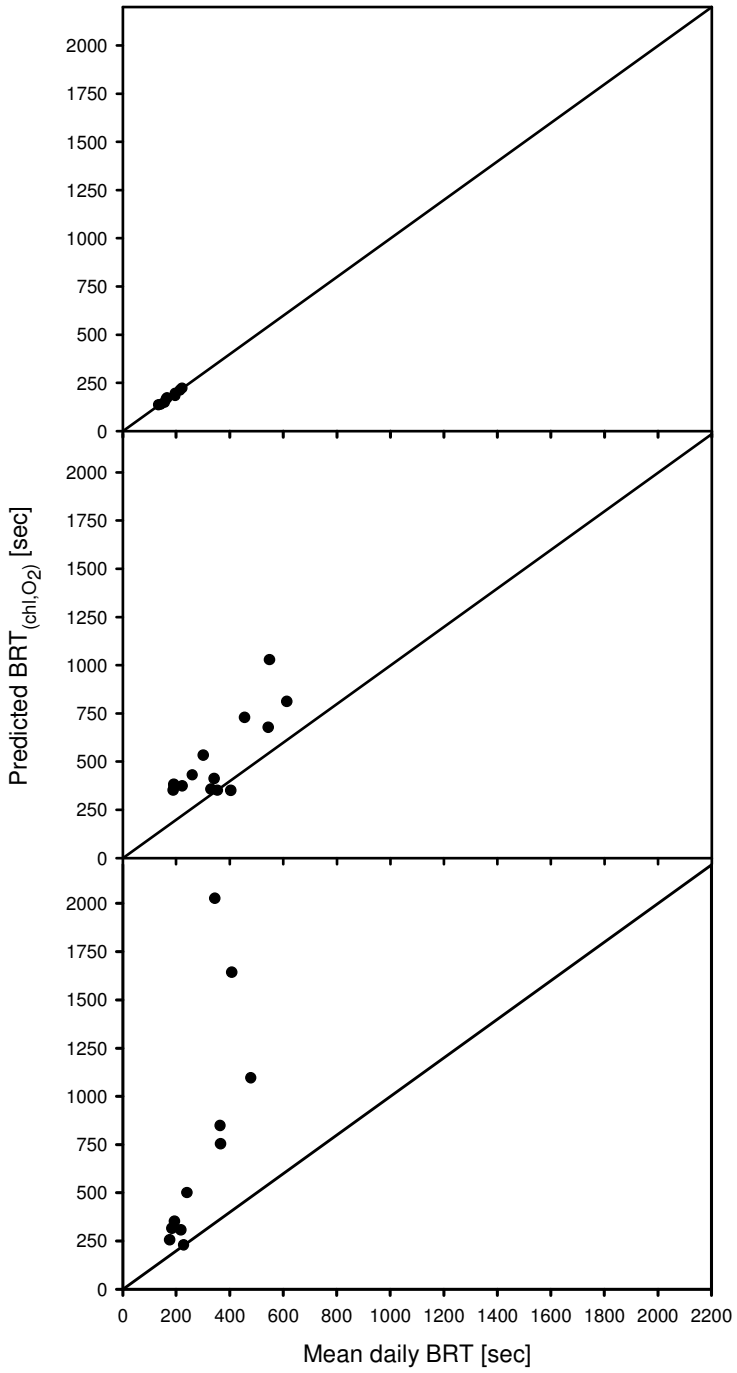

Figure 4.4 Summary Figure of measured BRT versus predicted BRT for Kiel Firth water growth experiments.
a: Experiment 1; b: Experiment 2 with mean daily mf BRT; c: Experiment 3 with mean daily mf BRT; black solid line shows the 1:1 ratio.

4.4.4 Dissolved organic carbon

A consistent covariation between BRT and DOC concentration was not found in any of the phytoplankton growth experiments. For all growth experiments, DOC increased with increasing chlorophyll concentration, but the concentrations and rates of increase became significantly higher during the stationary and senescent phase. These results generally agree with the findings of other studies conducted by Lee and Wakeham (1989), Williams (1990) and Norrman *et al*. (1995), who also reported that DOC production rates were higher during the senescent phase of a phytoplankton bloom compared to the exponential growth phase. The increase of DOC concentrations during the senescent phase of the phytoplankton growth experiments may be attributed to nutrient stress as already discussed by Jensen (1984) and Williams (1990), particularly for experiments 1, 2 and 3, when the cultures became depleted in silicate. Bacterial induced cell lysis of phytoplankton cells during the senescent phase, described by Imai *et al*. (1993) was likely to have contributed to the higher DOC levels observed during senescent phases. Another factor accounting for the increases in DOC concentration could also be the bacterial release of DOC from capsular material, which was described and discussed by Stoderegger and Herndl (1998). A contribution of bacterially produced DOC is likely as the bacteria numbers increased towards the end of the growth experiments (during the senescent phase), even though this is not well represented by the results of bacteria numbers due to the problems of attachment of bacteria to tank walls and tubes as discussed in section 4.2. Bacterial counts were carried out on material collected on a filter with a pore size of 0.2 µm and therefore include free living bacteria as well as bacteria attached to phytoplankton cells stained by acridine orange (see section 2.5.5). With respect to the absolute DOC concentrations, the growth experiments with Kiel Firth water revealed higher concentrations, ranging from 260-400 µmol l^{-1} than the monoculture growth experiments. This is due to the high background DOC levels in Kiel Firth water and the Baltic Sea, generally averaging ~300-400 µmol C l^{-1} as measured by Ferrari *et al*. (1996). High background DOC levels in Kiel Firth water (and the Baltic Sea) result from the high amounts of chromophoric dissolved organic matter (CDOM) in the Baltic Sea, (Ferrari *et al*., 1996; Ferrari and Dowell, 1998). The range of DOC values in the monoculture growth experiments, (140-170 µmol l^{-1} for experiment 5 and 130-250 µmol l^{-1} for experiment 6) as well as the concentration increases during the senescent phase agree with DOC concentrations measured during mesocosm diatom growth experiments by Mopper *et al*. (1995). The minor increase in DOC concentration during the *Phaeocystis* experiment can be accounted for by (i) the lower

chlorophyll concentrations and thus lesser amounts of dissolved organic material and (ii) the resistance of *Phaeocystis* to microbial degradation due to its tight colony skin, described by Hamm *et al*. (1999). Despite the lack of complete covariation between DOC content and BRT, it still cannot be excluded that no interrelation between DOC and BRT existed. Background values of DOC were significantly high (>250 µmol l^{-1}) especially for Kiel Firth water at the beginning of experiments as mentioned earlier. Background values of >100 µmol C l^{-1} also existed for the monoculture growth experiments with *Phaeocystis* and *Nitzschia closterium*. It can be argued, that especially for Kiel Firth water, a large fraction of the dissolved organic material was present in the form of CDOM and thus was likely to have been inert, as Hansell and Carlson (2002) state that the reactive fractions are usually rapidly consumed by heterotrophic bacteria. Additionally, oxygen saturation was not sufficient at the beginning of experiments to initiate bubble growth and to thus enable accumulation of dissolved and colloidal organic material on bubble surfaces. With increasing chlorophyll concentration, oxygen saturation increased, resulting in decelerated bubble dissolution and thus increased BRT for experiments 1, 2, 3 and 6. It is possible that the observed increases in BRT were significantly enhanced by the increases of the DOC concentrations and the accumulation of organic material on the surfaces of bubbles, reducing the rise velocity of bubbles and slowing down the gas exchange from bubbles to the surrounding water. Further increases of DOC concentration during the senescent phase should not have had much influence on BRT due to declines in oxygen saturation and the resulting enhanced bubble dissolution. The degree of DOC contribution to BRT is further unresolved as no information was obtained about its chemical composition. The chemical composition determines the surface activity of DOM as was shown by studies of Leppard (1995), who investigated the composition of algal mucilages and Zhou *et al*. (1998), who assessed surface active carbohydrates in seawater. It is likely that a large fraction of the DOC produced by phytoplankton were reactive, surface active polysaccharides, as shown by the studies of Leppard (1995) and Lancelot (1995). Additionally to reduced bubble dissolution resulting from high oxygen saturation, surface active polysaccharides may have stabilised the bubbles by accumulation on the bubble surfaces and the formation of a rigid cap (Patro *et al*., 2000), thus contributing to increased BRT. However, from the results of DOC concentrations and corresponding BRT for the different growth experiments, it is evident that phytoplankton exudates in the form of DOC were not the only influence on BRT.

4.5 Effect of phytoplankton growth and its influence on air bubble residence time with respect to:

4.5.1 Surface tension

Contrary to the results of Nägeli and Schanz (1991) and Slauenwhite and Johnson (1996), who found decreases in the surface tension of water samples containing phytoplankton monocultures (range of 8.9 mN m^{-1} for *Clamydomonas rheinhardii* and 5.1 mN m^{-1} for *Oscillatoria agardhii* see Table 4.3) and a reduction in bubble surface tension for seawater containing phytoplankton (range of 5.3 mN m^{-1} for *Nitzschia pungens* see Table 4.3), no significant reduction in surface tension was detectable with the SITA f60 tensiometer over the different stages of growth for experiments 2 (range of 0.9 mN m^{-1}) and 4 (range of 0.4 mN m^{-1}), for which surface tension measurements were carried out. This included the investigation of accumulation of surface active substances with time, which was achieved using the auto-mode of the instrument (see section 2.5.8) and which revealed no significant reduction in surface tension within the timeframe of 60 seconds. It can be argued, that most likely this timeframe is not long enough to accumulate sufficient surface active material, especially if it is compared to the potential lifetime of bubbles at increasing BRT (assuming that BRT is a representative value of the lifetime of a bubble). However, test measurements were carried out with dense monocultures of *Nitzschia closterium* (4.3×10^5 cells $ml^{-1} \pm 4.7 \times 10^4$) and *Phaeocystis* ($1.4 \times 10^6$ cell $ml^{-1} \pm 2.1 \times 10^5$ cells ml^{-1}) using a different surface tension measurement instrument, the Profile Analysis Tensiometer PAT-1 (Sinterface Technologies), which enables monitoring of surface tension over time spans of several minutes. The principle of the PAT-1 is based on the analysis of the shape of a pendent and sessile drop via a profile fitting technique. The general theory of this measurement method is based on a liquid meniscus which is subjected to gravity, taking a shape which corresponds to the minimum of the total energy of the system (i.e. sum of the bulk plus interfacial energy). The interfacial energy depends on the interfacial tension. The fitting software of the instrument fits a Laplacian curve to the observed drop profile. The experimental profile is compared with the calculated Laplacian curve. From the difference between experimental and theoretical profile, the surface tension can be calculated. Further details on this method are given in Loglio *et al*. (2001). Results of these test measurements are shown in Figure 4.5 and do not reveal significant changes in surface tension with increasing adsorption time. However, the surface tension of *Nitzschia closterium* was lower (mean surface tension ~ 72 mN m^{-1}) than the surface tension of *Phaeocystis* and F/2 nutrient medium (mean surface tension ~ 74-75 mN m^{-1}), indicating that possibly some

surface active substances were produced by *Nitzschia closterium* which initially lowered the surface tension but did not lead to a further decline in surface tension with increasing adsorption time.

To date few studies have investigated the surface tension of algal samples and Nägeli and Schanz (1991) and Slauenwhite and Johnson (1996) have used different species (including freshwater species) to the ones investigated in this study (see Table 1.3) as well as different measurement methods of surface tension. Nägeli and Schanz used a ring tensiometer and Slauenwhite and Johnson investigated bubble surface tension by spinning single bubbles in a rotating cell. For both studies (Nägeli and Schanz and Slauenwhite and Johnson) the range between minimum and maximum surface tension was significantly greater than for any of the experiments from this study (Table 4.3). Due to the larger sample volume needed for the ring tensiometer method, larger quantities of surfactant may have been available during Nägeli's and Schanz' investigations. The influence of algae on surface tension may be species specific, this being another possibility why Nägeli and Schanz and Slauenwhite and Johnson detected an influence. However, especially with regards to *Phaeocystis*, it is remarkable and unexpected that no surface activity could be detected, as this organism is well known for its foaming capacity, described by Lancelot (1995) that in turn is attributed to the release of surface active polysaccharides (Lancelot and Rousseau, 1994; Lancelot, 1995) resulting in regularly occurrences of foam accumulation along Dutch and German North Sea beaches as reported by Bätje and Michaelis (1986). Additionally, Hoagland *et al*. (1993) state that diatoms are well known to release large amounts of polysaccharides during all stages of growth, many of which are known to be surface active, as discussed by Zutic *et al*. (1981), Mopper *et al*. (1995) and Zhou *et al*. (1998). In all growth experiments DOC concentrations were high but evidently the organic material present in the tank water was not sufficiently surface active to significantly influence surface tension. One explanation for this may be that the surface active polysaccharides produced during phytoplankton blooms, that, according to Gershey (1983) should be predominantly of high molecular weight, were rapidly consumed by heterotrophic bacteria as has been described by Amon and Benner (1994 and 1996). However, Zutic *et al*. (1981) detected significant surface activity in various marine phytoplankton cultures that were non-axenic. It is possible that despite the lack of change in surface tension, some surfactants were produced during the growth experiments conducted in study that contributed to some extent to the changes in BRT in the tank system but were beyond the detection limits of the tensiometers used.

Experimental results of surface tension measurements								Surface tension measurements from literature						
Exp. No.	**Algal species**	**Temp. (°C)**	**Sal.**	**Min. surface tension (mN/m)**	**Max. surface tension (mN/m)**	**Range**	**Mean standard deviation**	**Algal species**	**Min. surface tension (mN/m)**	**Max. surface tension (mN/m)**	**Range**	**Temp. (°C)**	**Sal.**	**Reference**
2	*Thalassionema nitzschioides; Skeletonema costatum; Thalsassiosira* sp.*; Nitzschia closterium*	12°C	16.6	73.3	74.2	0.9	0.3	*Oscillatoria agardhii*	66.5	71.6	5.1	20	0	Nägeli and Schanz (1991)
								Clamydomonas rheinhardii	62.5	71.4	8.9	20	0	
4	*Chaetoceros muelleri*	18°C	31.0	73.36	73.72	0.4	0.07	*Nitzschia pungens*	67	72.3	5.3	?	?	Slauenwhite and Johnson (1996)

Table 4.3 Summary table of minimum and maximum surface tension values and range for experiments 2 and 4 and from the literature.

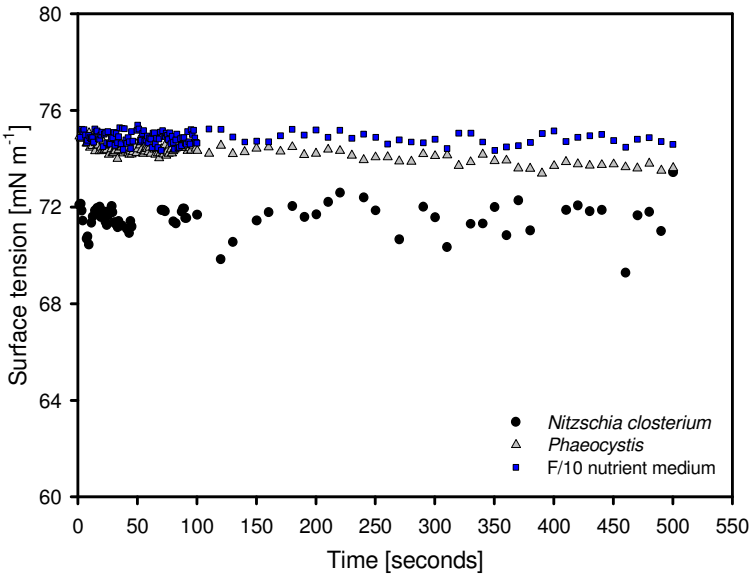

Figure 4.5 Changes in surface tension with time for filtered *Phaeocystis* and (unfiltered) *Nitzschia closterium* determined with the PAT-1.
PAT-1 measurements were carried out by the Department of Analytical Chemistry – University of Geneva.

4.5.2 Bulk water viscosity

Results of bulk water viscosity for the different growth experiments reveal that bulk water viscosity was not influenced significantly by phytoplankton growth, as no covariation with chlorophyll concentration or DOC existed except for experiment 6 with *Nitzschia closterium*, where a slight increase in bulk water viscosity occurred during days 8-13, when chlorophyll concentration was high. The ranges between minimum and maximum viscosity for all other growth experiments were only marginally greater than the mean standard deviations (Table 4.4), indicating that variations in viscosity between the different days were more likely resulting from experimental errors than from real effects. These results generally agree with findings of Mopper *et al*. (1995) who also detected only marginal changes in viscosity of a similar order of magnitude (0.937-0.945 mm^2 sec^{-1}) during a diatom bloom in a tank system. However, comparison with results of Petkov and Bratkova (1996, Table 4.4) reveal that contrary to the results of this study, they detected distinct increases in viscosity with increasing algal density as indicated by the greater range between minimum and maximum viscosity compared to this study. Reasons for this could be differences in algal biomass investigated in this study and that of Petkov and Bratkova. Species specific influence on viscosity may also account for the differences in range. Comparison between these results also shows that minimum viscosity was much higher in the cultures and natural phytoplankton populations used in this study. Most likely

this can be attributed to (i) the different temperatures of viscosity measurements (12 and 18°C opposed to 25 and 35°C) as well as (ii) different salinities (0 opposed to 14.5-31) and (iii) different nutrient media. Experimental error resulting from visual judgement of the flow time through the capillary as well as small errors in the sample volume may account for the outliers observed for experiments 2 (day 12.5) and 5 (day 1.5). However, absolute values of bulk water viscosity differed significantly between the different growth experiments. Factors that can account for this are first of all the differences in temperature, as viscosity measurements were always carried out at the experimental temperature of the tank system (i.e. either 12°C or 18°C). Viscosity was found to have been generally higher for experiments 1 and 2 carried out at a temperature of 12°C compared to experiments 5 and 6 carried out at 18°C (Table 4.4). Secondly, the order of magnitude of viscosity may have been specific to the algal species and their exudates. Despite higher water temperature, the highest viscosity values were measured during experiment 4. Reasons for this are unclear and cannot be attributed to the high chlorophyll concentrations of the samples, as the first two measurements (refer to Figure 3.47 days 0.5 and 5.5) were conducted with filtered seawater before the addition of nutrient medium and algae when bulk water viscosity was already 1.242 mm^2 sec^{-1}. Furthermore, the viscosity experiment (Figure 3.96) with different concentrations of *Chaetoceros muelleri* revealed lower viscosities for much higher chlorophyll concentrations compared to the viscosity values of experiment 4 despite equal measurement temperature and salinity. It is possible that the high viscosity values for experiment 4 may have resulted from DOM present in the tank water samples. The fact that viscosity values for experiment 5 (*Phaeocystis*) were higher than for experiment 6 (*Nitzschia closterium*) at equal temperatures and salinities further emphasises that factors such as the concentration and composition of dissolved organic matter or the composition and texture of the cells may have influenced bulk water viscosity. This is supported by the results of Myklestad (1972), who measured differences in viscosity for different concentrations of extracellular polysaccharide solutions isolated from *Chaetoceros affinis* in seawater. The fact that viscosity measurements in algal cultures is not necessarily dependent on cell density but is species specific was shown by Petkov and Bratkova (1996), who detected a slightly higher viscosity of a *Scenedesmus acutus* sample with an algal density of 2.13 g l^{-1} (0.93 mPa sec) than for a density of 5.11 g l^{-1} (0.9 mPa sec) at a temperature of 35°C. At a lower water temperature of 25°C, the sample with lower algal density also had a lower viscosity (Table 4.4). They also measured high viscosities for *Porphyridium sordidum* (Table 4.4) and attributed this to

enhanced polysaccharide excretion. Differences in the composition of DOC could also account for the higher viscosities of *Phaeocystis* compared to the lower viscosities of *Nitzschia closterium*.

Influence of viscosity on BRT

No detectable covariation of bulk water viscosity with chlorophyll concentration and DOC content was found for the various phytoplankton growth experiments conducted in this study. However, the differences in the order of magnitude of viscosity between the different growth experiments may have resulted in different bubble rise velocities for those experiments when supersaturation of the water was high and bubble residence time was not defined largely by bubble dissolution but by bubble rising. Unfortunately these effects cannot be separated as (i) both parameters, oxygen saturation as well as order of magnitude of bulk water viscosity differed for all growth experiments and (ii) rise velocity of bubbles could not be measured.

Experimental results of viscosity measurements								Viscosity measurements from the literature						
Exp. No.	**Algal species**	**Temp. (°C)**	**Sal.**	**Min viscosity (mPa sec)**	**Max viscosity (mPa sec)**	**Range**	**Mean Stan. Dev.**	**Algal species**	**Temp. (°C)**	**Sal.**	**Min viscosity (mPa sec)**	**Max Viscosity (mPa sec)**	**Range**	**Reference**
1	*Stephanopyxis turris; Rhizosolenia* sp.; *Asterionella japonica; Nitzschia closterium*	12	14.5	1.19	1.20	0.01	0.008	*Scenedesmus acutus*	 25 35 25 35	0	Medium I: 0.92 0.75 Medium III 1.02 0.82	Medium I: 1.05 0.86 Medium III 1.12 0.90	 0.13 0.11 0.1 0.08	Petkov and Bratkova (1996)
2	*Thalassionema nitzschioides; Skeletonema costatum; Thalassiosira* sp.*; Nitzschia closterium*	12	16.6	1.19	1.20	0.01	0.004	*Chlorococcum* sp.	 25 35	0	Medium I: 0.92 0.75	Medium I 1.44 1.15	 0.3 0.22	Petkov and Bratkova (1996)
4	*Chaetoceros muelleri*	18	31	1.24	1.25	0.01	0.004							
5	*Phaeocystis*	18	31	1.07	1.08	0.01	0.002	*Porphyridium sordidum*	25	0	0.95	2.62	1.67	Petkov and Bratkova (1996)
6	*Nitzschia closterium*	18	31	0.90	0.92	0.02	0.002							

Table 4.4 Summary table of minimum, maximum viscosity and range for phytoplankton growth experiments and from the literature.
The calculation of the range does not include outliers as these are considered to be measurement errors. Instead of the kinematic viscosity, the dynamic viscosity (including the density of the water samples) was calculated for the minimum and maximum values of the phytoplankton growth experiments for better comparison with viscosity values from the literature.

4.5.3 Surface shear viscosity

Results of surface shear viscosity measurements for different phytoplankton monocultures revealed that the influence of phytoplankton on this parameter is species specific. Furthermore, it depends on the growth phase of the culture and the presence of cells in the sample. None of the cultures except *Nitzschia closterium* showed a significant influence on the surface shear viscosity. The surface shear viscosities of *Thalassiosira rotula*, *Thalassiosira punctigera* and *Phaeocystis* were identical to the shear viscosity of cell-free F/2 nutrient medium. For these samples, surface shear viscosity was characterised by a slight decline from approximately 6-7 μNs m^{-1}, reaching zero after ~300 minutes. As this order of magnitude is close to the detection limit of the shear rheometer, it is difficult to account for the decline. One hypothesis is that at first, the surface active component of the sample quickly altered the mechanical properties of the interface by stabilising it, resulting in slightly higher surface shear viscosities (Krägel, personal communication). Due to proximate adsorption of other competitive molecules at the interface, the structure of the adsorption layer may have been modified in a way that its mechanical properties changed again, resulting in decreasing surface shear viscosities. For *Nitzschia closterium* however, surface shear viscosity of the stock culture behaved different from that of the remaining algal species as well as F/2 nutrient medium. The increase during the first 250 minutes may have resulted from the adsorption of surface active substances to the interface, forming compact mechanical structures through the unfolding and consequent interactions of protein molecules, thus enhancing the surface shear viscosity, as described by Wüstneck *et al*. (1996). The compact mechanical structures may have resulted from the formation of polymer networks, also known as polymer gels, originating from the aggregation of DOM and colloidal DOM produced by the algae into larger aggregates (Chin *et al*., 1998). This assumption is strengthened further as *Nitzschia closterium* was found to be the main phytoplankton species responsible for exopolymer material in the Northern Adriatic Sea leading to the mucilage phenomenon as described by Revelante and Gilmartin (1991). During the stable phase of surface shear viscosity (from 250-700 minutes), the equilibrium adsorption layer was established, as described by Miller *et al*. (1996). The fact that no further increase in surface shear viscosity occurred may be attributed to the large number of competing molecules at the interface, making it more difficult for these to unfold as it was discussed by Wüstneck *et al*. (1996) who investigated the formation of adsorption layers of model proteins. The decline in surface shear viscosity during the last 400 minutes may have been a result of denaturing of the compact adsorption layer due to enhanced

bacterial activity. At this point in time, it is likely that desorption of surface active molecules from the pre-established equilibrium adsorption layer had started (Miller *et al*., 1996), possibly also as a result of decelerated phytoplankton metabolism. Another possibility may be the rearrangement and displacement of molecules at the interface, which could have resulted in decreasing surface shear viscosity (Krägel, personal communication). The results summarised in Figures 3.93 and 3.94 show that increases in surface shear viscosity in *Nitzschia closterium* samples occurred during the exponential growth phase (days 3 and 4) when the number of cells was already very large. Reasons for this could be that at the very beginning of exponential phytoplankton growth, the phytoplankton cell number and the resulting amount of surface active organic material produced was not sufficient enough to result in the formation of an adsorption layer with compact mechanical characteristics. The surface shear viscosity of the *Nitzschia closterium* culture at the beginning of exponential growth thus showed the same behaviour as that for F/2 nutrient medium. The similar result of surface shear viscosity on day 7 may have been due to decreased production of surface active compounds and enhanced denaturing due to enhanced bacterial activity. As the results of filtered and unfiltered samples of surface shear viscosity measurements with *Nitzschia closterium* show, the presence of phytoplankton cells in the sample is essential in order for compact adsorption layers to develop. Possibly, the cells themselves contributed to the formation of a compact structure at the air-water interface, especially because *Nitzschia closterium* has the tendency to aggregate. It is more likely though that the presence of cells is a continuous source of dissolved and colloidal organic matter, thus enabling the adsorption of surface active polymer networks at the air-water interface. When the phytoplankton cells were removed from the sample through filtration, the continuous production of planktonic DOM was interrupted, explaining why no increase in surface shear viscosity took place.

Influence of surface shear viscosity on BRT

Unfortunately, there is no direct way of investigating the influence of surface shear viscosity on BRT. However, the relationship between surface shear viscosity and BRT could be explained as follows: Increased surface shear viscosity could have led to a decrease in bubble coalescence as a result of the mechanical resistance at the bubbles surface. This in turn would have resulted in longer residence times at high oxygen supersaturations (when small bubbles did not dissolve immediately), as smaller bubbles rise more slowly than larger bubbles. The formation of a rigid cap on the surface of the

bubbles, resulting from compact mechanical structures as described by Dukhin *et al.* (1998) would have led to essential deceleration of the bubble rise velocities, thus contributing to increasing BRT. Furthermore, the formation of polymer networks at the surface of the bubbles possibly reduced the diffusion of gas from bubbles into the surrounding water. The species specific effect of increased surface shear viscosity may be one factor accounting for the higher BRT values for the growth experiments with natural Kiel Firth water and the monoculture growth experiment with *Nitzschia closterium* besides the effect of oxygen supersaturation on BRT. For all Kiel Firth water growth experiments, *Nitzschia closterium* was among the dominating algal species, although it was never the most abundant species. Despite the much lower cell numbers of *Nitzschia closterium* per millilitre for the Kiel Firth water growth experiments as well as the monoculture growth experiment with *Nitzschia closterium* compared to the cell numbers of the laboratory culture used for the determination of surface shear viscosity (Table 4.5), *Nitzschia closterium* may still have caused some increase in surface shear viscosity during the growth experiments and thus contributed to some degree to the increases in BRT.

Experiment number	**Highest cell number of *Nitzschia closterium* per ml**
1	No cell count data available but *Nitzschia closterium* was among natural algal population in the tank system
2	0.13×10^3 (day 6)
3	4.1×10^3 (day 7)
6	28×10^3 (day 10)
Surface shear viscosity experiment	360×10^3 (day 4)

Table 4.5 Summary table of maximum cell numbers of *Nitzschia closterium* for phytoplankton growth experiments and surface shear viscosity experiment.

4.6 Effects of substantial changes in surface tension, bulk water viscosity and surface shear viscosity on air bubble residence time

A model polysaccharide (Gum Xanthan) and a model surfactant (Triton X 100) were used to selectively investigate the influence of large changes in bulk water viscosity, surface shear viscosity and surface tension on BRT.

Gum Xanthan

Results of measurements of BRT with the model polysaccharide Gum Xanthan indicate that an increase in bulk fluid viscosity led to increased BRT, however, the viscosity increase needed to be fairly large (0.4 $mm^2\ sec^{-1}$) in order for BRT to increase markedly. As Gum Xanthan also changed the rheological properties of the air-water interfaces (as

shown in Figure 3.90), these results verify that in general, not only supersaturation and thus decelerated bubble dissolution can increase BRT, but the bulk phase rheological properties as well as interfacial rheology can have a significant effect on BRT. Reasons for the increase in BRT for the experiment with Gum Xanthan are most likely similar to those that have been discussed in sections 4.5.1 and 4.5.3. Increased viscosity of the Gum Xanthan solution and a high surface shear viscosity would have resulted in reduced bubble coalescence as well as decelerated rise velocity due to the formation of a mechanically stable adsorption layer on the bubbles' surfaces. Furthermore, the gas diffusion from the bubble to the surrounding water was most likely decelerated due to the adsorption of polymers on the surfaces of bubbles. However, as bulk water viscosity as well as surface shear viscosity were enhanced strongly through the addition of Gum Xanthan, it is unlikely that the order of magnitude of increase in BRT resulting from changes in bulk viscosity and surface shear viscosity in this model experiment was similar during the phytoplankton growth experiments or would be likely to occur in the ocean. As bulk phase viscosities measured for experiment 4 (growth experiment with *Chaetoceros muelleri*) were of a similar order of magnitude to those of the model polysaccharide solution, it seems more likely that rather than the bulk water viscosity, the surface shear viscosity and consequently the change in the mechanical characteristics of the bubbles' surfaces may have been the dominant factor with respect to the increased BRT. However, in order to investigate the effect of changes in bulk water viscosity and surface shear viscosity during phytoplankton growth experiments, a measure of bubble rise velocity is needed.

Triton X 100

The model surfactant Triton X 100 was chosen to investigate specifically the influence of surface tension changes on BRT. The experiment with Triton X 100 shows that increasing surfactant concentrations and thus decreasing surface tensions enhanced BRT. The surfactant concentrations that were chosen for the experiment ranged from a very low concentration of 10^{-6} µmol l^{-1}, that did not result in detectable changes in surface tension with the SITA f-60 tensiometer to a high surfactant concentration of 2.5×10^{-4} µmol l^{-1}, which is the CMC (critical micelle concentration) of this particular surfactant (Krägel, personal communication). As the results indicate, a marginal surfactant concentration of 10^{-6}µmol l^{-1} already led to increased BRT. The fact that this low surfactant concentration did not result in a measurable decrease in surface tension indicates that even though a decrease in surface tension was also not detected during the phytoplankton growth

experiments, an influence of phytoplankton produced surfactants on BRT may still have existed. The adsorption time of the bubble pressure tensiometer may have been too short for the adsorption of sufficient amounts of surfactant to significantly alter the surface tension. The increase of BRT with increasing Triton X 100 concentration and decreasing surface tension can be explained by the build up of an adsorption layer as the bubbles rise towards the surface, which was in turn dependent on the adsorbed amount of surfactant (Miller *et al*., 1998). The strength and composition of the adsorption layer thus changed the mechanical properties of the bubble's surface which should have resulted in different rise velocities and possibly reduced bubble coalescence. The investigation of changes in interfacial properties of bubbles and changes in bulk water viscosity through the use of different concentrations of model substances show that changes in the rheological parameters indeed have an effect on BRT. However, with respect to the phytoplankton growth experiments, the influence of rheological parameters on BRT must have been much smaller. The amount and composition of surfactants present during the model experiments was definitely very different compared to those produced by the phytoplankton.

5 Chapter Five. Summary and general conclusions

5.1 Summary of results

The effect of phytoplankton on the residence time of air bubbles in seawater has not previously been investigated. Knowledge of the interrelation between phytoplankton growth and its related parameters on bubble residence time is of importance in order to understand bubble dynamics in the ocean, especially with respect to seasonal variations in surface and subsurface bubble clouds. This is in turn of great importance with respect to air-sea gas exchange processes as well as defence applications.

In order to assess the influence of phytoplankton growth-specific parameters on subsurface BRT, a laboratory tank system was developed with BRT determined from acoustic sampling. Real environmental conditions were simulated including the injection of bubble plumes by a breaking impulse. Investigations of artificially induced phytoplankton blooms with natural plankton communities from Kiel Firth as well as with algal monocultures showed that for strong increases of phytoplankton standing stock, a consequent increase in BRT occurred, provided that the water was sufficiently supersaturated with oxygen. If the water was undersaturated with oxygen, an increase in BRT failed to appear despite increasing phytoplankton biomass.

Investigations of other phytoplankton-related metabolic parameters such as the concentration of DOC revealed a steady increase over the growth period of the phytoplankton populations for all experiments, however, a direct correlation with BRT was not found. Measurements of surface tension and bulk water viscosity that were carried out for several phytoplankton growth experiments in the tank system, showed no dependency of these parameters on phytoplankton biomass or DOC concentration within the resolution of the methods available. Measurements of surface shear viscosity of several phytoplankton monocultures revealed a significant increase only for *Nitzschia closterium*.

Investigations of BRT with different concentrations of a model surfactant and a model polysaccharide proved that changes in the rheological parameters (bulk water viscosity, surface shear viscosity and surface tension) led to significant increases in BRT.

5.2 Conclusions

The results of this study have shown that phytoplankton growth has a significant influence on air bubble residence time in seawater. The parameter that was directly influenced by phytoplankton photosynthesis and that was identified as a necessary precondition for major changes of BRT was the oxygen saturation of the water. Furthermore, during the course of growth experiments, BRT corresponded well with the photosynthesis-respiration (light-dark cycle) induced changes in oxygen saturation, for oxygen saturations below 150%, emphasising the dependency of BRT on the oxygen saturation of the water. The results of the saturation experiments with deionised water however indicate that oxygen supersaturation on its own in a non biological, particle-free system does not show any significant influence on BRT. Changing the total gas saturation of the water by bubbling with air and by temperature variations had a greater influence on BRT than increasing the oxygen saturation alone, indicating that in non-biological systems, nitrogen saturation seems to be the more important factor influencing BRT. However, the importance of oxygen saturation for BRT in relation to phytoplankton growth becomes obvious considering the two growth experiments, when, despite a large increase in chlorophyll concentration, the water remained undersaturated with oxygen and consequently no significant increase in BRT occurred. Thus it can be concluded that the major factor that governs BRT is the dissolution of small air bubbles. Increasing supersaturation slows down the dissolution of small bubbles and the diffusion of oxygen from the supersaturated tank water, counter-balancing the pressure gradient and leading to the stabilisation and growth of small bubbles. The phytoplankton growth experiments have shown that a certain threshold in oxygen saturation has to be achieved for major changes to occur in BRT, so that small bubbles do not dissolve immediately after their formation but can remain in the water for longer periods of time. This threshold was found to be between 110-140% oxygen saturation and is considered to be specific with respect to the species composition of the phytoplankton.

However, the fact that oxygen saturation on its own showed no significant effect on BRT as indicated by the gas saturation experiments leads to the conclusion that BRT in phytoplankton growth experiments is not only dependent on the saturation of the water with oxygen but is also determined by other phytoplankton-related parameters.

From the findings of several other investigations that were presented in the introductory part of this study it became apparent that phytoplankton produce surface active organic material, that is capable of reducing the surface tension of air-water interfaces and thus

should have significant influence on the size, surface structure, rise velocity and gas diffusion of air bubbles in water. However, it was not possible within the scope of this study to come to a definite conclusion about the production and influence of surface active material by phytoplankton and its effects on BRT. The results have shown that over the different growth phases of a phytoplankton experiment, the concentration of DOC in the water increased, indicating that the algae in the tank system produced significant amounts of DOM. It was not possible to detect greater surface activity in the samples with high DOC concentration, however, reasons for this are unclear and may well be linked to methodological limitations in comparison to the amounts and surface activity of material produced. However, it is also possible that the material produced by phytoplankton during senescence, when DOC concentrations increased was not surface active. The fact that *Nitzschia closterium* had a significant effect on the surface shear viscosity demonstrates that at least some phytoplankton species have the ability to build up adsorption layers and thus alter the mechanical properties of an air-water interface. Nonetheless, resulting from the findings of other authors and indications in the results of the phytoplankton growth experiments (e.g. increasing DOC concentration and influence of *Nitzschia closterium* on the surface shear viscosity) it is very likely that during the phytoplankton growth experiments, dissolved as well as particulate organic matter accumulated on the surfaces of the bubbles and thus decelerated their rise velocity, prevented their ability to coalesce and inhibited bubble dissolution. The assumption that other parameters in addition to oxygen saturation caused the increases in BRT during phytoplankton growth is reinforced by the fact that the regression models of oxygen saturation differed significantly for the phytoplankton growth experiments. However, this part of the study remains uncertain as the design of the laboratory tank system and the acoustic determination of BRT unfortunately provided no direct information on the rise velocity of bubbles, their size distributions and their size changes as they rose through the water column. But the fact that even in undersaturated deionised water, where bubble dissolution proceeds rapidly, the addition of large amounts of model substances, which are known to alter the mechanical properties of an interface, the viscosity and the surface tension resulted in longer BRT, demonstrates that changes of the interfacial properties of air bubbles have strong effects. Thus it is very likely that BRT was to some extent influenced by changes in interfacial properties during the phytoplankton growth experiments.

5.3 Suggestions for further work

To further clarify the influence of phytoplankton growth on the residence time of air bubbles in seawater, it will be necessary to focus much more on the influence of particulate, colloidal and dissolved organic matter on the rheological properties of bubbles as this aspect of the current research could not be solved satisfactorily. For this, a different methodological approach will be needed. First of all, it will be vital that the bubbles and their rise through the water column can be observed and thus possible changes in shape and size of the bubbles and maybe even accumulation of material may be recorded. Secondly, the determination of bubble rise velocity will be essential as this gives information on the degree of surfactant contamination of the bubbles. Thirdly, the creation of bubbles of a defined size, possibly via a fine capillary or a micro-size frit would help in determining more precisely the influence of phytoplankton and their exudates on bubble rise velocity and bubble dissolution.

With respect to future *in situ* observations of BRT for example in the wake of a ship, it will be important to record several plankton-related chemical and biological parameters besides the physical and chemical parameters. The determination of phytoplankton biomass, major species composition as well as above all the measurement of dissolved oxygen saturation in the surface waters will be of importance for further investigations of *in situ* BRT. Seasonal investigations of BRT in association with biological as well as chemical parameters in productive regions, where extensive plankton blooms occur during spring and autumn would be of great importance.

6 Appendices

Appendix A

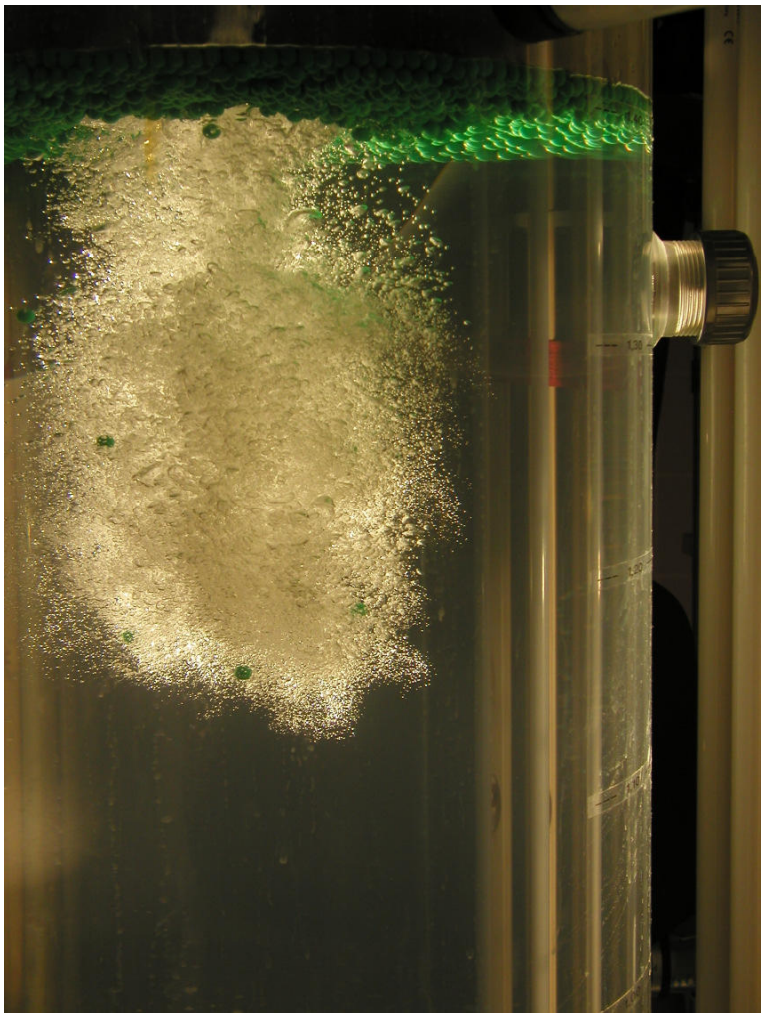

Figure 6.1 Bubble cloud injection.

Appendix B

Transducers
Hydrophones
HYDROPHONE

TC 4014

The TC 4014 broad-band spherical hydrophone offers a very wide usable frequency range with excellent omni-directional characteristics in all planes.

The overall receiving characteristics makes the TC 4014 an ideal transducer for making absolute underwater sound measurements up to 480 kHz. The wide frequency range also makes the TC 4014 perfect for calibration purposes, particularly in higher frequencies.

The TC 4014 incorporates a low-noise 26dB preamplifier providing signal conditioning for transmission over long underwater cables. The TC 4014 features an insert calibration facility which allows for a reliable test of the hydrophone.

The TC 4014 is available with integrated SUBCONN BGH MGP connector. Ask for TC 4039.

Description	
Usable Frequency Range:	15 Hz-480 kHz
Linear Frequency range:	30 Hz to 100 kHz ±2 dB 25 Hz to 250 kHz ±3 dB
Horizontal Directivity Pattern:	Omnidirectional ±2dB at 100kHz
Vertical Directivity Pattern:	270° ±2dB at 100 kHz
Receiving sensitivity: (re 1V/µPa)	-186dB ±3dB
Operating Depth:	900 metres
Survival Depth:	1200 metres
Operating temperature range:	-2° to +55° Celsius
Storage temperature range:	-40° to +80° Celsius
Weight in Air:	650 g without cable
Max. output voltage:	>2.8 Vrms (at 12V DC)
Supply voltage:	12 to 24 V DC
High pass filter:	15 Hz -3dB
Power consumption:	50 m W

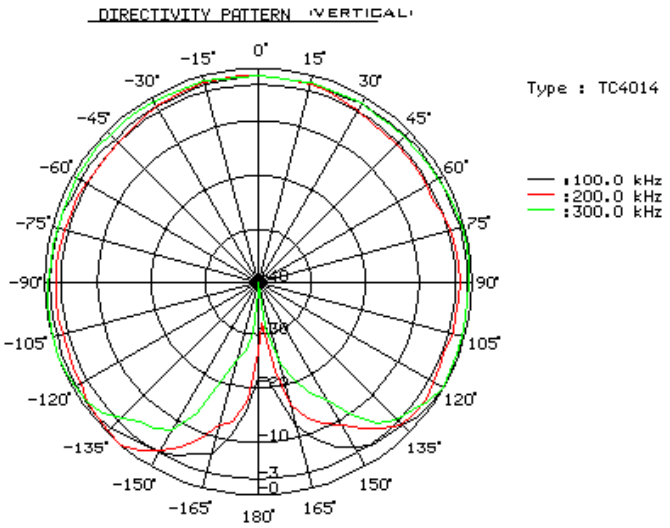
DIRECTIVITY PATTERN (VERTICAL)
0°
15°
30°
45°
60°
75°
90°
105°
120°
135°
150°
165°
180°
-15°
-30°
-45°
-60°
-75°
-90°
-105°
-120°
-135°
-150°
-165°
-10
-3
-0
Type : TC4014
:100.0 kHz
:200.0 kHz
:300.0 kHz

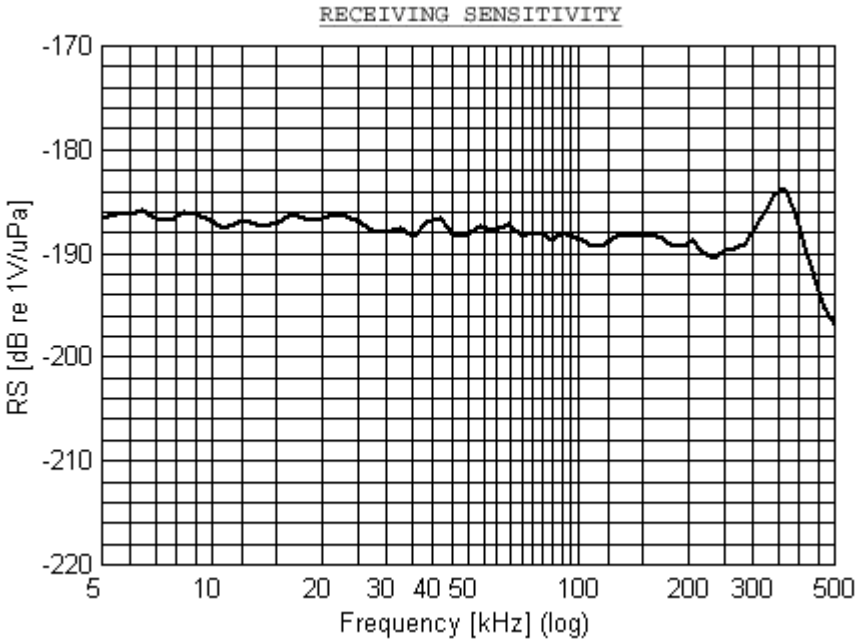
RECEIVING SENSITIVITY
RS [dB re 1V/uPa]
-170
-180
-190
-200
-210
-220
5
10
20
30
40
50
100
200
300
500
Frequency [kHz] (log)

Transducers
Hydrophones
HYDROPHONE

TC 4034

The TC 4034 broadband spherical hydrophone provides uniform omnidirectional characteristics over a wide frequency range of 1Hz to 480 kHz.

The overall receiving characteristics makes the TC 4034 an ideal transducer for making absolute underwater sound measurements up to 480 kHz. The wide frequency range also makes the TC 4034 perfect for calibration purposes, particularly in higher frequencies.

Usable Frequency range:	1 Hz-470 kHz +3, -10 dB
Linear Frequency range:	1 Hz to 250 kHz +1, -4 dB
Transmitting sensitivity: (re 1 µPa/V at 1 m)	122 dB ±3 dB (at 100 Hz)
Receiving sensitivity: (re 1V/µPa)	-218dB ±3 dB (at 250 Hz)
Horizontal Directivity Pattern:	Omnidirectional ±2 dB at 100kHz
Vertical Directivity Pattern:	>270° ±3 dB at 300 kHz
Nominal Capacitance:	3nF
Operating Depth:	900 metres
Survival Depth:	1000 metres
Operating temperature range:	-2° to +80° Celsius
Storage temperature range:	-40° to +80° Celsius
Encapsulating material:	Chloroprene
Metal body:	Alu-bronze
Cable (length and type):	10 m shielded pair DSS-2MIL-C915
Connector type:	BNC
Weight in Air:	1.6 kg

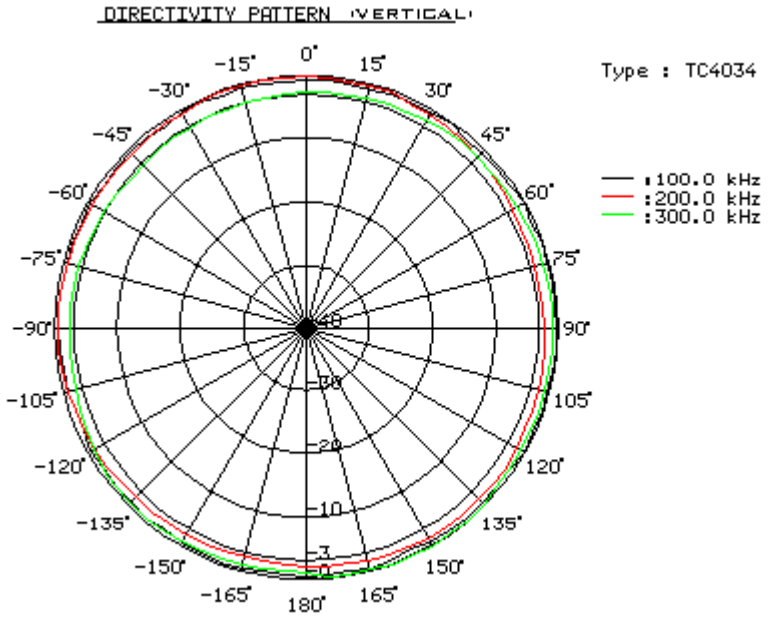
DIRECTIVITY PATTERN (VERTICAL)
Type : TC4034
:100.0 kHz
:200.0 kHz
:300.0 kHz
0°
15°
30°
45°
60°
75°
90°
105°
120°
135°
150°
165°
180°
-15°
-30°
-45°
-60°
-75°
-90°
-105°
-120°
-135°
-150°
-165°
-3
-10
-20

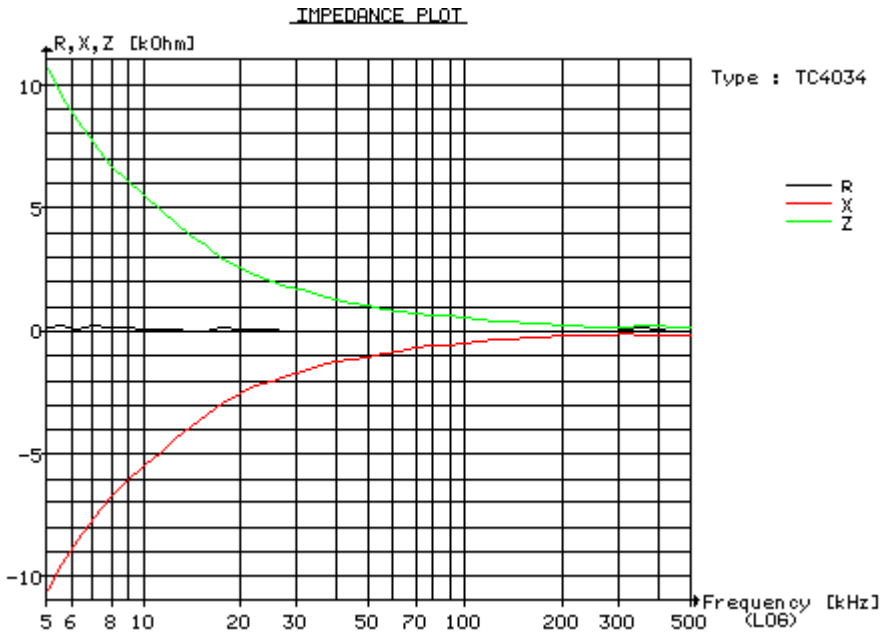
IMPEDANCE PLOT
R,X,Z [kOhm]
Type : TC4034
R
X
Z
10
5
0
-5
-10
5 6 8 10 20 30 50 70 100 200 300 500
Frequency [kHz]
(L06)


RECEIVING SENSITIVITY
RS [dB re 1V/uPa]
-200
-210
-220
-230
-240
Type : TC4034
5 6 8 10 20 30 50 70 100 200 300 500
Frequency [kHz]
(L06)

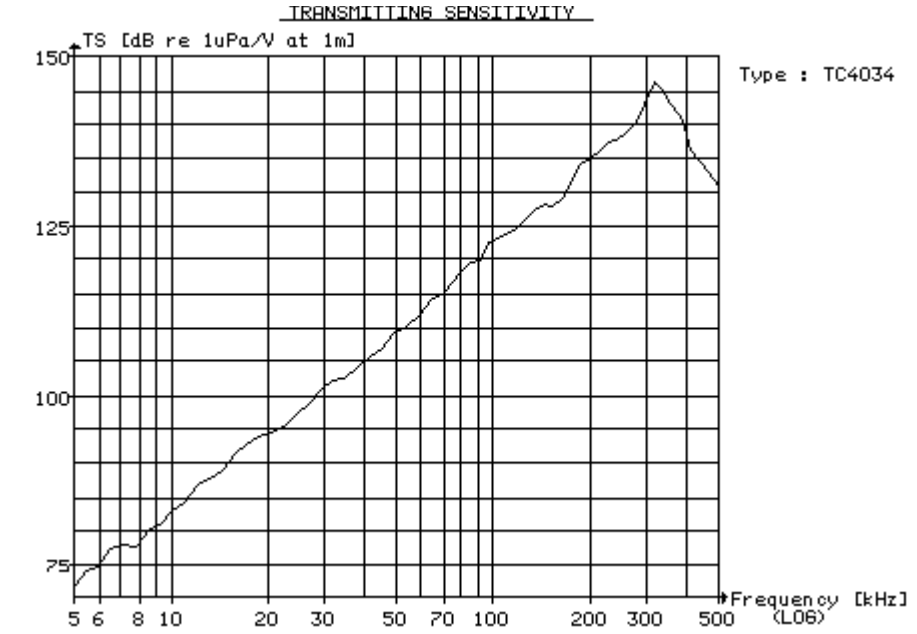
TRANSMITTING SENSITIVITY
TS [dB re 1uPa/V at 1m]
150
125
100
75
Type : TC4034
5 6 8 10 20 30 50 70 100 200 300 500
Frequency [kHz]
(L06)

Model ITC-1042

Spherical Omnidirectional Transducer

Model ITC-1042

The Model ITC-1042 spherical transducer offers broadband omnidirectional transmitting and receiving response with efficiencies of over 50%. This transducer is fabricated of Channelite-5400 lead zirconate titanate ceramic and is particularly well suited for noise sources as a broadband hydrophone and applications where an omnidirectional response is required. This unit can be supplied with Channelite-5800 for high power applications.

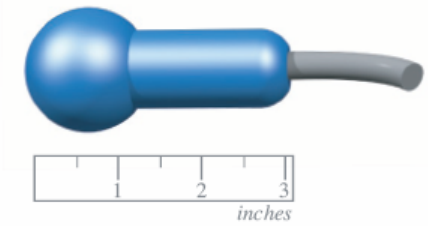

Specifications (Nominal)

Type	Projector/Hydrophone
Resonance Frequency f_r	79 kHz
Depth	1250 meters
Envelope Dimensions (in.)	1.4D
TVR at f_r	148 dB//µPa/V@1m
Midband OCV	-200 dB//1V/µPa
Suggested Band	.01 - 100 kHz
Beam Type	Spherical
Input Power	100 watts

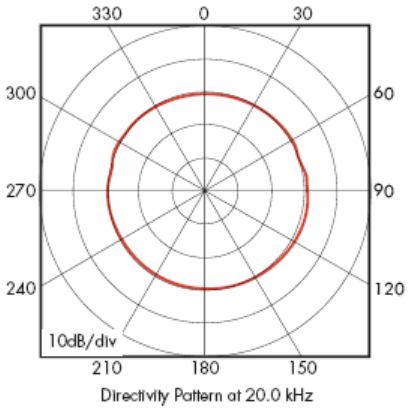

Directivity Pattern at 20.0 kHz

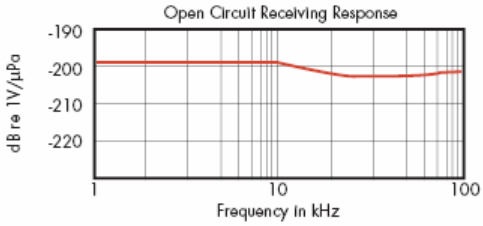

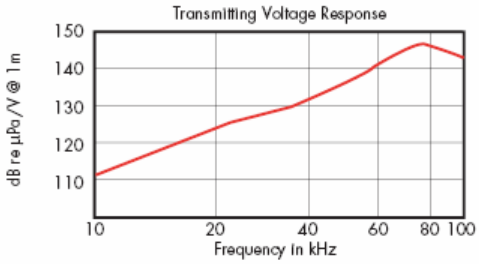

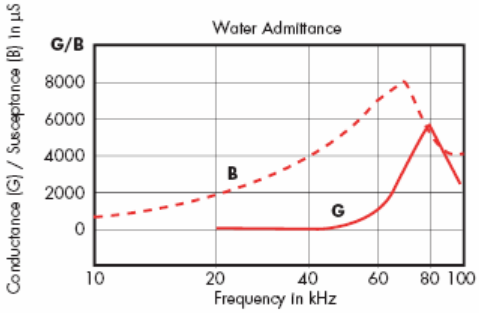

International Transducer Corporation
869 Ward Drive, Santa Barbara, CA 93111
805.683.2575 • 805.967.8199 FAX
www.itc-transducers.com

Appendix C

Figure 6.2 Tank system illumination.

Appendix D

No	Parameter recorded in header file
1	Measurement number
2	Start of measurement: Year
3	Month
4	Day
5	Hour
6	Minute
7	Second
8	1/10 second
9	Identification of measurement type (0 =standard measurement,1 =reference measurement, 3 =test)
10	Identification of outgoing acoustic signal (0 =passive,1 =frequency pulse,2 = ambient pulse)
11	Identification of quality (0 =bad,1 =constricted, 2 =good)
12	Water type
13	Depth of hydrophones [cm]
14	Sound velocity [m/sec]
15	Sampling rate [Hz]
16	Perpendicular period [msec]
17	Number of AD-converter channels
18	Amplification channel 1 [dB]
19	Amplification channel 2 [dB]
20	Amplification channel 3 [dB]
21	Amplification channel 4 [dB]
22	Amplification channel 5 [dB]
23	Amplification channel 6 [dB]
24	Bubble cloud injection at ping no. per frequency
25	Total number of pings
26	Values per ping
27	Height of water outlet of supply tank above large tank bottom [cm]
28	Diameter of water outlet [cm]
29	Water volume injected [litres]
30	Illumination [0 = no illumination; 1 = illumination on]
31	Impulse count of flow meter
32	Cut-off frequency filter 1 [High precision filter 6611A]
33	Cut-off frequency filter 2 [TP Kemo VBF8]
34	Water level of large tank before bubble splash [cm]
35	Water level of supply tank [cm]
36	Surface covering [0= without plastic balls; 1 = with plastic balls]
37	Set-temperature of tank system [°C]
38	Water temperature at beginning of measurement [°C]
39	Water temperature at finishing of measurement [°C]
40	Salinity at beginning of measurement
41	Salinity at finishing of measurement
42	Oxygen Saturation [%]
43	Water temperature as measured by oxygen electrode [°C]

44	Duration of acoustic measurement [min]
45	Time of bubble injection [sec]
46	Duration of turbulence phase [sec]
47	Duration of quiescent phase [sec]
48	Duration of bubble injection [sec]
49	Number of acoustic measurements defined
50	Amplitude carrier signal [mV]
51	Set-pulselength [µsec]
52	Number of frequencies per measurement
53-76	Frequency 1-24 [Hz]
77	Maximum amplitude [mV]
78-102	Amplitudes 1-24 [mV]

Table 6.1 Parameters recorded in header files.

From 16.10.2002-2003

Determination of calibration factor for Fluorometer

Dilute 1 mg Chla-Std in 250 ml 90% acetone.
Corresponds to 4 mg/L oder 4 µg/ml = Standard solution

For calibration the standards are set up in 10 ml vials

Spectrophotometric determination of chlorophyll concentration:

from stand.solu. x ml to 10 ml	theor.corresp.to µg to 10 ml	theor.corresp to. µg/l	E.* 10^{-3} 750 nm	E.* 10^{-3} 665 nm	Standard- set up in ml 90% acetone	Photometer cuvette size cm	desired value Jgofs-Formel Photometer Chl a µg/sample (in10mlAc.)	Photometer Chl a with ex-coeff. µg/l Ac	Jgofs-Formula Photometer Chla with ex-coeff. mg/l Acetone
0.0250	0.1	10	0.007	0.012	10	5	0.114	11.406	0.011
0.0500	0.2	20	0.008	0.015	10	5	0.160	15.969	0.016
0.2000	0.8	80	0.006	0.031	10	5	0.570	57.032	0.057
0.2500	1	100	0.006	0.036	10	5	0.684	68.438	0.068
0.5000	2	200	0.005	0.065	10	5	1.369	136.877	0.137
0.7500	3	300	0.005	0.088	10	5	1.893	189.346	0.189
1.0000	4	400	0.006	0.120	10	5	2.601	260.066	0.260
1.2500	5	500	0.006	0.147	10	5	3.217	321.661	0.322
2.0000	8	800	0.006	0.233	10	5	5.179	517.851	0.518
2.5000	10	1000	0.008	0.290	10	5	6.433	643.322	0.643

Table 6.2 Determination of factor for fluorometric chlorophyll *a* analysis.

Determination of factor for fluorometric Chl a determination

FLUOROMETER formula after Welschmeyer

theor corresp.	Photometer Chla with ex-coeff.	FLUOROMETER Reading before	Volume	Calibration factor	Actual value Chl a	Deisred value Photometer Chla with Ex-coeff.		
					in10mlAc	in1LAc	in1LAc	in1LAc
µg auf 10 ml	mg/l	Raw	ml	K	µg/sample	ug/10mll	ug/l	mg/l
0.1	0.011	1.205	10	0.0094659	0.115	0.114	11.406	0.011
0.2	0.016	1.630	10	0.0097969	0.156	0.160	15.969	0.016
0.8	0.057	5.960	10	0.0095691	0.569	0.570	57.032	0.057
1	0.068	7.180	10	0.0095318	0.686	0.684	68.438	0.068
2	0.137	14.300	10	0.0095718	1.366	1.369	136.877	0.137
3	0.189	20.100	10	0.0094202	1.920	1.893	189.346	0.189
4	0.260	26.900	10	0.0096679	2.570	2.601	260.066	0.260
5	0.322	34.100	10	0.0094329	3.258	3.217	321.661	0.322
8	0.518	54.200	10	0.0095544	5.178	5.179	517.851	0.518
10	0.643	67.500	10	0.0095307	6.449	6.433	643.322	0.643
			Mean:	0.0095542				

Table 6.2 continued

Appendix F

Reagents for spectrophotometric analyses of dissolved inorganic nutrients

Nitrate

Buffer:	75 g ammonium chloride were dissolved in 5 L distilled water. The solution was adjusted to pH 8.5 with approximately 12 ml ammonia. The buffer is sTable.
Sulphanilamide:	5g sulphanilamide and 50 ml concentrated hydrochloric acid were transferred into 500 ml distilled water, dissolved and made up to 1 L.
Coupling reagent:	0.5g N-(1-naphtyl)-ethylendiamine-dihydrochloride (NED) were dissolved in 1 L distilled water together with 1 ml of a surfactant (Brij 35,10%).
Reductor:	Granulated cadmium was separated from finer cadmium using an 800 µm sieve, washed with diluted HCl (~7%) and shaken with 1% copper sulphate solution. It was washed 5 times with deionised water and filled into the reductor glass. Cu settled on the Cd from the $CuSO_4$ solution, forming local cells and hence improving reactivity.
NO_3^- stock solution:	0.85 g sodium nitrate, dried at 110°C and cooled in a desiccator were dissolved in deionised water and filled up to a volume of 1000 ml (= 100 µmol ml^{-1} NO_3^-).

Nitrite

Sulphanilamide:	0.5 g sulphanilamide were dissolved in a small volume of deionised water. 5 ml of concentrated HCl (37%) were added and filled up to 50 ml with deionised water.
Coupling reagent:	0.05 g N-(1-naphtyl)-ethylendiamine-dihydrochloride were dissolved in 50 ml deionised water and stored in a brown glass bottle.
NO_2^- stock solution:	0.6896 g sodium nitrite ($NaNO_2$) dried at 110°C and cooled in a desiccator were filled to 1000 ml in a volumetric flask (= 10 µmol NO_2^- ml^{-1}).

Phosphate

Sulphuric acid, 4.5mol/L:	250 ml concentrated H_2SO_4 (98%) were added carefully to 750ml distilled water and diluted to 1 L.
Acidified ascorbic acid:	10 g ascorbic acid were dissolved in 50 ml water, then 50 ml sulphuric acid were added.
Mixing reagent:	12.5 g $(NH_4)6Mo_7O_{24}$ ·$4H_2O$ were dissolved in 125 ml water. 0.5 g $K(SbO)C_4H_4O_6$ were also dissolved in 20 ml water. The

	molybdate solution was added to 350 ml sulphuric acid, stirring continuously. The tartrate solution was added and mixed well.
PO_4^{3-} stock solution:	1.361 g dried potassium hydrogen phosphate were dissolved in deionised water and filled up in a volumetric flask to 1000 ml (= 10 µmol ml^{-1}).

Silicate

Oxalic acid:	10 g oxalic acid dihydrate $(COOH)_2 \cdot 2H_2O$ were dissolved in 100 ml distilled water.
Ascorbic acid:	2.8 g ascorbic acid, $C_6H_8O_6$ were dissolved in 100 ml distilled water.
Mixed reagent:	38 g $(NH_4)6Mo_7O_{24} \cdot 4H_2O$ were dissolved in 300 ml water. This solution was added to 300 ml sulphuric acid (see phosphate).

Appendix G

Calibration curves and equations for determination of dissolved organic carbon (DOC)

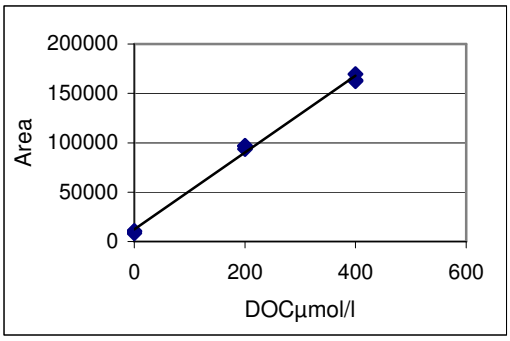

Calibration curve for DOC calculation for experiment 1 (DIMATEC TOC 100 analyser)

$R^2 = 0.9952$
DOC = 388.77x area + 2447

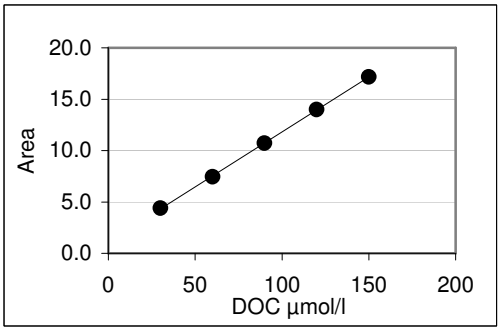

Calibration curve for DOC calculation for experiment 6 samples 1.1-8.1(Shimadzu TOC-V_{CSN})

$R^2 = 0.9999$
DOC = 9.352 x area - 10.504

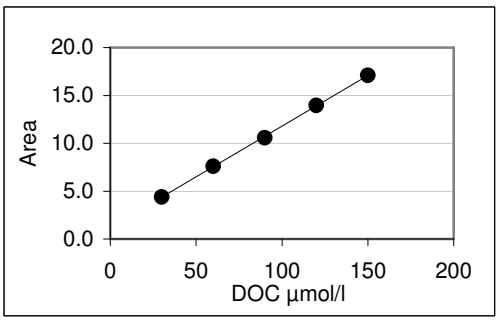

Calibration curve for DOC calculation for experiment 6 samples 8.2-15.2 (Shimadzu TOC-V_{CSN})

$R^2 = 0.9997$
DOC = 9.447 x area - 11.331

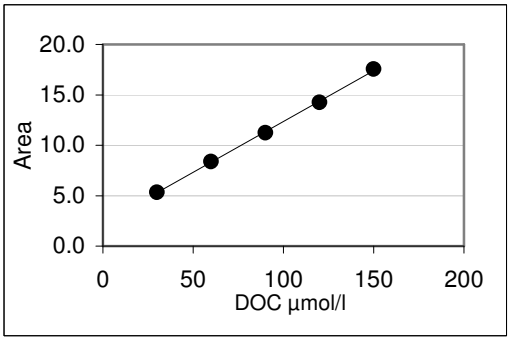

Calibration curve for DOC calculation for experiment 6 samples 15.3-21.3 (Shimadzu TOC-V_{CSN})

$R^2 = 0.9995$
DOC = 9.910 x area - 22.542

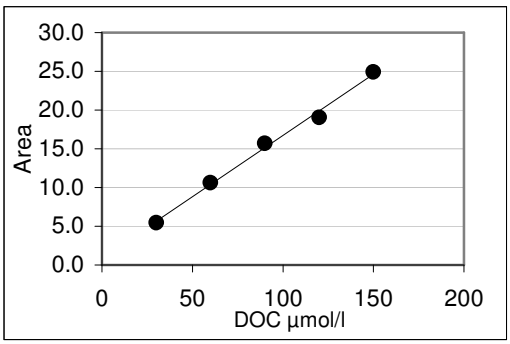

Calibration curve for DOC calculation for experiment 5
samples 1.1-8.3 (Shimadzu TOC-V_{CSN})

R^2 = 0.9947
DOC = 6.336 x area - 5.971

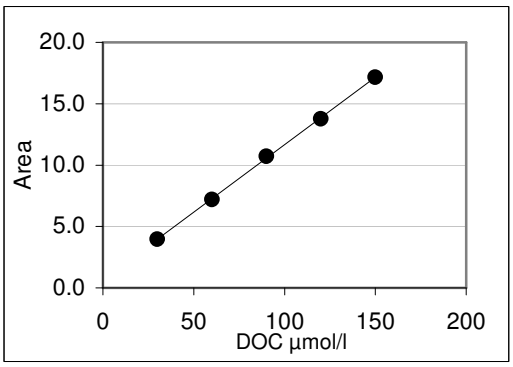

Calibration curve for DOC calculation for experiment 5
samples 9.1-11.3 (Shimadzu TOC-V_{CSN})

R^2 = 0.9996
DOC = 9.107x area - 6.151

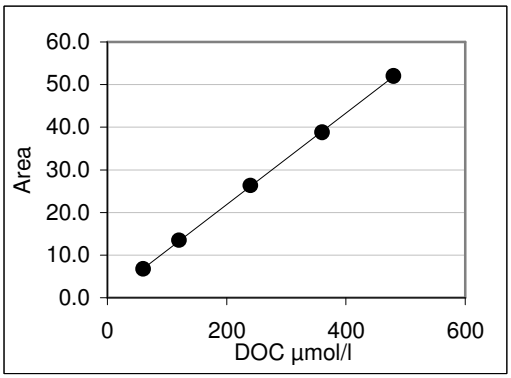

Calibration curve for DOC calculation for experiment 4
samples 1.1-9.3 (Shimadzu TOC-V_{CSN})

R^2 = 0.9999
DOC = 9.332 x area –4.065

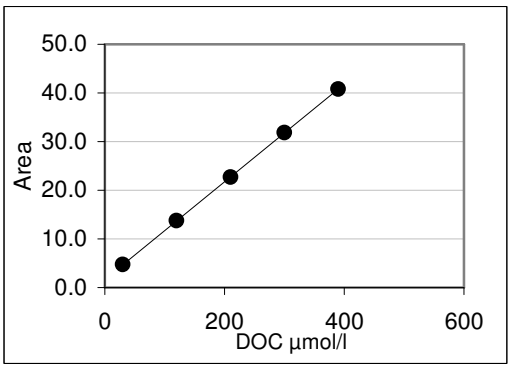

Calibration curve for DOC calculation for experiment 4 samples 10.1-11.3 (Shimadzu TOC-V_{CSN})

R^2 = 1.0000
DOC = 9.972 x area – 16.869

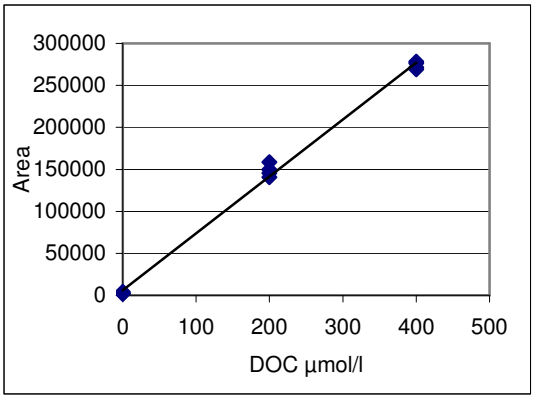

Calibration curve for DOC calculation for experiment 3 samples 1.1-6.3 (Shimadzu TOC 5000A)

$R^2 = 0.9965$
DOC = 0.0015 x area – 8.2844

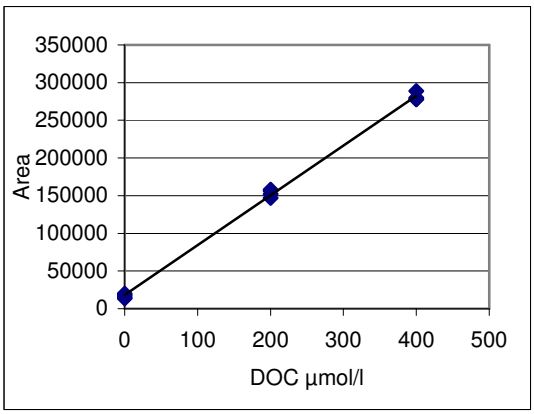

Calibration curve for DOC calculation for experiment 3 samples 7.1-13.3 (Shimadzu TOC 5000A)

$R^2 = 0.9983$
DOC = 0.0015 x area – 27.108

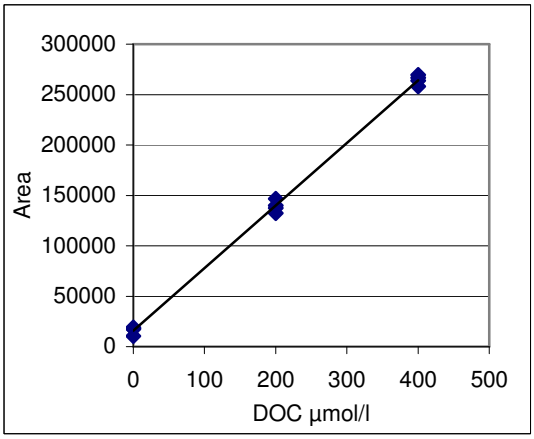

Calibration curve for DOC calculation for experiment 3 samples 14.1-19.3 (Shimadzu TOC 5000A)

$R^2 = 0.9982$
DOC = 0.0016 x area – 24.961

Appendix H

Reagents for determination of dissolved oxygen after Winkler

Manganese (II) chloride:	Dilute 100 g of $Mn(II)Cl_2$ in 250 ml distilled water.
Alkaline Iodide solution:	Dilute 75 g KOH in little distilled water, then add 100 g KI and fill up to 250 ml.
0.01 M iodate solution:	Dilute 325.0 mg potassium-hydrogen- iodate $KH(IO_3)$ whilst warming up and fill up to 1000 ml with distilled water.
0.2M thiosulfate solution:	Dilute 49.5 mg $Na_2S_2O_3$ into 1 L distilled water. Then dilute this solution 1:10 (0.02 M).
Sulphuric acid:	Concentrated sulphuric acid (98%) is diluted 1:1.

Appendix I

Nutrient medium (F/2) for phytoplankton cultures (Guillard and Ryther, 1962)

$NaNO_3$ stock solution:	75 g $NaNO_3$ were dissolved in a volumetric flask with 1 L deionised water.
Na_2HPO_4 stock solution:	5 g Na_2HPO_4 are dissolved in a volumetric flask with 1 L deionised water.
Na_2SiO_3 stock solution:	30 g Na_2SiO_3 • 9 H_2O were dissolved in a volumetric flasks with 1 L deionised water.
HCl:	200 ml concentrated HCl were filled up to 1 L with deionised water in a volumetric flask. 10 ml of Na_2SiO_3 stock were adjusted with the HCl to pH 7.1.
Vitamin mix stock solution:	1 mg B12, 1 mg biotin and 200 mg thiamine• HCl were dissolved in a volumetric flask with 1 L of deionised water.
Metal stock a:	150 mg $ZnSO_4$•$7H_2O$, 100 mg $CuSO_4$•$5H_2O$, 120 mg $CoSO_4$•$7H_2O$, 2 g $MnSO_4$•H_2O were dissolved in a volumetric flask with 100 ml deionised water.
Metal stock b:	5 g $FeCl_3$•$6H_2O$ were dissolved in a volumetric flask with 100 ml deionised water.
Metal stock c:	$NaMoO_4$•$2H_2O$ were dissolved in a volumetric flask with 100 ml deionised water.

Appendix J

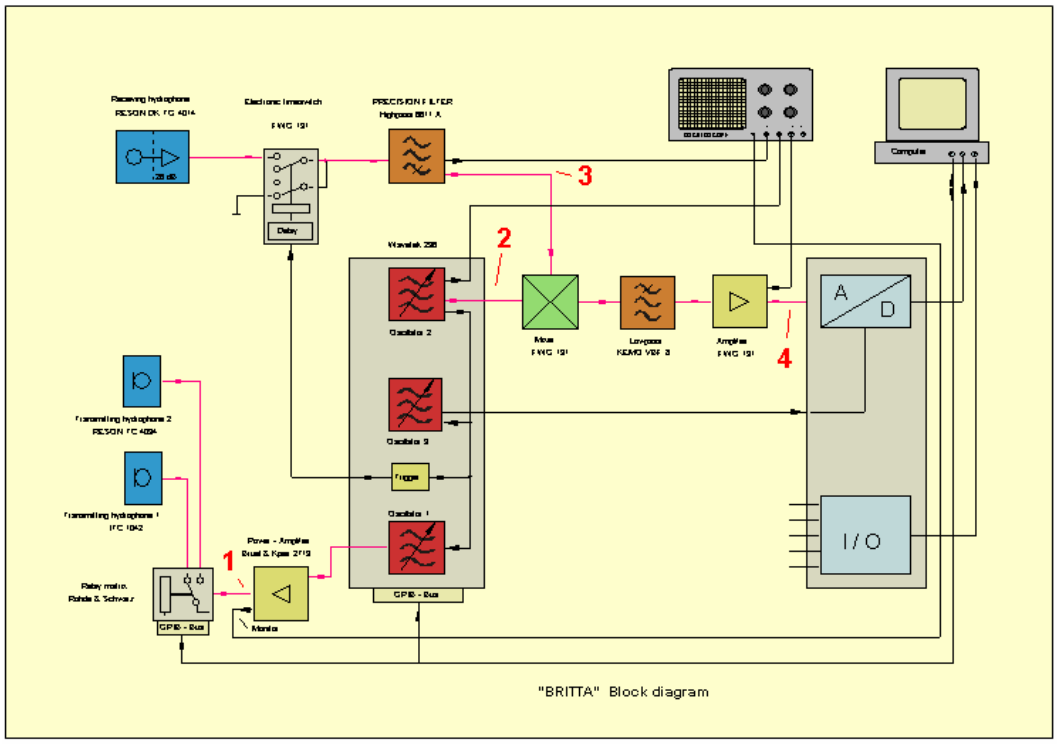

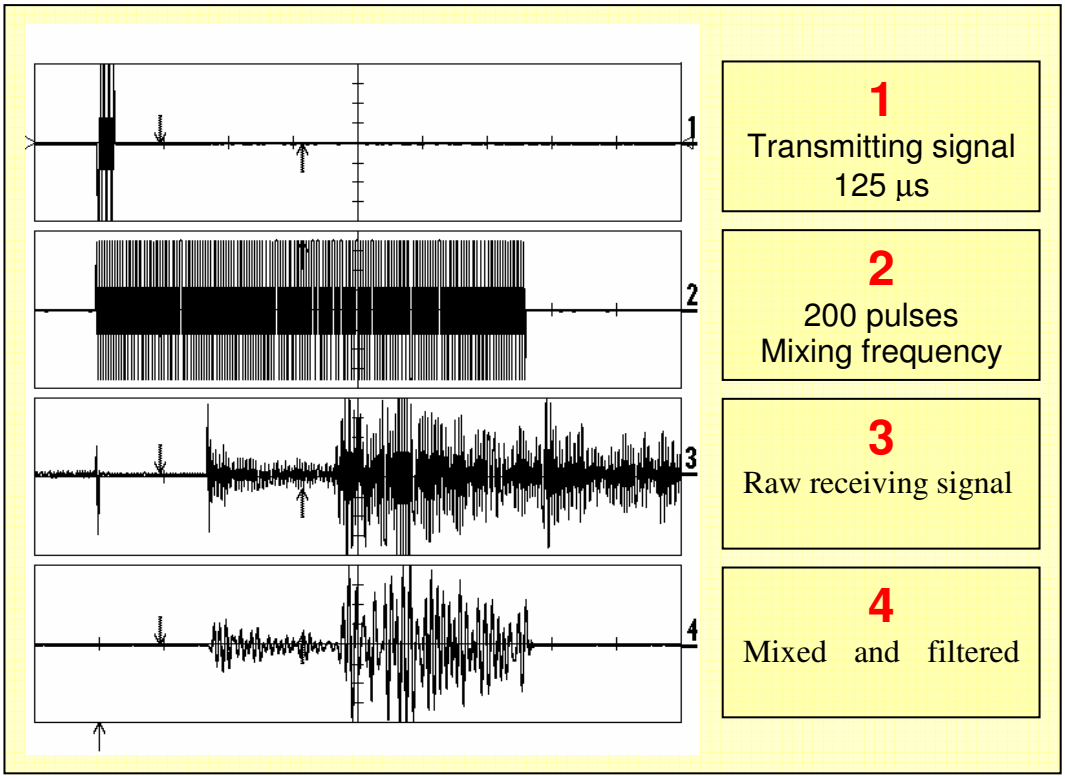

Figure 6.3 Signal assignment of transmitting and receiving signal.

Appendix K

Number	Date	Type of experiment	Main result
1	15.03.02-28.03.02	Measurements with Kiel Firth water at 12°C	No data
2	28.03.02-08.04.02	Measurements with Kiel Firth water at 12°C	No data
3	26.06.02-02.08.02	Measurements with Kiel Firth (mixed diatom species) water at 18°C 12hour daily illumination but no nutrient addition	Decline in chlorophyll concentration, oxygen saturation and BRT with time
4	26.08.02-02.08.02	Measurements with Kiel Firth water at 18°C (*Prorocentrum minimum, Prorocentrum micans*) 12 hour daily illumination but no nutrient addition	Decline in chlorophyll concentration, oxygen saturation and BRT with time
5	05.11.02-28.11.02	Growth experiment with *Chaetoceros muelleri* at 18°C, Salinity 32	No data due to complete malfunction of fill level sensor
6	08.01.03-11.02.03	Reference measurements 18°C	Decline in BRT after filling of the tank system for the first couple of days
7	24.02.03-13.03.03	Reference measurements 18°C	Decline in BRT after filling of the tank system for the first couple of days
8	21.03.03-31.03.03	Measurements with filtered Kiel Firth water at 18°C Salinity = 11.3	Increase in BRT during days 1-3, followed by a decline in BRT
9	30.04.03-23.05.03	Measurements with deionised water enriched with bacteria and nutrient medium	Oxygen saturation almost 0, decline in BRT
10	02.07.03-03.07.03	Acidification of filtered North Sea water to decrease buffer capacity of seawater	No difference in BRT
11	20.08.03-27.08.03	Deionised water with NaOCl solution (2-3 mg Cl/litre to investigate bacterial effect	No significant effect
12	01.09.03-16.09.03	Growth experiment with Kiel Firth water	No growth occurred in the tank system
13	16.09.03-25.09.03	Measurements with deionised water and di-methylphtalate	Addition of di-methylphthalate had no effect on BRT
14	25.09.03-04.10.03	Reference measurements with deionised water. Start of BRT measurements 4 days after filling of tank system.	Decline in BRT during first couple of days of measurement still occurred
15	26.02.04-02.03.04	Growth experiment with Kiel Firth water	No data due to malfunction of tank system

Table 6.3 Remaining experiments carried out in the tank system.

Appendix L

Matlab Scripts Median filtering of BRT data and Fourier Analysis of BRT data

```
%Median filtering of BRT data
%March 2004
%Verena Kuhnhenn  IFM-Geomar


clear all
close all
format long g

%Loading of BRT data file
cd C:\Daten\Akustik\z8f_files
[FILE, PATH] = uigetfile('*.txt', 'open_file:')
infile=[PATH FILE];
a=load(infile);

%Defining number of BRT measurements for which median filter will be
applied
i=input('first measurement number:')
j=input('last measurement number:')

i1=find(a(:,1)==i)
j1=find(a(:,1)==j)

%Creating new data matrix with all BRT data which will be median-filtered
a_neu=a(i1:j1,:);

highest=input('define highest possible BRT values: ')% Define maximum
value of BRT included i.e. eliminate outliers
ind=find(a_neu(:,3)<highest);
a_neu=a_neu(ind,:); %Create new data matrix of BRT without outliers

disp(a_neu(1,2))% Display time of first BRT measurement
t0=input('first day of measurement:')
dezimalzeit=a_neu(:,2)-t0; %Create vector with converted matlab date
format into decimal days

plot(dezimalzeit,a_neu(:,3),'+--')%Plot original BRT data without
outliers
hold

med=medfilt1(a_neu(:,3),4);%Application of median filter of order no.4 to
BRT data

plot(dezimalzeit,med,'*g--') %Plot median-filtered BRT data on same graph
as original BRT data
axis([0 dezimalzeit(end)+0.5 0 800])

b=[dezimalzeit,med]; %Create new matrix with median filtered BRT data
hold off
cd C:\Daten\Akustik\files_für_sigmaplot\medianfiltered

text=input('name_for_new_file_ending_txt: ','s')

dlmwrite(text,b,'\t') %Save median filtered BRT data in ascii format
```

```
%Fourier Analysis (Fast Fourier Transform-FFT) of median-filtered bubble
residence time data
%3rd March 2005
%Verena Kuhnhenn  IFM-Geomar


clear all;
close all;


%Loading of median-filtered BRT data file
cd C:\Daten\Akustik\files_für_sigmaplot\medianfiltered


[filename,PN]=uigetfile('*.txt','Datei zu öffnen: ');
a=load(filename);


%Interpolation of BRT data to 512 data points using Matlab function
'nearest'
%(All data points must have same distance i.e. time difference for FFT)
xi=linspace(a(1,1), a(end,1),512)';
bubble=interp1(a(:,1),a(:,2),xi,'nearest');


%FFT discrete Fourier transform of the noisy
%signal y is found by taking the 512-point fast Fourier transform (FFT):
X=fft(bubble,512);


%Selecting all absolute numbers
Z=abs(X)./512;


%Creation of frequency axis 'f'. This involves deviding the measurement
period of the experiment (e.g. 14.85 days)
%by the number of data points of the Fourier analysis. Only the first 256
data points are selected as the remaining
%data points are a reflection of the data. The direct-current fraction is
removed by removing the first 4 data points
%from the plot.


f=(4:256)/a(end,1);


%Plotting Fourier analysis
 h=plot(f,Z(4:512),'-x')
```

Appendix M

Data Tables for all phytoplankton growth experiments

Time (dec. days)	Salinity	Temp (°C)	NO_3^- (µmol /l)	NO_2- (µmol/l)	PO_4^{3-} (µmol/l)	Si (µmol/l)	Chl *a* (µg/l)	Viscos. (mm^2/sec)	Sigma Viscos.	O_2 (mg/l)	O_2 %	DOC (µmol/l)
0.4597	14.4	12.0	93.87	0.85	0.75	9.97	0.54	1.1868	0.007	8.61	87.52	304.47
1.4063	14.4	12.0	114..97	1.78	0.73	18.11	1.25	1.1956	0.008	8.69	88.33	302.17
2.491	14.4	12.0	76	1.73	0.25	3.53	4.38	1.1954	0.012	10.82	109.98	271.41
3.4521	14.4	12.0	75.89	2.16	0.13	1.88	7.59	1.1966	0.006	13.58	138.04	324.6
6.3958	14.4	12.0	65.62	1.96	0.5	1.57	5.81	1.1879	0.007	15.45	157.04	339.57
7.4667	14.4	12.0	60.62	2.01	0.87	2.28	4.51	1.1939	0.010	14.79	150.43	321.89
8.4167	14.4	12.0	32.3	3.05	0.23	1.74	4.16	1.1926	0.006	14.13	143.75	364.45
9.4278	14.4	12.0	37.99	1.66	0.18	1.25	3.71	1.2021	0.010	12.85	130.73	396.59
10.4222	14.4	12.0	35.34	1.17	0.15	2.5	3.97	1.1053	0.007	13.14	133.67	348.21

Table 6.4 Biological, chemical, physical and physico-chemical parameters for experiment 1.

Time (dec. days)	Salin.	Temp. (°C)	NO_3^- (µmol/l)	σ NO_3^-	NO_2^- (µmol/l)	σ NO_2^-	PO_4^{3-} (µmol/l)	σ PO_4^{3-}	Si (µmol/l)	σ Si	Chl (µg/l)	σ Chl
0.6303	32.3	18.0	8.122	0.14	0.1	0.02	0.8	0.02	18.98	0.22	-	-
5.4792	32.3	18.0	0.958	0.07	0.13	0.01	0.23	0.03	22.15	0.24	-	-
6.5153	32.3	18.0	0.358	0.08	0.07	0.03	0.14	0.02	19.27	0.28	-	-
7.5042	32.3	18.0	0.268	0.08	0.04	0.01	0.12	0.02	17.81	0.2	17.34	2.1
7.6229	32.3	18.0	282.14	0.80	0.11	0.01	9.67	0.03	33.99	0.1	-	-
8.3389	32.3	18.0	261.17	2.2	0.47	0.01	7.29	0.07	31.55	0.25	17.58	0.3
8.7069	32.3	18.0	-	-	-	-	-	-	-	-	-	-
9.3417	32.3	18.0	208.87	0.97	0.99	0.03	6.18	0.02	26.26	0.28	18.42	1.78
10.3028	32.3	18.0	207.108	1.29	0.86	0.02	5.01	0.02	22.34	0.22	32.12	0.81
10.6986	32.3	18.0	-	-	-	-	-	-	-	-	-	-
11.4153	32.3	18.0	152.494	0.61	0.68	0.02	3.52	0.03	16.66	0.04	53.1	4.11
11.6875	32.3	18.0	-	-	-	-	-	-	-	-	-	-
12.3854	32.3	18.0	123.61	0.71	0.47	0.01	1.74	0.04	13.83	0.1	62.0	1.33
12.6736	32.3	18.0	-	-	-	-	-	-	-	-	-	-
13.4583	32.3	18.0	104.1	0.3	0.37	0.01	0.44	0.03	7.09	0.18	72.0	3.16
13.7236	32.3	18.0	-	-	-	-	-	-	-	-	-	-
14.3743	32.3	18.0	88	0.5	0.32	0.01	0.11	0.04	5.4	0.16	66.68	4.05
14.7028	32.3	18.0	-	-	-	.	-	-	-	-	-	-
15.4007	32.3	18.0	74.9	0.1	0.47	0.02	0.19	0.02	0.75	0.04	70.57	2.13
16.4778	32.3	18.0	69.8	0.2	0.4	0	0.07	0.01	0.53	0.06	-	-
17.4493	32.3	18.0	59.8	0.4	0.56	0.03	0.16	0.02	0.5	0.02	50.43	0.79
18.4222	32.3	18.0	48.56	0.21	0.76	0.01	0.16	0.02	0.78	0.08	46.24	2.29
18.691	32.3	18.0	-	-	-	-	-	-	-	-	-	-

Viscos. (mm^2/sec)	σ Visc.	O_2 (mg/l)	σ O_2	O_2 (%)	σ O_2 (%)	pH	Surf tens. (mN/m)	σ Surf. Tens.	TBN (ml^{-1})	σTBN	Mean Cell Vol. ($µm^3$)	Bact.Bio-mass (µgC/l)
1.2409	0.004	7.27	0.19	93.33	2.47	7.71	73.67	0.08	978350	208674	0.11486	21.038
1.2413	0.002	3.88	0.05	49.84	0.55	7.48	73.61	0.06	4335427	1441947	0.18206	131.605
-	-	3.4	0.01	43.63	0.13	7.44	73.65	0.07	-	-	-	-
1.276	0.005	3.86	0.03	49.5	0.33	7.46	73.36	0.08	1142245	605221	0.19339	34.227
-	-	4.09	0.01	52.48	0.21	7.46	-	-	2403042	610556	0.32388	106.948
1.2495	0.004	3.21	0.02	41.2	0.24	7.47	73.67	0.07	1922074	617567	0.2593	73.117
-	-	2.71	0.01	34.77	0.24	7.46	-	-	-	-	-	-
1.2517	0.009	284	0	36.44	0.04	7.45	73.69	0.08	3735797	171639	0.13587	100.728
1.2479	0.00	3.47	0.01	44.46	0.08	7.52	73.54	0.07	3648307	1385026	0.19051	117.338
-	-	-	-	-	-	7.64	-	-	-	-	-	-
1.2445	0.005	5.44	0.03	69.83	0.37	7.76	73.63	0.07	3123371	1094348	0.15471	90.53
-	-	-	-	-	-	7.75	-	-	-	-	-	-
1.285	0.006	5.77	0.1	74.1	1.28	7.79	73.63	0.07	3657056	1189138	0.21374	129.019
-	-	-	-	-	-	7.81	-	-	-	-	-	-
1.2524	0.004	5.9	0.07	75.69	0.89	7.84	73.41	0.06	4949165	1393537	0.14716	138.335
-	-	-	-	-	-	7.77	-	-	-	-	-	-
1.2512	0.005	5.11	0.01	65.6	0.15	7.78	73.53	0.07	4891750	1951179	0.10881	113.247
-	-	-	-	-	-	7.77	-	-	-	-	-	-
1.2475	0.004	4.82	0.03	61.81	0.47	7.71	73.72	0.09	5695559	1322754	0.09143	120.264
1.2451	0.004	4.16	0.07	53.43	0.96	7.7	73.54	0.07	5822755	2020148	0.15115	164.492
1.2495	0.004	3.3	0.03	42.33	0.41	7.61	73.51	0.07	4133873	974745	0.15342	116.859
1.2494	0.006	2.37	0.03	30.47	0.27	7.53	73.55	0.06	4616159	1754415	0.1419	121.284
-	-	-	-	-	-	-	-	-	-	-	-	-

Table 6.5 Biological, chemical, physical and physico-chemical parameters for experiment 2.

Time (dec. days)	Salin.	Temp. (°C)	NO_3^- (µmol/l)	σ NO_3^-	NO_2^- (µmol/l)	σ NO_2^-	PO_4^{3-} (µmol/l)	σ PO_4^{3-}	Si (µmol/l)	σ Si	Chl (µg/l)	σ Chl
0.63	16.6	12.0	10.63	0.78	0.71	0.03	0.68	0.25	26.11	0.28	-	-
0.7	16.6	12.0	204.64	13.6	0.74	0.03	12.15	0.68	47.24	2.39	1.68	0.2
1.43	16.6	12.0	204.48	16.76	0.74	0.09	11.99	0.93	50.72	6.97	2.18	0.26
2.48	16.6	12.0	219.78	11.56	0.88	0.02	11.94	0.67	40.81	1.63	5.01	0.08
3.52	16.6	12.0	218.53	15.38	1.27	0.02	12.37	0.95	24.91	2.73	11.95	0.4
4.5	16.6	12.0	201.27	5.19	2.16	0	10.1	0.41	6.6	0.45	26.21	2.76
5.53	16.6	12.0	205.8	14.66	2.75	0.02	9.32	0.32	2.17	0.8	33.57	4.84
6.46	16.6	12.0	153.22	0	2.67	0.2	8.36	0.25	3.38	0.73	26.67	2.11
7.47	16.6	12.0	147.44	11.57	2.72	0.14	7.38	0.1	2.9	0.06	23.91	2.11
8.44	16.6	12.0	152.84	14.58	2.87	0	7.02	0.54	1.79	0.51	19.31	0
9.51	16.6	12.0	162.02	20.46	2.81	0.07	7.39	0.72	2.94	2.56	13.66	0.2
10.49	16.6	12.0	164.1	7.32	2.82	0.03	6.97	0.49	5.22	1.05	6.9	0
11.47	16.6	12.0	178.97	4.27	2.69	0.05	6.01	0.03	2.31	0.53	10.12	0.4
12.46	16.6	12.0	176.92	4.16	2.71	0.04	5.87	0.08	0.63	0.86	10.58	0.8
13.61	16.6	12.0	166.85	2.29	2.58	0.12	6.64	0.1	1.6	0.4	11.63	0.16

O_2 (mg/l)	σ O_2	O_2 (%)	σ O_2 (%)	pH	TBN (ml^1)	σTBN	Mean Cell Vol. ($µm^3$)	DOC (µmol/l)	σ DOC	Viscos. (mm^2/sec)	σ Visc.
-	-	-	-	7.72	-	-	-	-	-	-	-
9.98	0.07	102.8	0.7	-	-2759139	478526	0.18584	-	-	1.1972	0.0116
9.95	0.05	102.6	0.48	7.9	-	-	-	265.4	6.66	-	-
10.29	0.12	106.13	1.26	8.04	5498708	1240806	0.12268	273.5	7.33	-	-
11.76	0.16	121.19	1.58	8.23	-	-	-	-	-	-	-
15.36	0.2	158.29	2.11	8.43	5766223	725427	0.1566	261.83	2.16	1.1972	0.0116
17.59	0.31	181.3	3.25	8.52	-	-	-	279.28	4.36	1.2008	0.001
16.44	0.05	169.38	0.52	8.68	17556203	2760674	0.15877	298.07	3.39	1.2008	0.001
15.06	0.08	155.15	0.76	8.66	-	-	-	308.71	7.11	1.2	0.0071
13.42	0.02	138.2	0.17	8.68	13344433	3025014	0.12974	291.79	5.62	1.198	0.0028
12.07	0.09	124.38	0.92	8.68	-	-	-	306.52	1.86	1.2006	0.0019
11.12	0.07	114.61	0.69	8.58	5472461	1759568	0.13175	317.56	3.61	1.199	0.0022
10.55	0.04	108.72	0.39	8.65	-	-	-	325.46	2.02	1.1988	0.0022
10.44	0.04	107.55	0.44	8.66	7016649	2129672	0.18526	335.78	3.84	1.2012	0.0024
10.72	0.04	110.42	0.42	8.77	-	-	-	338.87	3.51	-	-

Table 6.6 Biological, chemical, physical and physico-chemical parameters for experiment 3.

Time (dec. days)	Salin.	Temp. (°C)	NO_3^- (µmol/l)	σ NO_3^-	NO_2^- (µmol/l)	σ NO_2^-	PO_4^{3-} (µmol/l)	σ PO_4^{3-}	Si (µmol/l)	σ Si	Chl (µg/l)	σ Chl	DOC (µmol/l)
3.2653	16.2	12.0	13.18	2.47	0.3	0.01	0.08	0.02	1.58	0.34	-	-	-
3.3903	16.2	12.0	168.78	3.27	0.3	0.01	9.66	0.04	11.82	2.81	4.8	0.6	292
4.3458	16.2	12.0	161.94	0.57	0.66	0.22	7.75	0.16	7.52	0.6	9.7	1.19	291.2
5.4313	16.2	12.0	141.52	1.82	1	0.25	7.77	0.05	0.58	0.74	39.5	0.8	291.2
6.3549	16.2	12.0	112.79	2.8	1.25	0.08	7.47	0.06	8.82	2.73	58.9	3.47	321
7.5431	16.2	12.0	95.65	4.04	1.39	0.01	4.59	0.13	2.15	0.25	41.8	6.52	329.7
8.4625	16.2	12.0	89.25	3.95	1.35	0.01	3.37	0.07	0.92	0.3	29.4	3.98	325
9.3931	16.2	12.0	86.8	0.36	1.35	0.02	2.97	0.04	1.83	1.14	26.2	0	247.1
10.425	16.2	12.0	82.46	0.58	1.43	0.03	3.09	0.01	4.59	1.35	14.3	0.4	340
11.5396	16.2	12.0	77.29	0.9	1.39	0.01	2.69	0.01	3.2	1.68	9.4	0.4	351.8
12.541	16.2	12.0	73.94	0.42	1.41	0.03	2.55	0.01	0.32	0.24	8.7	0.4	364.4
13.5431	16.2	12.0	69.86	1.83	1.39	0.04	2.42	0.02	0.57	0.19	7.6	0.69	369.6

σ DOC	O_2 (mg/l)	σ O_2	O_2 (%)	σ O_2 (%)	pH	TBN (ml^{-1})	σTBN	Mean Cell Vol. (μm^3)	Bact.Biomass (µgC/l)
-	-	-	-	-	-	-	-	-	-
7	10.54	0.01	108.4	0.12	-	11023662	2041185	0.09761	244.77
3.6	10.92	0.12	112.2	1.27	8.3	10175688	3271417	0.12653	250.80
3.6	15.26	0.12	256.9	1.21	8.59	5737958	1541831	0.07693	110.21
3.6	21.84	0.26	224.5	2.66	8.9	3371004	1043165	0.16431	94.31
15.7	23.23	0.67	238.8	6.95	9.13	3702113	1338486	0.19189	116.71
3.8	21.66	0.2	222.7	2.11	9.22	6275008	2155502	0.20603	200.36
17.9	19.43	0.36	199.8	3.77	9.12	6747818	2030274	0.15395	189.13
4.1	17.98	1.12	184.8	11.45	9.14	5766233	1461601	0.2702	218.03
8.7	16.11	0.12	165.6	1.27	9.11	4788774	2256156	0.24166	155.73
7.32	14.96	0.09	153.8	0.88	9.11	4593193	1838462	0.27705	161.45
3.55	12.63	1.79	129.8	1.79	9.11	3735797	1270691	0.23932	119.01

Table 6.7 Biological, chemical, physical and physico-chemical parameters for experiment 4.

Time (dec. days)	Salin	Temp (°C)	NO_3^- (µmol/l)	σ NO_3^-	NO_2^- (µmol /l)	σ NO_2^-	PO_4^{3-} (µmol /l)	σ PO_4^{3-}	Chl (µg/l)	σ Chl	DOC (µmol/l)	σ DOC	σ Visc.
1.5932	31.5	18.0	289.12	26.54	0.14	0.05	9.75	0.67	1.26	0.04	155.5	2	0.0021
2.4302	31.5	18.0	293.1	47.45	0.11	0.02	8.66	1.2	1.33	0.11	147.3	11.6	0.0018
3.4576	31.5	18.0	283.77	2.73	0.18	0.03	9.91	0.1	2.39	0.44	153	8.5	0.0018
4.3896	31.5	18.0	274.39	8.6	0.24	0.01	10.41	0.34	3.26	0.16	143.8	13.1	0.0055
5.492	31.5	18.0	266.39	7.88	0.22	0	9.16	0	3.98	0.17	145.6	6.2	0.0017
7.389	31.5	18.0	231.14	8.13	0.3	0.01	8.89	0.23	4.37	0.8	146.1	5.7	0.0021
8.3945	31.5	18.0	331.15	82.5	0.31	0.01	8.79	0.68	4.37	0.4	142.8	8.5	0.0017
9.4458	31.5	18.0	322.43	19.54	0.33	0.04	8.12	0.48	3.95	0.21	153.5	3.2	0.0017
10.4875	31.5	18.0	304.88	13.24	0.42	0.02	8.66	0.01	3.08	0	154.5	7.2	0.0017
11.4757	31.5	18.0	308.88	6.95	0.37	0.07	8.09	0.48	2.02	0.16	159.6	0.6	0.0021
12.6227	31.5	18.0	452.11	43.05	0.49	0.05	13.28	0.41	0.9	0	167.8	7.9	0.0017

Viscos. (mm^2/sec)	O_2 (mg/l)	σ O_2	O_2 (%)	σ O_2 (%)	pH	TBN (ml^{-1})	σTBN	Mean Cell Vol. (µm^3)	Bacterial Biomass (µgC/l)
1.0614	7.09	0.07	90.95	0.88	7.85	897482	431567	0.10926	21.174
1.0808	6.92	0.07	88.69	0.9	7.87	860896	247612	0.09967	18.971
1.0812	7.35	0.04	94.24	0.52	7.89	869295	155409	0.23027	31.712
1.0810	7.73	0.03	98.56	0.31	7.92	1253671	353057	0.16562	36.946
1.0800	8.21	0.02	104.61	0.26	7.99	2064749	296571	0.16744	61.655
1.0780	8.38	0.04	106.7	0.25	8.05	3390611	605820	0.14405	95.508
1.0790	8.36	0.06	107.1	0.2	8.07	1850887	566753	0.11735	44.455
1.0780	8.29	0.04	105.88	0.28	8.05	1249348	380374	0.07866	23.32
1.0809	8.09	0.03	103.25	0.28	8.1	913071	310728	0.09807	18.76
1.0811	7.75	0.05	98.8	0.59	8.03	1184023	347701	0.12127	28.91
1.0765	7.38	0.04	94.15	0.54	8.03	1505847	322658	0.12644	39.06

Table 6.8 Biological, chemical, physical and physico-chemical parameters for experiment 5.

Time (dec. days)	Salin.	Temp. (°C)	NO_3^- (µmol/l)	σ NO_3^-	NO_2^- (µmol/l)	σ NO_2^-	PO_4^{3-} (µmol/l)	σ PO_4^{3-}	Si (µmol/l)	σ Si	Chl (µg/l)	σ Chl	DOC (µmol/l)	σ DOC
1.6319	31	18.0	319.44	9.69	0.38	0.01	11.47	0.7	25.09	0.62	21.05	2.74	136.3	15.1
2.4618	31	18.0	303.31	4.22	0.42	0.04	9.98	0.07	28.92	0.11	10.71	1.13	147.8	14.7
3.4521	31	18.0	299.23	1.16	0.34	0.06	9.27	0.1	28.36	0.41	11.43	0.54	131.7	7.5
4.3952	31	18.0	290.57	6.83	0.39	0.03	8.77	0.16	29.41	1.67	14.52	0.31	133.1	1.4
5.4848	31	18.0	285.06	10.28	0.4	0.1	8.59	0.01	29.95	1.68	16.88	0.77	127.9	2
6.4944	31	18.0	292.36	0.96	0.47	0.01	8.12	0.3	30.48	0.29	21.78	ß	131	4
7.4292	31	18.0	277.11	7.71	0.38	0.01	8.02	0.08	17.79	1.05	18.51	3.93	144.1	2.3
8.4069	31	18.0	286.82	4.6	0.42	0.04	7.45	0.42	20.57	1.81	23.96	0	157.2	16.4
9.4153	31	18.0	273.25	13.27	0.34	0.06	7.49	0.58	24.72	6.89	25.41	0.63	152	3.6
10.4292	31	18.0	271.25	9.99	0.39	0.03	7.45	0.35	21.84	0.62	25.05	1.09	151.9	5.8
11.4056	31	18.0	278.94	9.34	0.4	0.1	7.29	0.49	20.52	0.29	23.41	2.31	157.8	2.9
12.509	31	18.0	264.19	2.23	0.47	0.01	7.2	0.05	21.15	0.4	25.77	2.27	163.3	1.5
13.5229	31	18.0	163.27	7.59	0.53	0.04	6.94	0.43	21.37	1.43	17.42	1.09	168.3	4.1
14.4354	31	18.0	249.68	7.06	0.5	0.02	6.16	0.13	22.42	1.83	22.87	1.09	176.9	4.3
15.4035	31	18.0	247.06	1.74	0.6	0.08	6.35	0.56	21.42	0.27	24.32	2.27	188	2.3
16.4319	31	18.0	240.16	2.05	0.58	0.05	5.83	0.2	22.52	0.64	22.51	0.63	195.3	12.5
17.4187	31	18.0	130.07	7.47	0.62	0.03	5.42	0.31	22.6	0.33	16.7	0.63	205.5	4.1
18.4472	31	18.0	226.56	6.49	0.68	0.04	5.34	0.08	22.65	0.27	11.07	0.31	223.5	3
19.4368	31	18.0	225.33	2.24	0.68	0.01	5.39	0.05	22.74	0.31	5.08	0.31	234.4	4.5
20.5681	31	18.0	224.48	1.65	0.68	0.05	5.67	0.02	22.6	0.64	2	0.13	233.3	3.7
21.3681	31	18.0	222.27	2.62	0.75	0.01	5.84	0.06	22.19	0.69	1.42	0.11	245.4	1.6

Table 6.9 Biological, chemical, physical and physico-chemical parameters for experiment 6.

Time (dec. days)	Viscos. (mm^2/sec)	σ Visc.	O_2 (mg/l)	σ O_2	O_2 (%)	σ O_2 (%)	pH	TBN (ml^{-1})	σTBN	Mean Cell Vol. (μm^3)	Bact.Biomass (µgC/l)
1.6319	0.9048	0.0082	7.93	0.24	110.97	3.05	7.73	3405087	1029166	0.25922	131.025
2.4618	0.9056	0.0061	7.77	0.06	98.92	0.86	7.89	4788055	933549	0.38497	234.085
3.4521	0.9092	0.0027	8.71	0.09	110.97	1.13	7.98	5459338	1313914	0.28918	224.907
4.3952	0.9096	0.0022	9.67	0.05	123.09	0.58	8.07	7115273	1649647	0.27364	286.901
5.4848	0.9088	0.003	10.92	0.04	139.04	0.48	8.18	9347147	2358475	0.19901	313.517
6.4944	0.9092	0.0027	11.39	0.05	145.05	0.6	8.24	8175883	1980154	0.3072	362.919
7.4292	0.9152	0.0033	11.29	0.03	143.78	0.36	8.28	1903231	644631	0.29745	81.387
8.4069	0.9152	.0033	11.37	0.02	144.9	0.26	8.35	1287692	358575	0.28203	53.607
9.4153	0.9128	0.0033	11.46	0.03	146	0.39	8.38	2312143	592211	0.34633	105.944
10.4292	0.9136	0.0022	11.51	0.07	146.56	0.86	8.37	3057229	767034	0.25808	120.699
11.4056	0.9112	0.0018	11.31	0.03	155.09	0.45	8.44	4184909	1011163	0.2636	167.687
12.509	0.916	0.0037	9.12	0.01	116.16	0.05	8.37	5217867	1756284	0.24663	200.174
13.5229	0.9128	0.0018	10.89	0.01	138.68	0.12	8.47	5579879	558319	0.21343	200.565
14.4354	0.9104	0.0022	10.52	0.04	134.03	0.47	8.44	5046388	1108849	0.2567	197.329
15.4035	0.9221	0.0018	10.4	0.05	132.42	0.55	8.48	5144376	1072473	0.2584	199.372
16.4319	0.9104	0.0022	9.93	0.06	126.51	0.78	8.48	7532836	131359	0.24084	283.863
17.4187	0.908	0.004	8.93	0.38	113.79	4.92	8.48	9737568	2273646	0.15632	282.354
18.4472	0-9072	0.0044	7.77	0.07	98.94	0.84	8.42	9823308	2184811	0.22638	346.517
19.4368	0.9104	0.0022	6.2	0.1	78.96	1.27	8.33	8288161	1715306	0.29188	344.21
20.5681	0.9096	0.0022	5.03	0.26	64.03	3.27	8.27	3683303	1295868	0.12119	83.711
21.3681	0.9096	0.0022	4.83	0.12	61.53	1.47	8.23	-	-	-	-

Table 6.9 continued

7 References

Alldredge, A.L., Passow, U., Logan, B.E. (1993). The abundance and significance of a class of large, transparent organic particles in the ocean. *Deep Sea Research*, **40**, 1131-1140.

Amon, R.M.W., Benner, B. (1994). Rapid cycling of high-molecular-weight dissolved organic matter in the ocean. *Nature*, **369**, 549-552.

Amon, R.M.W., Benner, B. (1996). Bacterial utilisation of different size classes of dissolved organic matter. *Limnology and Oceanography*, **41**, 41-51.

Asher, W.E., Karle, L.M., Higgins, B.J., Farley, P.J. (1996). The influence of bubble plumes on air-seawater gas transfer velocities. *Journal of Geophysical Research*, **101**, 12027-12041.

Bargu, S., Marinovic, B., Mansergh, S., Silver, M.W. (2003). Feeding responses of krill to the toxin-producing diatom *Pseudo-nitzschia*. *Journal of Experimental Marine Biology and Ecology*, **284**, 87-104.

Bätje, M., Michaelis, H., (1986). *Phaeocystis pouchetii* blooms in the East Frisian coastal waters (German Bight, North Sea). *Marine Biology*, **93**, 21-27.

Billard, J-Y., Gindroz, B., Cerrutti, P., Geistdoerfer, P. (1994). An equipment for simultaneous nuclei and biological activity measurements in deep sea water. *Oceans 94 (Held in conjunction with OSATES 94). Oceans engineering for today's technology and tomorrow's preservation -- Proceedings*, *13-16 September 1994, Brest France -- Vol. 2.* Institute of electrical and electronics engineers. New York (USA): pp. II.377-II.382.

Blanchard, D.C. (1963). The electrification of the atmosphere by particles from bubbles in the sea. *Progress in Oceanography,* **1**, 71-202.

Blanchard, D.C., Woodcock, A.H. (1957). Bubble formation and modification in the sea and its meteorological significance. *Tellus*, **9**, 145-158.

Bowyer, P. (1992). The rise of bubbles in a glass tube and the spectrum of bubbles produced by a splash. *Journal of Marine Research*, **50**, 521-543.

Bowyer, P., Woolf, D.K. (2004). Gas exchange and bubble induced supersaturation in a wind wave tank. *Journal of Atmospheric and Oceanic Technology*, **21**, 1925-1935.

Brockmann, U.H., Ittekkot, V., Kattner, G., Eberlein, K., Hammer, K.D. (1983). Release of dissolved organic substances in the course of phytoplankton blooms. In: Sündermann, J. (ed.) *North Sea Dynamics*. Springer Verlag. Berlin: pp. 530-548.

Burger, S.R., Blanchard, D.C. (1983). The persistence of air bubbles at a seawater surface. *Journal of Geophysical Research*, **88**, 7724-7726.

Carey, W.M., Fitzgerald, J.W., Monahan, E.C., Wang, Q. (1993). Measurement of sound produced by a tipping trough with fresh and salt water. *Journal of the Acoustical Society of America,* **93** (6), 3178-3192.

Cartmill, J.W., Su, M.-Y. (1993). Bubble size distribution under saltwater and freshwater breaking waves. *Dynamics of Atmospheres and Oceans*, **20**, 25-31.

Chen, W., Wangersky, P.J. (1996). Production of dissolved organic carbon in phytoplankton cultures as measured by high-temperature catalytic oxidation and ultraviolet photo-oxidation methods. *Journal of Plankton Research*, **18**, 1201-1211.

Chin, W-C., Orellana, M.V., Verdugo, P. (1998). Spontaneous assembly of marine dissolved organic matter into polymer gels. *Nature*, **391**, 568-572.

Cipriano, R.J., Blanchard, D.C. (1981). Bubble and aerosol spectra produced by a laboratory 'breaking wave'. *Journal of Geophysical Research*, **86**, 8085-8092.

Clay, C.S., Medwin, H. (1977). *Acoustical oceanography: Principles and applications*. John Wiley. New York. 544 pp.

Clift, R., Grace, J.R., Weber, M.E. (1978). *Bubbles, drops and particles.* Academic. San Diego. California. 380 pp.

Coffin, R.B., Connolly, J.P., Harris, P.S. (1993). Availability of dissolved organic carbon to bacterioplankton examined by oxygen utilization. *Marine Ecology Progress Series*, **101**, 9-22.

Craig, V.S.J., Ninham, B.W., Pashley, R.M. (1993). Effect of electrolytes on bubble coalescence. *Nature*, **364**, 317-319.

Crawford, G.B., Farmer, D.M. (1987). On the spatial distribution of ocean bubbles. *Journal of Geophysical Research*, **92**, 8231-8243.

Dafner, E.V., Wangersky, P.J. (2002). A brief overview of modern directions in marine DOC studies Part I.-Methodological aspects. *Journal of Environmental Monitoring,* **4**, 48-54.

Dahl, P.H. (2001). Bubble clouds and their transport within the surf zone as measured with a distributed array of upward-looking sonars. *Journal of the Acoustical Society of America*, **109**, 133-142.

Datta, R.L., Napier, D.H., Newitt, D.M. (1950). The properties and behaviour of gas bubbles formed at a circular orifice. *Transactions of the Institute of Chemical Engineering*, **28**, 14-26.

Deane, G.B., Stokes, M.D. (2002). Scale dependence of bubble creation mechanisms in breaking waves. *Nature*, **418**, 839-844.

Decho, A.W. (1990). Microbial exopolymer secretions in ocean environments: Their role(s) in food webs and marine processes. *Oceanography and Marine Biology: An Annual Review*, **28**, 73-153.

Detsch, R.M. (1990). Dissolution of 100 to 1000µm diameter air bubbles in reagent grade water and seawater. *Journal of Geophysical Research*, **95**, 9765-9773.

Detwiler, A. (1979). Surface active contamination of air bubbles in water. In: Mittal, K.L. (ed.) *Surface contamination: Genesis, detection and control*. Plenum. New York: pp. 993-1007.

Farmer, D.M., McNeil, C.L., Johnson, B.D. (1993). Evidence for the importance of bubbles in increasing air-sea gas flux. *Nature*, **361**, 620-623.

Ferrari, G.M., Dowell, M.D., Grossi, S., Targa, C. (1996). Relationship between the optical properties of chromophoric dissolved organic matter and total concentration of dissolved organic carbon in the southern Baltic Sea region. *Marine Chemistry*, **55**, 299-316.

Ferrari, G.M., Dowell, M.D. (1998). CDOM absorptions characteristics with relation to fluorescence and salinity in coastal areas of the southern Baltic Sea. *Estuarine, Coastal and Shelf Science*, **47**, 91-105.

Fogg, G.E., (1965). *Algal cultures and phytoplankton ecology*. University of Wisconsin Press. Madison. 126 pp.

Fogg, G.E. (1977). Excretion of organic matter by phytoplankton. *Limnology and Oceanography*, **22**, 576-577.

Frew, N.M., Goldman, J.C., Dennett, M.R., Johnson, A.S. (1990). Impact of phytoplankton-generated surfactants on air-sea gas exchange. *Journal of Geophysical Research*, **95**, 3337-3352.

Garrett, W.D. (1967). Damping of capillary waves at the air-sea interface by oceanic surface active material. *Journal of Marine Research*, **25**, 279-291.

Gat, J.R., Shatkay, M. (1991). Gas exchange with saline waters. *Limnology and Oceanography*, **36**, 988-997.

Gershey, R.M. (1983). A bubble adsorption device for the isolation of surface active organic matter in seawater. *Limnology and Oceanography*, **28**, 395-400.

Giullard, R.R.L., Ryther, J.H. (1962). Studies of marine planktonic diatoms. I. *Cyclotella nana* Hustedt and *Detonula confervacea* (Cleve). *Canadian Journal of Microbiology*, **8**, 229-239.

Grasshoff, K., Kremling, K., Erhard, M. (eds.) *Methods of seawater analysis* 3rd edition. Verlag Chemie. Weinheim. 600 pp.

Haberman, W.L., Morton, R.K. (1953). An experimental investigation of the drag and shape of air bubbles rising in various liquids. *The David W. Taylor Model Basin.* 55, Navy Department. Washington 7 D.C.

Hamm, C.E., Simson, D.A., Merkel, R., Smetacek, V. (1999). Colonies of *Phaeocystis globosa* are protected by a thin but tough skin. *Marine Ecology Progress Series*, **187**, 101-111.

Hansell, D.A., Carlson, C.A. (2002). *Biogeochemistry of marine dissolved organic matter*. Academic Press. London. 774 pp.

Harris, I.A., Detsch, R.M. (1991). Small air bubbles in reagent grade water and seawater-2. Dissolution of 20- to 500µm-diameter bubbles at atmospheric pressure. *Journal of Geophysical Research*, **96**, 8907-8910.
Hellebust, J.A. (1965). Excretion of some organic compounds by marine phytoplankton. *Limnology and Oceanography*, **10**, 192-206.

Hellebust, J.A. (1974). Extracellular products. In: Stewart, W.D. (ed.) *Algal physiology and biochemistry*. *Botanical Monographs 10*. Blackwell Scientific. Oxford: pp. 838-854.

Hoagland, K.D., Rosowski, J.R., Gretz, M.R., Roemer, S.C. (1993). Diatom extracellular polymeric substances: function, fine structure, chemistry and physiology. *Journal of Phycology*, **29**, 537-566.

Hobbie, J.E., Daley, R.J., Jasper, S. (1977). Use of nuclepore filters for counting bacteria by fluorescence microscopy. *Applied and Environmental Microbiology*, **33**, 1225-1228.

Humphrey, G.F. Wootton, M. (1966). Comparison of techniques used in the determination of phytoplankton pigments. Unesco Monographs on Oceanographic Methodology. Paris: pp. 37-63.

Hwang, P.A., Poon, Y.-K., Wu, J. (1991). Temperature effects on generation and entrainment of bubbles induced by a water jet. *Journal of Physical Oceanography*, **21**, 1602-1605.

Imai, I., Ishida, Y., Hata, Y. (1993). Killing of marine phytoplankton by a gliding bacterium *Cytophaga* sp., isolated from the coastal sea of Japan. *Marine Biology*, **116**, 527-532.

Ittekkot, V. (1982). Variations of dissolved organic matter during a plankton bloom: Qualitative aspects, based on sugar and amino acid analysis. *Marine Chemistry*, **11**, 143-158.

Jeffrey, S.W., Humphrey, G.F. (1975). New spectrophotometric equations for determining chlorophylls a, b, c1 and c2 in higher plants, algae and natural phytoplankton. *Biochemie und Physiologie der Pflanzen (BPP)*, **167**, 191-194.

Jenkinson, I.R. (1993). Bulk-phase viscoelastic properties of seawater. *Oceanologica Acta*, **16**, 317-334.

Jenkinson, I.R., Biddanda, A. (1995). Bulk-phase viscoelastic properties of seawater: relationship with plankton components. *Journal of Plankton Research*, **17**, 2251-2274.

Jensen, A. (1984). Excretion of organic carbon as function of nutrient stress. In: Holm-Hansen, O., Bolis, L., Gilles, R. (eds.) *Marine phytoplankton and productivity.* Springer Verlag. Berlin: pp. 61-72.

Johnson, B.D., Cooke, R.C. (1979). Bubble populations and spectra in coastal waters: A photographic approach. *Journal of Geophysical Research*, **84**, 3761-3766.

Kaehler, P., Bjornsen, P.K., Lochte, K., Antia, A. (1997). Dissolved organic matter and its utilisation by bacteria during spring in the Southern Ocean. *Deep-Sea Research*, **44**, 341-353.

Keeling, R.F. (1993). On the role of large bubbles in air-sea gas exchange and supersaturation in the ocean. *Journal of Marine Research*, **51**, 237-271.

Kepkay, P.E. Particle aggregation and the biological reactivity of colloids. *Marine Ecology Progress Series*, **109**, 293-304.

Kolaini, A.R., Crum, L.A., Roy, R.A. (1994). Bubble production by capillary-gravity waves. *Journal of the Acoustical Society of America*, **95**, 1913-1921.

Kolovayev, P.A. (1976). Investigation of the concentration and statistical size distribution of wind produced bubbles in the near-surface ocean layer. *Oceanology*, **15**, 659-661.

Krägel, J., Siegel, S., Miller, R., Born, M., Schano, K.-H. (1994). Measurement of interfacial shear rheological properties: an automated apparatus. *Colloids and Surfaces A: Physicochemical and Engineering Aspects*, **91**, 169-180.

Krägel, J., Stortini, A.M., Degli-Innocenti, N., Loglio, G., Cini, R., Miller, R. (1995). Dynamic interfacial properties of marine microlayers. *Colloids and Surfaces A: Physicochemical and Engineering Aspects*, **101**, 129-135.

Lancelot, C., Rousseau, V. (1994). Ecology of *Phaeocystis*-dominated ecosystems: the key role of colony forms. In: Leadbeater, B., Green, J. (eds.) *The Prymnesiophyte Algae. Systematics Association* (special volume, No. 51). Oxford University Press: pp. 229-245.

Lancelot, C. (1995). The mucilage phenomenon in the continental coastal waters of the North Sea. *The Science of the Total Environment*, **165**, 83-102.

Larsson, U., Hagström, A. (1979). Phytoplankton exudate release as an energy source for the growth of pelagic bacteria. *Marine Biology*, **52**, 199-206.

Lee, C., Wakeham, S.G. (1989). Organic matter in seawater: Biogeochemical processes. In: Riley, J.P. (ed.). *Chemical Oceanography.* Vol. 9. Academic Press. London: pp. 1-51.

Leppard, G.G. (1995). The characterization of algal and microbial mucilages and their aggregates in aquatic ecosystems. *The Science of the Total Environment*, **165**, 103-131.

Leifer I., Patro, R., Bowyer, P. (2000). A study on the temperature variation of rise velocity for large clean bubbles. *Journal of Atmospheric and Oceanic Techology*, **17**, 1392-1402.

Liss, P.S., Merlivat, L. (1986). Air-sea gas exchange rates: introduction and synthesis. In: Buat-Menard, P. (ed.). *The role of air-sea exchange in geochemical cyling.* Reidel. Dordrecht: pp. 113-127.

Loewen, M.R., O'Dor, M.A., Skafel, M.G. (1996). Bubbles entrained by mechanically generated breaking waves. *Journal of Geophysical Research,* **101**, 20795-20796.

Loglio, G., Pandolfini, P., Miller, R., Makievski, A.V., Ravera, F., Ferrari, M., Liggieri, L. (2001). Drop and bubble shape analysis as tool for dilational rheology studies of interfacial layers. In: Möbius, D., Miller, R. (eds.). *Novel methods to study interfacial layers. Studies in Interface Science*. Vol. **11**. Elsevier. Amsterdam: pp. 439-484.

Longuet-Higgins, M.S., Cokelet, E.D. (1978). The deformation of steep surface waves on water. Part II: Growth of normal mode instabilities. *Proceedings of the Royal Society of London*, **364**, 1-28.

McConnell, S.O. (1988). Acoustic measurements of bubbole densities at 15-50 Hz. In: Kerman, B.R. (ed.). *Sea Surface Sound*. Kluwer Academic Publishers. Boston: pp. 237-252.

McDaniel, S.T. (1988) Acoustical estimates of subsurface bubble densities in the open ocean and coastal waters. In: Kerman, B.R. (ed.). *Sea Surface Sound*. Kluwer Academic Publishers. Boston: pp. 225-235.

McIntyre, F. (1986). On reconciling optical and acoustical bubble spectra in the mixed layer. In: Monahan, E.C. and MacNiocaill, G. (eds.). *Oceanic whitecaps and their role in air-sea exchange processes.* Kluwer Academic Publishers. Boston: pp. 75-94.

Medwin, H. (1970). In situ acoustic measurements of bubble populations in coastal ocean waters. *Journal of Geophysical Research*, **75**, 599-611.

Merlivat, L., Memery, L. (1983). Gas exchange across an air-water interface: Experimental results and modelling of bubble contribution to transfer. *Journal of Geophysical Research*, **88**, 707-724.

Miller, R., Krägel, J., Wüstneck, R., Wilde, P.J., Li, J.B., Fainerman, V.B., Loglio, G., Neumann, A.W. (1998). Adsorption kinetics and rheological properties of food proteins at air/water and oil/water interfaces. *Nahrung*, **42**, 225-228.

Mitsuyasu, H., Bock, E.J. (2001). The influence of surface tension. In: Jones, I.S.F., Yoshiaki, T. (eds.), *Wind stress over the ocean*. Camebridge University Press: pp.242-253.

Möller Jensen, L. (1983). Phytoplankton release of extracellular organic carbon, molecular weight composition , and bacterial assimilation. *Marine Ecology Progress Series*, **11**, 39-48.

Monahan, E.C., Dam, H.G. (2001). Bubbles: An estimate of their role in the global oceanic flux of carbon. *Journal of Geophysical Research*, **106**, 9377-9383.

Monahan, E.C., Zietlow, C.R. (1969). Laboratory comparisons of freshwater and saltwater whitecaps. *Journal of Geophysical Research*, **74**, 6961-6966.

Mopper, K., Zhou, J., Ramana, K.S., Passow, U., Dam, H.G., Drapeau, D.T. (1995). The role of surface active carbohydrates in the flocculation of a diatom bloom in a mesocosm. *Deep-Sea Research*, **42**, 47-73.

Mulhearn, P.J. (1981). Distribution of microbubbles in coastal waters. *Journal of Geophysical Research*, **86**, 6429-6434.

Myklestad, S.M. (1972). Production of carbohydrates by the marine diatom *Chaetoceros affinis* var. *willei* (Gran) Hustedt. II. Preliminary investigation of the extracellular polysaccharide. *Journal of experimental marine Biology and Ecology*, **9**, 137-144.

Myklestad, S.M. (1977). Production of carbohydrates by marine planktonic diatoms. II. Influence of the N/P ratio in the growth medium on the assimilation ratio, growth rate, and production of cellular and extracellular carbohydrates by *Chaetoceros affinis* var. *willei* (Gran) Hustedt and *Skeletonema costatum* (Grev.) Cleve. *Journal of Experimental Marine Biology and Ecology*, **29**, 161-179.

Myklestad, S.M. (1995). Release of extracellular products by phytoplankton with special emphasis on polysaccharides. *The Science of the Total Environment*, **165**, 155-164.

Nägeli, A., Schanz, F. (1991). The influence of extracellular algal products on the surface tension of water. *Internationale Revue gesamten Hydrobiologie*, **76**, 89-103.

Nalewajko, C., Lean, D.R.S. (1972). Growth and excretion in planktonic algae and bacteria. *Journal of Phycology*, **8**, 361-366.

Nightingale, P.D., Liss, P.S. (2004). Gases in seawater. In: Elderfield, H. (Vol. ed.). *Treatise on geochemistry Volume 6. The oceans and marine geochemistry* Executive eds.: Holland, H.D., Turekian, K.K. Elsevier. Amsterdam: pp. 49-81.

Norrman, B., Zweifel, U.L., Hopkinson, C.S., Fry, B. (1995). Production and utilisation of dissolved organic carbon during an experimental diatom bloom. *Limnology and Oceanography*, **40**, 898-907.

Patro, R., Leifer, I., Bowyer, P. (2001). Better bubble process modeling : Improved bubble hydrodynamics parameterisation. In: Donelan, M., Drennan, W., Salzmann, E.S., Wanninkhof, R. (eds). *Gas transfer and water surfaces*, AGU Monograph **127**: pp. 315-320.

Peltzer, E.T. (1994). Shipboard determination of total organic carbon by a high temperature combustion / discrete injection technique.
http://www.mbari.org/~etp3/doc1/proto.txt

Peltzer, E.T. (1996). Instructions for DOC/TOC sampling.
http://www.mbari.org/~etp3/doc1/sample.txt

Peltzer, R.D., Griffin, O.M. (1988). Stability of a three-dimensional foam layer in seawater. *Journal of Geophysical Research*, **93**, 10804-10812.

Petkov, G.D., Bratkova, S.G. (1996). Viscosity of algal cultures and estimation of turbulency in devices for the mass culture of microalgae. *Algological Studies*, **81**, 99-104.

Ramsey, W.L. (1962). Dissolved oxygen in shallow near-shore water and its relation to possible bubble formation. *Limnology and Oceanography*, **8**, 453-461.

Rapp, R.J., Melville, W.K. (1990). Laboratory measurements of deep water breaking waves. *Philosophical Transactions of the Royal Society of London* A, **331**, 735-800.

Revelante, N., Gilmartin, M. (1991). The phytoplankton composition and population enrichment in gelatinous macroaggregates in the Northern Adriatic during the summer of 1989. *Journal of Experimental Marine Biology and Ecology*, **146**, 217-233.

Rosenstock, B., Simon, M. (2001). Sources and sinks of dissolved free amino acids and protein in a large and deep mesotrophic lake. *Limnology and Oceanography*, **46**, 644-654.

Sandler, B.M., Selivanovskii, D.A., Sokolov, A.Yu. (1982). New data on the concentration of gas bubbles with radii from 6 to 20 μm in the sea. *Soviet Physics Technical Physics*, **27**, 1038-1039.

Scott, J.C. (1975). The role of salt in whitecap persistence. *Deep Sea Research*, **22**, 651-657.

Sharp, J.H. (1973). Size classes of organic carbon in seawater. *Limnology and Oceanography*, **18**, 441-447.

Sharp, J.H. (1977). Excretion of organic matter by marine phytoplankton. Do healthy cells do it? *Limnology and Oceanography*, **22**, 381-399.

Shatkay, M., Ronen, D. (1992). Bubble populations and gas exchange in hypersaline solutions: A preliminary study. *Journal of Geophysical Research*, **97**, 7361-7372.

Simon, M., Azam, F. (1989). Protein content and protein synthesis rates of planktonic marine bacteria. *Marine Ecology Progress Series*, **51**, 201-213.

Skop, R.A., Tseng, R-S, Brown, J.W. (1993). Effects of salinity and surface tension on microbubble-mediated sea-to-air transfer of surfactants. *Journal of Geophysical Research*, **98**, 8489-8494.

Slauenwhite, D.E., Johnson, B.D. (1996). Effect of organic matter on bubble surface tension. *Journal of Geophysical Research*, **101**, 3769-3774.

Slauenwhite, D.E., Johnson, B.D. (1999). Bubble shattering: Differences in bubble formation in fresh water and seawater. *Journal of Geophysical Research*, **104**, 3265-3275.

Stoderegger, K., Herndl, G.J. (1998). Production and release of bacterial capsular material and ist subsequent utilization by marine bacterioplankton. *Limnology and Oceanography*, **43**, 877-884.

Stoderegger, K., Herndl, G.J. (1999). Production of exopolymer particles by marine bacterioplankton under contrasting turbulence conditions. *Marine Ecology Progress Series*, **189**, 9-16.

Stramska, M., Marks, R., Monahan, E.C. (1990). Bubble-mediated aerosol production as a consequence of wave breaking in supersaturated (hyperoxic) seawater. *Journal of Geophysical Research*, **95**, 18281-18288.

Terrill, E.J., Melville, W.K. (2000). A broadband acoustic technique for measuring bubble size distributions: Laboratory and shallow water measurements. *Journal of Atmospheric and Oceanic Technology*, **17**, 220-239.

Thorpe, S.A. (1982). On the clouds of bubbles formed by breaking wind-waves in deep water, and their role in air-sea gas transfer. *Philosophical Transactions of the Royal Society of London A*, **304**, 155-210.

Thorpe, S.A. (1986). Measurements with an automatically recording inverted echo sounder, ARIES and the bubble clouds. *Journal of Physical Oceanography*, **16**, 1462-1478.

Thorpe, S.A. (1988). The horizontal structure and distribution of bubble clouds. In: Kerman, B.R. (ed.). *Sea surface sound*. Kluwer Academic Publishers. Boston: pp.173-183.

Thorpe, S.A., Bowyer, P., Woolf, D.K. (1992). Some factors affecting the size distribution of oceanic bubbles. *Journal of Physical Oceanography*, **22**, 382-389.

Thorpe, S.A., Hall, A.J. (1987). Bubble clouds and temperature anomalies in the upper ocean. *Nature*, **328**, 48-51.

Trevorrow, M.V., Vagle, S., Farmer, D.M. (1994). Acoustical measurements of microbubbles within ship wakes. *Journal of the Acoustical Society of America*, **95**, 1922-1930.

Tsen, R-S., Viechnicki, J.T., Skop, R.A., Brown, J.W. (1992). Sea-to-air transfer of surface active organic compounds by bursting bubbles. *Journal of Geophysical Research*, **97**, 5201-5206.

Utermöhl, H. (1958) Zur Vervollkommnung der quantitativen Phytoplankton-Methodik. *Mitteilungen. Internationale Vereiningung für Theoretische und Angewandte Limnologie*, **9**, 1–38.

Vagle, S., Farmer, D.M. (1992). The measurement of bubble-size distributions by acoustical backscatter. *Journal of Atmospheric and Oceanic Technology*, **9**, 630-644.

Vieira, A.A.H., Myklestad, S. (1986). Production of extracellular carbohydrate in culture of *Ankistrodesmus densus* Kors. (Chlorophyceae). *Journal of Plankton Research*, **8**, 985-994.

Wallace, G.T., Duce, R.A. (1978). Open-ocean transport of particulate trace metals by bubbles. *Deep Sea Research*, **25**, 827-835.

Wallace, D.W.R., Wirick, C.D. (1992). Large air-sea gas fluxes associated with breaking waves. *Nature*, **365**, 694-696.

Wang, Q., Monahan, E.C. (1995). *The Influence of salinity on the spectra of bubbles formed in breaking wave simulations.* In: Buckingham, M.J and Potter, J.R. (eds). *Sea Surface Sound '94, Proceedings of the III International Meeting on Natural Physical Processes Related to Sea Surface Sound*. World Scientific. Singapore: pp.312-319.

Welschmeyer, N.A. (1994). Fluorometric analysis of chlorophyll a in the presence of chlorophyll b and pheopigments. *Limnology and Oceanography*, **39**, 1985-1992.

Wildt, R. (1968) *Physics of sound in the sea*. Gordon and Breach. New York. 118 pp.

Williams, P.M., Carlucci, A.F., Henrichs, S.M., Van Vleet, E.X., Horrigan, S.G., Reid, F.M.H., Robertson, K.J. (1986). Chemical and microbiological studies of sea-surface films in the southern gulf of California and off the west coast of Baja California. *Marine Chemistry*, **19**, 17-98.

Williams, P.J. le B. (1990). The importance of losses during microbial growth: commentary on the physiology, measurement and ecology of the release of dissolved organic material. *Marine Microbial Food Webs*, **4**, 175-206.

Woolf, D.K. (1997). Bubbles and their role in gas exchange. In: Liss, P.S. and Duce, R.A. (eds.) *The sea surface and global change.* Cambridge University Press: pp. 173-205.

Woolf, D.K., Thorpe, S.A. (1991). Bubbles and the air-sea exchange of gases in near-saturation conditions. *Journal of Marine Research*, **49**, 435-466.

Wu, J. (1981). Bubble populations and spectra in near-surface ocean : Summary and review of field measurements. *Journal of Geophysical Research*, **86**, 457-463.

Wu, J. (1988). Bubbles in the near-surface ocean: A general description. *Journal of Geophysical Research*, **93**, 587-590.

Wu, J. (1992). Individual characteristics of whitecaps and volumetric description of bubbles. *IEEE Journal of Oceanic Engineering*, **17**, 150-158.

Wu, J. (1994). Bubbles in the near-surface ocean: Their various structures. *Journal of Physical Oceanography*, **24**, 1955-1964.

Wüstneck, R., Krägel, J., Miller, R., Wilde, P.J., Clark, D.C. (1996). The adsorption of surface active complexes between β-casein, β-lactoglobulin and ionic surfactants and their shear rheological behaviour. *Colloids and surfaces A: Physicochemical and Engineering Aspects*, **114**, 255-265.

Zakharkov, S.P., Sandler, B.M., Selivanovskiy, D.A., Sokolov, A.Yu., Starodubtsev, Ye.G., Stunzhas, P.A. (1991). Gas bubbles and phytoplankton in seawater. *Oceanology*, **31**, 440-441.

Zhou, J., Mopper, K., Passow, U. (1998). The role of surface active carbohydrates in the formation of transparent exopolymer particles by bubble adsorption of seawater. *Limnology and Oceanography*, **43**, 1860-1871.

Zlotnik, I., Dubinsky, Z. (1989). The effect of light and temperature on DOC excretion by phytoplankton. *Limnology and Oceanography*, **34**, 831-839.

Zutic, V., Cosovic, B., Marcenko, E., Bihari, N. (1981). Surfactant production by marine phytoplankton. *Marine Chemistry*, **10**, 505-520.